RUTHENIUM OLEFIN METATHESIS COMPLEXES:

CATALYST DEVELOPMENT AND MECHANISTIC STUDIES

Thesis by

DONDE R. ANDERSON

In Partial Fulfillment of the Requirements for the degree of

Doctor of Philosophy

CALIFORNIA INSTITUTE OF TECHNOLOGY

Pasadena, California

2008

(Defended July 27, 2007)

For my birth mom

ᴥ WE ARE LINKED BY BLOOD, AND BLOOD IS MEMORY WITHOUT LANGUAGE. ଔ

-JOYCE CAROL OATES, *I LOCK MY DOOR UPON MYSELF*

ACKNOWLEDGEMENTS

There have been many highs and lows over the past five years, and I wouldn't change a thing. I have benefited from the professors, fellow grad students, post-docs, undergrads and staff, and I thank them all for their contribution to my thesis and/or my sanity.

First, I have to thank my 8th-grade earth science teacher at Central Middle School in Broken Arrow, OK: Mrs. Smith. The experiments we did in her class were the beginning of my interest in science (until then math and English were my favorite subjects). Then, in my senior year of high school at OSSM, my biochemistry professor, Dr. Dell, set me up to do research at the University of Oklahoma with Prof. Keith Strevett in the Dept. of Environmental Science and Engineering. This was my first introduction to research and I became fascinated with the idea of finding out something that no one else has ever discovered.

During my undergraduate years, I explored many different research areas from molelcular biology to non-linear dynamics to biophysics (Prof. Pill Soon Song at the University of Nebraska-Lincoln, Prof. Paul Umbanhowar at Northwestern University, Prof. Bob Austin at Princeton University), but it was working in Prof. SonBinh Nguyen's lab at Northwestern that led me on the chemistry path. His pure excitement for chemistry and high standards were both demanding and compelling. SonBinh helped me in countless ways, including with fellowship applications and propelled me to Caltech. He has been kind, genuine, honest and helpful (in addition to stubborn and thrifty) even as I have continued my studies here. He will always be my advisor.

Keith Watson was my graduate student mentor in SonBinh's lab. He has always had an unshakable faith in my abilities. I never understood it, but I seriously appreciated it. Life has come full circle since I will be joining Keith at Dow Chemical this fall. Who would've guessed back in 2000 that the grad student who was stuck with me would eventually recruit me and we would become co-workers. Hopefully we won't have to share a hood again.

I am so thankful for Bob's decision to let me into the group. His management style, which I believe can be summarized as "treat a lady as she is and she will stay as she is; treat a lady as she could be and she will grow to be all she can," has been frustrating and difficult at times, but, as he once told me, it wasn't meant to be easy. Maybe we don't remember that often enough. Seriously, the Grubbs group has been awesome (especially that Nobel thing)….and I'm not just saying that because I'm leaving. Also a huge thanks for letting me study in Japan for 2 months during my time at Caltech—I had a blast and I don't think most professors would have been as generous. Thanks Bob for putting up with all my random research projects, career interests (should I postdoc? With whom should I postdoc? Should I be a professor? Do I have what it takes to be a professor? Should I interview for industrial positions? What position should I take???) and rants. I hope I've made enough desserts over the years to make it up to you! If only I'd known about your penchant for banana cream pie earlier.

My committee—Brian Stoltz, Jackie Barton and John Bercaw—has been greatly accommodating in all of the scheduling issues—thank you (for passing me)! I want to especially thank Brian. I remember calling him one night when I was a prospective student to tell him that I didn't think I belonged at Caltech because I wasn't smart enough.

Another professor might have not cared at all about some random prospective, but Brian was encouraging and, well, I did end up at Caltech! Thanks Brian!

While at Caltech, I've worked on projects with a lot of (really smart) people. In chronological order, I'd like to thank Drew Waltman who introduced me to organometallic chemistry via nickel chemistry. I also want to thank "King" James Tsai, Christiane Marti and Soon Hong for working together on the use of tin ligands for metathesis catalyst. Thanks also to Jacob Berlin who donated various chiral ligand precursors and chiral ruthenium complexes to me for the Rh hydrosilylation project (and later for the olefin-binding studies). I'd like to thank Prof. Guy Bertrand and his group members Vincent Lavallo and Carsten Praesang at UC, Riverside for sending me some really cool carbene precursors to work with. I have also benefited much from Dr. Yann Schrodi, Thay Ung, Garik Mkrtumyan, and Jeanie Connor at Materia, Inc. for all of their discussions and experimental expertise (and to Materia for generation donation of many ruthenium precursors!). Prof. Dan O'Leary at Pomona College spent a year on sabbatical in the Grubbs group, and I don't think I would have been able to complete this thesis without his insightful and helpful NMR experiments and discussions. Dr. O's passion for his work and family are an inspiration for the rest of us. I also worked with Daniel Hickstein, an undergraduate at Pomona College, who did his senior thesis on ruthenium-olefin complexes; I hope I didn't scare him away from synthetic chemistry! I expect we'll see great things from Hickstein (I at least expect a postcard from him while on his Churchill fellowship in England)! While at Caltech, I also had the pleasure of mentoring a SURF student, Louis Ciardulli from University of Florida, Gainesville. He was a great student who had to listen to my "particular" and "precise" ways of doing things for many weeks. I hope he winds up back here at Caltech!

A shout out here for Zono Sushi and Chipotle for giving me (and a bunch of my friends) free lunch through their business card drawing. I was *so* excited when Chipotle opened on Lake—it reminds me of my undergrad days in Evanston. One of the other great food-related events was when Trader Joe's opened up on Lake/Del Mar. I will miss TJs. And, since returning from Japan where the ramen and udon were delicious, Kansai in Old Town has become one of my favorite spots for dinner.

All of the staff that keep Caltech Chemistry running should receive more recognition than they do. Thanks to Linda Clark, Dian Buchness, Tom Dunn, Mona Shagholi, Scott Ross, Larry Henling, Mike Day, Anne Penney Joe Drew, Terry James, Laura Howe for everything they do to make grad students time at Caltech bearable. Also, a big thanks to everyone who works to keep up the rose gardens/grounds/ponds; it's a great place to just sit and enjoy the day (yeah, I did that a couple of times).

I thank everyone who helped me out during the job interviewing process. There were lots of drafts of my CV, research summary, research slides and job talk slides to be analyzed and there were always willing participants. The Grubbs group is always willing to help out its members and that's one of the things I am so grateful for. I want to thank BP, Dow, DuPont, Rohm and Haas and BASF for offering me gainful employment. It's good to know that the past five years have molded me into someone that people are willing to take a chance on.

One of the greatest things about the Grubbs group is all the people you get to know just by virtue of working with them. I've met people from all over the world, including Canada, Chile, China, England, France, Germany, Greece, Japan, Korea, Norway, Romania,

Russia, Spain, Sweden, Switzerland, and Taiwan. It's been great to learn about so many different cultures. I want to thank all the graduate students I've overlapped with: Bill Ward, Tae-Lim Choi, Dan Sanders, Oren Scherman, Christie Morrill, Drew Waltman, Isaac Rutenberg, Jacob Berlin, Tim Funk, Andy Hejl, Jason Jordan, Erin Guidry, Irina Gorodetskaya, Soon Hong, Kevin Kuhn, John Matson, Paul Clark, Angela Blum, Jean Li, Chris Daeffler, Matt Whited and newcomer Keith Keitz. There have been numerous postdocs and scholars as well: Daryl Allen, Katie Campbell, Stu Cantrill, Emmanuelle Despagnet-Ayoub, Greg Beutner, Cheol Cheung, Paula Diaconescu, Chris Douglas, Jon Efskind, Steve Goldberg, Connie Hou, Takashi Koike, Jen Love, Christiane Marti-Meyers, Al Nelson, Mike Page, Tobias Ritter, Patricio Romero, Joseph Samec, Sebastian Smidt, Ian Stewart, James Tsai, Georgios Vougioukalakis, and Masao Yanagawa. I have enjoyed getting to know everyone in addition to all the chemistry I've soaked up (hopefully) from just being around such smart people.

A shout out to all the girls who've been in the group and come along for our weekly "girls' lunch" outings. What's done/said at girls' lunch stays at girls' lunch, except for those times when we let boys come with us.

One of the few things that has made grad school bearable is all of my friends who have been there to listen, complain, empathize, sympathize, hang with, and drink with (vide infra!).

Erin Guidry kept me sane by listening to all my gripes and empathizing. Pizza and cheesecake nights (and framboise) were awesome. She was always up for driving to get good food, from Korean food to chipotle (back when it was far away). Erin made grad student life bearable, and even fun at times! She's always good for a pep talk or a good ol' rant. I have been considerably enriched in many ways, including all of the supramolecular chemistry knowledge I've gained through osmosis! I'll miss being around her 60 + hours a week. ☺

Irina Gorodetskaya kept me sane with all the shopping therapy. Random trips to the beach, to malls and for dinner. Did someone say outlet mall? Or ice cream? She drove me all over LA and then some. She made me like LA, even though I still LOVE Chicago. Her car is *the* most beautiful I have ever seen. I'm going to miss my shopping buddy. Good luck interviewing and don't forget you promised to take me to Russia someday!

Soon Hong was a great labmate and friend. We spent many nights talking about our non-functional projects and trying to help and encourage each other! I've certainly appreciated learning about Korean culture from him. I'm so happy for him, Jamie and their cutie-pie son, David. Congrats on being the first from our class to graduate!

Dan O'Leary was a great collaborator and friend. 2D NOESY, EXSY, HOESY, HMQC, HMBC, COSY—thanks for teaching me! Hi Maggie, Frances, and Katie—you're too cute. Am I still in the Yoda club??? And June, the cook in the family, was always kind enough to let me stay for (Thanksgiving, Christmas, anytime) dinner! Dan listened to my "trials and tribulations" as a grad student and didn't laugh (in my face anyway). He's been like the Dad I never had! I am going to miss *my* NMR and *my* guesthouse.

Paula Diaconescu was one of the few real inorganic chemists to postdoc in our group and needless to say we all benefited from her glovebox wisdom. Paula has been great to talk to about science and everything else. I have semi-converted her into a Cook's illustrated

fan. Opera. Vlad. The arts. UCLA. Romania. Marriage. Learning to drive. I'm so glad she has kept in touch and been willing to drive all the way to Pasadena to hang out occasionally. I hope she has time some day to slow down a bit!

Andy Hejl (or is it Hail or Hale?) was an awesome labmate. The Hodge. The Ath. Marzipan. Fudge. Survivor. Lists. Darts. Random facts. Jeopardy. Eating better. Tim and Andy's Thanksgiving Extravaganza! He had good interviewing advice (I did get a job after all). Andy was always good for an opinion on whatever it was you were thinking about (chemistry, sports, tv, history…). Good darts.

Katie Campbell has been a lot of fun to be in lab with. Ruby. Puff pastry. Socks with pom poms. Lack of sleep. Spinach quesadilla. Pizza. Canada. Hockey. Edmonton. Lab ball. I had fun not participating in races up the stairwell. Katie has been a great listener and friend. Go Canada! I'll always think of her when I drink Tim Horton's when I move to Michigan.

John Matson is the hottest guy I've *ever* met. Beef! John keeps perhaps the best notebook I've ever seen in the group. We were baymates for a short while before the renovation made us adjacent baymates. Is the benzene-d_6 column leaking again?? Aren't you glad I badgered you into learning how to use the glovebox? Morn'un. He did well as King of the group pub crawls. Who's up for riding the bull???

Tobias Ritter was one of the most talented post-docs I met while in the group. He laughed at my 'american education' aka my lack of encyclopedic chemistry knowledge. But I always received good advice, though I didn't ever get a guarantee that my reactions would work like Irina did. Blue bug. Germany. Switzerland. Crazy hours. Short jeans. Ann and her wonderful cooking.

Chris Douglas is another of the really smart postdocs I've overlapped with. Rh. por. Ros. Mac 'n cheese. Thailand. Hard-core organic synthesis. The Renovation. U Minnesota. Glazed ham. Ernie's. Chris is quiet and reserved at first, but once you get to know him, you'll know differently. I know that Chris will be a great professor. I hope he learns to value his skills and knowledge as much as the rest of us do.

Daryl Allen, the Canadian who refused a ticket to an NHL hockey game. Daryl gave me a hard time, but I probably deserved it for all the Canadian jokes. But seriously, hetero-man's excitement about heterogeneous catalysis was awesome. He has mad editing skills; I should know since there's always something on his desk with my name on it! He's one of the coolest guys to hang out and talk about anything under the sun.

Drew Waltman took me under his wing, sortof, when I first joined the Grubbs group. Hooting like an owl. Nickel. Rohm and Haas. birdwatching. Chumbawumba. Drew could make you laugh at any time via robot dancing or any number of other methods.

Christiane Marti-Meyers was a great labmate. She always had time to listen to my questions or think about my project. She had lots of good stories to tell about the ETH. How I wished we'd had dishwashers like the Swiss. Congrats to her on her new baby boy!

Emmanuelle Despagnet was always fun to commiserate about projects with. She was the first one to introduce me to outlet malls! She was a fun office mate to have around. Bonne chance!

viii

Tim Funk and the cat limo will forever be etched together in my memory. Tim's straightforward, tell it like it is personality made him a great person to get advice from. Tim and Andy's Thanksgiving Extravaganza. Beer. The Ath. Funcadamo. Golf. Surfing. Total Synthesis. Merck. Gettysberg.

Dan Sanders was a wonderful resource to have around the lab! He knew everything about polymers since he practically had a separate PhD in it. Sports, of any kind. Loveline. Goggles. Cereal, for breakfast, lunch and maybe dinner.

Ron Walker—at first I had a difficult time with his Louisiana accent, but it's all good now! Ron's been a lot of fun to be in lab with, especially now that he's not buried in the back of 217 church! BBQ, barbecue, barbeque. Shrimp, crawfish, fresh seafood. Ron never comes to group functions like the infamous Grubbs group pub crawls, so I'm not sure if he's technically in the group yet (j/k!). Good luck to you and Tammy (go Captain of Crush Gripper!)

Kevin Kuhn and his wife Melissa have been fun to get to know. Mac. Stella. Moving. ROMP. Kevin's winding path in projects has probably come the closest to my own in the group. I'm glad things are starting to fall into place and I'm excited to see the cool results that are undoubtedly just around the corner!

Jen Love was one of the first postdocs I met in the Grubbs group. She has also been one of the nicest and smartest people I've had the good fortune of interacting with, even after she left for UBC. She passed on lots of good Grubbs group lore and Jedi Olefin Metathesis Barbie to me!

Jason Jordan's always been willing to lend a helping hand no matter how busy he was. Jason was also kind enough to show *Battlestar Galactica* on the big screen in 151 Crellin on the weekends! Who are the other cylons????

Connie Hou and I shared a glovebox after Paula left and we managed to never fight over it! Nickel Nickel Nickel. Trimers and prep HPLCs that don't work. Chinese New Year! Rice, yum! Din Tai Fung! She brought yummy snacks from the Chinese grocery store! She was also a great officemate and was subjected to my woes a lot. Good luck at Symyx, I'm sure we'll be meeting again in the near future!

Patricio Romero—Pato! Are you Chilenese? Are you from Canada? It's been fun getting to know you and gossip with you! And Carola too! I'm jealous of all the cool places that you get to visit because of the BP project. It's been cool to chat about science and to learn something about Chile!

Georgios Vougioukalakis has been a great labmate. Exxxxxxcellent! George always shared his afternoon snacks with us—yum! I've enjoyed learning about Greece and the small (400 person) weddings held there. Good luck to you and Christina!
Bill Ward and Stu Cantrill took me to coffee many a time when I was just starting at Caltech. They always had lots of good group gossip and advice on how things operate in the Grubbs group! Ah, the pink raspberry latte and the Brain Freeze!

Bercaw, Peters, Stoltz and MacMillan group members (and their stockrooms) have been really cool to learn from and hang out with! I've enjoyed getting lots of helpful advice from

everyone. The camaraderie among groups is one of the awesome, and perhaps unique, strengths of Caltech. I hope it never changes.

Amongst non-Grubbs group people, Claire Jacobs, Smith Nielsen, John Keith and Katie Saliba have been fun to hang out with, get coffee/drinks with, watch movies with, and have tea parties with. They've been a much-needed occasional break from metathesis speak! Go Northwestern! Gotta love the el. And Katie, I hope you get some sleep some day!

Linda Syme keeps Bob's schedule and keeps him mostly on time! Nobel symposium/reunion meetings, ISOM meetings, grandkid and travel stories. She has the scoop on all the group history and on Bob…if you have questions, ask her first!

Pat Anderson was great to work with to organize Friday IOS! She was understanding of all the last-minute changes and helped us change the budgetary allowances so we could go to the Ath occasionally! I'll drink to that!

Tom Dunn has fixed everything in our lab, three times at least. Gloveboxes, printers, NMR spectrometers, IKA hot plates. He is a friendly and funny personality with mad skills that are undervalued and overlooked too often. He is *always* so helpful. Thanks Tom for all of your help and especially your encouragement during the job interviewing season!

Larry Henling keeps telling me that my crystals are bad, but that maybe we can get something from them. He asks which crystal *I* think we should put on next as if I might know something. Larry continually manages to get structures from the worst crystals and tries to teach you something in the meantime as well. I almost stole his "nano-butter" idea for one of my props, but I thought twice about stealing it (because there were witnesses to his original pitch of the idea). Thanks for all the x-ray structures!

Scott Ross has overlooked my breaking an NMR tube in hg1 and still allows me to use the NMR facility. His willingness to help everyone do what they want while teaching them a little on the way is invaluable. If the NMR facility is working, you can bet that Scott (and the GLAs) is to be thanked.

Mona Shahgoli has kept me sane with the availability of a functioning mass spec facility. Thank you Mona!

My labmates in Prof. Mitsuo Sawamoto's group at Kyoto University: Aya-Chan, Chihiro-san, Tera-chan, Katsube-san, Nishi-san, Hirosue-san, Inagaki-san. They were so kind, helpful and cheerful to me during my stay! I had a great time learning about culture, scientific culture, language and traveling throughout Japan. They made living in a country where I don't speak the language fun!

Sherry Suyu was my first roommate in the Cats. Weekly grocery shopping to Ranch99 and other Asian markets with a little lunch or dinner on the side. Sinbala! Din Tai Fung! Young Dong Tofu House! Fosselman's Ice Cream! She reminded me that there's more to life than chemistry (there's astrophysics too!). I hope to visit you during your postdoc in Germany!

Fatemeh Afshari was my best friend during my undergrad days. Occasional visits to her in Boston and her family in Chicago. Persian food. Persian dill. Saffron. Dentistry. Harvard people. Chicago. T = L. Midtown. Her family has become like another home to me.

Jenny Birnbaum was my best friend at OSSM where I went to high school. She reminds me that no one has it figured out! She's out to save the environment meanwhile I'm gonna be working at a chemical company….I hope we can still be friends ☺ I'll soon be joining her in the ranks of people who have a 'real' job!

Maria Oh got me through some very tough times and encouraged me in countless ways. She was always an understanding place to visit and she referred me to Dr. Shon. It was one of the best pieces of advice I've received.

Liz Shon, I can't really put into words how much I valued my weekly therapy sessions. I don't know how I stumbled into her office, but I'm terrified to think that I almost didn't. She has helped me through many periods of anxiety, depression and sadness in order to become a (hopefully) better version of myself. Like grad school, it hasn't always been a pleasant experience, but if it had been, what would I have learned? I am indebted, grateful and sad to be leaving.

Jane Jeong Trenka and the other 150,000–200,000 Korean adoptees spread throughout the world who have given me a sense of community just by virtue of existing. I have found people with whom I share many experiences despite our scattered geographical locations and adoptive cultures. Thanks especially to those have begun to express their experiences through poetry, fiction, non-fiction and blogs.

Sunny weather and awesome beaches. It almost made grad school worthwhile.

ABSTRACT

The field of olefin metathesis has grown to include organometallic chemists who strive to develop more efficient catalysts and to understand their mechanism of activity and decomposition, synthetic organic chemists who construct complex molecules utilizing existing catalysts and continually find challenging reactions in need of more efficient catalysts, and polymer chemists who utilize current catalysts to synthesize polymers with an ever-widening array of functional groups and structures in a controlled manner. This thesis describes the exploration of new ligands for olefin metathesis catalysts and the investigation of the model compounds of olefin metathesis reaction intermediates.

Chapter 2 describes the synthesis, characterization, activity and kinetic selectivity of ruthenium olefin metathesis complexes bearing cyclic (alkyl)(amino)carbenes (CAACs). The activity of phosphine-free CAAC-ruthenium complexes is significantly affected by steric interactions. By decreasing the steric bulk of the ligand, a new catalyst with activity comparable to that of existing NHC-ruthenium (N-heterocyclic carbene) complexes has been synthesized. Additionally, these complexes exhibit unusual E/Z-diastereoselectivity and ethenolysis selectivity relative to previously studied NHC-ruthenium complexes.

Chapter 3 describes the exploration of 3- and 6-membered carbenes as ligands for ruthenium olefin metathesis complexes. Stable silver-cyclopropenylidene adducts were synthesized and utilized as carbene transfer reagents in the presence of ruthenium precursors. Although good conversions were observed, isolation of cyclopropenylidene-ruthenium complexes was unsuccessful. Ruthenium complexes of 6-membered 'borazine'-like carbenes were isolated, characterized and evaluated for ring-closing metathesis activity.

Chapter 4 describes the development of a model system to study ruthenium-olefin complexes relevant to the mechanism of olefin metathesis. Upon addition of the ligand precursor 1,2-divinylbenzene to $(H_2IMes)(py_2)(Cl)_2Ru=CHPh$ (H_2IMes = 1,3-dimesityl-4,5-dihydroimidazol-2-ylidene), two ruthenium-olefin adducts are formed. Based on ^1H NMR spectroscopy experiments and X-ray crystallographic analysis, the solution phase

and solid-state structure of these complexes is assigned. Exploration of the generality of these observations through variation of the *N*-heterocyclic carbene ligand and the ligand precursor are also presented.

Appendix 1 describes the screening of transitional-metal salts and ligands for the non-oxidative hydration of styrene. Appendix 2 describes the investigation of a prior report of intramolecular olefin hydroalkoxylation with ruthenium, copper and silver salts. Appendix 3 describes the evaluation of chiral NHCs as ligands for ruthenium and rhodium hydrosilylation catalysts. Appendix 4 describes the investigation of tin(II) halides as ligands for ruthenium olefin metathesis catalysts. Appendix 5 contains X-ray crystallographic analysis parameters of the structures presented in this thesis.

TABLE OF CONTENTS

# CHAPTER 1

Introduction

Introduction

Olefin metathesis is the formation of new carbon-carbon double bonds from existing carbon-carbon double bonds via a metallacyclobutane intermediate (eq 1.1). The olefin metathesis reaction has evolved from a novel observation resulting from ill-defined catalysts to a standard method for the synthesis of new C–C double bonds with well-defined catalysts.[1,2] Olefin metathesis is employed by synthetic organic, polymer and materials chemists[1,3] and has been utilized in a variety of applications, including the synthesis of agrochemicals and pharmaceuticals.[4,5]


thermodynamically controlled process
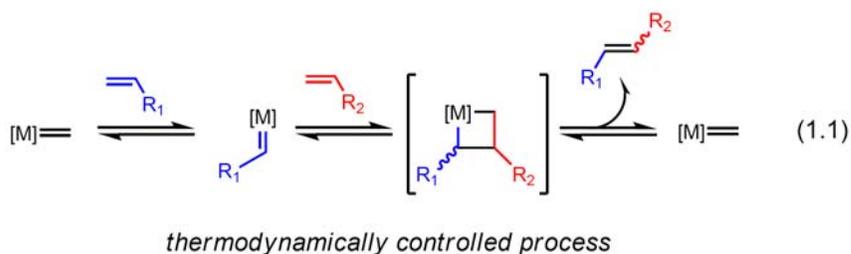
Olefin metathesis was first discovered in the 1950s and its history[3,6] includes the development of titanium,[7] tungsten,[8-12] molybdenum,[10,13,14] ruthenium[15-17] and rhenium[18] catalysts (Chart 1.1). Its contribution to the field of chemistry is demonstrated by the award of the 2005 Nobel prize to Richard Schrock, Robert Grubbs and Yves Chauvin whose research pioneered the synthesis of active, well-defined olefin metathesis catalysts.

Chart 1.1. Examples of olefin metathesis catalysts
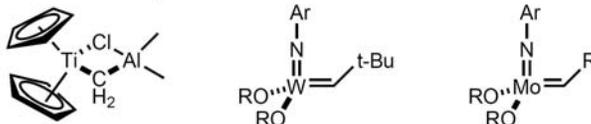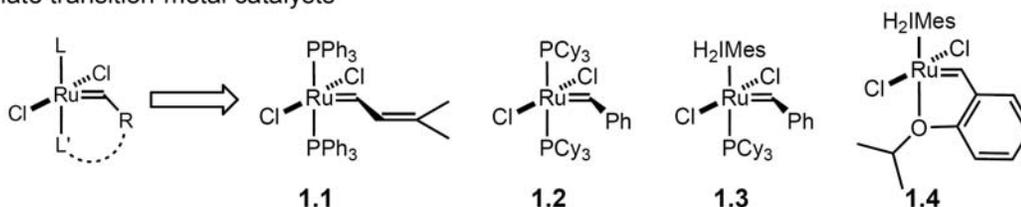
Metathesis Reactions

The broad applicability of olefin metathesis is due in part to the wide array of olefins that can be formed, including terminal, internal, cyclic, and macrocyclic olefins and polymers (Figure 1.1). Depending on reaction concentration, α,ω-dienes can undergo ring-closing metathesis (RCM) to form cyclic olefins or acyclic diene metathesis (ADMET) to form linear polymers. Strained cyclic olefins undergo ring-opening metathesis polymerization (ROMP) to provide polymers. Intermolecular reaction of two olefins provides a new olefin in cross metathesis (CM) reactions; if one cross partner is a strained cyclic olefin, a ring-opening cross metathesis (ROCM) reaction may occur. Due to the typical thermodynamic control of metathesis reactions, these reactions often utilize a driving force (e.g., release of volatile products such as ethylene, release of ring strain, or formation of a more stable olefin product) to favor the formation of a single product.

Terminal Olefin Intermolecular Reactions

Cross Metathesis (CM)

Ring-Opening Cross Metathesis (ROCM)

Diene Metathesis Reactions

Ring-Closing Metathesis (RCM)

Acyclic Diene Metathesis (ADMET)

Ring-Opening Metathesis Polymerization (ROMP)
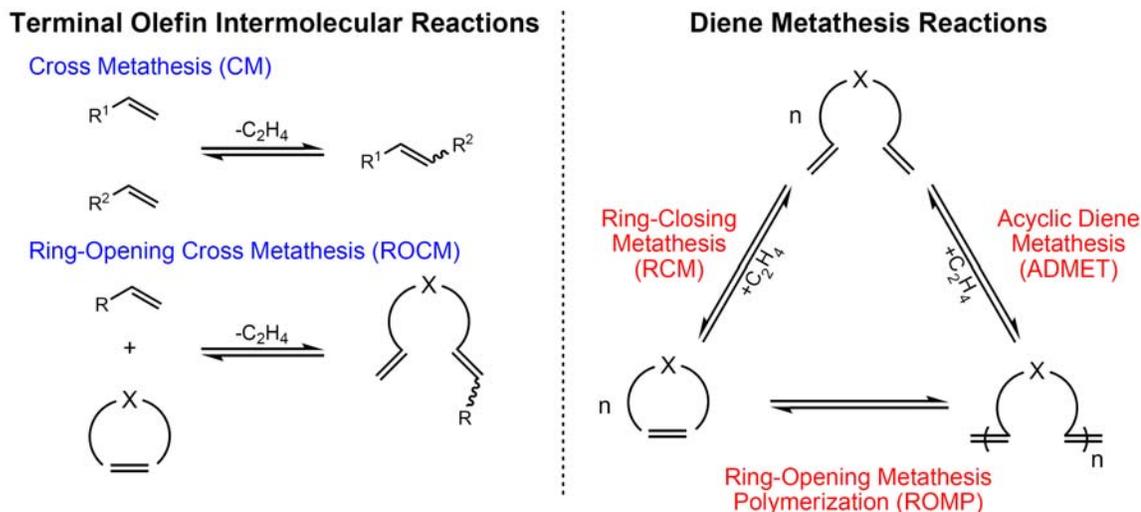
Figure 1.1. Types of olefin metathesis reactions commonly employed.

Overview and Future Outlook of Ruthenium Olefin Metathesis Complexes

Mechanism and Mechanistic Intermediates

The mechanism of olefin metathesis, as proposed by Chauvin and Herisson in 1971,[19] involves a metal alkylidene center that binds olefin, forms a metallacyclobutane, and subsequently undergoes cycloreversion to provide another metal alkylidene and an olefin product (Figure 1.2).

1.2: L = PCy_3
1.3: L = Mes–N⌣N–Mes
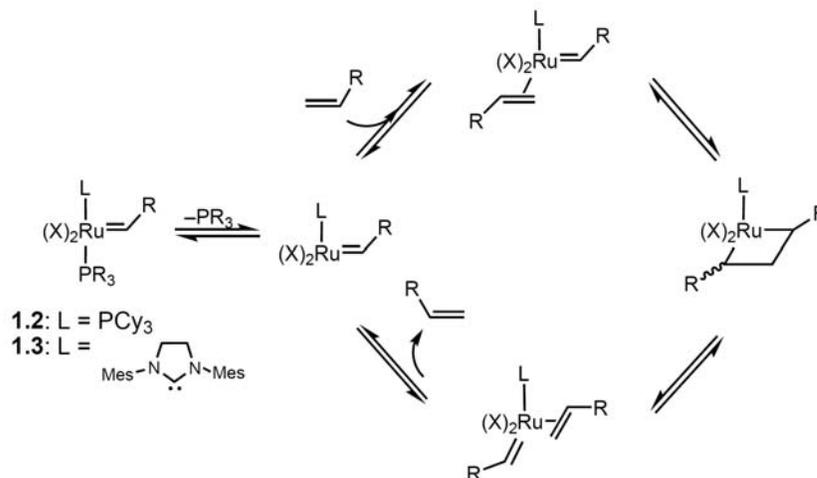
Figure 1.2. Degenerate olefin metathesis catalytic cycle.

It has been established through kinetic studies that for ruthenium initiators **1.2** and **1.3**, initiation is achieved through rate-determining phosphine dissociation.[20-22] Although catalyst **1.3** is more active for a variety of metathesis reactions than catalyst **1.2**, it initiates slower than catalyst **1.2**; however, **1.3** has a higher olefin affinity than **1.2** which results in an overall more efficient catalyst.[21-23] Initiation studies of catalyst **1.4**, which contains a chelating alkylidene group, demonstrated that the rate-limiting step is olefin binding.[24] Based on exchange studies, dissociation of the ether moiety is fast relative to olefin coordination, thus implying that initiation is not an associative process.

Although the general mechanism of olefin metathesis has been accepted for many years, few details concerning the geometry of the ruthenium-olefin and ruthenacyclobutane species have been reported. These species are difficult to observe due to their short-lived presence in most metathesis reactions. However, recent studies have provided new details concerning the geometry of ruthenium-olefin complexes[25-27] and ruthenacyclobutane complexes.[28-30] Experimental evidence thus far supports a side-bound model for NHC-ruthenium-olefin complexes and a C_2-symmetric ruthenacyclobutane complex. As these studies utilize model complexes to mimic typical reaction intermediates, the generality of these results has not been determined. Indeed, many questions remain, including: 1) Is it possible for a ruthenium-olefin complex to isomerize from side- to bottom-bound or vice versa (Scheme 1.1)? If so, does it occur on a time scale relevant to a typical metathesis turnover? 2) Can ruthenacyclobutane complexes interconvert prior to cycloreversion? If so, does it occur on a time scale relevant to a typical metathesis turnover? 3) Which step is lower: olefin binding or

ruthenacyclobutane formation?   4) Is olefin binding or ruthenacyclobutane formation

selectivity-determining?

Scheme 1.1.   Possible ruthenium-olefin and ruthenacyclobutane interconversion
processes
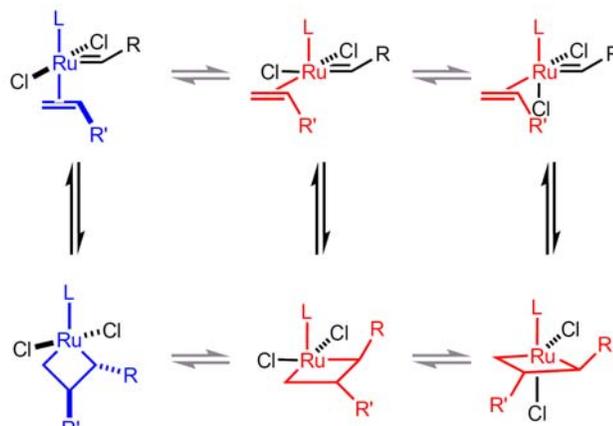
Ligand Effects

The development of more efficient olefin metathesis catalysts has been achieved

through the investigation of new ligand frameworks. Nearly all ruthenium metathesis

catalysts are based on the $X_2L_2Ru=CHR$ framework.   Nguyen and co-workers first

synthesized the first well-defined ruthenium olefin metathesis catalysts based on the

$Cl_2(PPh_3)_2Ru=CHR$ scaffold; these bis(phosphine) catalysts (e.g., **1.1**) are commonly

referred to as first-generation catalysts and showed reactivity for the polymerization of

highly strained monomers such as norbornene.[16,17] Schwab and co-workers subsequently

reported the use of PCy_3 in place of PPh_3 to generate complex **1.2**, which enabled the

next major advance toward more reactive and stable catalysts.[31]   Although these

ruthenium catalysts generally demonstrated lower activity than molybdenum catalysts,

they were less sensitive to oxygen and water impurities and could thus be easily handled

on the benchtop.

In 1999, Scholl and co-workers replaced one phosphine ligand with a saturated N-heterocyclic carbene ligand to provide complex **1.3**.[32] The use of a stronger σ-donating ligand enabled significant advances in substrate scope, such as bulk or electron-deficient olefins, and catalyst stability. In 2000, Hoveyda and co-workers reported the exchange of the remaining phosphine ligand of **1.3** for a chelating ether moiety to produce **1.4**, a more stable catalyst.[33] In addition to the H$_2$IMes ligand, several other types of carbenes have been examined as ligands for ruthenium complexes. These include unsymmetrically substituted NHCs,[34,35] 4-membered NHCs,[36] 6-membered NHCs,[37] chelating NHCs,[38-40] and non-diamino-based NHCs.[41]

Challenging Reactions

Although olefin metathesis catalysts have made impressive advances over the last several decades, several important areas of catalyst development remain (Figure 1.3). The design and development of ruthenium catalysts for enantioselective olefin metathesis processes has been an ongoing research target.[42-45] Utilizing a gearing-type interaction to create a chiral environment near the ruthenium center, Grubbs and co-workers have enabled successful application of these catalysts to asymmetric ring-opening cross and ring-closing metathesis reactions. Additionally, design of a chelating NHC featuring a BINOL-like moiety has also been employed by Hoveyda and co-workers for the development of asymmetric metathesis catalysts. However, a general asymmetric olefin metathesis catalyst has yet to be developed.

Other areas of significant interest include the development of catalysts with a broader substrate scope or with desired kinetic selectivity. Olefins containing both steric

hindrance and electron-withdrawing substituents, such as α-methylstyrene, are unreactive with current catalysts. Recently, the formation of tetrasubstituted olefins has been achieved through ring-closing metathesis,[46,47] however intermolecular reactions remain challenging. Ethenolysis[48] and E/Z-diastereoselective[49] olefin metathesis reactions both require kinetic selectivity, unlike the typically observed thermodynamic control; catalysts for these applications are highly desirable, yet relatively little progress has been achieved thus far. The development of more efficient catalysts for a variety of applications continues to be an important goal!
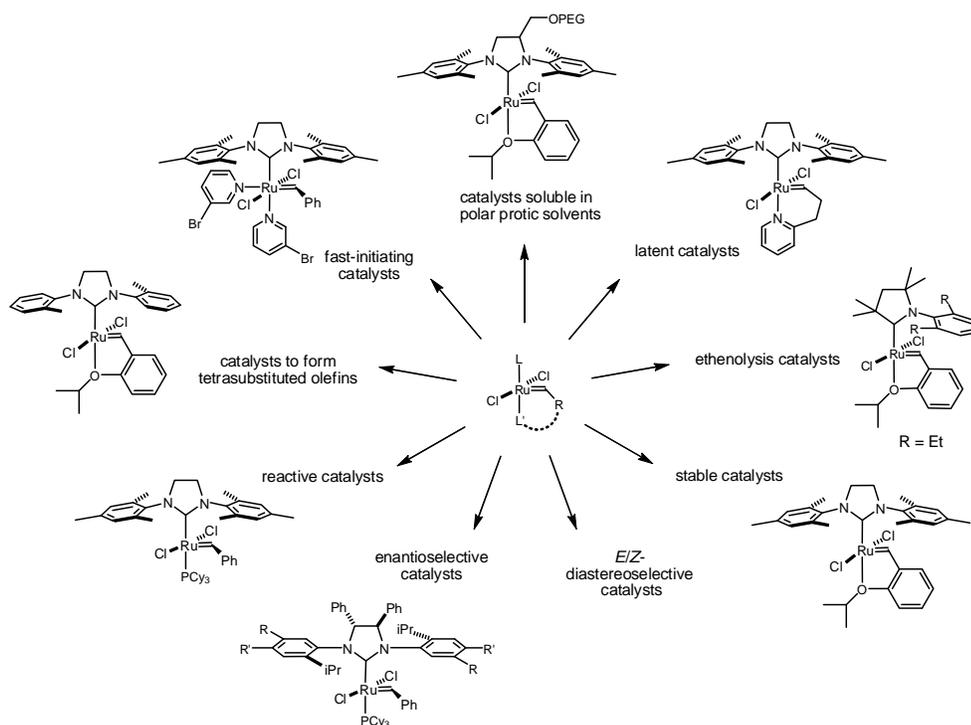

Figure 1.3. Evolution of metathesis catalysts for different applications.

References

(1)   Grubbs, R. H. *Handbook of Metathesis*; Wiley-VCH: Weinheim, 2003.

(2)   Ivin, K. J.; Mol, J. C. *Olefin Metathesis and Metathesis Polymerization*; Academic Press: San Diego, CA, 1997.

(3)   Grubbs, R. H. *Tetrahedron* **2004**, *60*, 7117.

(4)   Pederson, Richard L.; Fellows, Ingrid M.; Ung, Thay A.; Ishihara, H.; Hajela, Sharad P. *Advanced Synthesis & Catalysis* **2002**, *344*, 728.

(5)   Thayer, A. M. *Chem. Eng. News* **2007**, *85*, 37.

(6)   Grubbs, R. H. *Angew. Chem. Int. Ed.* **2006**, *45*, 3760.

(7)   Tebbe, F. N.; Parshall, G. W.; Ovenall, D. W. *J. Am. Chem. Soc.* **1979**, *101*, 5074.

(8)   Quignard, F.; Leconte, M.; Basset, J. M. *J. Mol. Catal.* **1986**, *36*, 13.

(9)   Wengrovius, J. H.; Schrock, R. R.; Churchill, M. R.; Missert, J. R.; Youngs, W. J. *J. Am. Chem. Soc.* **1980**, *102*, 4515.

(10)   Kress, J. R. M.; Russell, M. J. M.; Wesolek, M. G.; Osborn, B. P. *J. Chem. Soc., Chem. Commun.* **1980**, 431.

(11)   Schrock, R. R.; DePue, R. T.; Feldman, J.; Schaverien, C. J.; Dewan, J. C.; Liu, A. H. *J. Am. Chem. Soc.* **1988**, *110*, 1423.

(12)   Couturier, J.-L.; Paillet, C.; Leconte, M.; Basset, J.-M.; Weiss, K. *Angew. Chem., Int. Ed. Eng.* **1992**, *31*, 628.

(13)   Schrock, R. R.; Murdzek, J. S.; Bazan, G. C.; Robbins, J.; DiMare, M.; O'Regan, M. *J. Am. Chem. Soc.* **1990**, *112*, 3875.

(14)   Schrodi, Y.; Pedersen, R. L. *Aldrichimica Acta* **2007** *40*, 45.

(15)   Novak, B. M.; Grubbs, R. H. *J. Am. Chem. Soc.* **1988**, *110*, 960.

(16)   Nguyen, S. T.; Grubbs, R. H.; Ziller, J. W. *J. Am. Chem. Soc.* **1993**, *115*, 9858.

(17)   Nguyen, S. T.; Johnson, L. K.; Grubbs, R. H.; Ziller, J. W. *J. Am. Chem. Soc.* **1992**, *114*, 3974.

(18)   Toreki, R.; Vaughan, G. A.; Schrock, R. R.; Davis, W. M. *J. Am. Chem. Soc.* **1993**, *115*, 127.

(19)   Herisson, J. L.; Chauvin, Y. *Makromol. Chem.* **1971**, *141*, 161.

(20)   Dias, E. L.; Nguyen, S. T.; Grubbs, R. H. *J. Am. Chem. Soc.* **1997**, *119*, 3887.

(21)   Sanford, M. S.; Love, J. A.; Grubbs, R. H. *J. Am. Chem. Soc.* **2001**, *123*, 6543.

(22)   Sanford, M. S.; Ulman, M.; Grubbs, R. H. *J. Am. Chem. Soc.* **2001**, *123*, 749.

(23)   Love, J. A.; Sanford, M. S.; Day, M. W.; Grubbs, R. H. *J. Am. Chem. Soc.* **2003**, *125*, 10103.

(24)   Hejl, A. Ph.D. thesis, California Institute of Technology, 2007.

(25)   Tallarico, J. A.; Bonitatebus, P. J.; Snapper, M. L. *J. Am. Chem. Soc.* **1997**, *119*, 7157.

(26)   Trnka, T. M.; Day, M. W.; Grubbs, R. H. *Organometallics* **2001**, *20*, 3845.

(27)   Anderson, D. R.; Hickstein, D. D.; O'Leary, D. J.; Grubbs, R. H. *J. Am. Chem. Soc.* **2006**, *128*, 8386.

(28)   Romero, P. E.; Piers, W. E. *J. Am. Chem. Soc.* **2005**, *127*, 5032.

(29)   Romero, P. E.; Piers, W. E. *J. Am. Chem. Soc.* **2007**, *129*, 1698.

(30)   Wenzel, A. G.; Grubbs, R. H. *J. Am. Chem. Soc.* **2006**, *128*, 16048.

(31)   Schwab, P.; France, M. B.; Ziller, J. W.; Grubbs, R. H. *Angew. Chem. Int. Ed.* **1995**, *34*, 2039.

(32)   Scholl, M.; Ding, S.; Lee, C. W.; Grubbs, R. H. *Org. Lett.* **1999**, *1*, 953.

(33)   Kingsbury, J. S.; Harrity, J. P. A.; Bonitatebus, P. J., Jr.; Hoveyda, A. H. *J. Am. Chem. Soc.* **1999**, *121*, 791.

(34)   Vougioukalakis, G. C.; Grubbs, R. H. *Organometallics* **2007**, *26*, 2469.

(35)   Vehlow, K.; Maechling, S.; Blechert, S. *Organometallics* **2006**, *25*, 25.

(36)   Despagnet-Ayoub, E.; Grubbs, R. H. *Organometallics* **2005**, *24*, 338.

(37)   Yun, J.; Marinez, E. R.; Grubbs, R. H. *Organometallics* **2004**, *23*, 4172.

(38)   Van Veldhuizen, J. J.; Garber, S. B.; Kingsbury, J. S.; Hoveyda, A. H. *J. Am. Chem. Soc.* **2002**, *124*, 4954.

(39)   Funk, T. W. Ph.D. thesis, California Institute of Technology, 2006.

(40)   Bielawski, C. W.; Benitez, D.; Grubbs, R. H. *Science* **2002**, *297*, 2041.

(41)   Anderson, D. R.; Lavallo, V.; O'Leary, D. J.; Bertrand, G.; Grubbs, R. H. *Angew. Chem. Int. Ed.* **2007**, *119*, in press.

(42)   Seiders, T. J.; Ward, D. W.; Grubbs, R. H. *Org. Lett.* **2001**, *3*, 3225.

(43)   Funk, T. W.; Berlin, J. M.; Grubbs, R. H. *J. Am. Chem. Soc.* **2006**, *128*, 1840.

(44)   Berlin, J. M.; Goldberg, S. D.; Grubbs, R. H. *Angew. Chem. Int. Ed.* **2006**, *45*, 7591.

(45)   VanVeldhuizen, J. J.; Gillingham, D. G.; Garber, S. B.; Kataoka, O.; Hoveyda, A. H. *J. Am. Chem. Soc.* **2003**, *125*, 12502.

(46)   Berlin, J. M.; Campbell, K.; Ritter, T.; Funk, T. W.; Chlenov, A.; Grubbs, R. H. *Org. Lett.* **2007**, *9*, 1339.

(47)   Stewart, I. C.; Ung, T.; Pletnev, A. A.; Berlin, J. M.; Grubbs, R. H.; Schrodi, Y. *Org. Lett.* **2007**, *9*, 1589.

(48)   Burdett, K. A.; Harris, L. D.; Margl, P.; Maughon, B. R.; Mokhtar-Zadeh, T.; Saucier, P. C.; Wasserman, E. P. *Organometallics* **2004**, *23*, 2027.

(49)   Deshmukh, P. H.; Blechert, S. *Dalton Trans.* **2007**, 2479.

CHAPTER **2**

Synthesis, Activity and Kinetic Selectivity of
Ruthenium Olefin Metathesis Catalysts Bearing Cyclic (Alkyl)(Amino)Carbenes

This chapter was taken in part from:

Anderson, D. R.; Lavallo, V.; O'Leary, D. J.; Bertrand, G.; Grubbs, R. H. *Angew. Chem. Int. Ed.* **2007**, in press.

Anderson, D. R.; Ung, T.; Mkrtumyan, G.; Bertrand, G.; Schrodi, Y.; Grubbs, R. H. *Organometallics* **2007**, submitted.

Introduction

The evolution of olefin metathesis into a reaction routinely used to form new carbon-carbon double bonds has been enabled by the development of well-defined transition-metal catalysts.[1,2] Many metathesis catalysts based on the $L_2X_2Ru=CHR$ scaffold have been synthesized in an effort to increase catalyst stability, activity and substrate scope.[3-10] A significant gain in these areas was achieved after exchanging a single PCy_3 ligand of **2.1** with H_2IMes (H_2IMes = 1,3-dimesityl-4,5-dihydroimidazol-2-ylidene), an N-heterocyclic carbene (NHC), to produce catalyst **2.2** (Chart 2.1).[5] These results are attributed to the increased σ-donor ability of H_2IMes over PCy_3, which increases the affinity for π-acidic olefins relative to σ-donating phosphines.[11] Additionally, exchange of the remaining PCy_3 ligand with a chelating ether moiety provides a more stable complex, catalyst **2.3**.[6]

Chart 2.1. Commonly utilized ruthenium olefin metathesis catalysts

2.1   2.2   2.3
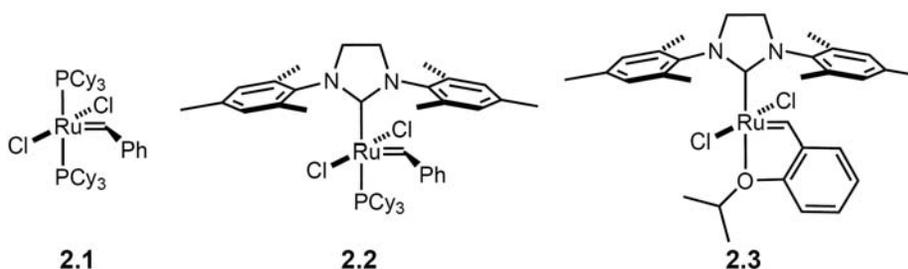
Although complexes **2.1–3** are efficient catalysts for many polymerizations and ring-closing, ring-opening and cross metathesis reactions, several olefin metathesis processes remain challenging.[12] In particular, the development of catalysts that favor the formation of kinetically controlled rather than thermodynamically controlled products is an area of significant interest. Indeed, highly active and stable NHC-containing catalysts

such as **2.2** and **2.3** generally produce mixtures of the most stable products containing more trans olefins than cis olefins, or internal olefins than terminal olefins (ethenolysis).[13,14]

An *E/Z*-diastereoselective olefin metathesis catalyst would enable the efficient synthesis of *E*- or *Z*-olefins, an attractive goal of synthetic chemistry.[1] However, the *E/Z* diastereoselectivity of an olefin metathesis reaction is often controlled by the thermodynamic stability of the olefin isomers rather than the selectivity of the catalyst. The product *E/Z* ratio of the homodimerization of a terminal olefin is a result of primary and secondary metathesis processes (Figure 2.1). Primary metathesis is composed of two reactions: the reaction of a ruthenium methylidene species with terminal olefin to produce a ruthenium alkylidene species, which subsequently reacts with terminal olefin to generate *E*- or *Z*-olefins. The selectivity of the primary metathesis reactions depends on the geometry of the olefin approach and coordination to the ruthenium-alkylidene complex.[15,16]
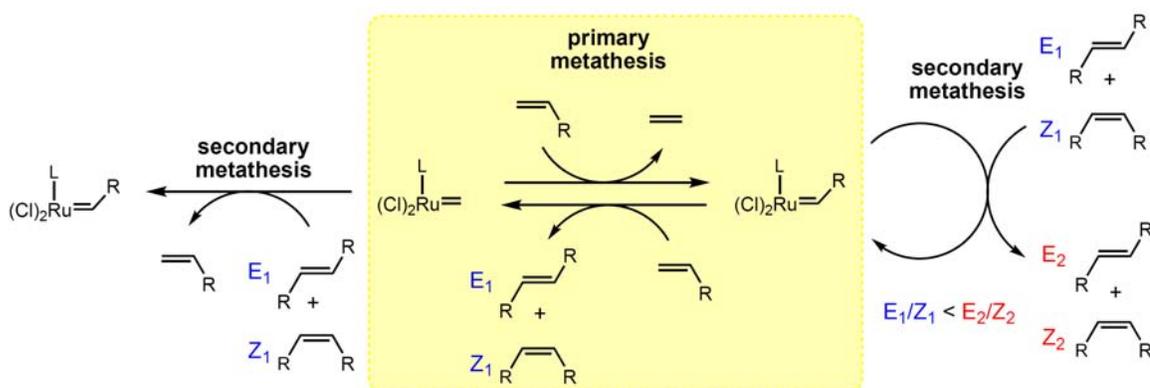

Figure 2.1. Primary and secondary metathesis processes affecting *E/Z*-diastereoselectivity in olefin metathesis.

Secondary metathesis processes involve reactions of the product *E-* and *Z*-olefins with ruthenium alkylidene and methylidene species (Figure 2.1). In general, secondary metathesis results in the interconversion of the isomers, supplying an increased yield of the more thermodynamically stable isomer.[17,18] In addition to the different *E/Z* diastereoselectivities of these reactions, the relative rates of each reaction may also be different because *Z*-olefins are generally more reactive than *E*-olefins.[19]

As a result of these competing processes, the *E/Z* product ratio at lower conversions is more reflective of the selectivity of primary metathesis processes, whereas at higher conversions an increase in the *E/Z* ratio is typically observed due to secondary metathesis of the *Z*-olefin to the more thermodynamically favorable *E*-olefin.[20]

Another targeted kinetic process is ethenolysis, the cross metathesis of ethylene with an internal olefin to provide terminal olefins without significant production of internal olefins. Typically, the observed product distribution reflects the increased stability of internal olefins relative to terminal olefins.[13]

The ethenolysis catalytic cycle involves two primary metathesis reactions: the reaction of a ruthenium methylidene species with an internal olefin to produce a terminal olefin and ruthenium alkylidene species, which then reacts with ethylene to regenerate the ruthenium methylidene species and yields a second terminal olefin (Figure 2.2).
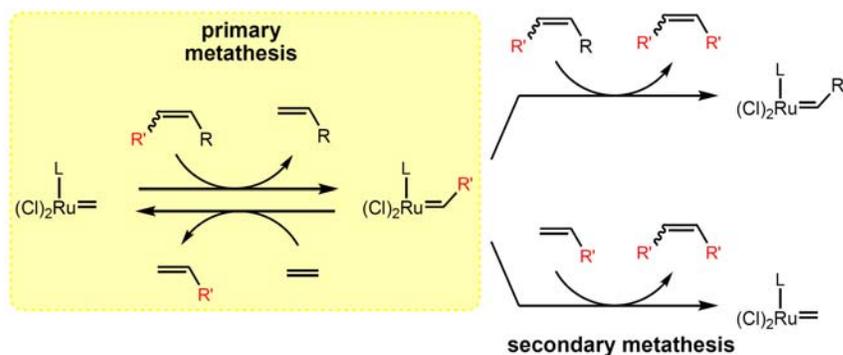
Figure 2.2. Primary, secondary and self metathesis processes during ethenolysis reactions.

Self metathesis and secondary metathesis processes compete with primary metathesis reactions and produce undesired internal olefins (Figure 2.2).[13] Self metathesis of the substrate occurs when a ruthenium alkylidene species binds an internal olefin (instead of ethylene), resulting in the formation of a new internal olefin. Secondary metathesis occurs when a ruthenium alkylidene species reacts with a terminal olefin (rather than ethylene) to generate an internal olefin. As with *E*/*Z*-diastereoselective olefin metathesis, secondary metathesis results in the conversion of kinetic products into more thermodynamically stable products. Although numerous catalysts have been examined for *E*/*Z*-diastereoselective olefin metathesis and ethenolysis, no clear trend for ligand development has emerged.

Recently, the synthesis of cyclic (alkyl)(amino)carbenes (CAACs) in which one amino group from an NHC has been replaced by an alkyl group was reported.[21] The greater σ-donor ability of carbon versus nitrogen results in more electron-donating ligands, as indicated by the ν_{CO} of *cis*-Rh(Cl)(CO)$_2$L complexes (L = H$_2$IMes, ν_{CO} =1996, 2081 cm^{-1}; L = **2.5b**, ν_{CO} = 1994, 2077 cm^{-1}).[22] The exchange of an sp^2-hybridized nitrogen atom for an sp^3-hybridized carbon atom also changes the steric environment

relative to NHCs. Although most NHCs are C_{2v} symmetric, the CAACs reported to date

are C_s or C_1 symmetric, which may have implications for the microscopic reversibility of

the olefin binding and cycloreversion steps in the metathesis catalytic cycle.[15,23] The

unique properties of CAACs led us to explore the utility of this new class of stable

carbenes in olefin metathesis.

Results and Discussion

Synthesis and Activity

We first chose to investigate carbenes **2.5a,b** which can be prepared from their

respective salts **2.4a,b** (Scheme 2.1). [21,24] These ligands each contain an *N*-DIPP (DIPP =

2,6-diisopropylphenyl) group and vary the steric bulk at the quaternary carbon adjacent to

the carbene center with either two Me groups (**2.5a**) or a spiro-fused cyclohexyl group

(**2.5b**). Upon addition of potassium hexamethyldisilazide (KHMDS) to salts **2.4a,b** at 22

°C in benzene, the corresponding carbenes **2.5a,b** are observed in good conversion as

measured by ^{1}H NMR spectroscopy.

Scheme 2.1. Synthesis of carbenes **2.5a,b**
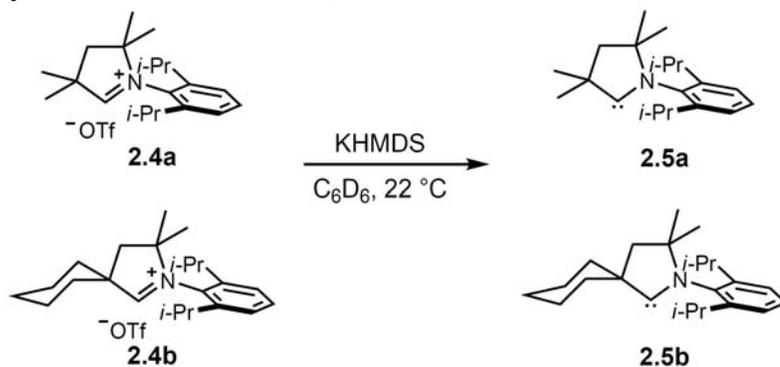
Ruthenium olefin metathesis catalysts bearing a pyridine ligand typically undergo facile ligand exchange with stronger donors such as phosphines or NHCs.[25] Thus, upon addition of pyridine complex **2.6**[26] to an NHC, the resulting ruthenium complex is typically coordinated by a carbene ligand and a phosphine ligand (e.g., **2.2**), rather than a pyridine ligand. However, upon treatment of pyridine complex **2.6** with carbenes **2.5a,b** (generated in situ), no evidence for the expected phosphine complexes was observed by ^{1}H or ^{31}P NMR spectroscopy (eq 2.1). Instead, air-sensitive pyridine adducts **2.7a,b** were isolated in modest yields.
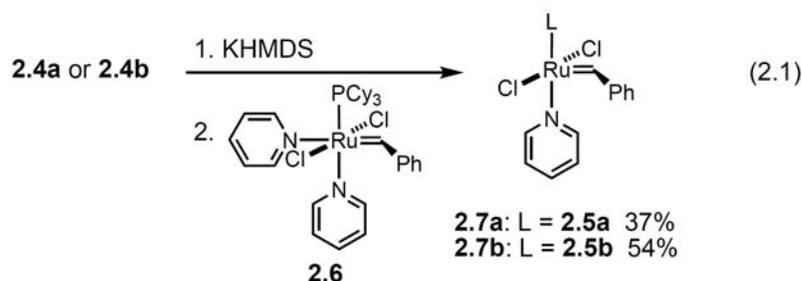
Interestingly, even upon addition of 5 equiv PPh$_3$ to **7a**, no evidence for the exchange of pyridine with phosphine was observed by ^{1}H or ^{31}P NMR spectroscopy after 3 d at 60 °C. This could be a result of either steric congestion around the ruthenium center or the increased donating ability of the coordinated cyclic(alkyl)(amino) carbene relative to NHC ligands.

X-ray crystallographic analysis of compounds **2.7a,b** was conducted. These complexes exhibit a distorted square pyramidal geometry with the benzylidene ligand in the apical position (Figure 2.3). The bond lengths and angles of the pyridine catalysts **2.7a,b** are similar to those of (H$_2$IMes)(py)$_2$(Cl)$_2$Ru=CHPh (**2.8**) (see experimental section).[25] The Ru–C$_{carbene}$ bond distance is ~ 0.05 Å shorter than in **2.8** which is

consistent with increased σ-donating ability of CAACs relative to H₂IMes. In addition, the Ru-C$_{benzylidene}$ bond length is ~ 0.03 Å shorter in **2.7a,b** compared to **2.8**, possibly a result of the trans influence of the additional pyridine ligand in **2.8**.
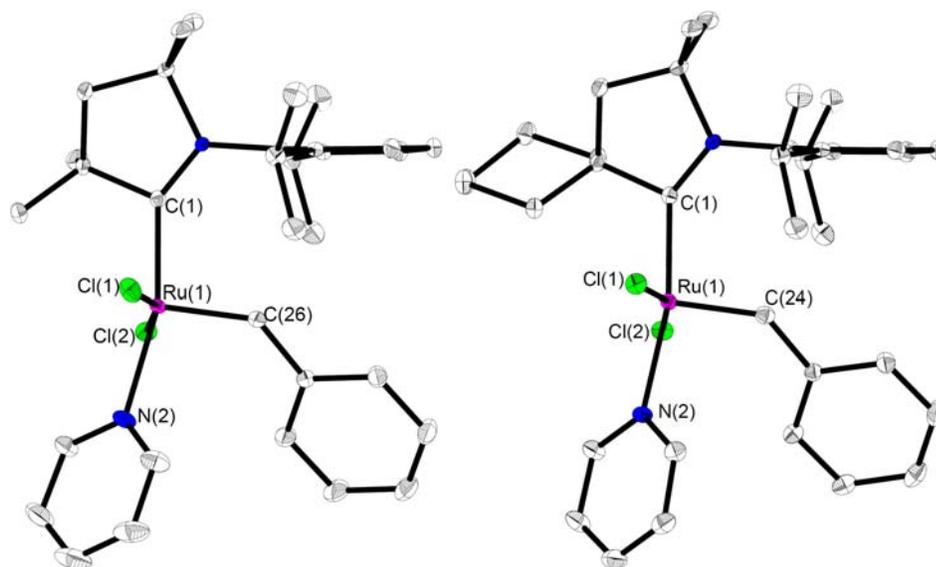

Figure 2.3. Structural drawings of **2.7a,b**. Thermal ellipsoids drawn at 50% probability and hydrogens omitted for clarity.

The efficiency of catalysts **2.7a,b** was examined in the ring-closing metathesis of diethyl diallylmalonate (**2.9**) (eq 2.2). Maximum conversions to cyclopentene **2.10** observed by ¹H NMR spectroscopy were less than 50% after 24 h at 22 °C or 60 °C, which is attributed to catalyst decomposition. These results are consistent with previously studied pyridine-containing catalysts.[20] For comparison, complexes **2.2** and **2.3** can achieve 95% conversion to **2.10** in 30 and 20 min respectively at 30 °C and 1 mol% catalyst loading.[20]

(2.2)
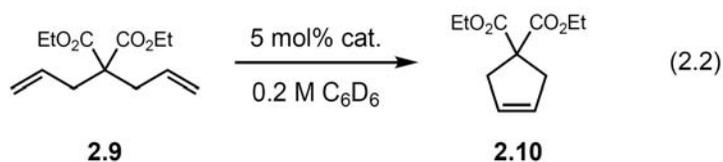
To examine the possibility of stabilizing the pyridine complexes, a catalyst containing a chelating alkylidene was synthesized. Although initial synthetic attempts were made utilizing **2.7a** and 2-butenylpyridine, a more facile in situ route was devised in which salt **2.4a**, KHMDS, ruthenium precursor **2.6** and 2-butenylpyridine were stirred together in benzene at 50 °C (eq 2.3). Ruthenium complex **2.11** was isolated in 26–28% yield. X-ray crystallographic analysis of **2.11** showed a shortening of the Ru–C$_{carbene}$ bond length by ~ 0.05 Å and lengthening of the Ru–N bond by ~ 0.08 Å; all other bond lengths and angles are similar to its H$_2$IMes analog (Figure 2.4).[27] However, catalyst **2.11** was inactive for the ring-closing metathesis of **2.9** at 22 °C.


(2.3)
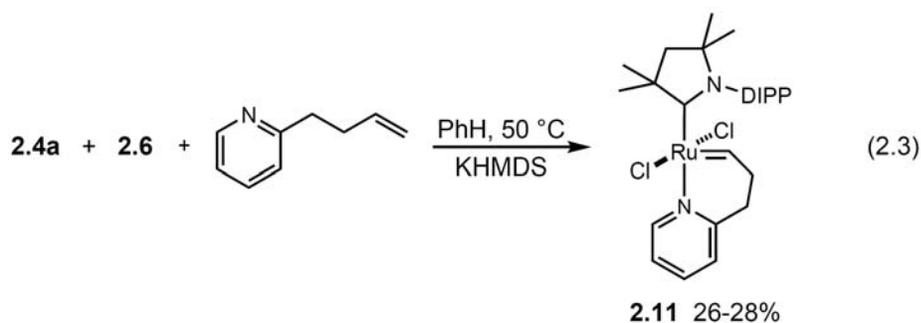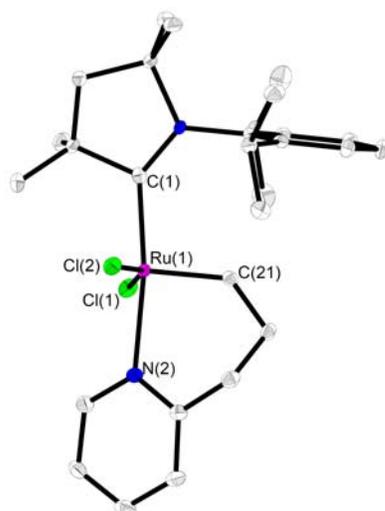
Figure 2.4. Structural drawing of **2.11**. Thermal ellipsoids drawn at 50% probability and hydrogens omitted for clarity.

Additionally, bis(tricyclopentyl)phosphine complex **2.12** was examined as a ruthenium source to form complex **2.13**. It was hypothesized that if steric effects were responsible for the formation of pyridine complexes **2.7a**,**b** (rather than the analogous phosphine complexes), then the slightly smaller cone angle of PCp_3 relative to PCy_3 and the smaller alkylidene moiety might enable the isolation of complex **2.13**. Upon addition of carbene **2.5a** (prepared in situ) to **2.12**, a new alkylidene resonance in the ^{1}H NMR spectrum was observed at 20.1 ppm (d) (eq 2.4). However, the new ruthenium complex was not **2.13**, but rather **2.14** in which the carbene has inserted into the C-H bond of the vinyl alkylidene moiety as verified by X-ray crystallographic analysis (Figure 2.5). Although relatively uncommon, C-H insertion reactions of carbenes have been previously reported.[28-32]

$$2.4a \xrightarrow[\text{2.}]{\text{1. KHMDS}} \qquad \textbf{2.13} \; 0\% \qquad \textbf{2.14} \; 39\% \qquad (2.4)$$

2.12
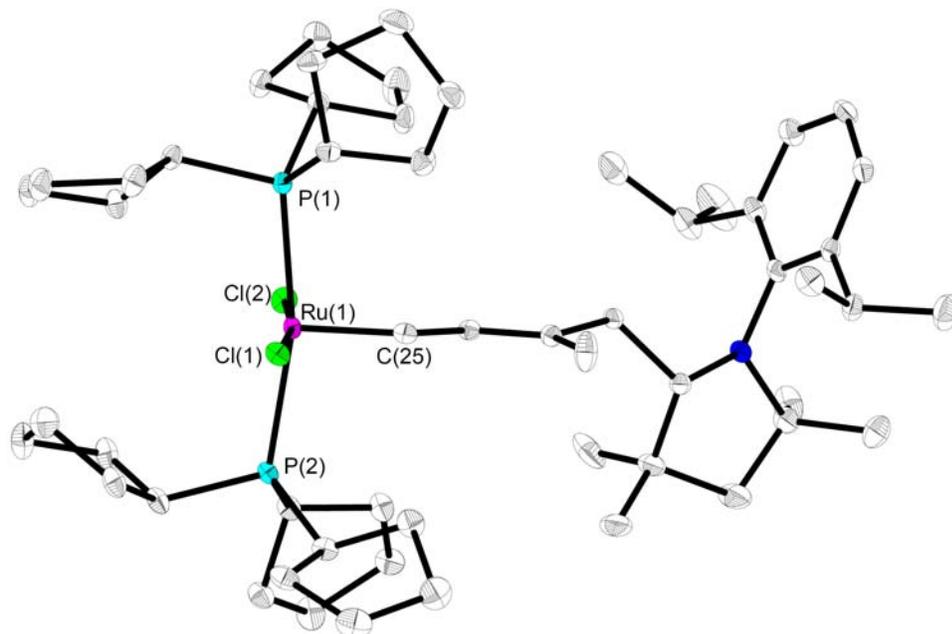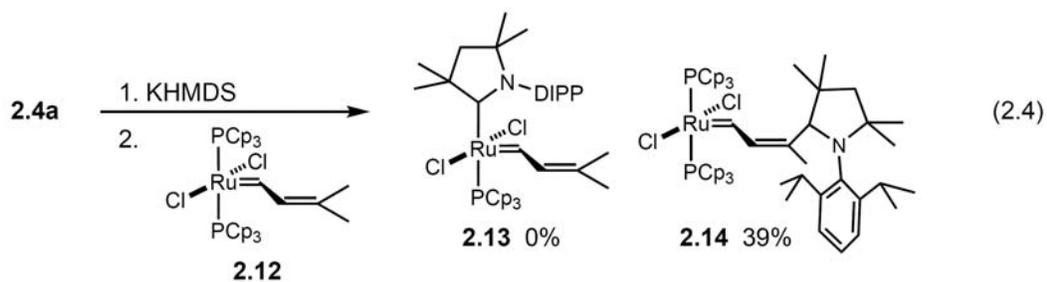
Figure 2.5. Structural drawing of **2.14**. Thermal ellipsoids drawn at 50% probability and hydrogens omitted for clarity.

To obtain stable, active complexes, we next targeted complexes **2.16a,b**. Upon addition of **2.5a,b** (prepared in situ) to ruthenium precursor **2.15**,[8] catalysts **2.16a,b** were isolated and purified in good yields by column chromatography (eq 2.5). Chelating ether complexes **2.16a,b** are air- and moisture-stable compounds.
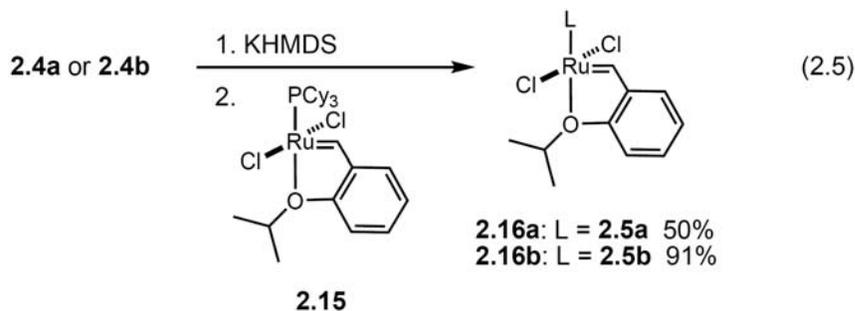
Similar to complexes **2.7a,b**, the solid-state structures of **2.16a,b** show a distorted square pyramidal structure with the benzylidene moiety at the apical position (Figure 2.6). Comparing complexes **2.16a,b** with the H_2IMes-containing analog **2.3**, the Ru–$C_{carbene}$ bond distances are ~ 0.04–0.05 Å shorter and the Ru–O bond distances are 0.04–0.09 Å longer than in complex **2.3** (see experimental section).[6] These observations are consistent with the increased σ-donating properties of ligands **2.5a,b** over their NHC counterparts.
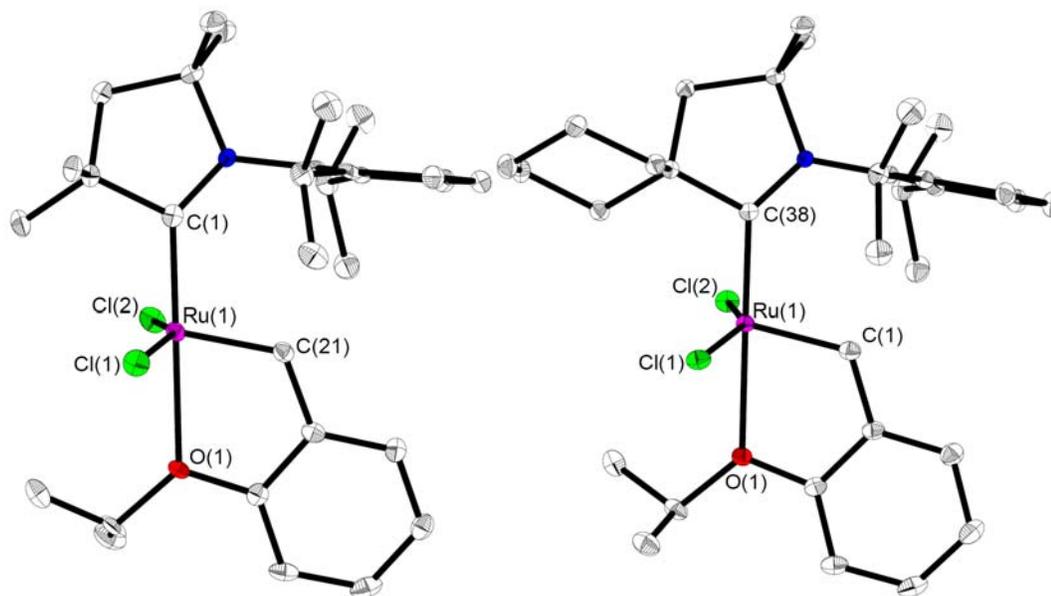

Figure 2.6. Structural drawings of **2.16a,b**. Thermal ellipsoids drawn at 50% probability and hydrogens omitted for clarity.

In all solid-state structures obtained, the CAAC exhibits the same orientation relative to the benzylidene group (Figure 2.7). The *N*-aryl ring is located above the benzylidene moiety while the quaternary carbon adjacent to the carbene center is positioned over an empty coordination site. In the case of pyridine complexes **2.7a,b**, this observed preference may be due to π-π stacking between the *N*-aryl ring and the benzylidene ring. For chelating ether complexes **2.16a,b** this structural preference may be a result of negative steric interactions between the Me groups on the quaternary carbon adjacent to the carbene carbon and the benzylidene proton (Figure 2.7). From this side-view, it is apparent that the benzylidene proton would be in close contact with one Me group on the quaternary carbon center if the ligand were rotated 180° relative to the remainder of the molecule.
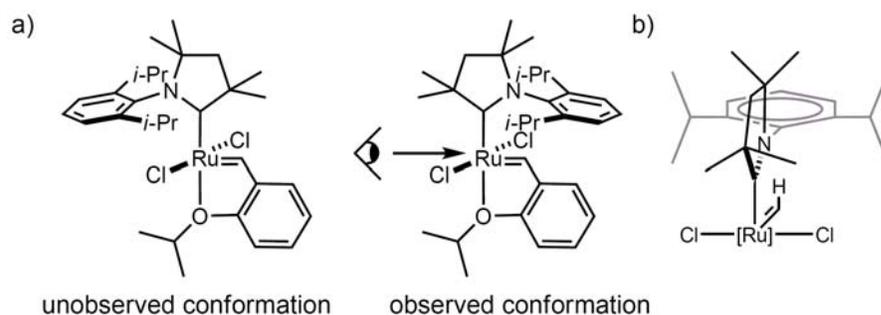

Figure 2.7. a) Unobserved and observed conformations of catalyst **2.16a**. b) View of the observed conformation of complex **2.16a** looking down the Ru=CHR bond.

^{1}H NMR spectroscopic data suggest that the solid-state conformation of **12a,b** is maintained in solution. 2D-ROESY experiments performed on complexes **2.16a,b** in C_6D_6 at 22 °C demonstrate Overhauser effects between the benzylidene resonance and the aryl protons on the *N*-DIPP moiety, the equivalent methine resonances of the aryl isopropyl groups, and the enantiotopic Me groups facing the benzylidene proton (Figure

2.7b). Overhauser effects are not observed between the benzylidene proton and the gem-dimethyl(ene) groups adjacent to the carbene center. This interaction might be expected if there is fast exchange between two orientations of the carbene ligand relative to the ruthenium benzylidene.

The efficiency of catalysts **2.16a,b** was examined in the ring-closing metathesis of **2.9**, **2.17a**, and **2.17b** (eq 2.6). At 1 mol% catalyst loading, chelating ether catalysts **2.16a,b** achieved 97% and 95% conversion of diethyl diallylmalonate (**2.9**) after heating at 60 °C for 3.3 h and 10 h, respectively. Uninitiated catalyst is observed for both catalysts even at high conversions, indicating that only a fraction of added catalyst is engaged in the reaction. Catalyst **2.16a** converts **2.17a** to 95% of tri-substituted olefin **2.18a** in 20 h at 60 °C, whereas catalyst **2.16b** achieves 96% conversion after 48 h at 60 °C. However, catalysts **2.16a,b** showed no reactivity in the conversion of **2.17b** to tetra-substituted olefin **2.18b**.

1 mol% cat.

0.1 M C_6D_6

(2.6)

2.17a: R' = H
2.17b: R' = Me

R = CO_2Et

2.18a: R' = H
2.18b: R' = Me
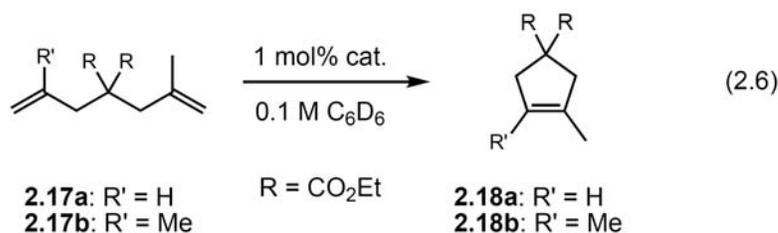
One application in which low catalyst activity at room temperature is desirable is in the development of latent catalysts which do not initiate at room temperature, but are highly active at elevated temperatures.[27,33] Latent catalysts are particularly useful for industrial applications such as injection molding processes. Ruthenium olefin metathesis catalysts are typically evaluated for latent activity through the polymerization of dicyclopentadiene (DCPD) at low catalyst loadings (eq 2.7). Evaluation of complexes

2.16a,**b** in the ROMP of dicyclopentadiene demonstrate slow initiation (long string time) even as the polymerization proceeds to generate heat (Figure 2.8). Ideally, a DCPD exotherm should look like a step function with a sharp transition.[27,33]


$$(2.7)$$
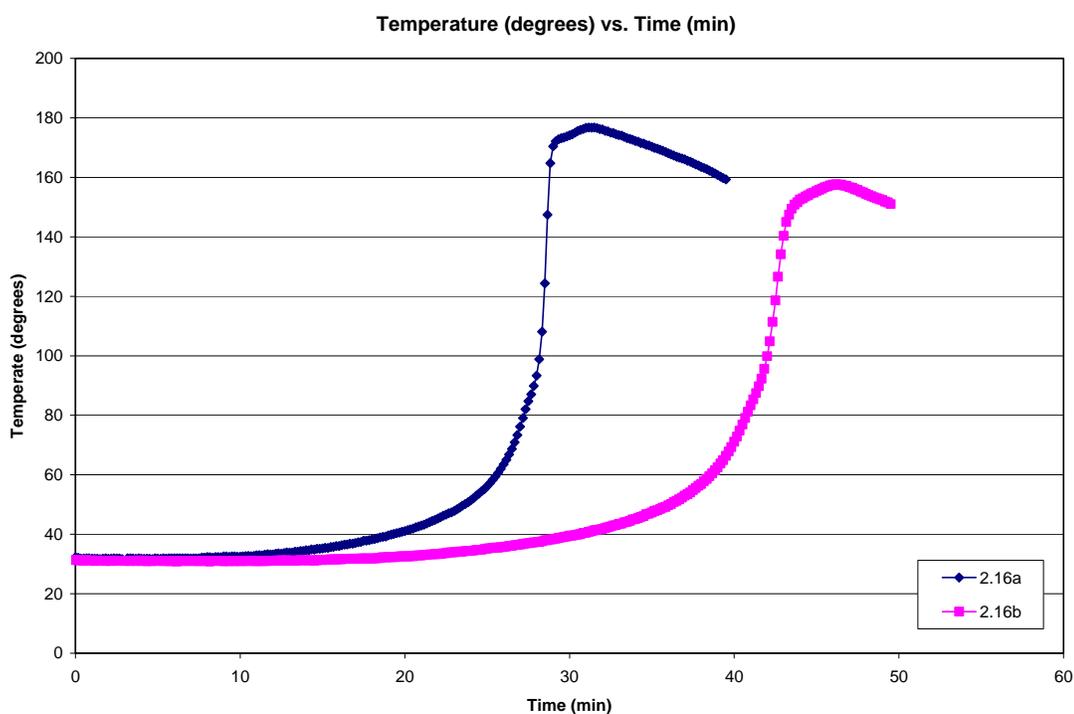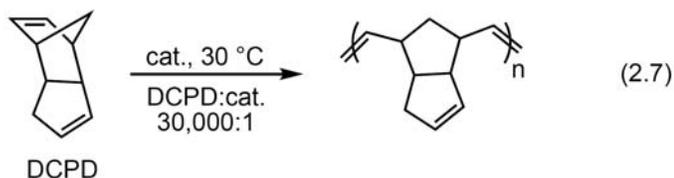
Figure 2.8. Exotherm plot for ROMP of DCPD with **2.16a** (blue diamonds) and **2.16b** (purple squares) (30,000:1 M/C, 30 °C).

We hypothesized that negative steric interactions could be responsible for the lower activity of catalysts **2.16a,b** relative to **2.2** and **2.3**. CAACs without the quaternary carbon center adjacent to the carbene carbon are not synthetically accessible; thus, decreasing the steric bulk of the *N*-aryl ring was targeted. Both the *N*-mesityl (**2.19**) and

N-DEP (DEP = 2,6-diethylphenyl) (**2.20**) substituted salts were synthesized; deprotonation of **2.19** and **2.20** under a variety of conditions did not afford the desired free carbenes (eq 2.8). In situ deprotonations of **2.19** and **2.20** with KHMDS at −78 °C in THF in the presence of ruthenium precursor **2.19** were also attempted. Although **2.21** was not observed by NMR spectroscopy, complex **2.22** could be observed and isolated. Similar to **2.16a,b**, complex **2.22** is an air- and moisture-stable solid. X-ray diffraction studies of catalyst **2.22** show similar bond lengths and angles to **2.16a,b** (Figure 2.9).

(2.8)

2.19: Ar = mesityl
2.20: Ar = 2,6-diethylphenyl

2.21: Ar = mesityl 0%
**2.22**: Ar = 2,6-diethylphenyl 18%
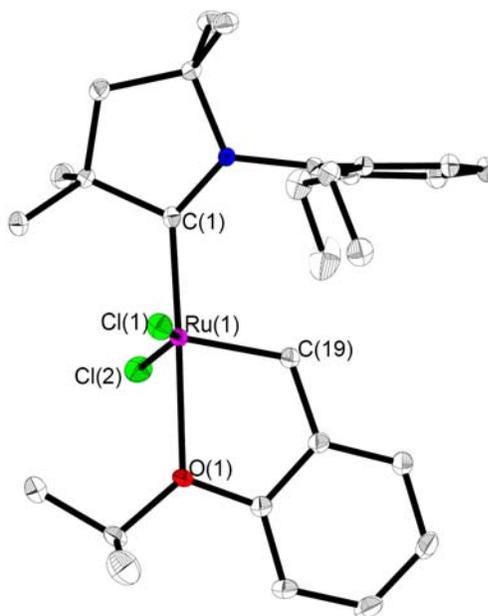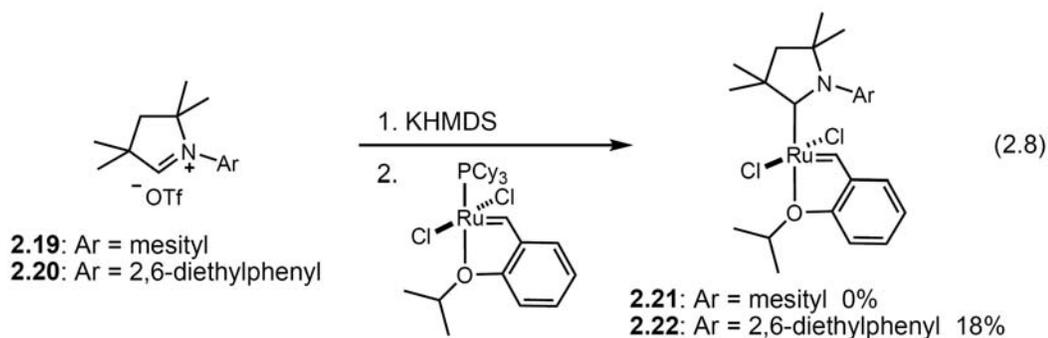
Figure 2.9. Structural drawing of **2.22**. Thermal ellipsoids drawn at 50% probability and hydrogens omitted for clarity.

Catalyst **2.22**, which differs from **2.16a** only by replacing *N*-DIPP with *N*-DEP, demonstrates significantly increased activity in the formation of di- and tri-substituted olefins.   In the presence of 1 mol% **2.22**, 95% conversion of **2.9** to substituted cyclopentene **2.10** is observed in 15 min at 30 °C, as compared to 3 h at 60 °C required for catalyst **12a** (Table 2.1).   Catalyst **2.22** achieves 95% conversion of **2.17a** to tri-substituted cyclopentene **2.18a** at 30 °C in 1 h, which is comparable to catalysts **2.2** and **2.3**.   However, catalyst **2.22** showed no reactivity in the conversion of **2.17b** to **2.18b**.

Table 2.1. Activity comparison of catalysts **2.16a**, **2.16b**, **2.22**, **2.2**, and **2.3**.

catalyst	% conversion to **2.9→2.10**	% conversion **2.17b→2.18b**
2.16a	97% (3.3 h at 60 °C)	95% (20 h at 60 °C)
2.16b	95% (10 h at 60 °C)	96% (48 h at 60 °C)
2.22	95% (15 min at 30 °C)	95% (1 h at 30 °C)
2.2	95% (30 min at 30 °C)	95% (45 min at 30 °C)
2.3	95% (20 min at 30 °C)	95% (45 min at 30 °C)

Upon addition of 30 equiv ethyl vinyl ether to complex **2.22** in C_6D_6, two new benzylidene resonances at 14.09 ppm (m) and 13.97 ppm (m) are observed in a 1:5 ratio via ^{1}H NMR spectroscopy (eq 2.9). Addition of pentane to the resulting solution enabled the isolation of yellow-orange crystals. X-ray crystallographic analysis demonstrated the formation of a dimeric, ruthenium Fisher carbene complex **2.23** (Figure 2.10). Previous studies by Grubbs and Hejl also reported the observation of two new species during initiation experiments with chelating ether ruthenium complexes and butyl vinyl ether;[34] however, in those studies, the reaction products were unable to be successfully isolated. The formation of complex **2.23** in the presence of excess ethyl vinyl ether, a reactive

cross partner and potential ligand, may be a result of the stability of dinuclear ruthenium

complexes with bridging chlorides.

(2.9)

2.23
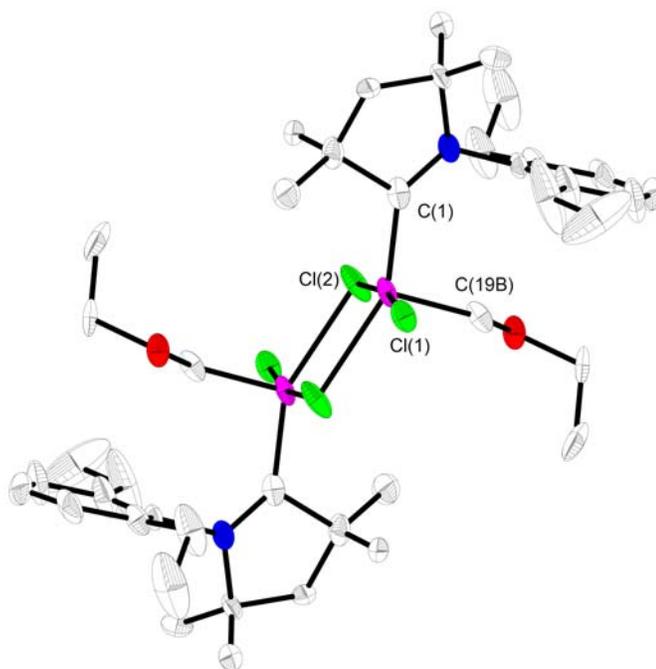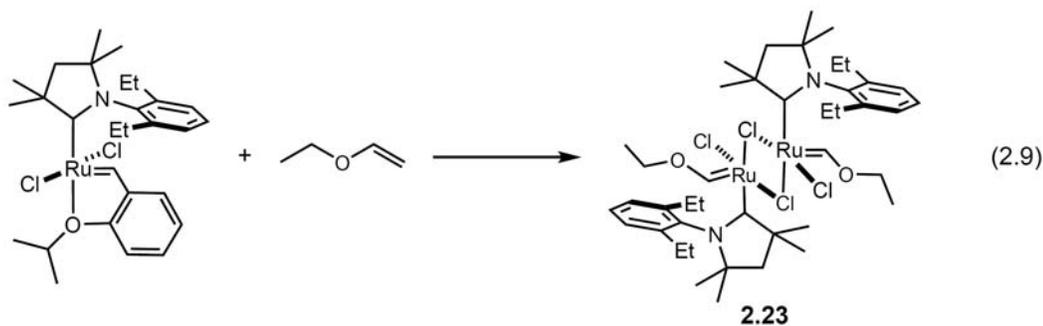
Figure 2.10. Structural drawing of **2.23**. Thermal ellipsoids drawn at 50% probability and hydrogens omitted for clarity. Selected bond distances (Å): Ru(1)–C(1) = 1.822(10), Ru(1)–C(19B) = 1.857(18), Ru(1)–Cl(1) = 2.3743(8), Ru(1)–Cl(2) = 2.4819(8).

The dramatic increase in activity observed after slightly decreasing the steric bulk

of the *N*-aryl group is attributed to catalyst initiation. We postulate that catalyst initiation

requires dissociation of the ether moiety and rotation of the benzylidene ring into a plane

parallel to the *N*-aryl group to open a coordination site for incoming olefin.[35] For

complexes **2.16a,b** this process may be sterically unfavorable, thus resulting in poor

initiation (Figure 2.11).   The steric bulk of the ortho-aryl substituents may have a

significant effect on initiation for two reasons.   First, the Ru–C$_{carbene}$ bond length is

slightly shorter than in NHC analogs, thus bringing the aryl ring in closer proximity to the

ruthenium center.   Second, the quaternary carbon adjacent to the *N*-aryl group restricts

rotation around the *N*-aryl bond and the C$_{aryl}$-C$_{i Pr}$ bond, as indicated by NMR

spectroscopy experiments discussed earlier.
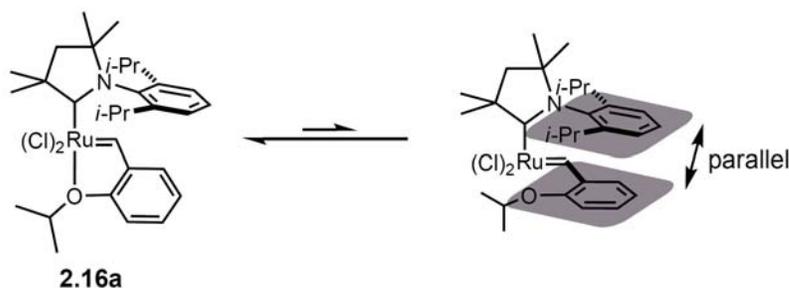
Figure 2.11. Proposed rotation required for catalyst initiation.

Interestingly, substitution of the *N*-mesityl groups in complex **2.3** with *N*-DIPP

groups[36] results in a catalyst with increased activity for the ring-closing metathesis of **2.9**

(97% conversion in 13 min vs. 20 min).[35] However, this bulkier catalyst differs from the

CAAC complexes due to the absence of substitution at the carbon adjacent to the nitrogen

atom.

Kinetic Selectivity: *E/Z* diastereoselectivity

Recently, our group reported the evaluation of catalyst *E/Z* selectivity by

examining the cross metathesis of 2 equiv of *cis*-1,4-diacetoxy-2-butene (**2.24**) with

allylbenzene (**2.25**) in the presence of 2.5 mol% catalyst in CH_2Cl_2 at 25 °C to produce

(*E*)- or (*Z*)-4-phenylbut-2-enyl acetate (**2.26** and **2.27**, respectively) (eq 2.10).[20] To

compensate for the slow or fast reaction rates observed, catalysts were compared via plots

of *E*/*Z* ratio vs. conversion rather than *E*/*Z* ratio vs. time. Both bis(phosphine) and NHC-

containing ruthenium catalysts show similar *E*/*Z* ratios (~ 3−4) at conversions below 60%

(Figure 2.12). At higher conversions, NHC-containing catalysts provide a mixture of

products containing a higher *E*/*Z* ratio of ~ 6−10 due to secondary metathesis of **2.27** to

2.26.
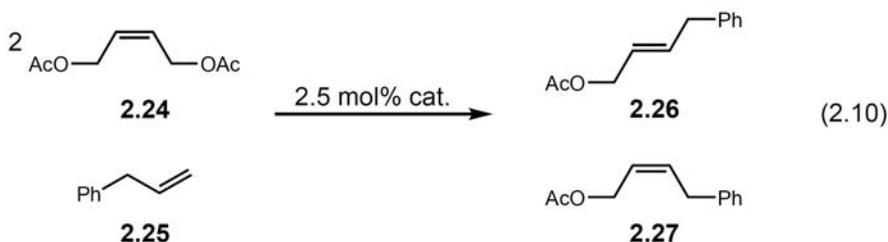
As shown in Figure 2.12, catalysts **2.16a,b** and **2.22** exhibit enhanced *E*/*Z*

diastereoselectivity for the formation of *Z*-olefins over catalysts **2.1−3**. Below 60%

conversion to the heterocoupled products **2.26** and **2.27**, catalysts **2.16a,b** and **2.22**

demonstrate *E*/*Z* ratios of 1.5−2.5. At 70% conversion, catalysts **2.16a,b** and **2.22**

provide *E*/*Z* ratios of ~ 3 compared to catalyst **2.2** which provides a ratio of ~ 6. Similar

E/*Z* ratios were observed by Blechert and co-workers utilizing a ruthenium complex

bearing an unsymmetrically substituted NHC.[37]
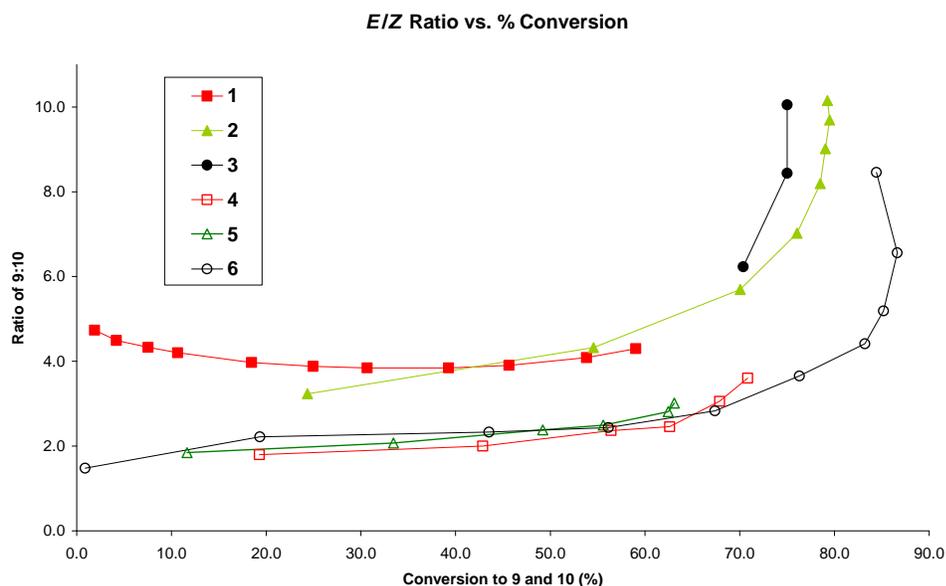
Figure 2.12. Plot of *E*/*Z* ratio of cross products vs. % conversion for catalysts **2.16a**,**b** and **2.22** in comparison with previously studied catalysts **2.1**–**3**.

Interestingly, catalyst **2.22** achieves ~ 60% conversion to product in 1 h at 22 °C, whereas catalysts **2.16a**,**b** require 32 h and 48 h at 60 °C, respectively. These results indicate that the higher *E*-selectivity observed is not simply due to a less active catalyst that is slow to isomerize olefins. Rather, these carbenes impart a change in the inherent catalyst selectivity.

Kinetic Selectivity: Ethenolysis Activity

Ethenolysis has been investigated for several decades as a method to transform internal olefins derived from seed oils to terminal olefin feedstocks.[38] However, an ethenolysis catalyst that is both highly efficient and highly selective has yet to be developed.[13]

Previous detailed studies of catalysts **2.1**[13] and PCy$_3$Cl$_2$Ru=CH(2-(OCH(CH$_3$)$_2$-)C$_6$H$_4$) **2.28**[39,40] in the ethenolysis of methyl oleate (**2.29**) demonstrated their high selectivity for the production of terminal olefins 9-methyl decenoate (**2.30**) and 1-decene (**2.31**) over self-metathesis products 1,18-dimethyl 9-octadecenoate (**2.32**) and 9-octadecene (**2.33**) (eq 2.11). At 100 ppm, catalysts **2.1** and **2.28** achieve 58% and 51% conversion to **2.30** and **2.31** with 93% and 94% selectivity, resulting in 5,400 and 4,800 TONs, respectively. Lowering the catalyst loading of **2.1** from 100 ppm to 35 ppm results in a significant increase in TONs to 12,900 with 94% selectivity for ethenolysis products over self-metathesis products. However, further decreasing the catalyst loading of **2.1** to 10 ppm did not result in increased TONs. The highest TONs reported to date is 14,047 for a bis(9-cyclohexyl-9-phospha-9*H*-bicyclonane) ruthenium complex.[41] The efficiency of first-generation Grubbs-type catalysts is limited by two major factors: catalyst decomposition due to the instability of the propagating methylidene species and catalyst inhibition by the ethenolysis products.[13]

$$(2.11)$$
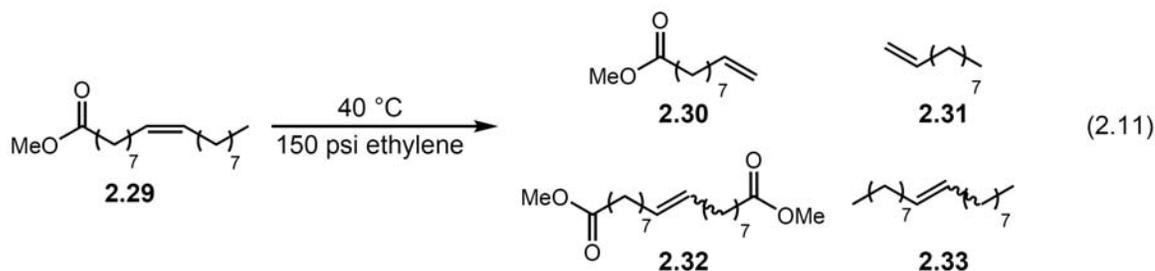
Conversely, NHC-containing systems **2.2** and **2.3** demonstrate relatively low selectivity for the synthesis of desired terminal olefins (Table 2.2). At 100 ppm, catalysts **2.2** and **2.3** produce only 28% and 20% yield of ethenolysis products **2.30** and **2.31** with product selectivities of 44% and 33% respectively. The remaining products of these

reactions are self-metathesis products **2.32** and **2.33**. Interetingly, for the ethenolysis of

2.29, bis(phosphine) catalyst **2.1** outperforms NHC-containing catalysts **2.2** and **2.3**.

Catalysts **2.16a**,**b** and **2.22** were evaluated for the ethenolysis of methyl oleate

(**2.29**) under the same conditions (150 psi ethylene, neat **2.29**, 40 °C) (Table 2.2). At

loadings of 100 ppm, catalysts **2.16a**,**b** and **2.22** exhibited good selectivity (73–94%) for

terminal olefins **2.30** and **2.31** and achieved TONs ranging from 4,200 to 5,600. By

lowering the catalyst loading of **2.22** to 10 ppm, TONs of 35,000 were achieved.[42]

Catalyst **2.22** exhibits the highest activity for the ethenolysis of methyl oleate to date and

represents a new direction of catalyst development in this area

Table 2.2. Comparison of ruthenium catalysts in the ethenolysis of **2.29**[a]

Cat.	Cat./11 (ppm)	Time (min)[b]	Conv. (%)[c]	Selectivity (%)[d]	Yield (%)[e]	TON[f]
2.1	100	120	58	93	54	5,400
2.1	35	240	48	94	45	12,900
2.1	10	120	13	>97	13	12,700
2.28	100	30	51	94	48	4,800
2.2	100	120	64	44	28	2,800
2.3	100	30	60	33	20	2,000
2.16a	100	1,320	61	92	56	5,600
2.16a	50	1,200	61	93	57	11,400
2.16b	100	360	46	94	43	4,200
2.22	100	<30	73	73	53	5,300
2.22	35	60	75	75	56	16,000
2.22	10	<30	42	83	35	35,000

[a] General conditions: neat **2.29**, 150 psi ethylene, 40 °C
[b] Time to maximum conversion
[c] Conversion = 100 − [(final moles of **2.29**) ∗ 100 / (initial moles of **2.29**)]
[d] Selectivity = (moles of ethenolysis products **2.30** + **2.31**) ∗ 100 / (moles of total products **2.30** + **2.31** + **2.31** + **2.32**)

[e] Yield = (moles of ethenolysis products **2.30** + **2.31**) ∗ 100 / (initial moles of **2.29**) =
Conversion ∗ Selectivity/100
[f] TON = Yield ∗ [(moles of **2.29**) / (moles of cat.)]

Summary

CAAC-ruthenium complexes **2.16a**,**b** are active for the formation di- and tri-substituted olefins via ring-closing metathesis. Catalyst **2.22** differs from **2.16a**,**b** through replacement of the *N*-DIPP group with a *N*-DEP group; reducing the steric bulk of the ligand results in an increase in catalyst ring-closing metathesis activity to levels comparable to standard catalysts **2.2** and **2.3**. In addition, complexes **2.16a**, **2.16b** and **2.22** were examined in the cross metathesis of *Z*-1,4-diacetoxy-2-butene (**2.24**) and allyl benzene (**2.25**) and in the ethenolysis of methyl oleate (**2.29**). Complexes **2.16a**,**b** and **2.22** demonstrate increased selectivity for the formation of *Z*-olefins relative to commercially-available catalysts **2.1**–**3**. In the ethenolysis of methyl oleate, catalysts **2.16a**,**b** display high selectivities and TONs for the formation of terminal olefins, which are comparable to those of bisphosphine catalyst **2.1**. Complex **2.22** displays slightly lower selectivity, but achieves the highest TONs (35,000) observed to date.

Experimental
General Considerations

All reactions were carried out under a dry argon atmosphere using standard Schlenk techniques or in a nitrogen-filled glovebox unless otherwise noted. Toluene, pentane, benzene, and benzene-d$_6$ were purified by passage through activated A-2 alumina solvent columns and were degassed with argon prior to use. Unless otherwise noted, all compounds were purchased from Aldrich or Fisher. Diethyl diallymalonate

(**2.9**) was purchased from Aldrich and distilled prior to use. Ruthenium catalysts **2.6** and **2.15**, salts **2.4a,b**, **2.20**, and imine **2.A1** were prepared according to literature procedures.[21,26,39,43] Column chromatography was performed utilizing silica purchased from TSI Scientific, Cambridge, MA (60Å, pH 6.5–7.0). High-resolution mass spectrometry (HRMS) FAB data was obtained on a JEOL MSRoute mass spectrometer and ESI data was obtained on an Agilant LC TOF spectrometer. ^{1}H and ^{13}C NMR spectra were recorded on Varian Inova (300 and 500), Mercury 300 and Bruker Avance 300 spectrometers. 2D NMR spectra acquired on a Bruker Avance DPX 400 MHz NMR spectrometer equipped with a 5 mm dual ^{1}H/^{13}C Z-gradient probe. ^{1}H NMR chemical shifts are reported in ppm relative to SiMe$_4$ ($\delta = 0$) and referenced internally with respect to the protio solvent impurity. ^{13}C NMR spectra were referenced internally with respect to the solvent resonance.

General ring-closing metathesis procedure: An NMR tube with a screw-cap septum top inside a glovebox was charged with catalyst stock solution (0.016 M, 50 μL, 1 mol%) and C$_6$D$_6$ (0.75 mL). The sample was equilibrated at 30 °C (temperature determined by measuring the peak separation of an ethylene glycol standard) in the NMR probe before diethyl diallymalonate (**2.9**, 19.3 μL, 19.2 mg, 0.08 mmol, 0.1 M) was added via syringe. Data points were collected over an appropriate period of time using the Varian array function. Conversion of **2.9** to **2.10** was determined by comparing the ratio of the integration of the methylene protons in the starting material with those in the product. For reactions performed at elevated temperatures, the NMR sample was equilibrated in a heating bath at the appropriate temperature before addition of **2.9**. Conversion was determined utilizing the same method.

General cross metathesis procedure: utilized the procedure outlined in Ritter, T.; Hejl, A.; Wenzel, A. G.; Funk, T. W.; Grubbs, R. H. Organometallics **2006**, *25*, 5740 for reaction conditions and GC analysis. Reactions with catalysts 4–6 were performed in benzene rather than CH_2Cl_2. For catalysts 4 and 5, the reactions were heated to 60 °C. For each catalyst, 2–3 identical reactions utilizing different catalyst batches were performed and the data was averaged together.

General ethenolysis procedure: Ethenolysis reactions of research-grade methyl oleate were set up under an inert atmosphere in a glove box: a Fisher-Porter bottle equipped with a stir bar was charged with methyl oleate (> 99%) from Nu-Check-Prep (Elysian, MN) and further purified by filtration through activated alumina (15.0 g; 50.6 mmol). For ethenolysis reactions run with low catalyst loadings (i.e., catalyst loadings lower than 100 ppm), it is important to use freshly purified methyl oleate. A solution of olefin metathesis catalyst of an appropriate concentration was prepared in anhydrous dichloromethane (from Aldrich) and the desired volume of this solution added to the methyl oleate. The head of the Fisher-Porter bottle equipped with a pressure gauge and a dip-tube was adapted on the bottle. The system was sealed and taken out of the glove box to an ethylene line. The vessel was then purged 3 times with ethylene (Polymer purity 99.9 % from Matheson Tri Gas), pressurized to 150 psi and placed in an oil bath at 40 °C. The reaction was monitored by collecting samples into vials at different reaction times via the dip-tube. Immediately after collecting a sample, the reaction was stopped by adding 1 mL of a 1.0 M isopropanol solution of tris-hydroxymethylphopshine (THMP) to the vial. The samples were then heated for at least 1 hour at 60°C, diluted

with 1 mL of distilled water, extracted with 1 mL of hexanes and analyzed by gas

chromatography (GC).

GC analytical method for ethenolysis reactions: The GC analyses were run using

a flame ionization detector (FID). Column: Rtx-5 from Restek (30m x 0.25mm (ID) x

0.25μm film thickness). GC and column conditions: (Injector temperature: 250 °C;

Detector temperature: 280 °C; Oven temperature: Starting temperature: 100 °C, hold

time: 1 minute, ramp rate 10 °C/min to 250 °C, hold time: 12 minutes; Carrier gas:

Helium).

2.A1　　　　　3. Tf$_2$O　　　　　**2.19**
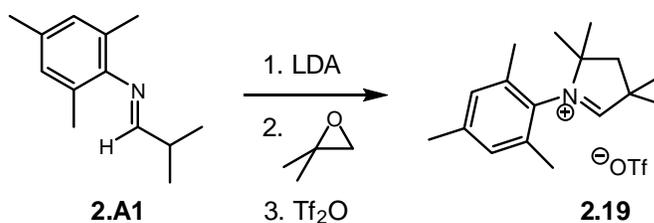
1-mesityl-2,2,4,4-tetramethyl-3,4-dihydro-2*H*-pyrrolium

trifluoromethanesulfonate (**2.19**): A solution of LDA (4.82 g, 45.0 mmol) in Et$_2$O (50

ml) was added at 0 °C to a stirred solution of imine **2.A1** (8.50 g, 45.0 mmol) in Et$_2$O (50

ml). The solution was warmed to room temperature and stirred for 2 h. After

evaporation of the solvent under vacuum, the residue was dissolved in Et$_2$O (100 ml), and

1,2-epoxy-2-methylpropane (4.19 mL, 47.2 mmol) was added drop-wise. After stirring

12 h at room temperature, Tf$_2$O (7.94 ml, 47.2 mmol) was added at −78 °C. The solution

was allowed to warm to room temperature and stirred for 1 h. After filtration, the

remaining solid was washed with Et$_2$O (60 ml) to give **2.19** as a white solid (10.79 g,

61%). ^{1}H NMR (CDCl$_3$, 300 MHz): δ = 9.15 (s, 1H; CH), 7.00 (s, 2H; H$_{ar}$), 2.38 (s, 2H;

CH$_2$), 2.30 (s, 3H; CH$_3$), 2.20 (s, 6H; CH$_3$), 1.63 (s, 6H; CH$_3$), 1.54 (s, 6H; CH$_3$);

^{13}C{1H} NMR (CDCl$_3$, 300 MHz): δ = 192.77 (CH), 141.21 (C$_{ar}$), 133.30 (C$_{ar}$), 130.75 (C$_{ar}$), 130.31 (C$_{ar}$), 120.88 (q, CF$_3$SO$_3^-$, ^{1}J(H-F) = 319.0 Hz), 84.39 (C), 49.19 (CH$_2$), 48.11 (C), 28.60 (CH$_3$), 26.54 (CH$_3$), 21.03 (CH$_3$), 19.27 (CH$_3$); HRMS (FAB) *m/z* (%): 244.2066 [M]$^+$ (100).

2.A2   2. (epoxide)   **2.20**   1. LDA   3. Tf$_2$O
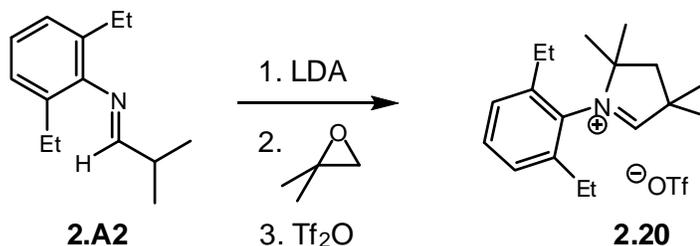
(E)-2,6-diethyl-N-(2-methylpropylidene)aniline (**2.A2**): To a solution of 2,6-diethyl-aniline (20 g, 0.134 mol) in toluene (100 ml) over 4Å molecular sieves, isobutraldehyde (7.89g, 0.1407 mol) was added. The mixture was heated to 60 °C for 16 hours and then filtered to remove the molecular sieves. The solution was concentrated under high vacuum and the viscous liquid used without any further purification (24.52 g, 90%). ^{1}H NMR (CDCl$_3$, 300 MHz): δ = 1.16 (t, 6H, ^{3}J(H,H) = 7.5 Hz; CH$_2$C*H$_3$), 1.26 (d, 6H; J = 6.8 Hz, CH(C*H$_3$)$_2$)), 2.48 (q, 4H, J = 7.5 Hz, CH$_2$CH$_3$), 2.71 (dsept., 1H, J = 6.8, 4.7 Hz, C*H(CH$_3$)$_2$), 7.15-6.9 (m, 3H), 7.56 (d, 1H, J = 4.7 Hz, N=C*H); ^{13}C{^{1}H} NMR (CDCl$_3$, 75 MHz): δ = 14.7 (CH$_3$), 19.0 (CH$_3$), 24.5 (CH$_2$), 34.9 (CH), 123.7 (CH$_{p-aryl}$), 126.2 (CH$_{m-aryl}$), 133.0 (C$_{i-aryl}$), 150.3 (C$_{o-aryl}$), 171.7 (N=C*H); HRMS (ESI): 204.1755 [M$^+$].

1-(2-ethyl-6-methylphenyl)-2,2,4,4-tetramethyl-3,4-dihydro-2*H*-pyrrolium trifluoromethanesulfonate (**2.20**):. Yield 80%. Mp: 90–92 °C. ^{1}H NMR (CDCl$_3$, 300

MHz): δ = 1.28 (dd, 6H, J = 7.5, 7.5 Hz, CH$_2$CH_3), 1.53 (s, 6H, CH$_3$), 1.71 (s, 6H, CH$_3$),

2.39 (s, 2H, CH$_2$), 2.49 (q, 2H, J = 7.5 Hz, CH_2CH$_3$), 2.54 (q, 2H, J = 7.5 Hz CH_2CH$_3$),

7.33 (d, 2H, J = 7.7 Hz), 7.49 (t, 1H, J = 7.7 Hz), 9.48 (s, 1H; N=CH); ^{13}C{^{1}H} NMR

(CDCl$_3$, 75 MHz): δ = 15.2 (CH$_3$), 25.1 (CH$_2$CH$_3$), 26.5 (CH$_3$), 28.4 (CH$_3$), 48.3 (CH$_2$),

49.3 (C), 84.0 (C), 122.2 (q, J(C-F) = 321.2 Hz, CF$_3$), 127.9 (CH$_{m-aryl}$), 130.8 (C$_{i-aryl}$),

131.5 (C$_{p-aryl}$), 139.6 (C$_{o-aryl}$), 192.8 (N=CH); HRMS (ESI): 258.2217 [M+].

Catalyst **2.7a**: To a 20-mL vial in the glovebox was added triflate salt **2.4a** (300

mg, 0.69 mmol), KHMDS (137 mg, 0.69 mmol), ruthenium precursor **2.6** (483 mg, 0.69

mmol) and benzene (8−10 mL). After 30 min, the reaction was filtered. The filtrate was

added to a 20-mL vial containing ruthenium precursor **2.6**. The reaction was stirred at

room temperature for 30 min. The reaction was placed under vacuum. The resulting

residue was extracted with Et$_2$O and washed 3 x 2 mL Et$_2$O. The solid was dissolved in

benzene, layered with Et$_2$O, and placed at −25 °C overnight. After filtration, the filtrate

was placed under vacuum to give a green solid (37%, 140 mg). ^{1}H NMR (C$_6$D$_6$, 300

MHz): δ = 19.25 (s, 1H, Ru=CHAr), 8.75 (d, 2H, J = 4.8 Hz), 7.75 (d, 2H, J = 7.5 Hz),

7.34-7.21 (m, 3H), 7.08 (t, 1H, J = 7.2 Hz), 6.86 (t, 2H, J = 7.8 Hz), 6.63 (t, 1H, J = 7.5

Hz), 6.31 (t, 2H, J = 6.8 Hz), 3.40 (septet, 2H, J = 6.5 Hz; CH(CH$_3$)$_2$), 2.35 (s, 6H), 1.92

(s, 2H), 1.20 (d, 6H, J = 6.9 Hz), 1.16 (d, 6H, J = 6.0 Hz, CH(CH$_3$)$_2$), 1.07 (s, 6H);

^{13}C{^{1}H} NMR (C$_6$D$_6$, 125 MHz): δ = 314.25, 273.08, 153.86, 153.06, 148.90, 136.60,

136.47, 129.92, 129.72, 128.93, 128.77, 126.36, 123.81, 78.79, 57.33, 51.75, 29.96, 29.53,

29.12, 27.97, 25.30, 25.24; HRMS (FAB) m/z (%): 547.1364 [M–py]$^+$ (97).

Catalyst **2.7b**: To a 20-mL vial in the glovebox was added triflate salt **2.4b** (161 mg, 0.34 mmol), KHMDS (76.9 mg, 0.39 mmol) and toluene (3 mL). The reaction was stirred at room temperature for 30 min, filtered through celite, and the filtrate concentrated to dryness. The resulting solid was redissolved in toluene (2 mL) and added to a 20-mL vial containing ruthenium complex **2.6** (215 mg, 0.31 mmol) and toluene (3 mL). The reaction was stirred at room temperature for 3 h and concentrated to dryness. The product was precipitated from toluene (~ 0.5 mL) and pentane (10 mL). The resulting solid was washed 2 x 5 mL pentane to provide a green powder (111 mg, 54%). A small impurity displaying only aryl protons in the ^{1}H NMR spectrum remained despite all purification attempts. ^{1}H NMR (C_6D_6, 300 MHz): δ = 19.36 (s, 1H, Ru=CHPh), 8.80 (br d, 2H, 4.8 Hz), 7.78 (d, 2H, 7.5 Hz), 7.42-7.22 (m, 3H), 7.14-7.07 (t, 1H, J = 7.6 Hz), 6.87 (t, 2H, J = 7.8 Hz), 6.64 (t, 1H, J = 7.8 Hz), 6.33 (t, 2H, J = 7.0 Hz), 3.79 (dt, 2H, J = 6.6 Hz), 3.44 (septet, 2H, J = 6.5 Hz), 2.68 (br d, 2H, J = 12.3 Hz), 2.06 (s, 2H), 1.87-1.29 (m, 6H), 1.22 (d, 6H, J = 6.6 Hz), 1.17 (d, 6H, J = 6.3 Hz), 1.09 (s, 6H); ^{13}C{^{1}H} NMR (C_6D_6, 125 MHz): δ = 315.29, 273.23, (159.03), (158.93), 154.06, 153.01, 148.87, 136.62, 136.52, (133.74), 130.04, 129.68, 128.95, 128.92, (127.94), (127.56), 126.38, 123.81, (123.26), 78.84, 63.68, 44.89, 35.27, 30.46, 29.15, 28.02, 26.29, 25.28 23.84 (numbers in parantheses: based on comparison to **2.7a**, these resonances may belong to the observed impurity); HRMS (FAB) m/z (%): 666.2093 [M]$^+$ (6).

Catalyst **2.11**: To a flame-dried, 25-mL flask in the glovebox was added **2.4a** (205 mg, 0.46 mmol), KHMDS (100 mg, 0,046 mg), **2.6** (330 mg, 0.46 mmol) and dry benzene (10 mL). Flask capped with a septum, removed from the glovebox and stirred at

22 °C for 20 min. 2-butenyl pyridine (60 μL, 0.46 mmol) was added via syringe, and the flask was heated at 50 °C. After 1 h, an additional portion of 2-butenyl pyridine (60 μL, 0.46 mmol) was added. After stirring an additional 2 h, the solvent was removed under vacuum. Purification by column chromatography (1:4 EtOAc:hexanes) led to the isolation of an orange solid (70 mg, 26%). ^{1}H NMR (C$_6$D$_6$, 300 MHz): δ = 18.63 (t, 1H, Ru=CH), 9.08 (dd, 1H, J = 1.5, 5.7 Hz), 7.25 (m, 3H), 6.79 (m, 1H), 6.53 (m, 1H), 6.39 (d, 1H, J = 6.0 Hz), 3.36 (s, 2H, J = 6.6 Hz, CH(CH$_3$)$_2$), 3.17 (t, 2H, J = 6.3 Hz, CH_2py), 2.36 (s, 6H, C(CH_3)$_2$CH$_2$), 1.82 (s, 2H, C(CH$_3$)$_2$CH_2), 1.82-1.77 (m, 2H), 1.23 (d, 6H, J = 6.6 Hz, CH(CH_3)$_2$), 1.15 (d, 6H, J = 6.6 Hz, CH(CH_3)$_2$), 1.03 (s, 6H, C(CH_3)$_2$CH$_2$); HRMS (FAB) m/z (%): 576.1622 [M]$^{+}$ (18).

Catalyst **2.14**: To a 4-mL vial in the glovebox was added **2.4a** (99 mg, 0.23 mmol), KHMDS (53 mg, 0.25 mmol) and toluene (3 mL). After 0.5−1 h, the reaction was filtered through a pad of celite. The filtrate was placed under vacuum, redissolved in toluene (3−4 mL) and added to a 20-mL vial containing **2.12**. After stirring at 22 °C for 4−6 h, the reaction was placed under vacuum. Toluene (~ 0.5 mL) was added followed by pentane (10 mL) to precipitate the product. After filtration, the solid was reprecipitated from toluene/pentane to provide a pink solid (67 mg, 39% yield). ^{1}H NMR (C$_6$D$_6$, 300 MHz): δ = 20.12 (d, 1H, 41 Hz, Ru=CH), 8.41 (d, 1H, J = 10.5 Hz), 7.14 (d, 1H, J = 2.7 Hz), 7.11-7.05 (m, 1H), 4.03 (m, 1H), 3.934 (s, 1H, J = 6.9 Hz), 3.38 (s, 1H, J = 6.3 Hz), 2.71-2.66 (m, 6H), 2.53 (dd, 1H), 2.28-1.06 (m, 79 H); ^{31}P{^{1}H} NMR (C$_6$D$_6$, 121 MHz): δ = 32.04; HRMS (FAB) m/z (%): 762.3304 [M]$^{+}$ (6).
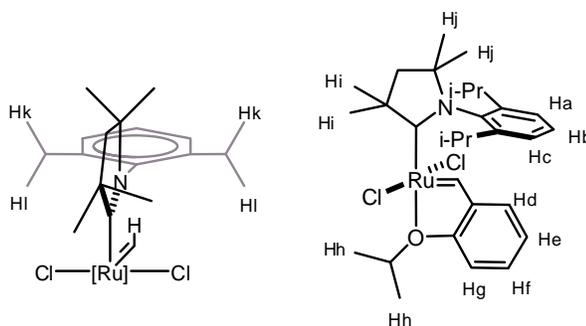
Catalyst **2.16a**: To a 20-mL vial in the glovebox was added triflate salt **2.4a** (100 mg, 0.23 mmol), KHMDS (55 mg, 0.25 mmol), and 3–4 mL benzene. After stirring 45 min at room temperature, the reaction was filtered. The filtrate was concentrated to dryness, dissolved in minimal toluene, and added to a 20-mL vial containing ruthenium complex **2.15** (135 mg, 0.23 mmol). The reaction was stirred at room temperature for 1 h, filtered, and washed 2 x 5 mL pentane. The green solid (70 mg, 50%) was dried under vacuum. ^{1}H NMR (C$_6$D$_6$, 300 MHz): δ = 16.45 (d, J = 0.6 Hz, 1H, Ru=CHR), 7.39-7.34 (m, 1H, Hb), 7.27-7.24 (m, 2H, Ha + Hc), 7.14-7.09 (m, 1H, Hf), 7.01 (dd, 1H, J = 1.5 Hz, 6.4 Hz, Hd), 6.65 (t, 1H, J = 7.5 Hz, He), 6.43 (d, 1H, J = 8.7 Hz, Hg), 4.66 (septet, 1H, J = 6 Hz, OCH(CH$_3$)$_2$), 3.18 (septet, 2H, J = 6.6 Hz, N-ArCH(CH$_3$)$_2$), 2.27 (s, 6H, Hi), 1.78 (s, 2H), 1.72 (br d, 6H, J = 6.3 Hz, Hh), 1.15 (d, 6H, J = 6.9 Hz, Hk), 0.98 (s, 6H, Hj), 0.93 (d, 6H, J = 6.6 Hz, Hl); ^{13}C{^{1}H} NMR (C$_6$D$_6$, 75 MHz): δ = 290.82, 268.91, 153.83, 149.32, 143.67, 137.55, 130.62, 129.94, 128.92, 126.25, 123.95, 122.29, 113.80, 77.79, 75.47, 56.81, 51.81, 29.93, 29.60, 29.08, 27.33, 24.72, 22.50; HRMS (FAB) m/z (%): 605.1777 [M+H]$^+$ (100).

Catalyst **2.16b**: To a 20-mL vial in the glovebox was added pyrrolium salt **2.4b** (155 mg, 0.33 mmol), KHMDS (69 mg, 0.35 mmol), complex **2.15** (182 mg, 0.32 mmol),

and 6–8 mL toluene. The reaction was stirred at room temperature for 4.5 h and concentrated to 1–2 mL. The crude product was purified by flash column chromatography (eluent: 9:1 toluene:hexanes) to provide a green solid (178 mg, 91%). ^{1}H NMR (C_6D_6, 300 MHz): δ = 16.44 (s, 1H, Ru=CHR), 7.28-7.14 (m, 1H), 7.04-6.98 (m, 2H), 6.90 (d, 1H, J = 7.2 Hz), 6.54 (t, 1H, J = 7.5 Hz), 6.32 (d, 1H, J = 8.4 Hz), 4.54 (septet, 1H, J = 6.1 Hz, OH(CH$_3$)$_2$), 3.66 (m, 2H, J = 3.3 Hz, 13.1 Hz), 3.10 (septet, 2H, J = 6.5 Hz, ArCH(CH$_3$)$_2$), 2.39 (d, 2H, J = 12.9 Hz), 1.80 (s, 2H), 1.78-1.25 (m, 6H), 1.05 (d, 6H, J = 6.6 Hz), 0.88 (s, 6H), 0.82 (d, 6H, J = 6.6 Hz); ^{13}C{^{1}H} NMR (C_6D_6, 75 MHz): δ = 291.81, 268.79, 153.82, 149.31, 147.20, 143.83, 137.57, 130.70, 129.91, 126.26, 124.08, 122.29, 113.87, 77.82, 75.35, 63.00, 44.76, 35.38, 30.47, 29.08, 27.35, 26.25, 24.77, 23.76, 22.57; HRMS (FAB) m/z (%): 645.2088 [M]$^+$ (26).

Catalyst **2.22**: To a 20-mL vial in the glovebox was added pyrrolium salt **2.20** (100 mg, 0.25 mmol), KHMDS (54 mg, 0.27 mmol), complex **2.15** (49 mg, 0.082 mmol) and stir bar. Vial capped with cap containing septum, removed from the glovebox and placed in a dry ice/acetone bath. A separate vial containing dry THF was also cooled in a dry ice/acetone bath. 5 mL of cooled THF added to starting materials via syringe. The reaction was stirred for 20 min in the cooling bath, and then warmed to room temperature and stirred 2 h. The crude product was purified by flash column column chromatography (9:1 toluene:hexanes) followed by recrystallization from slow diffusion of pentane into a concentrated solution of crude product in benzene. A green solid was isolated (8.7 mg, 18%). ^{1}H NMR (C_6D_6, 300 MHz): δ =16.42 (d, 1H, J = 0.6 Hz, Ru=CHAr,), MULTIPLET 7.03 (dd, H, J = 1.5 Hz, 9.4 Hz) 6.66 (dt, H, J = 0.9 Hz, 7.5 Hz) 6.43 (d, H,

J = 8.6 Hz), 4.66 (m, 1H, J = 6 Hz, OCH(CH$_3$)$_2$), 2.84 (m, 2H, J = 14.7 Hz, CH_2CH$_3$),

2.41 (m, 2H, J = 14.8 Hz, CH_2CH$_3$), 2.24 (s, 6H), 1.77 (s, 2H, CH$_2$), 1.70 (d, 6H, J = 6

Hz, CH(CH_3)$_2$), 0.95 (t, 6H, J = 7.5 Hz, CH$_2$CH_3), 0.92 (s, 6H); ^{13}C{^{1}H} NMR (C$_6$D$_6$,

125 MHz): δ = 292.86, 267.88, 153.39, 144.68, 144.39, 139.58, 130.62, 129.34, 127.434,

123.79, 122.31, 113.75, 78.24, 75.41, 56.63, 52.17, 30.04, 28.63, 25.55, 22.43, 15.32;

HRMS (FAB) *m/z* (%): 577.1434 [M]$^+$ (33).

2.35:   See procedure of Hejl, A. Ph.D. thesis, **2007**, California Institute of

Technology.for initiation kinetics (Chapter 3).   Modifications: utilized C$_6$D$_6$ in place of

tol-*d*$_8$.   NMR initiation kinetics measured (~2-3 h at room temperature), the NMR tube

was taken into the glovebox and pentanes added.   Small crystals formed overnight.

Table 2.A1. Selected bond distances (Å) and angles for **2.7a,b** and **2.8**

Selected bond distances (Å):			
	2.7a	**2.7b**	**2.8**
Ru–C$_{carbene}$	1.9778(10)	1.9876(13)	2.033(4)
Ru–C$_{benzylidene}$	1.8427(10)	1.8409(14)	1.873(4)
Ru–Cl(1)	2.3831(3)	2.3657(3)	2.3995(12)
Ru–Cl(2)	2.3713(3)	2.3853(3)	2.4227(12)
Ru–N	2.2089(9)	2.1989(12)	2.203(3)
			2.372(4)
Selected bond angles (deg):			
C$_{carbene}$–Ru–N	163.33(4)	166.72(5)	176.4(14)
C$_{benzylidene}$–Ru–N	97.52(4)	94.3(5)	87.07(15)
Cl(1)–Ru–Cl(2)	162.300(10)	161.68(13)	174.50(4)

Table 2.A2. Selected bond distances (Å) and angles for **2.16a,b, 2.22** and **2.3**

Selected bond distances (Å):				
	2.16a	**2.16b**	**2.3**	**2.22**
Ru–C$_{carbene}$	1.930(3)	1.9457(10)	1.981(5)	1.9482(14)
Ru–C$_{benzylidene}$	1.822(3)	1.8318(12)	1.828(5)	1.8367(14)
Ru–Cl(1)	2.3320(8)	2.3326(3)	2.328(12)	2.3297(5)
Ru–Cl(2)	2.3370(7)	2.3319 (3)	2.340(12)	2.3495(4)
Ru–O	2.325(2)	2.3539(8)	2.261(3)	2.2978(14)
Selected bond angles (deg):				
C$_{carbene}$–Ru–O	177.51(8)	175.84(3)	176.2(14)	178.07(6)
C$_{benzylidene}$–Ru–O	78.09(10)	77.74(4)	79.3(17)	78.54(6)
Cl(1)–Ru–Cl(2)	152.78(3)	151.627(11)	156.5(5)	154.542(17)

Table 2.A3. Selected bond distances (Å) and angles for **2.11** and **2.23**

Selected bond distances (Å):		
	2.11 (X=N)	**2.23** (X=Cl)

R = H

	2.11 (X=N)		**2.23** (X=Cl)
Ru–C$_{carbene}$	2.0000(3)	2.0459(10)	1.933(3)
Ru–C$_{benzylidene}$	1.8163(18)	1.8185(11)	1.822(10)
Ru–Cl(1)	2.3537(5)	2.3973(3)	2.3743(8)
Ru–Cl(2)	2.3752(5)	2.3662(3)	2.4819(8)
Ru–X	2.2159(15)	2.1355(9)	
Selected bond angles (deg):			
C$_{carbene}$–Ru–X	171.95(6)	170.21(4)	
C$_{benzylidene}$–Ru–X	89.63(7)	88.32(4)	
Cl(1)–Ru–Cl(2)	154.761(17)	164.406(11)	

NMR Spectroscopy Experiments

Details for the 2D experiments are as follows:

Gradient-enhanced 2D COSY experiment.[44] The **cosygs** pulse program was used with the following acquisition parameters: F2 and F1 sweep widths, 7184 Hz. F2 and F1 digital resolution, 7.01 Hz/pt. 256 FIDs recorded, each consisting of 4 scans and 1024 data points (AQ = 0.071 s). A recycle delay of (D1) of 1.5 s was employed. Processing parameters: unshifted sinusoidal apodization was applied in both dimensions prior to the Fourier transformation. **2.16a**: Figures 2.A1, 2.A2; **2.16b**: Figures 2.A9, 2.A10.

2D COSYLR experiment.[45] The **cosylr** pulse program was used with the following acquisition parameters: F2 and F1 sweep widths, 7184 Hz. F2 and F1 digital resolution, 7.01 Hz/pt. 128 FIDs recorded, each consisting of 8 scans and 1024 data points (AQ = 0.071 s). Refocussing delays of 100 ms and 200 ms were used in separate experiments. A recycle delay of (D1) of 2.0 s was employed. Zero-filling was applied once to achieve digital resolution of 3.5 Hz/pt in each dimension. Processing parameters: unshifted sinusoidal (SINE, SSB=0) apodization was applied in both dimensions prior to the Fourier transformation. **2.16a**: Figures 2.A3, 2.A4; **2.16b**: Figures 2.A11, 2.A12.

2D ROESY experiment.[46] The **roesytp.2** pulse program was used with the following acquisition parameters: F2 and F1 sweep widths, 7184 Hz. F2 and F1 digital resolution, 3.5 Hz/pt. 256 FIDs recorded, each consisting of 16 scans and 2048 data points (AQ = 0.142 s). The 800 ms spin lock consisted of 5404 cycles of phase-shifted pairs of 74 μs 180° pulses. A recycle delay of (D1) of 2.0 s was employed. Processing parameters: $\pi/2$ shifted sine^2 (QSINE, SSB=2) apodization was applied in both

dimensions prior to the Fourier transformation. **2.16a**: Figures 2.A5, 2.A6, 2.A7; **2.16b**:

Figures 2.A13, 2.A14.
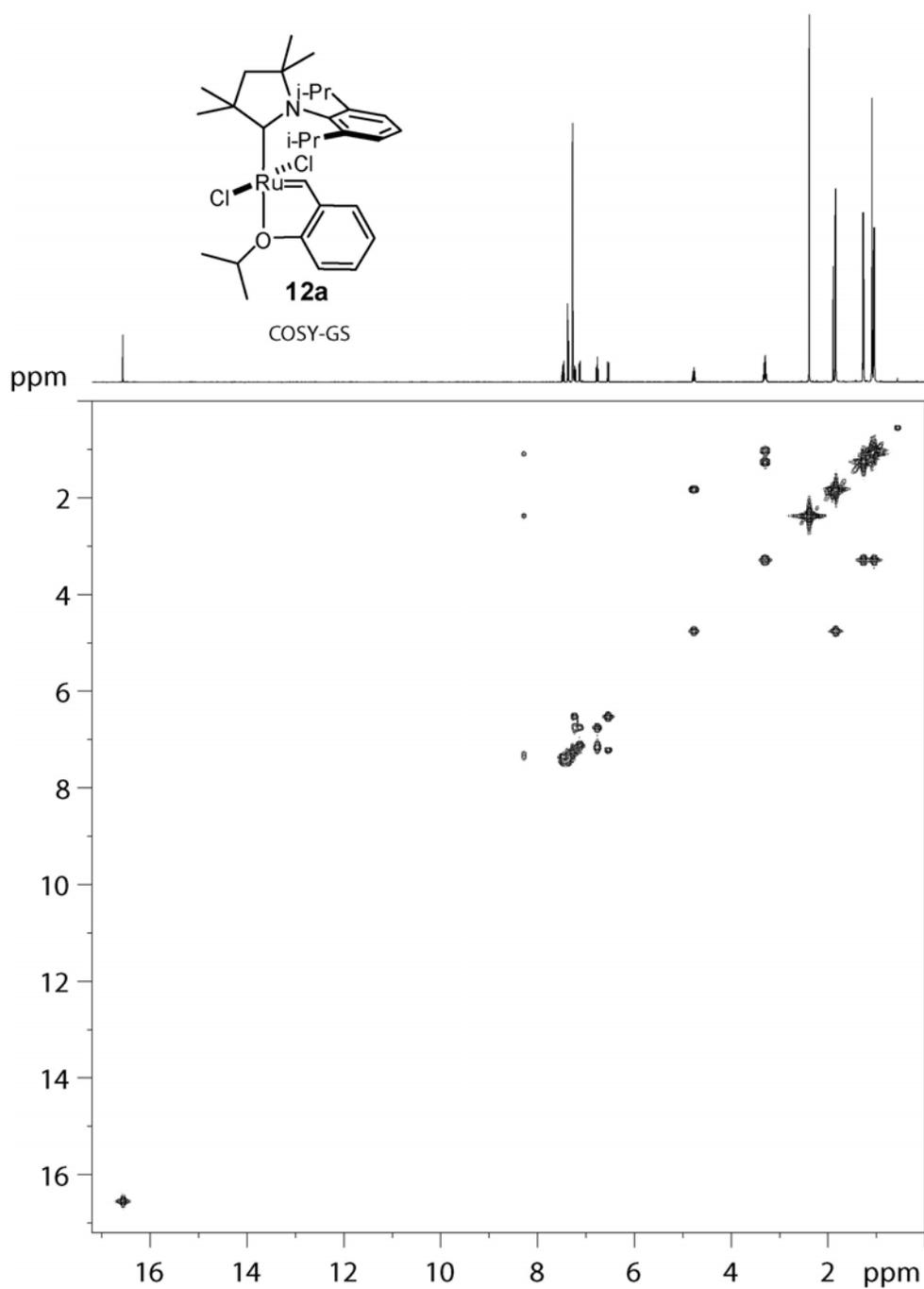
Figure 2.A1 400 MHz ^{1}H -^{1}H COSY spectrum for **2.16a** in C_6D_6 at 22 °C.
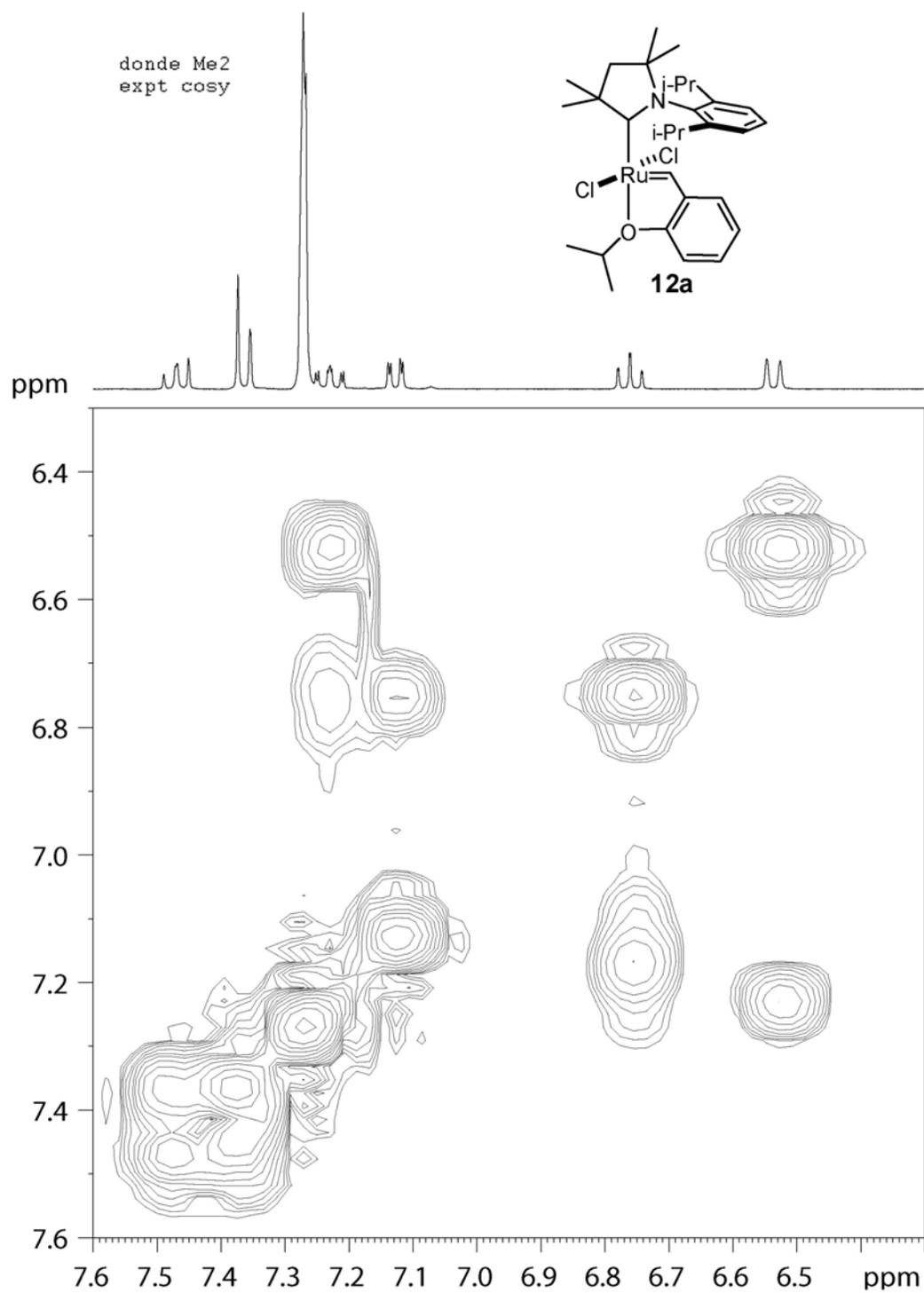
**Figure 2.A2.** 400 MHz ^{1}H -^{1}H COSY spectrum for **2.16a** in C_6D_6 at 22 °C.
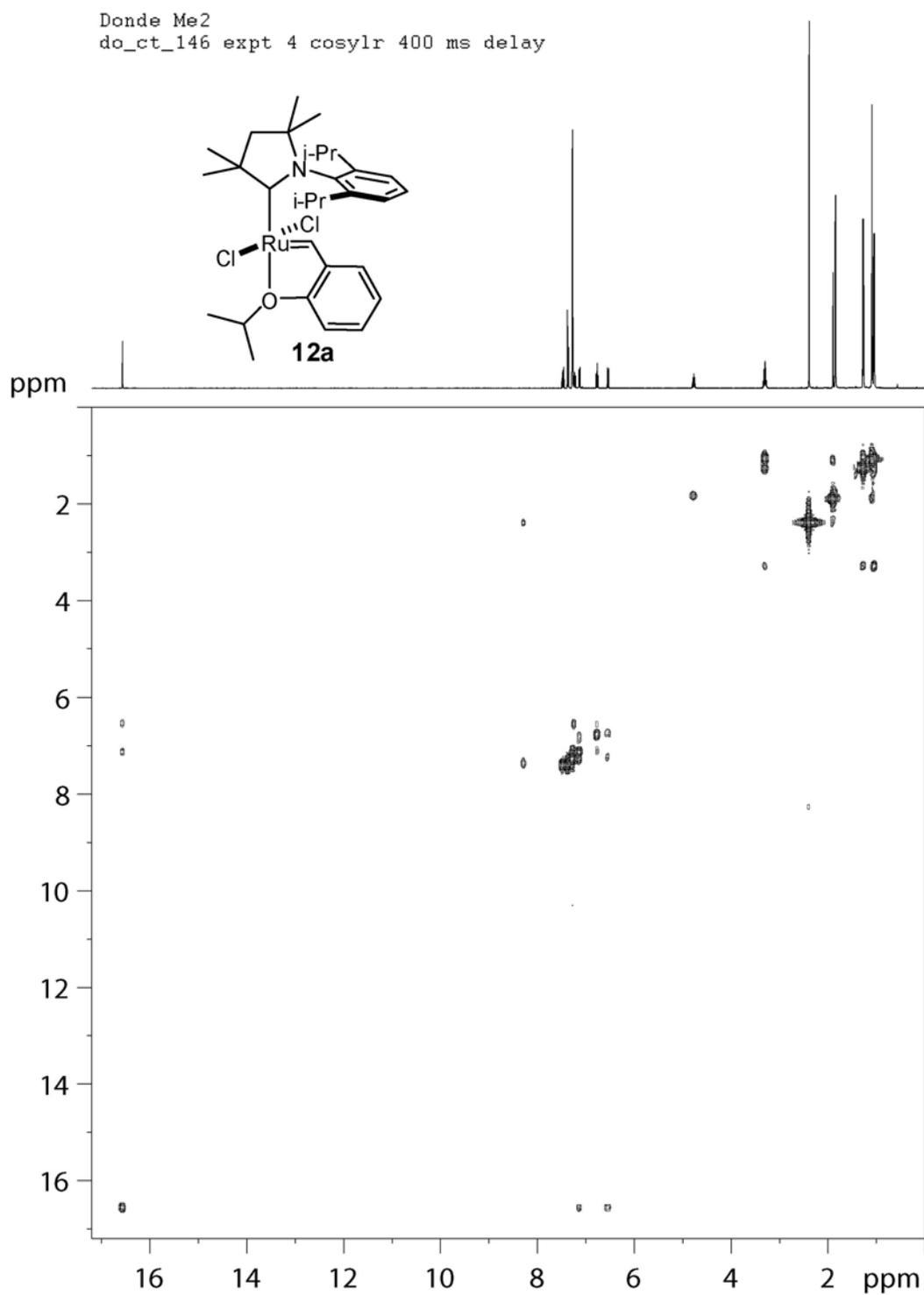
Figure 2.A3. 400 MHz ^{1}H -^{1}H COSYLR spectrum for **2.16a** in C$_6$D at 22 °C $_6$.
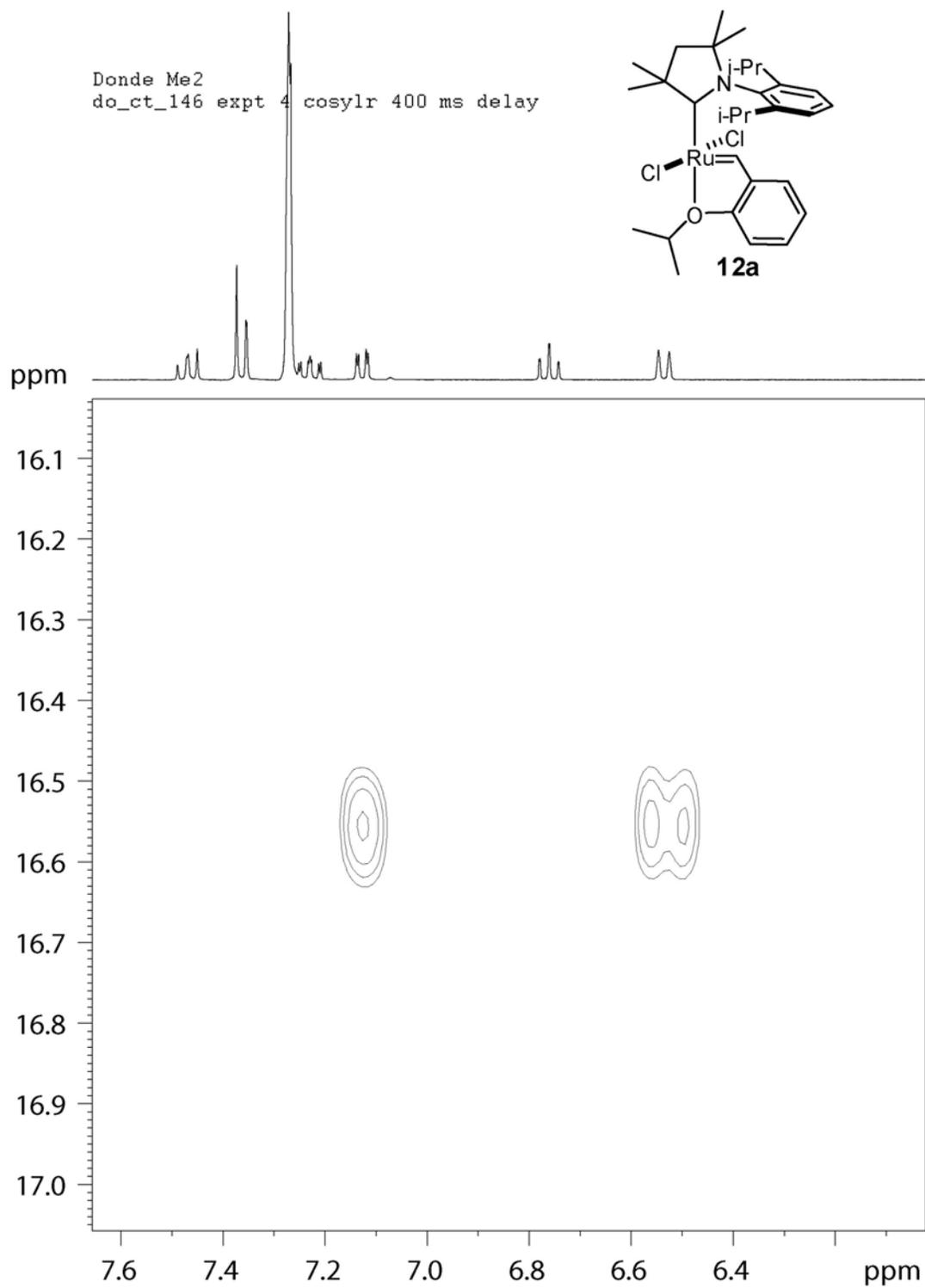
Figure 2.A4. 400 MHz ^{1}H -^{1}H COSYLR spectrum for **2.16a** in C_6D_6 at 22 °C.
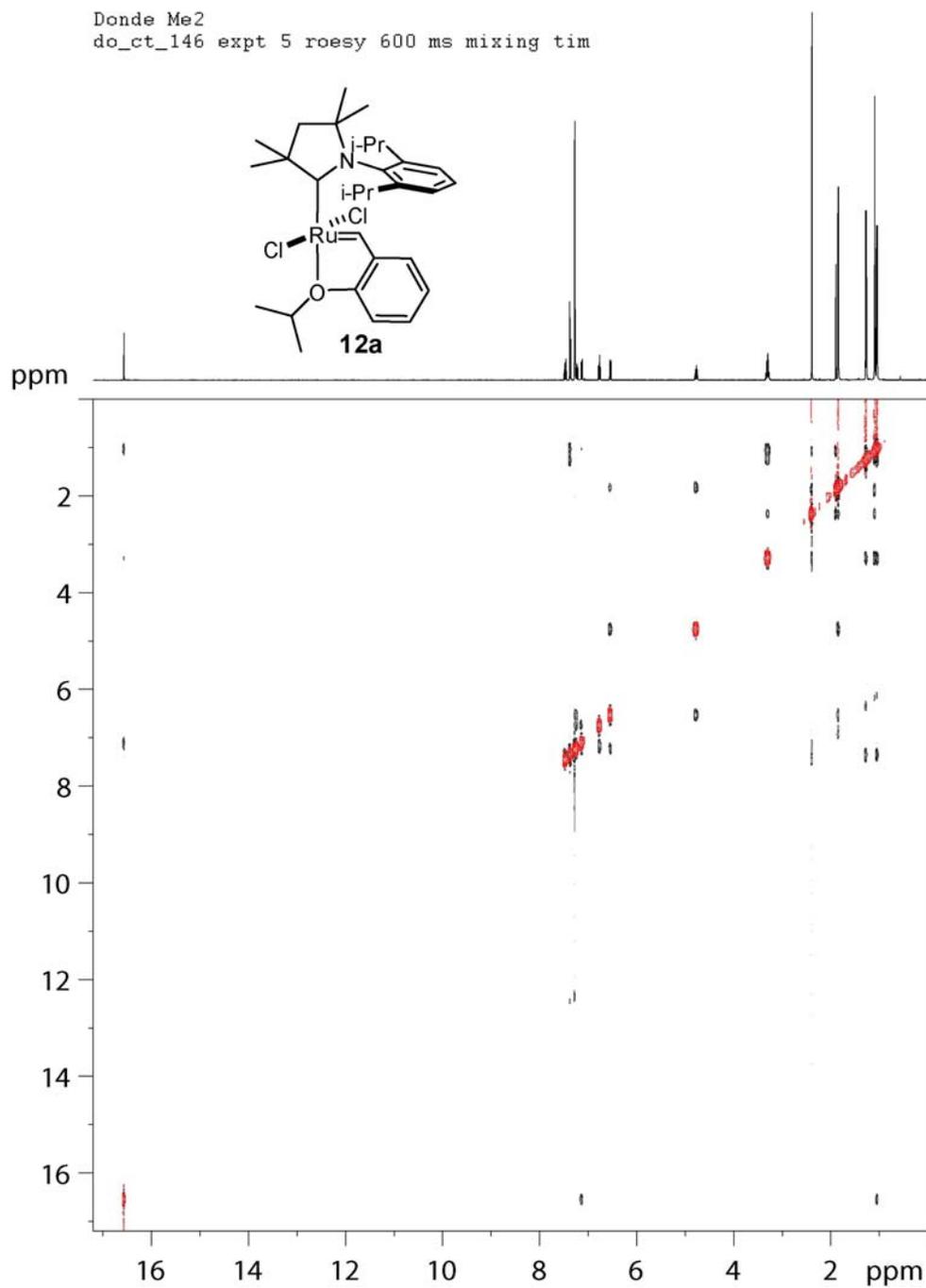
Figure 2.A5. 400 MHz ^{1}H-^{1}H ROESY spectrum for **2.16a** in C_6D_6 at 22 °C. Overhauser-derived crosspeaks are colored black, diagonal and exchange-derived crosspeaks are colored red.
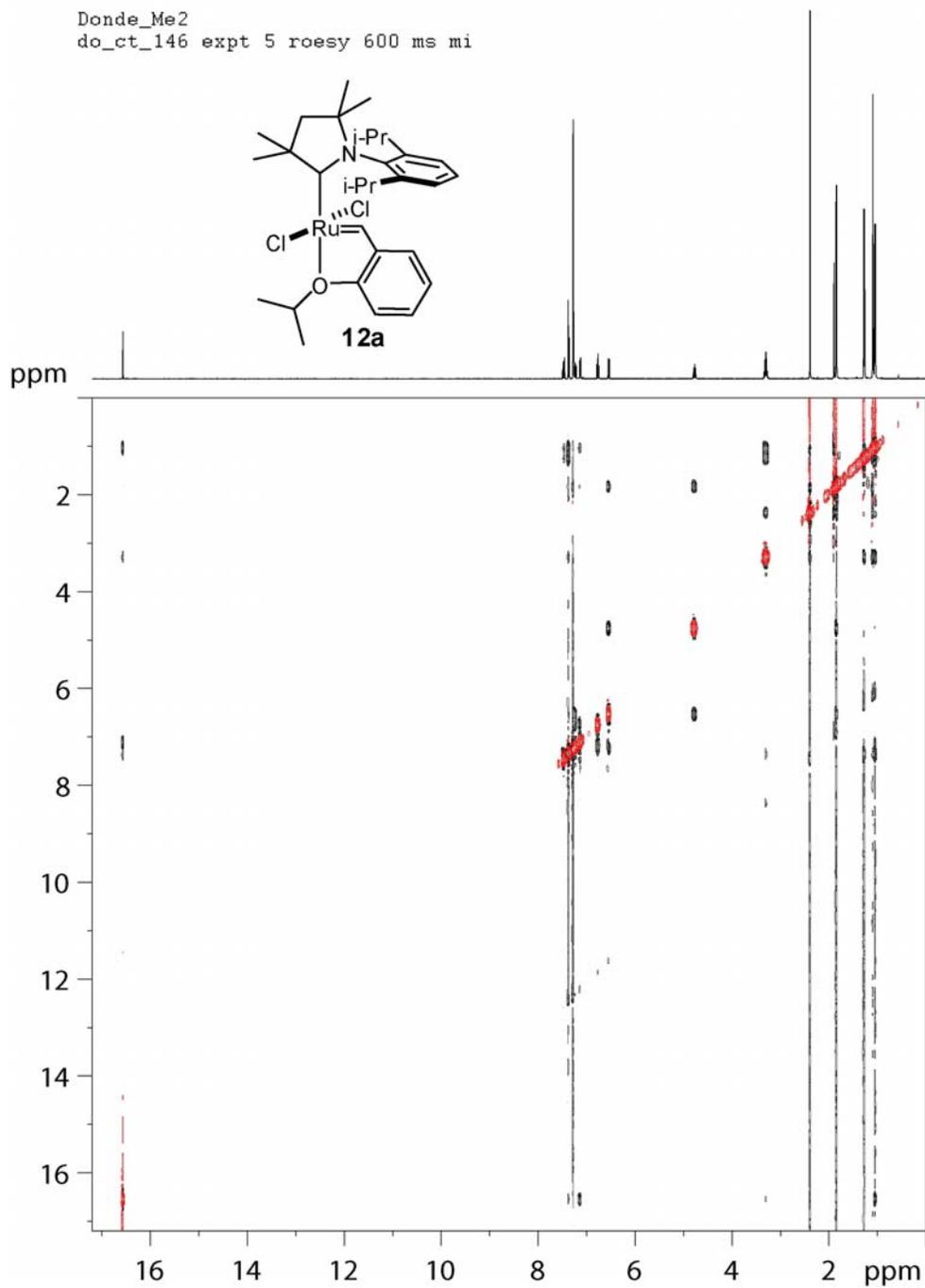
Figure 2.A6. 400 MHz ¹H-¹H ROESY spectrum for **2.16a** in C₆D₆ at 22 °C. Overhauser-derived crosspeaks are colored black, diagonal and exchange-derived crosspeaks are colored red.
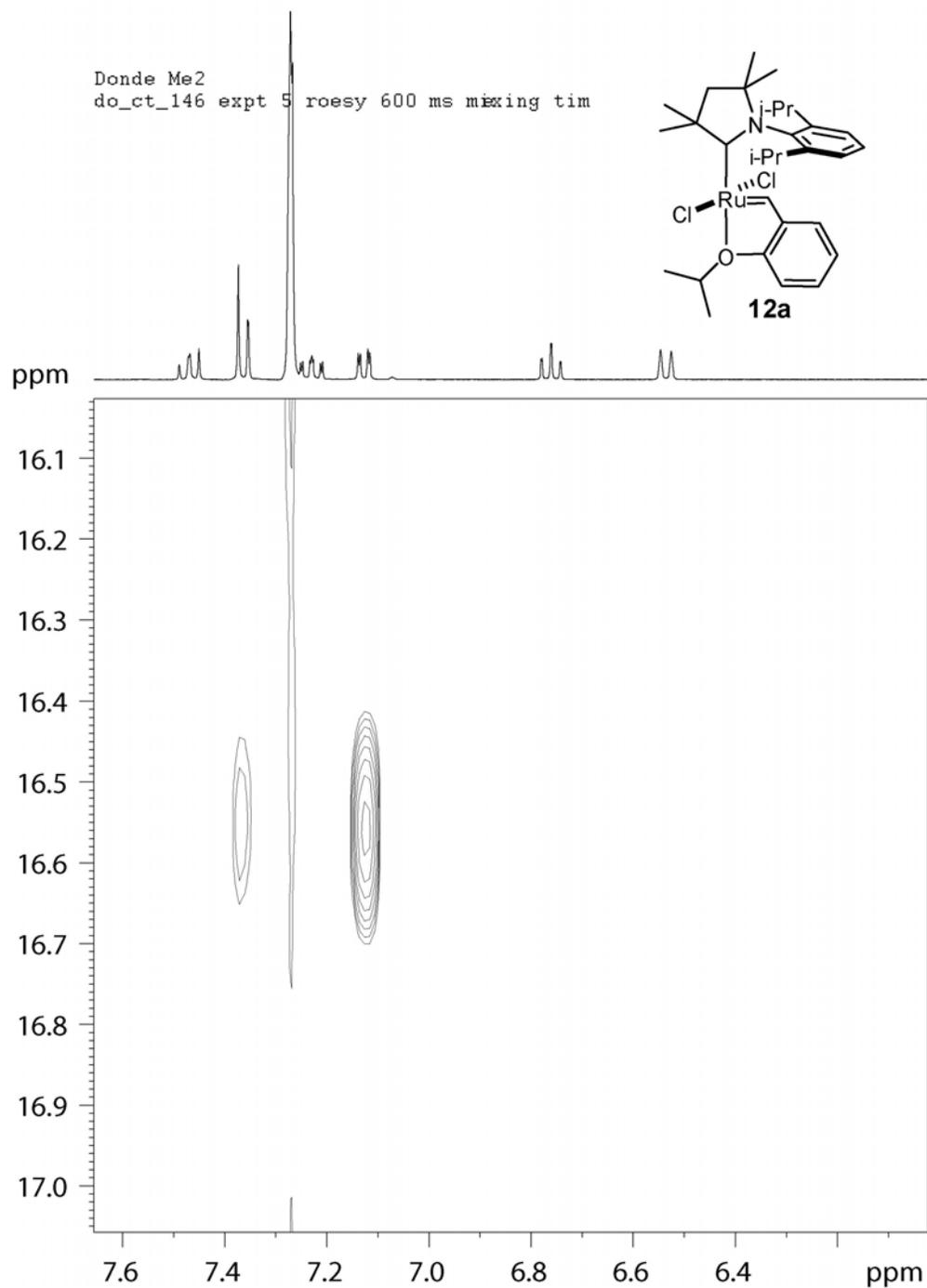
**Figure 2.A7.** 400 MHz ^{1}H-^{1}H ROESY spectrum for **2.16a** in C$_6$D$_6$ at 22 °C. Overhauser-derived crosspeaks are colored black, diagonal and exchange-derived crosspeaks are colored red.
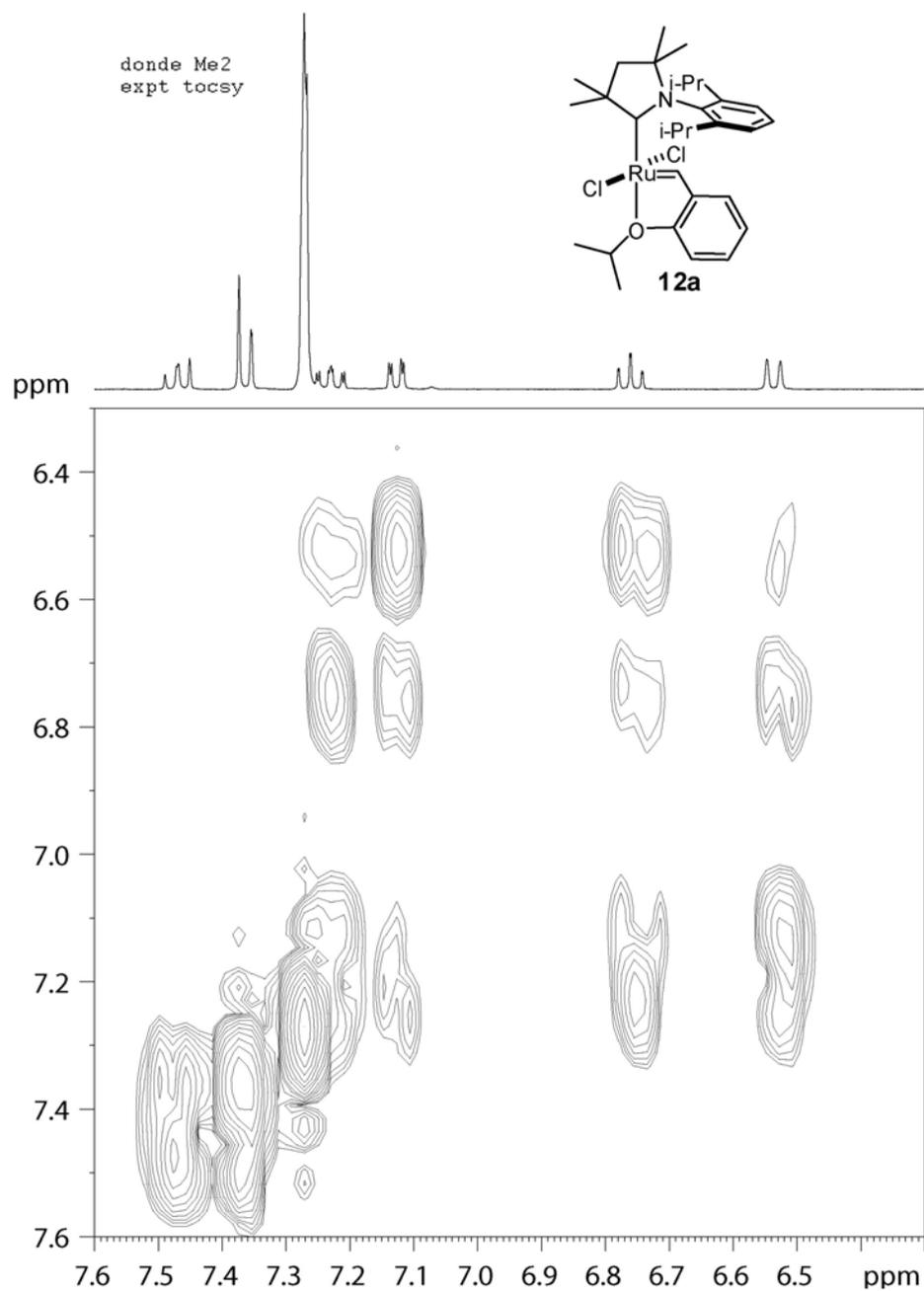
Figure 2.A8. 400 MHz ^{1}H-^{1}H TOCSY spectrum for **2.16a** in C_6D_6 at 22 °C.
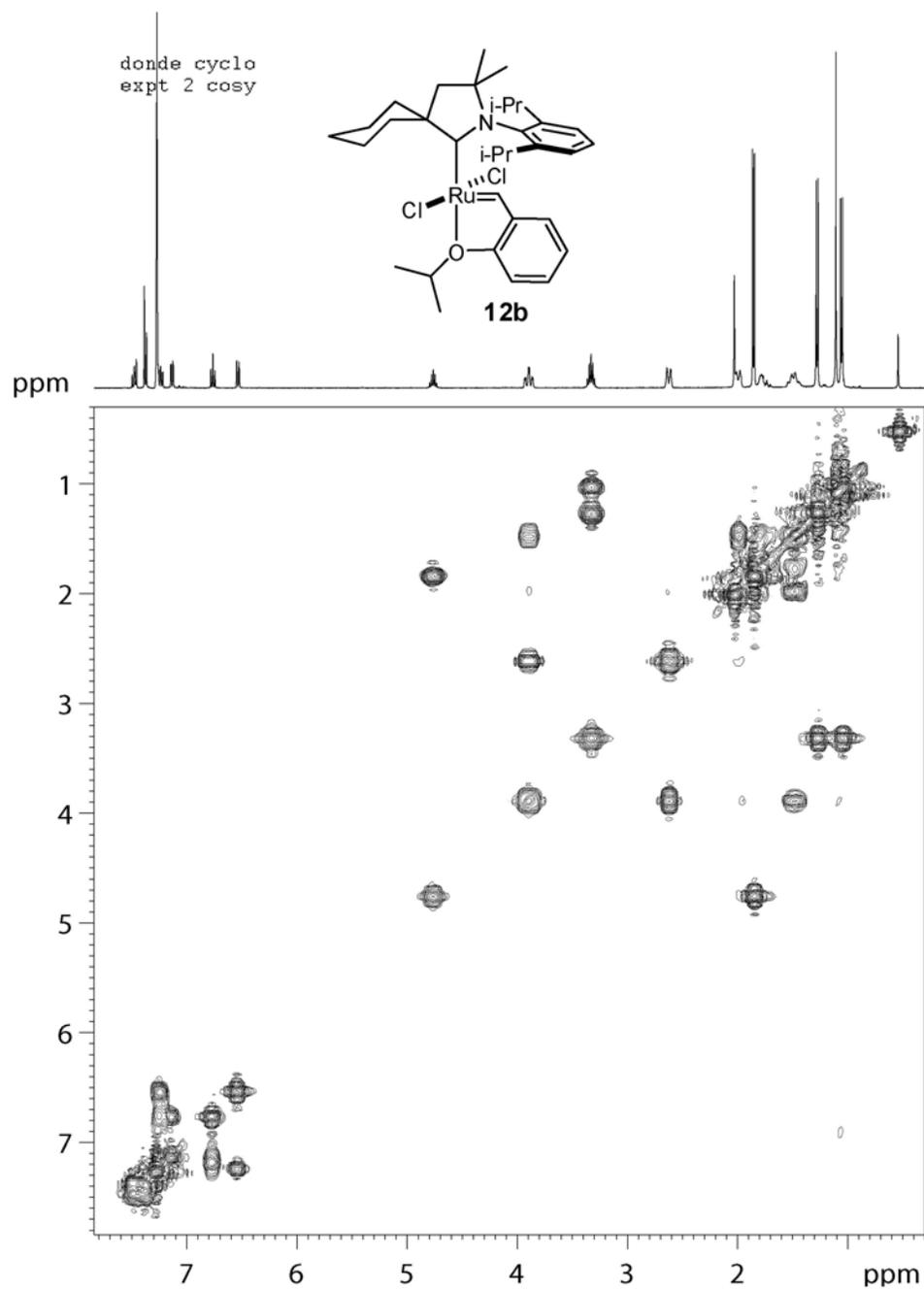
Figure 2.A9. 400 MHz ^{1}H-^{1}H COSY spectrum for **2.16b** in C_6D_6 at 22 °C.
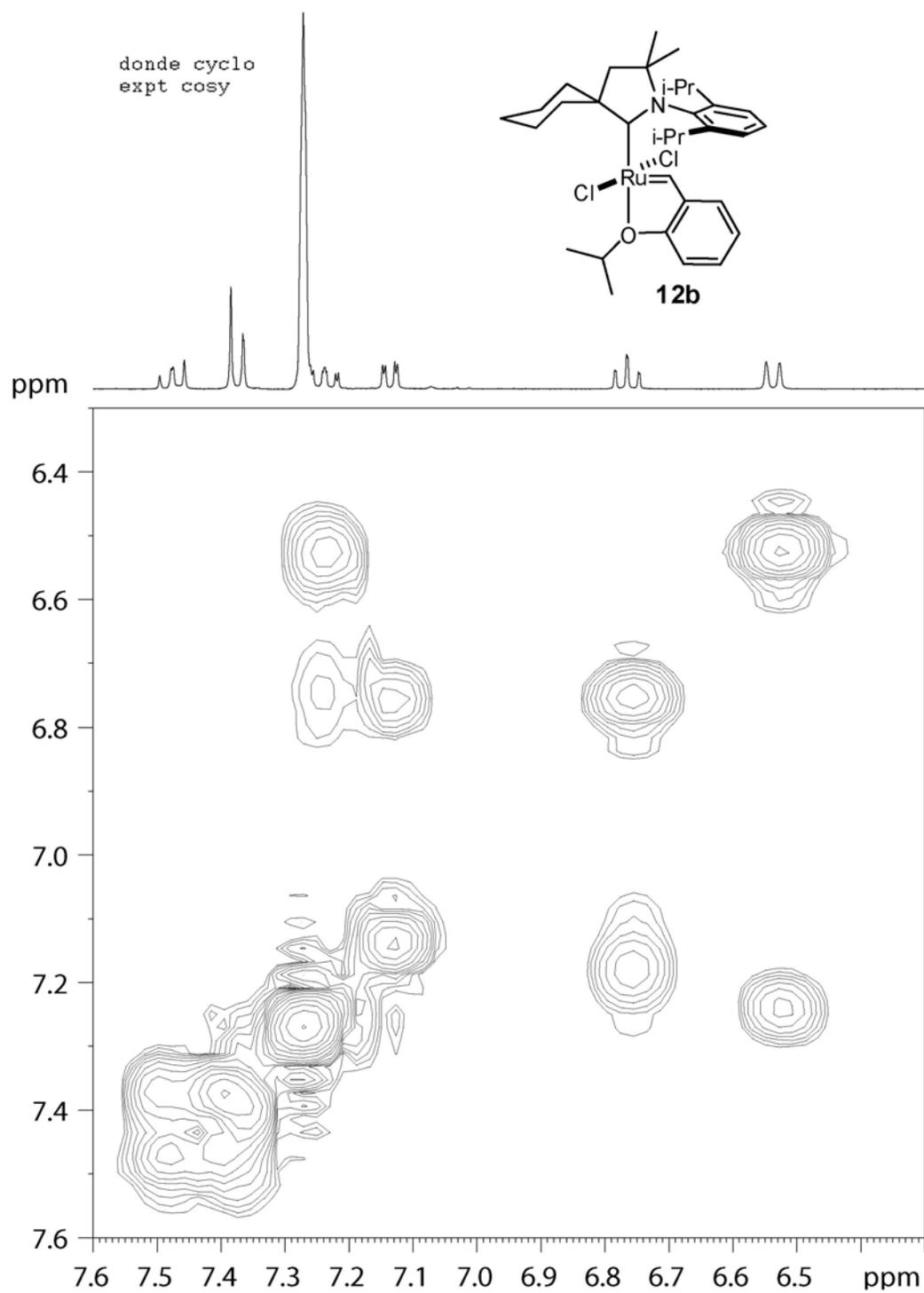
Figure 2.A10. 400 MHz ^{1}H-^{1}H COSY spectrum for **2.16b** in C$_6$D$_6$ at 22 °C.
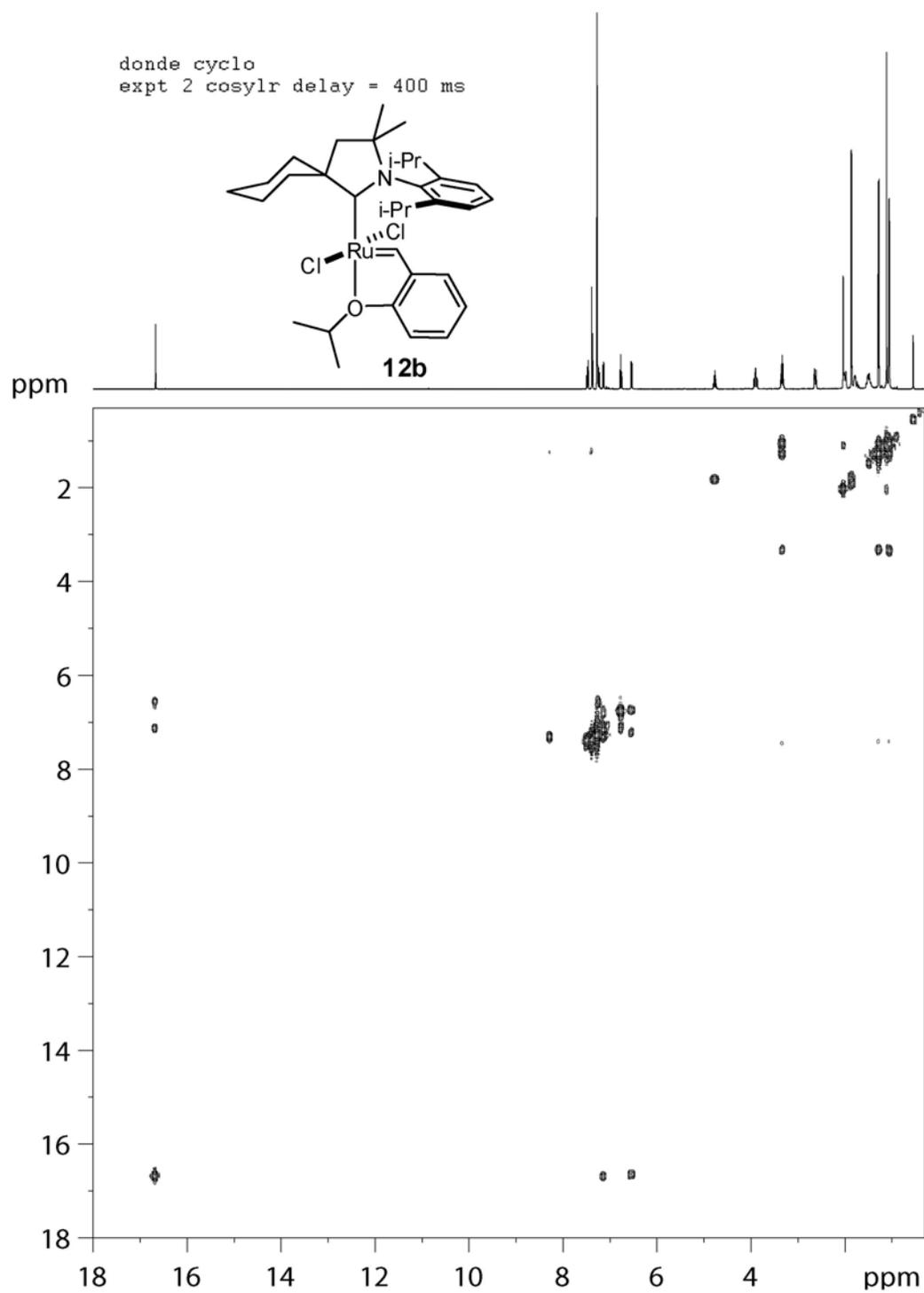
Figure 2.A11. 400 MHz ^{1}H-^{1}H COSYLR spectrum for **2.16b** in C_6D_6 at 22 °C.
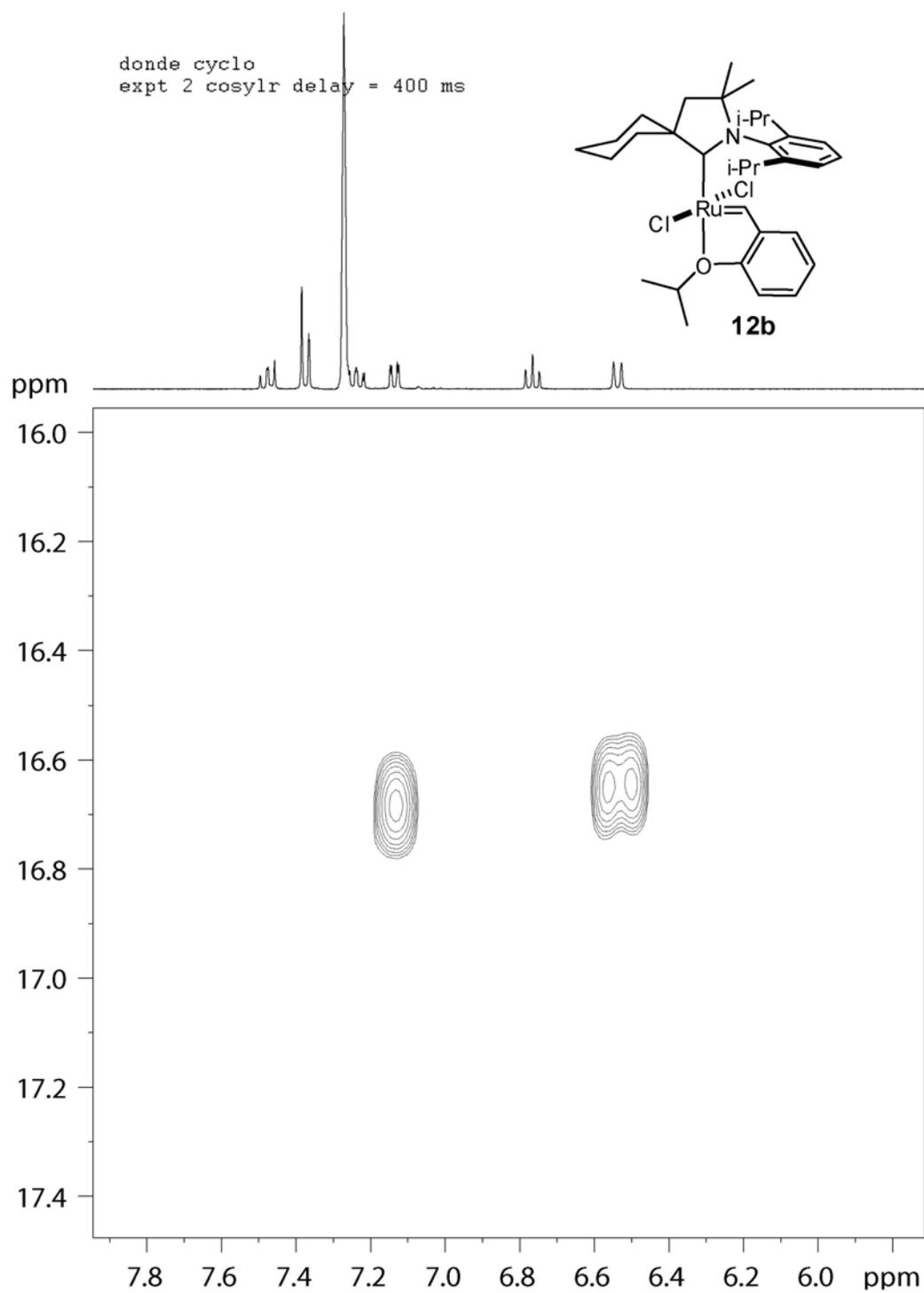
Figure 2.A12. 400 MHz ^{1}H-^{1}H COSYLR spectrum for **2.16b** in C_6D_6 at 22 °C.
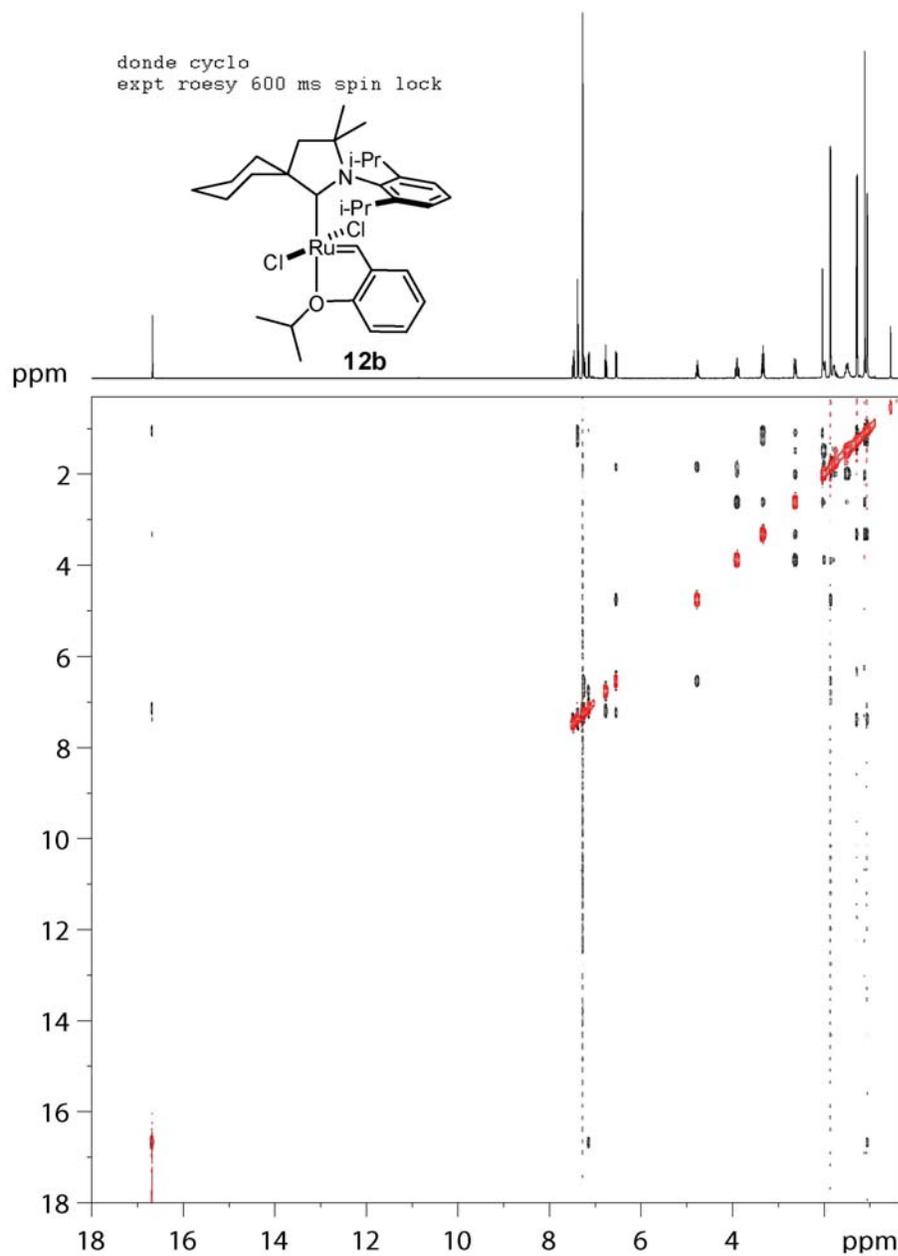
Figure 2.A13. 400 MHz ^{1}H-^{1}H ROESY spectrum for **2.16b** in C_6D_6 at 22 °C. Overhauser-derived crosspeaks are colored black, diagonal and exchange-derived crosspeaks are colored red.
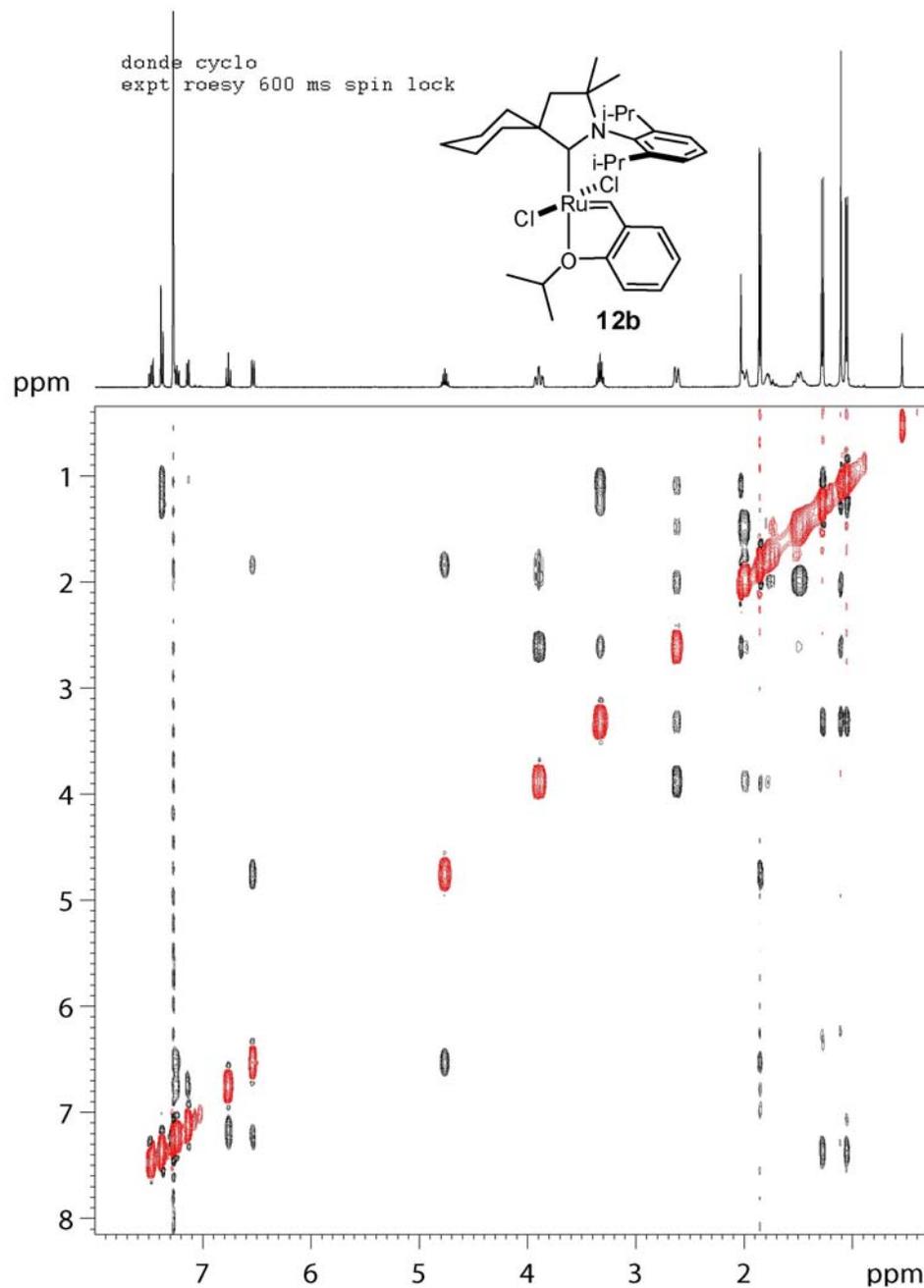
Figure 2.A14. 400 MHz ^{1}H-^{1}H ROESY spectrum for **2.16b** in C$_6$D$_6$ at 22 °C. Overhauser-derived crosspeaks are colored black, diagonal and exchange-derived crosspeaks are colored red.
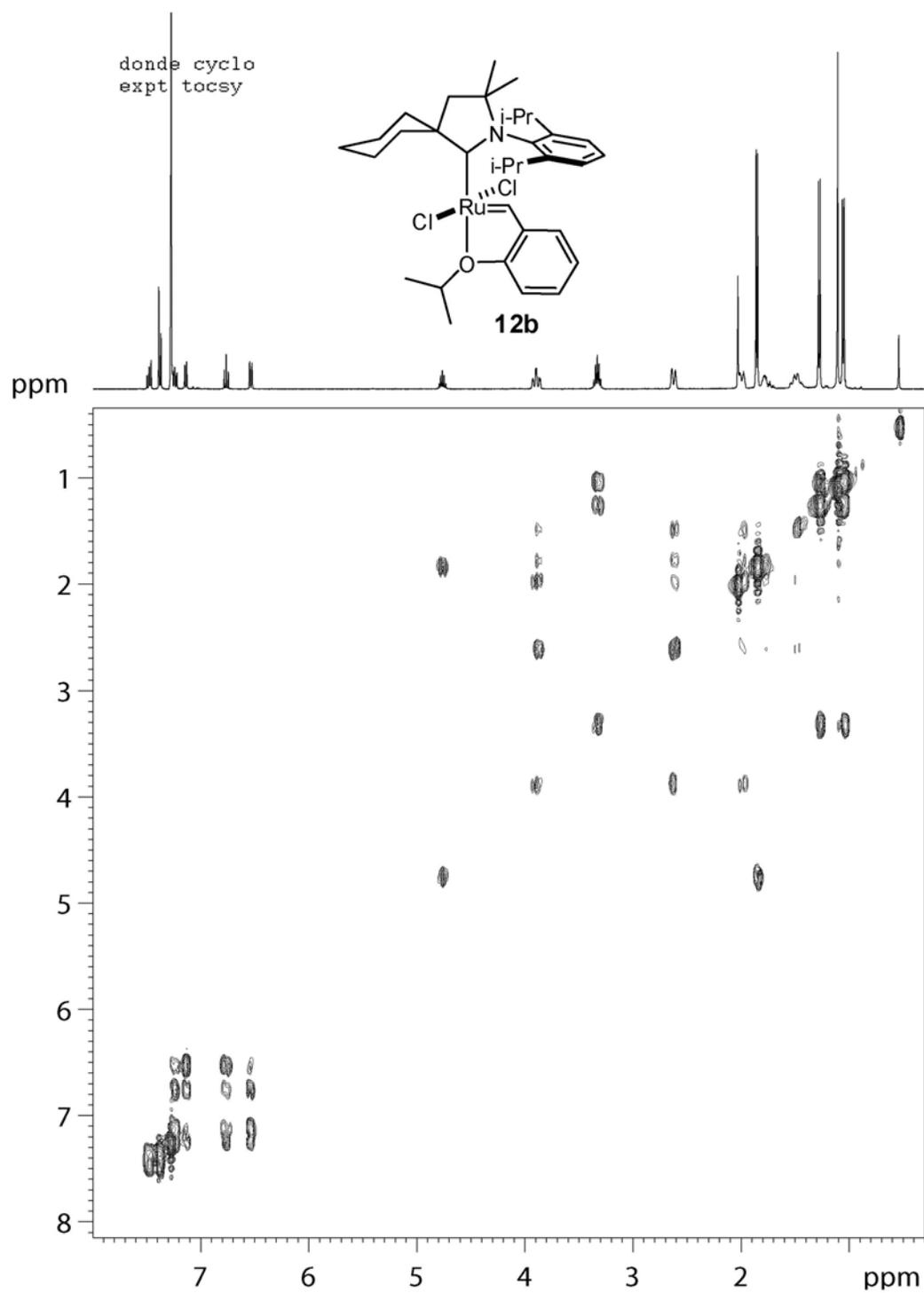
Figure 2.A15. 400 MHz ^{1}H-^{1}H TOCSY spectrum for **2.16b** in C$_6$D$_6$ at 22 °C.
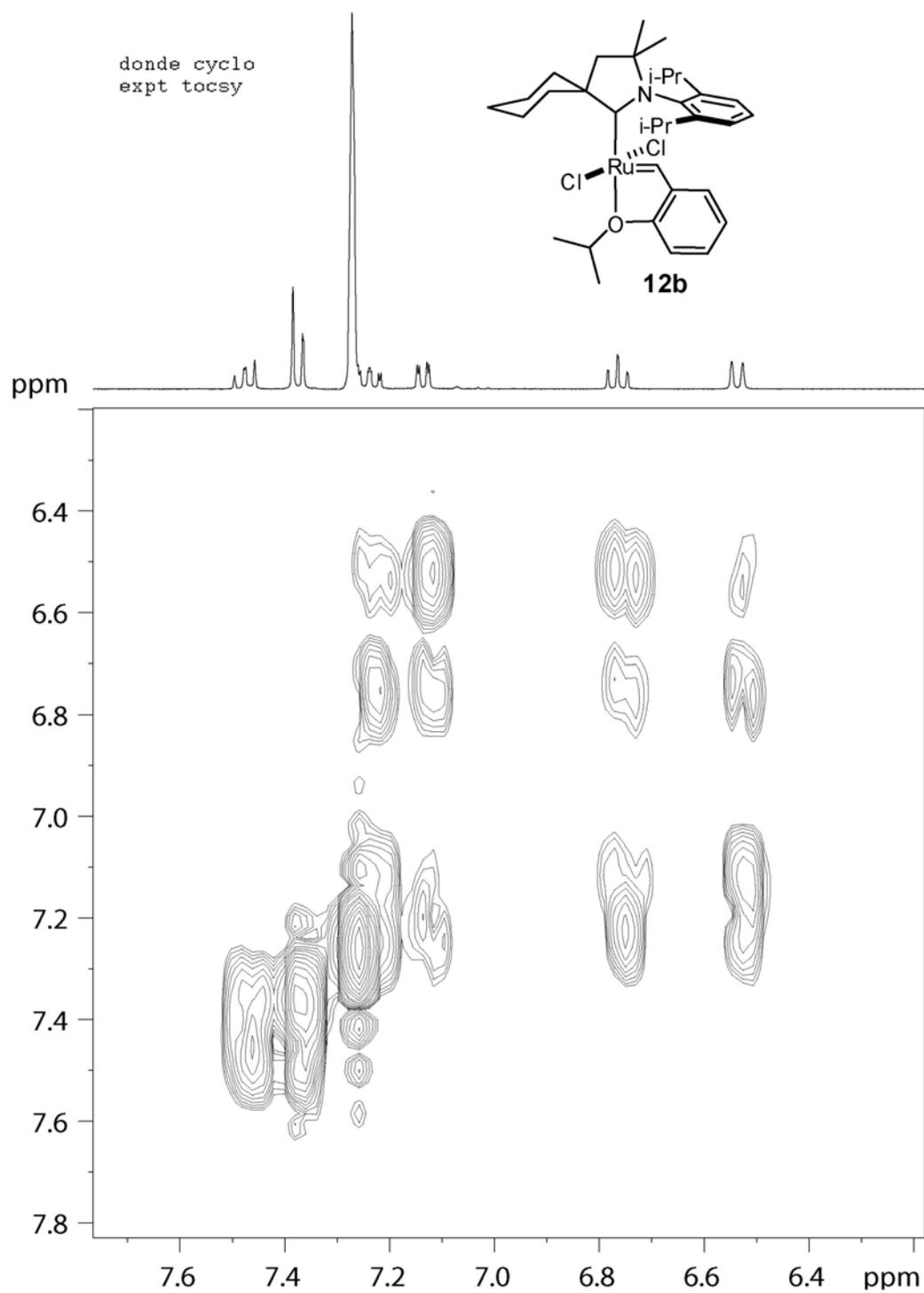
Figure 2.A16. 400 MHz ^{1}H-^{1}H TOCSY spectrum for **2.16b** in C_6D_6 at 22 °C.

References

(1)   Grubbs, R. H. *Handbook of Metathesis*; Wiley-VCH: Weinheim, 2003.

(2)   Ivin, K. J.; Mol, J. C. *Olefin Metathesis and Metathesis Polymerization*; Academic Press: San Diego, CA, 1997.

(3)   Schwab, P.; Grubbs, R. H.; Ziller, J. W. *J. Am. Chem. Soc.* **1996**, *118*, 100.

(4)   Nguyen, S. T.; Grubbs, R. H.; Ziller, J. W. *J. Am. Chem. Soc.* **1993**, *115*, 9858.

(5)   Scholl, M.; Ding, S.; Lee, C. W.; Grubbs, R. H. *Org. Lett.* **1999**, *1*, 953.

(6)   Garber, S. B.; Kingsbury, J. S.; Gray, B. L.; Hoveyda, A. H. *J. Am. Chem. Soc.* **2000**, *122*, 8168.

(7)   Yun, J.; Marinez, E. R.; Grubbs, R. H. *Organometallics* **2004**, *23*, 4172.

(8)   Despagnet-Ayoub, E.; Grubbs, R. H. *Organometallics* **2005**, *24*, 338.

(9)   Berlin, J. M.; Campbell, K.; Ritter, T.; Funk, T. W.; Chlenov, A.; Grubbs, R. H. *Org. Lett.* **2007**, *9*, 1339.

(10)   Stewart, I. C.; Ung, T.; Pletnev, A. A.; Berlin, J. M.; Grubbs, R. H.; Schrodi, Y. *Org. Lett.* **2007**, *9*, 1589.

(11)   Sanford, M. S.; Love, J. A.; Grubbs, R. H. *J. Am. Chem. Soc.* **2001**, *123*, 6543.

(12)   Thayer, A. M. *Chem. Eng. News* **2007**, *85*, 37.

(13)   Burdett, K. A.; Harris, L. D.; Margl, P.; Maughon, B. R.; Mokhtar-Zadeh, T.; Saucier, P. C.; Wasserman, E. P. *Organometallics* **2004**, *23*, 2027.

(14)   Deshmukh, P. H.; Blechert, S. *Dalton Trans.* **2007**, 2479.

(15)   Romero, P. E.; Piers, W. E. *J. Am. Chem. Soc.* **2007**, *129*, 1698.

(16)   Wenzel, A. G.; Grubbs, R. H. *J. Am. Chem. Soc.* **2006**, *128*, 16048.

(17)   Chatterjee, A. K.; Choi, T. L.; Sanders, D. P.; Grubbs, R. H. *J. Am. Chem. Soc.* **2003**, *125*, 11360.

(18)   Connon, S. J.; Blechert, S. *Angew. Chem. Int. Ed.* **2003**, *42*, 1900.

(19)   Ulman, M.; Grubbs, R. H. *Organometallics* **1998**, *17*, 2484.

(20)   Ritter, T.; Hejl, A.; Wenzel, A. G.; Funk, T. W.; Grubbs, R. H. *Organometallics* **2006**, *25*, 5740.

(21)   Lavallo, V.; Canac, Y.; Prasang, C.; Donnadieu, B.; Bertrand, G. *Angew. Chem. Int. Ed.* **2005**, *44*, 5705.

(22)   Lavallo, V.; Canac, Y.; DeHope, A.; Donnadieu, B.; Bertrand, G. *Angewandte Chemie, International Edition* **2005**, *44*, 7236.

(23)   Cavallo, L. *J. Am. Chem. Soc.* **2002**, *124*, 8965.

(24)   Jazzar, R.; Rian D., D.; Bourg, J.-B.; Donnadieu, B.; Canac, Y.; Bertrand, G. *Angew. Chem. Int. Ed.* **2007**, *46*, 2899.

(25)   Sanford, M. S.; Love, J. A.; Grubbs, R. H. *Organometallics* **2001**, *20*, 5314.

(26)   Dias, E. L. Ph.D., California Institute of Technology, 1998.

(27)   Hejl, A.; Day, M. W.; Grubbs, R. H. *Organometallics* **2006**, *25*, 6149.

(28)   Lloyd-Jones, G. C.; Alder, R. W.; Owen-Smith, G. J. J. *Chem. Eur. J.* **2006**, *12*, 5361.

(29)   Nyce, G. W.; Csihony, S.; Waymouth, R. M.; Hedrick, J. L. *Chem. Eur. J.* **2004**, *10*, 4073.

(30)   Arduengo, A. J., III; Calabrese, J. C.; Davidson, F.; Dias, H. V. R.; Goerlich, J. R.; Krafczyk, R.; Marshall, W. J.; Tamm, M.; Schmutzler, R. *Helv. Chim. Acta* **1999**, *82*, 2348.

(31)   Sole, S.; Gornitzka, H.; Schoeller, W. W.; Bourissou, D.; Bertrand, G. *Science* **2001**.

(32)   Korotikh, N. I.; Rayenko, G. F.; Shvaika, O. P.; Pekhtereva, T. M.; Cowley, A. H.; Jones, J. N.; Macdonald, C. L. B. *J. Org. Chem.* **1993**, *58*, 5762.

(33)   Ung, T.; Hejl, A.; Grubbs, R. H.; Schrodi, Y. *Organometallics* **2004**, *23*, 5399.

(34)   Hejl, A. Ph.D. thesis, California Institute of Technology, 2007.

(35)   Hejl, A. H. Ph.D., California Institute of Technology, 2007.

(36)   Courchay, F. C.; Sworen, J. C.; Wagener, K. B. *Macromolecules* **2003**, *36*, 8231.

(37)   Vehlow, K.; Maechling, S.; Blechert, S. *Organometallics* **2006**, *25*, 25.

(38)   Corma, A.; Iborra, S.; Velty, A. *Chem. Rev.* **2007**, *107*, 2411.

(39)   Kingsbury, J. S.; Harrity, J. P. A.; Bonitatebus, P. J.; Hoveyda, A. H. *J. Am. Chem. Soc.* **1999**, *121*, 791.

(40) Newman, T. H.; Rand, C. L.; Burdett, K. A.; Maughon, B. R.; Morrison, D. L.; Wasserman, E. P. 7119216, October 10, 2006.

(41) Forman, G. S.; McConnell, A. E.; Hanton, M. J.; Slawin, A. M. Z.; Tooze, R. P.; vanRensburg, W. J.; Meyer, W. H.; Dwyer, C.; Kirk, M. M.; Serfontein, D. W. *Organometallics* **2004**, *23*, 4824.

(42) Roelle, T.; Grubbs, R. H. *Chem. Commun.* **2002**, 1070.

(43) O. Daugulis, M. B. *Organometallics* **2002**, *21*, 5926.

(44) Hurd, R. *Journal of Magnetic Resonance* **1990**, *87*, 422.

(45) Bax, A.; Freeman, R. *Journal of Magnetic Resonance* **1981**, *44*, 542.

(46) Hwang, T.-L.; Shaka, A. *J. Am. Chem. Soc.* **1992**, *114*, 3157.

CHAPTER 3

Investigation of 3- and 6-membered Carbenes as Ligands for Ruthenium Olefin Metathesis Catalysts: Cyclopropenylidenes and 'Borazine'-like Carbenes

Introduction

　　To further improve olefin metathesis catalyst stability and activity, many ligands have been investigated. By replacing one phosphine ligand of the bis(phosphine) ruthenium complexe **3.1**[1] with an N-heterocyclic carbene (NHC) ligand, more stable and active catalysts such as **3.2**[2] and **3.3**[3] have been achieved (Chart 3.1). Recently, several NHC ligands have been utilized as ligands for ruthenium olefin metathesis catalysts, including unsymmetrical NHCs,[4,5] less bulky NHCs,[6-8] bulkier NHCs,[9,10] protic solvent solubility enhancing NHCs,[11-13] and 4-,[14] 5-,[15] and 6-membered non-traditional carbenes.[16,17] However, the synthesis of more efficient metathesis catalysts remains a challenging goal.[18,19]

Chart 3.1. Commonly utilized ruthenium olefin metathesis catalysts

3.1　　　　　　　**3.2**　　　　　　　**3.3**
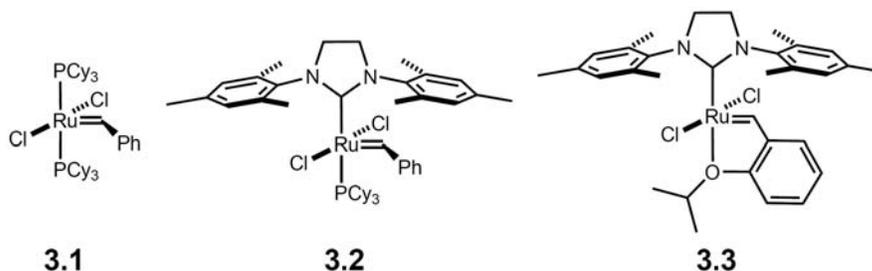
　　Recently, the Bertrand group reported the synthesis of several novel carbene architectures that are not based on the traditional 5-membered-ring framework, including cyclopropenylidenes[20,21] and six-π-electron six-membered-ring carbenes[22] containing a borazine-like core. We report herein the investigation of these new carbenes as ligands for ruthenium olefin metathesis catalysts.

Results and Discussion

Cyclopropenylidenes

Typically, deprotonation of the conjugate acid of a carbene provides the desired free carbene. Deprotonation of BPh_4^- salt **3.4** with KHMDS in Et_2O was previously reported to provide a modest 20% isolated yield of carbene **3.6** (Scheme 3.1).[20] Exchanging the BPh_4^- anion for BF_4^- enables the deprotonation of **3.5** with KHMDS at –78 °C in THF to yield carbene **3.6** with significantly fewer side products. An alternate synthetic route utilizes the addition of n-BuLi to BF_4^- salt **3.5** in Et_2O, to form lithium complex **3.7**, a polymeric material, in 48% yield.[21] Based on these results, the reactivity of several ruthenium precursors with complexes **3.6** and **3.7** was examined.

Scheme 3.1. Synthesis of **3.6** and **3.7**
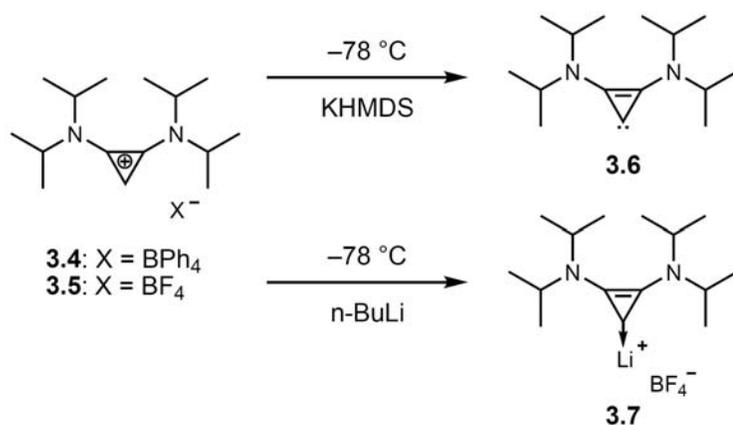
In situ deprotonation of **3.5** in the presence of ruthenium precursors **3.1**, **3.8** and **3.9** was attempted at –78 °C in THF (Chart 3.2). Deprotonation of **3.5** in the presence of ruthenium complex **3.1** led to the appearance of two new benzylidene resonances in the ^{1}H NMR spectrum (C_6D_6) of the reaction at 21.4 and 20.7 ppm (Scheme 3.2). In the presence of bispyridine adduct **3.8**, two new benzylidene resonances in the ^{1}H NMR

spectrum (C$_6$D$_6$) at 21.3 ppm and 20.7 ppm were observed. Additionally, deprotonation

of **3.5** in the presence of chelating-ether complex **3.9** led to three new benzylidene

resonances in the ^{1}H NMR spectrum (C$_6$D$_6$) at 18.4, 17.95 and 17.85 ppm. Unfortunately,

in all cases, no products could be isolated due to difficulties in product decomposition

and separation of product from starting materials.

Chart 3.2. Commonly-utilized ruthenium precursors

3.8   **3.9**
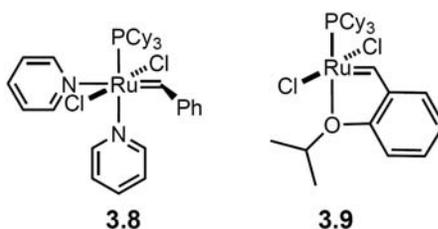
Scheme 3.2. In situ deprotonation of **3.5**
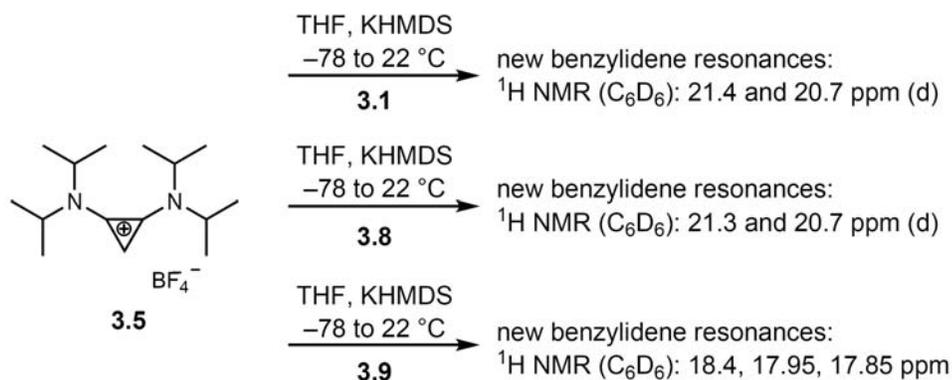
Transmetallation of complex **3.7** to bisphosphine precursor **3.1** in C$_6$D$_6$ at room

temperature did not proceed (Scheme 3.3). However, upon addition of 1 equiv **3.7** to

complex **3.8** in C$_6$D$_6$ at room temperature, evidence for two new benzylidene-containing

species at 21.4 and 21.3 ppm was observed by ^{1}H NMR spectroscopy. However, these

new products were formed in low conversions and could not be isolated.

**Scheme 3.3**. Transmetallation from lithium to ruthenium
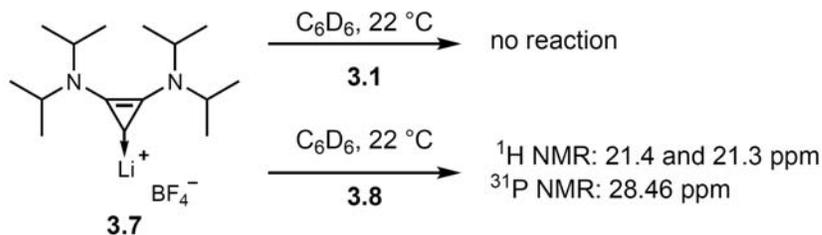
Although reactivity was observed between carbene complexes **3.6** and **3.7** and ruthenium precursors **3.1**, **3.8**, and **3.9**, the resulting compounds were formed in low yield and as a mixture of products. A higher-yielding synthetic route was targeted. Several methods for carbene generation have been reported in the literature; one facile route that has gained popularity recently is the synthesis of a silver carbene transmetallation reagent.[23] Typically, an imidazolium salt is added to 0.5 equiv of Ag_2O in the presence of 4 Å MS in CH_2Cl_2 to provide the desired silver carbene complex.[24] Upon addition of the silver carbene complex to the desired metal precursor, transmetallation is often achieved in good yields.

In the presence of Ag_2O and 4 Å MS, **3.5** underwent clean reaction to form a silver carbene complex (Scheme 3.4). However, due to the low coordinating ability of BF_4^-, bisligated, cationic silver complex **3.10** was formed. It has been previously shown that imidazolium salts with non-coordinating anions such as BF_4^- form bisligated cationic silver complexes.[24] Unfortunately, these complexes typically demonstrate low transmetallation ability. Indeed, complex **3.10** showed low reactivity with ruthenium complexes **3.1** and **3.8**.

Scheme 3.4. Synthesis and reactivity of bisligated silver carbene complex **3.10**
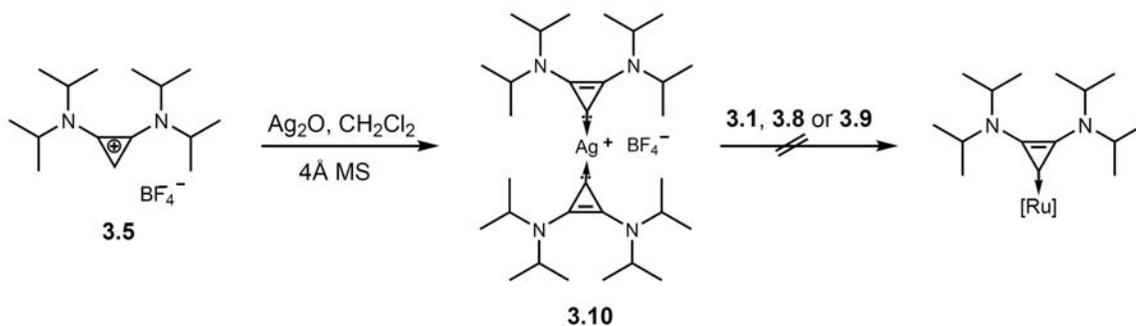
It has been demonstrated that the addition of a halide source, such as NBu$_4$Cl, to the reaction of an imidazolium salt containing a non-coordinating anion and Ag$_2$O leads to the formation of the desired mono-carbene silver chloride complex.[24] Upon addition of 1.1 equiv of NBu$_4$Cl to **3.5**, 0.5 equiv Ag$_2$O and 4 Å MS, the desired mono-ligated silver complex **3.11** is formed in good conversion (eq 3.1). Due to the high solubility of NBu$_4$BF$_4$ in organic solvents, separation from complex **3.11** was difficult to achieve. However, recrystallization from CH$_2$Cl$_2$/pentanes at –25 °C enabled isolation of pure **3.11**.

(3.1)
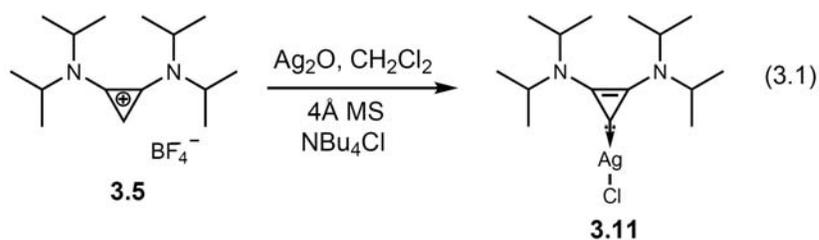
The purification of **3.11** through recrystallization had a dramatic effect on its reactivity with ruthenium precursors **3.1**, **3.8**, and **3.9**. Recrystallized **3.11** demonstrated much faster reaction rates (qualitative) and higher conversion to products than unrecrystallized **3.11** (Figure 3.1). Based on ^{1}H and ^{31}P NMR data, complexes **3.12** and

3.13 are hypothesized to be formed in these reactions; other complexes present may include a pyridine-bound complex or bis-ligated cyclopropenylidene-ruthenium complex. Unfortunately, attempts to isolate any products through column chromatography (under air or Ar), precipitation or recrystallization on a non-NMR scale were unsuccessful. Additionally, product decomposition was observed in crude reactions allowed to sit at room temperature for several hours, which may reflect the instability of the ruthenium-cyclopropenylidene complexes formed.
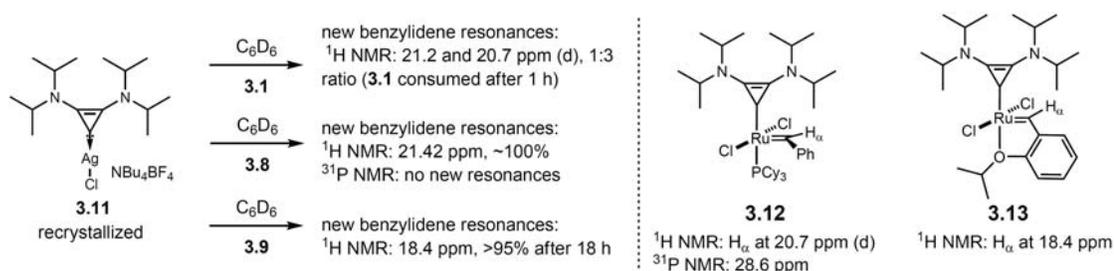

**Figure 3.1**. Reactivity of **3.11** with several ruthenium precursors.

6-membered NHCs

In 2005, Bertrand and co-workers reported the synthesis of a new 6-membered carbene based on a 'borazine'-like framework. By varying substituents on the nitrogen and boron atoms, these ligands can be separately electronically and sterically tuned.

We targeted carbenes **3.16** and **3.17**, which contain *N*-mesityl and *N*-cyclohexyl substituents, respectively. Salts **3.14** and **3.15** were cleanly deprotonated with KHMDS in C_6D_6 at room temperature to provide carbenes **3.16** and **3.17** (eq 3.2).

3.14: R = Mes, X = OTf
3.15: R = Cy, X = Br

3.16: R = Mes
3.17: R = Cy
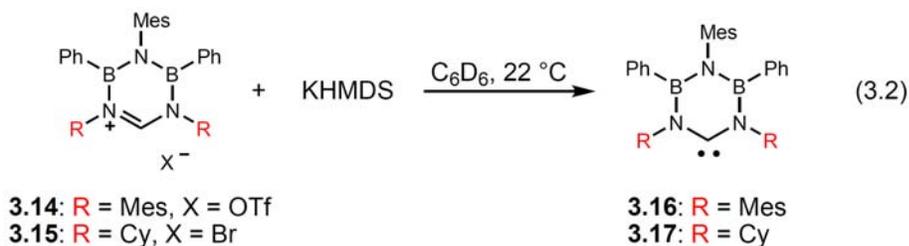
In the presence of a pyridine-containing ruthenium precursor **3.8**, **3.16** (formed in situ) forms a ruthenium complex with benzylidene resonance at 19.64 ppm; however, low conversion was observed under a variety of reaction conditions. In further reactivity studies, ruthenium precursor **3.9** and **3.16** form a new species with benzylidene resonance at 19.79 ppm after 2.5 hr at 50 °C (eq 3.3). This new complex **3.18** can be isolated by column chromatography in 51% yield.
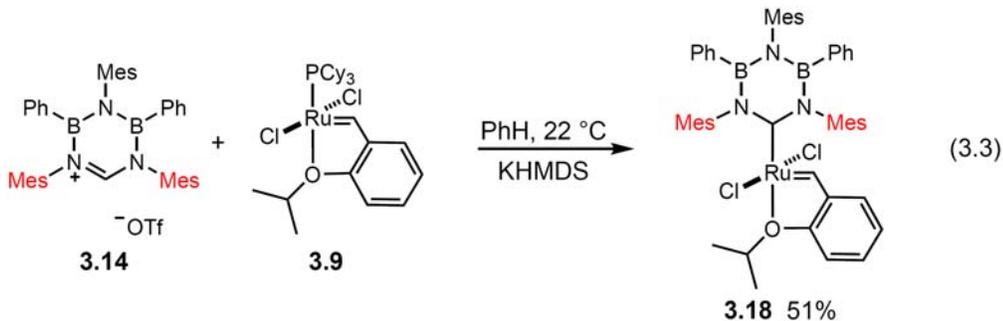
X-ray crystallographic analysis of **3.18** showed a square-pyramidal ruthenium center with the benzylidene moiety in the apical position (Figure 3.2). All bond lengths and angles are similar to those observed for complex **3.3**.
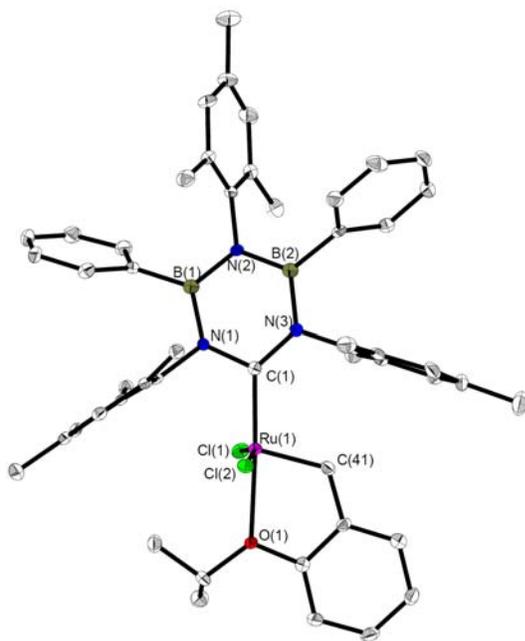
Figure 3.2. Structural drawing of **3.18**. Thermal ellipsoids drawn at 50% probability and hydrogens omitted for clarity. Selected bond distances (Å) and angles (deg): Ru–C(1) = 1.975(2), Ru–C(41) = 1.839(2), Ru–Cl(1) = 2.3489(6), Ru–Cl(2) = 2.3648(6), Ru–O(1) = 2.3072(15), Cl(1)–Ru–Cl(2) = 161.61(2), C(1)–Ru–O(1) = 174.19(8), C(41)–Ru–O(1) = 77.81(8).

Reactivity studies of carbene **3.17** with ruthenium precursors were also carried out. Due to the presence of a bromide counteranion in **3.15**, these reactions typically provided a mixture of complexes (starting material and product) in which zero, one or two chloride ligands on ruthenium have been exchanged for bromides. Although precursors **3.1** and **3.8** were examined in the presence of **3.17** (formed in situ), the resulting products were formed in low yield and were prone to decomposition. However, complex **3.19**, a mixture of halide isomers, was isolated from the reaction of **3.9** and **3.17** (formed in situ) (eq 3.4).
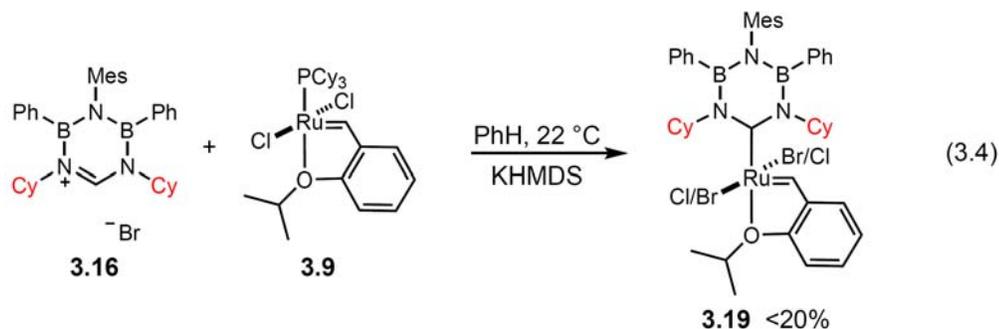
X-ray crystallographic analysis of **3.19** demonstrated the formation of a square-pyramidal ruthenium complex with the benzylidene moiety in the apical position (Figure 3.3). Interestingly, the plane of the carbene ring is twisted out-of-plane (with respect to the chelating benzylidene group), a possible result of steric crowding of the *N*-Cy group and benzylidene proton. All other bond lengths and angles are similar to those observed for **3.3** and **3.18**.
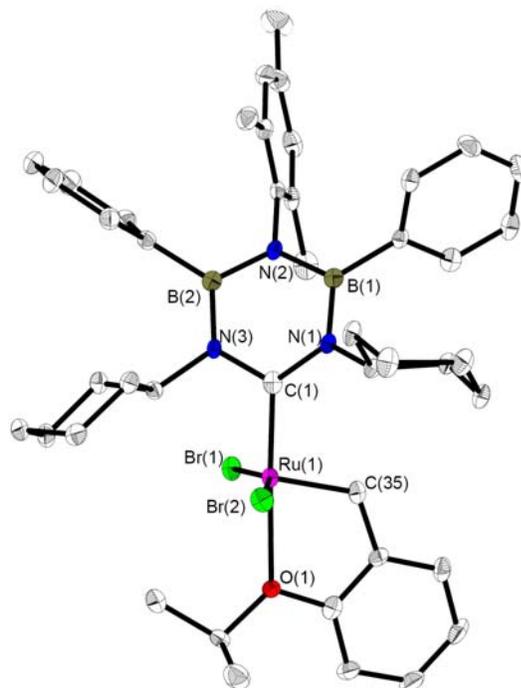

Figure 3.3. Structural drawing of **3.19**. Thermal ellipsoids drawn at 50% probability and hydrogens omitted for clarity. Selected bond distances (Å) and angles (deg): Ru–C(1) = 1.934(3), Ru–C(35) = 1.834(2), Ru–Br(1) = 2.342(10), Ru–Br(2) = 2.322(15), Ru–O(1) =

2.2959(18), Br(1)–Ru–Br(2) = 157.6(7), C(1)–Ru–O(1) = 175.35(8), C(35)–Ru–O(1) = 77.78(9).

The activity of catalyst **3.18** was examined in the ring-closing metathesis of diethyl diallylmalonate. Irreproducible conversions were measured by ^{1}H NMR spectroscopy. At best, 1 mol% catalyst **3.18**, yielded 66% of ring-closed product after 15 h at 40 °C in CD$_2$Cl$_2$, which is relatively low (catalysts **3.1**–**3.3** achieve > 95% conversion in < 45 min at 30 °C). The activity of catalyst **3.19** was not examined.

Summary

3- and 6-membered carbenes have been investigated as ligands for ruthenium olefin metathesis catalysts. Although a competent silver-cyclopropenylidene transmetallation complex was synthesized and demonstrated good reactivity with several ruthenium precursors, no ruthenium products were successfully isolated. In contrast, two new ruthenium complexes of 6-membered 'borazine'-like carbenes were synthesized and characterized by X-ray crystallography. Unfortunately, these complexes exhibited poor reactivity in the ring-closing metathesis of diethyl diallylmalonate.

Experimental

Catalyst **3.18**: To a 4-mL vial in the glovebox was added **3.14** (150 mg, 0.203 mmol), KHMDS (45 mg, 0.224 mmol) and benzene (ca. 1.5 mL). The reaction stirred for 30 min, filtered through celite and added to a 20-mL vial containing **3.9** (122 mg, 0.203 mmol). The vial was capped, taped, brought out of the glovebox, and placed in a 50 °C oil bath overnight. Upon concentration and purification by column chromatography (toluene), a green solid was isolated (60 mg, 51%). ^{1}H NMR (C$_6$D$_6$, 300 MHz): δ =

16.27 (s, 1H, Ru=C*H*Ar), 7.42-6.33 (m, 20H), 4.42 (sept, J = 6.3 Hz, 1H), 2.83 (s, 6H), 2.57 (s, 6H), 2.27 (s, 6H), 2.09 (d, 6H, J = 6.3 Hz), 1.68 (s, 3H) 1.11 (s, 3H), 1.09 (s, 3H); HRMS (FAB) *m*/*z* (%): 907.2995 [M]$^+$ (100%).

Catalyst **3.19**: To a 20-mL vial in the glovebox was added **3.15** (125 mg, 0.21 mmol), KHMDS (46 mg, 0.23 mmol), **3.9** (114 mg, 0.19 mmol) and PhH (4–5 mL). The vial was capped, taped, removed from the glovebox and placed in a 50 °C oil bath for 5 h. Upon concentration and purification by column chromatography (9:1 toluene:hexanes), a green solid was isolated (33mg, yield not determined). Major isomer: ^{1}H NMR (C$_6$D$_6$, 300 MHz): δ = 18.50 (s, 1H, Ru=C*H*Ar), 7.49 (dd, 1H, J = 1.5, 7.5 Hz), 7.42-7.26 (m, 5H), 7.11-6.89 (m, 5H), 6.75 (t, 1H, J = 7.8 Hz), 6.57 (d, 1H, J = 8.1 Hz), 6.30 (m, 1H), 5.67 (m, 1H), 4.84 (m, 1H), 4.72 (sept, 1H, J = 6.0 Hz), 3.10 (m, 2H), 2.41-2.25 (m, 2H), 2.14 (s, 3H), 2.08 (s, 3H), 1.81 (dd, 6H, J = 16, 6.0 Hz), 1.74-1.22 (m, 16H).

References

(1)   Schwab, P.; France, M. B.; Ziller, J. W.; Grubbs, R. H. *Angew. Chem. Int. Ed.* **1995**, *34*, 2039.

(2)   Scholl, M.; Ding, S.; Lee, C. W.; Grubbs, R. H. *Org. Lett.* **1999**, *1*, 953.

(3)   Garber, S. B.; Kingsbury, J. S.; Gray, B. L.; Hoveyda, A. H. *J. Am. Chem. Soc.* **2000**, *122*, 8168.

(4)   Vehlow, K.; Maechling, S.; Blechert, S. *Organometallics* **2006**, *25*, 25.

(5)   Vougioukalakis, G. C.; Grubbs, R. H. *Organometallics* **2007**, *26*, 2469.

(6)   Stewart, I. C.; Ung, T.; Pletnev, A. A.; Berlin, J. M.; Grubbs, R. H.; Schrodi, Y. *Org. Lett.* **2007**, *9*, 1589.

(7)   Berlin, J. M.; Campbell, K.; Ritter, T.; Funk, T. W.; Chlenov, A.; Grubbs, R. H. *Org. Lett.* **2007**, *9*, 1339.

(8)   Ritter, T.; Day, M. W.; Grubbs, R. H. *J. Am. Chem. Soc.* **2006**, *128*, 11768.

(9)   Dinger, M. B.; Mol, J. C. *Adv. Synth. Catal.* **2002**, *344*, 671.

(10)   Courchay, F. C.; Sworen, J. C.; Wagener, K. B. *Macromolecules* **2003**, *36*, 8231.

(11)   Hong, S. H.; Grubbs, R. H. *J. Am. Chem. Soc.* **2006**, *128*, 3508.

(12)   Gallivan, J. P.; Jordan, J. P.; Grubbs, R. H. *Tetrahedron Lett.* **2005**, *46*, 2577.

(13)   Jordan, J. P.; Grubbs, R. H. *Angew. Chem. Int. Ed.* **2007**, *46*, in press.

(14)   Despagnet-Ayoub, E.; Grubbs, R. H. *Organometallics* **2005**, *24*, 338.

(15)   Anderson, D. R.; Lavallo, V.; O'Leary, D. J.; Bertrand, G.; Grubbs, R. H. *Angew. Chem. Int. Ed.* **2007**, *119*, in press.

(16)   Yun, J.; Marinez, E. R.; Grubbs, R. H. *Organometallics* **2004**, *23*, 4172.

(17)   Yang, L. R.; Mayr, M.; Wurst, K.; Buchmeiser, M. R. *Chem. Eur. J.* **2004**, *10*, 5761.

(18)   Deshmukh, P. H.; Blechert, S. *Dalton Trans.* **2007**, 2479.

(19)   Thayer, A. M. *Chem. Eng. News* **2007**, *85*, 37.

(20)   Lavallo, V.; Canac, Y.; Donnadieu, B.; Schoeller, W. W.; Bertrand, G. *Science* **2006**, *312*, 722.

(21)   Lavallo, V.; Ishida, Y.; Donnadieu, B.; Bertrand, G. *Angew. Chem. Int. Ed.* **2006**, *45*, 6652.

(22)   Praesang, C.; Donnadieu, B.; Bertrand, G. *J. Am. Chem. Soc.* **2005**, *127*, 10182.

(23)   Herrmann, W. A. *Angew. Chem. Int. Ed.* **2002**, *41*, 1290.

(24)   Garrison, J. C.; Youngs, W. J. *Chem. Rev.* **2005**, *105*, 3978.

CHAPTER 4

Model Compounds of Ruthenium-Alkene Intermediates
in Olefin Metathesis Reactions

This chapter was taken in part from:

Anderson, D. R.; Hickstein, D. D.; O'Leary, D. J.; Grubbs, R. H. *J. Am. Chem. Soc.* **2006**, *128*, 8386.

Anderson, D. R.; O'Leary, D. J.; Grubbs, R. H. *Organometallics*, **2007**, submitted.

<u>Introduction</u>

With the advent of well-defined and stable catalysts, olefin metathesis has become a versatile synthetic tool for carbon-carbon double bond construction.[1,2] Among reported olefin metathesis catalysts, **4.1**[3,4] and **4.2**[5] have received significant attention from and widespread use by synthetic chemists due to their activity, functional-group tolerance and commercial availability.[6-10]

The general mechanism for transition-metal-catalyzed olefin metathesis, as proposed by Chauvin and co-workers, involves olefin binding to a metal alkylidene species, metallacyclobutane formation and subsequent generation of another olefin and metal alkylidene species.[11] Previous mechanistic studies of **1**[12] and **2**[13,14] in olefin metathesis reactions have focused on catalyst initiation and demonstrated that phosphine dissociates to generate coordinatively unsaturated ruthenium alkylidene species **3**, which can then bind an olefin and enter the catalytic cycle (Scheme 4.1). These studies enabled the design and synthesis of catalysts with higher initiation rates for use in living polymerizations.[15] However, few experimental studies[16,17] have been performed to provide an understanding of olefin binding geometry and metallacyclobutane formation;[18] these steps in the catalytic cycle are essential to the rational design of diastereoselective and enantioselective[19,20] catalysts.

Scheme 4.1. Initial steps of the mechanism of olefin metathesis
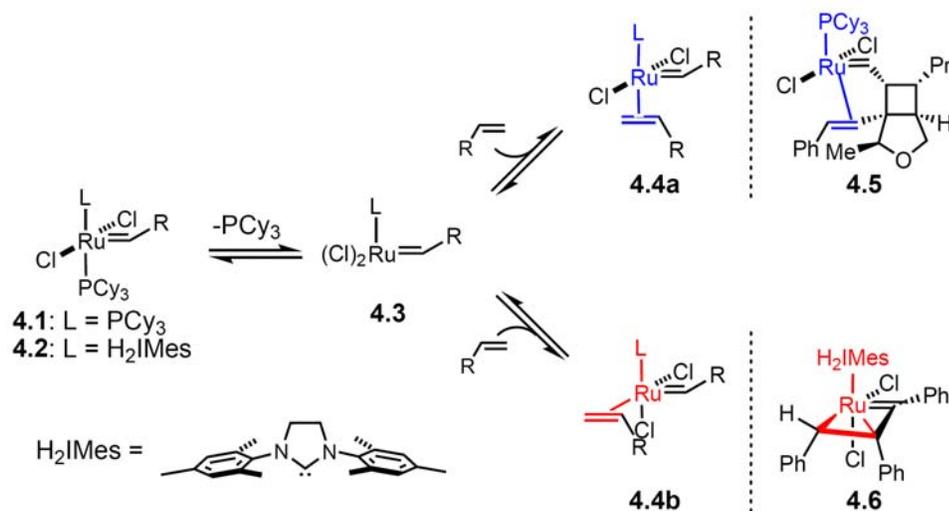
Postulated olefin binding scenarios include intermediate **4.3** either binding olefin preferentially trans (**4.4a**) or cis (**4.4b**) to the L-type ligand, or binding olefin non-preferentially through a mixture of intermediates **4.4a** and **4.4b**. (Scheme 4.1). Snapper and co-workers isolated complex **4.5** in which a chelating olefin is tethered through the alkylidene and coordinates trans to the PCy$_3$ ligand (bottom-bound).[21] Additional evidence for a bottom-bound mechanism was provided by Piers and co-workers who observed a C_{2v} symmetric ruthenacyclobutane by ^{1}H NMR spectroscopy.[10] Complex **4.6** was isolated by our group from the reaction of **4.2** and diphenylacetylene.[22] Although the bonding in **4.6** lies between a ruthenacyclopropane and a ruthenium-olefin complex, it is suggestive of a side-bound olefin intermediate. However, no studies have synthesized ruthenium-olefin adducts bearing *N*-heterocyclic carbenes (NHCs), ligands that enable the high activity, stability and selectivity observed for chiral and achiral olefin metathesis catalysts.

To study olefin binding in NHC-based ruthenium catalysts, we hypothesized that utilizing a chelating alkylidene would enable the isolation of stable complexes. Upon

addition of the ligand precursor diene to an appropriate ruthenium precursor, productive

metathesis would result in the desired ruthenium-olefin complex. Undesired reactions

include ring-closing metathesis and oligomerization of the diene. Additionally, to

facilitate the formation of a single ruthenium-olefin complex, a symmetrical diene

precursor was targeted.

Scheme 4.2. Synthetic strategy for ruthenium-olefin complexes

desired
Ru-olefin complex
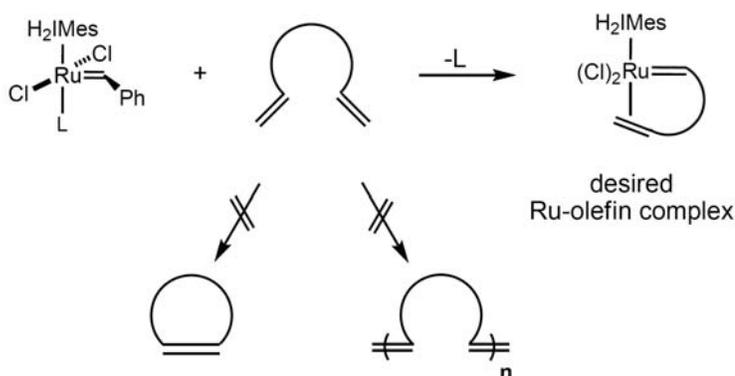
Results and Discussion

We chose to explore 1,2-divinylbenzene (**4.8**) as a chelating ligand precursor due

to its inability to undergo ring-closing metathesis and expected slow oliogomerization.[23]

Upon addition of **4.8** to a solution of **4.7** in benzene, two new species in a ratio of 2:3 are

initially observed by ^{1}H NMR spectroscopy (eq 4.1). In CD_2Cl_2 both reaction products

display six magnetically inequivalent Me groups and geminal olefinic protons that are

significantly shifted upfield to 3.37–3.59 ppm in the ^{1}H NMR spectrum. These

complexes were found to be competent metathesis catalysts at elevated temperatures.[24]

We envisioned three possible structural isomers based on **4.4a** and **4.4b**: one isomer

featuring a bottom-bound olefin (**4.9a**), a geometry similar to previously synthesized

chelating *i*-Pr ether catalysts,[25] and two side-bound isomers in which the terminal

methylene can either point away from (**4.9b**) or towards (**4.9c**) the NHC ligand (Figure 4.1).
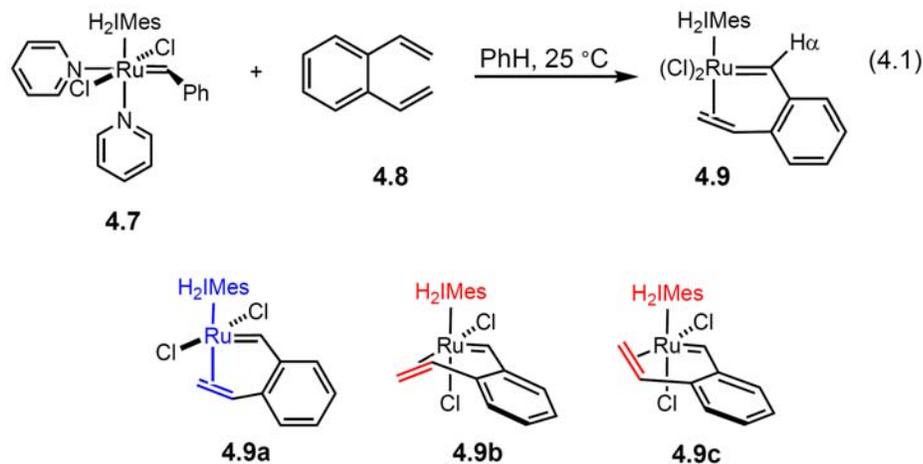
Figure 4.1. Structural isomers of **4.9**.

X-ray crystallographic analysis of crystals grown from slow diffusion of pentane into a CH$_2$Cl$_2$ solution of **4.9** showed a single compound, **4.9b**, in which the olefin is coordinated to ruthenium cis to the NHC (Figure 4.2). The C(29)–C(30) olefin bond length in **4.9b** (1.331(4) Å)[23] is close to that of free styrene (1.3245(16) Å),[26] suggesting a weak Ru-olefin interaction. However, the Ru–C(29) and Ru–C(30) bond lengths of **4.9b** (2.228(4) Å, 2.185(3) Å) are shorter than those found in **4.5** (2.362(5) Å, 2.339(5) Å) and **4.6** (2.356(4) Å, 2.221(4) Å).
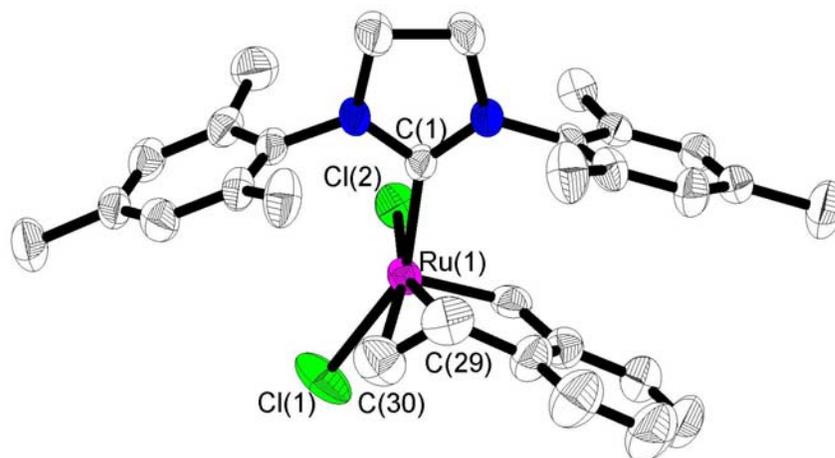
Figure 4.2. X-ray crystal structure of **4.9b**. Hydrogen atoms omitted for clarity. Thermal ellipsoids shown at 50% probability. Selected bond distances (Å) and angles (deg): Ru–C(1) =2.041(3), Ru–C(22) = 1.827(3), Ru–C(29) = 2.228(4), Ru–C(30) = 2.185(3), Ru–Cl(1) = 2.3926(9), Ru–Cl(2) = 2.3701(9), C(29)–C(30) = 1.331(4), Cl(1)–Ru–Cl(2) = 84.15(3), C(1)–Ru–Cl(1) = 152.57(9), C(30)–Ru–Cl(2) = 162.31(11).

A series of NMR spectroscopy experiments was performed to elucidate the geometry of the two compounds formed in eq 1. In 2D NOESY experiments, cross peaks are observed for the olefinic protons of each complex with Me groups on the mesityl rings (Figure 4.3). From consideration of internuclear distances in DFT-optimized structures,[27] these NOEs are consistent with side-bound complexes **9b** and **9c** but not bottom-bound compound **9a**. NOEs are observed for both isomers between H_b and a Me group on the mesityl ring. Complex **9b** would be expected to have NOEs between H_a and two Me groups on the mesityl rings; these are experimentally observed for the minor isomer. For compound **9c**, NOEs would be expected between H_c and two Me groups on the mesityl rings of the NHC and are observed for the major isomer. Based on this spectroscopic evidence, we assign **9b** as the minor isomer and **9c** as the major isomer observed in solution.
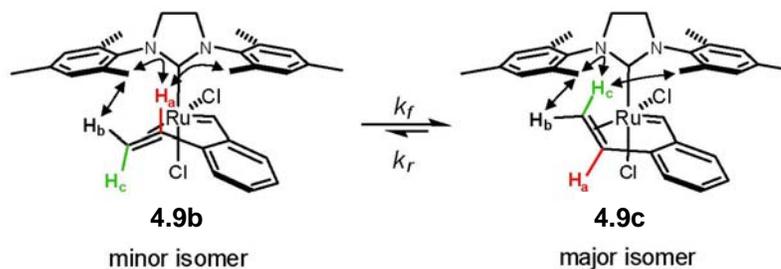
Figure 4.3. Structural assignments of solution isomers based on observed NOEs (indicated with arrows).

2D EXSY experiments reveal two dynamic exchange processes in complex **4.9** at 25 °C.[28] The first, observed only for isomer **4.9c**, is an *o*-Me group exchange ($k = 0.03$ s^{-1}) consistent with Ru–C$_{NHC}$ bond rotation.[29] The second process is **4.9b**↔**4.9c** interconversion, evidenced by exchange between all resolved **4.9b** and **4.9c** resonances. The forward rate constant (k_f) for this process was determined to be 0.08 ± 0.01 s^{-1}, which corresponds to $\Delta G^{\ddagger}_{298} = 18.9 \pm 0.1$ kcal/mol.

Variable-temperature ^{1}H NMR experiments of compounds **4.9b** and **4.9c** in CDCl$_2$CDCl$_2$ show coalescence of the benzylidene peaks at approximately 110 °C (Figure 4.4a–d). An Eyring analysis of the temperature-dependent forward rate constants, obtained from line shape analysis, was used to estimate the activation parameters. These are $\Delta H^{\ddagger} = 21.4 \pm 0.6$ kcal/mol, $\Delta S^{\ddagger} = 7.5 \pm 1.8$ eu. Therefore $\Delta G^{\ddagger}_{298} = 19.1 \pm 0.1$ kcal/mol, which is consistent with the EXSY-derived value.

Given the relatively high barrier to interconversion, we attempted to acquire a ^{1}H NMR spectrum at low temperature of the single compound identified by X-ray crystallography. Crystals dissolved in CD$_2$Cl$_2$ at −30 °C showed benzylidene protons in a 5:1 **4.9b**:**4.9c** ratio as compared to the room temperature ratio of 2:3 (Figures 4.4e,f).

Although not conclusive,[30] this is additional evidence for the **4.9b/4.9c** assignment described above.
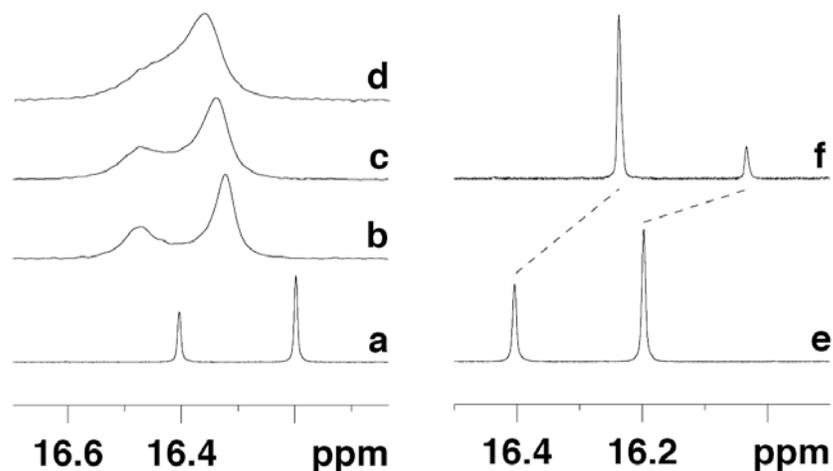

Figure 4.4. (a–d) Variable-temperature 400 MHz ^{1}H NMR data for the benzylidene resonances of a sample of adduct **4.9** dissolved in CDCl$_2$CDCl$_2$ at room temperature, with spectra recorded at a) 25 °C, b) 96 °C, c) 101 °C, and d) 106 °C. (e–f) 400 MHz ^{1}H NMR spectra of the benzylidene resonances of olefin adduct **4.9** dissolved and recorded in CD$_2$Cl$_2$ at e) 25 °C and f) −30 °C. The high field resonance is assigned to isomer **4.9c**.

Fluorinated NHC Complex

Recently, the increased initiation efficiency of complex **4.10** was reported and postulated to result from fluorine-assisted phosphine dissociation (Figure 4.5).[31] Although no solid-state Ru–F interaction is observed for complex **7**, possibly due to the steric bulk of the PCy$_3$ ligand, a Ru–F interaction (3.2 Å) is observed for chelating ether complex **4.11** in the solid state. Complex **4.12** was targeted to explore the effect of decreasing NHC steric bulk relative to H$_2$IMes and to determine if a Ru–F interaction could be observed in solid-state or solution-phase studies. Additionally, solution-phase structural analysis of complex **4.10** was performed for comparison with complex **4.12**.
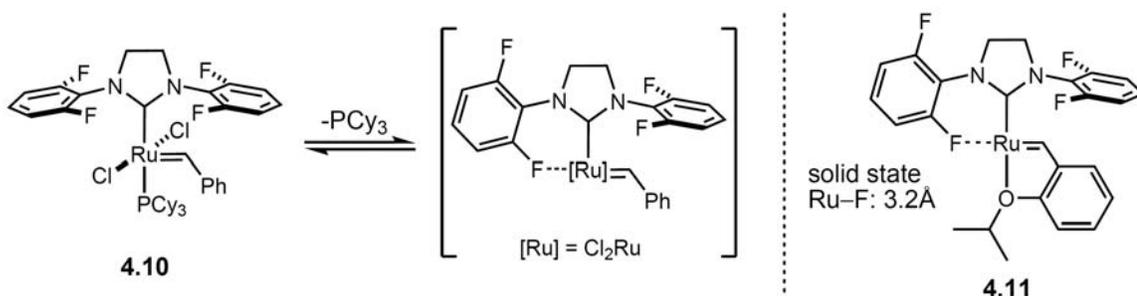
Figure 4.5. Ruthenium complexes of a fluorine-containing NHC.

Upon addition of 1,2-divinylbenzene (**4.8**) to complex **7** in C_6D_6, three new species with benzylidene resonances (H_α) at 17.44, 16.86, and 16.61 ppm are initially observed by ^{1}H NMR spectroscopy (eq 4.2). After 4 h at 22 °C, the resonance at 17.44 ppm is no longer observed. Upon precipitation with pentane, a yellow solid comprised of the two ruthenium-olefin complexes (isomers of **4.12**) with resonances at 16.57 and 16.42 ppm (1:1) in CD_2Cl_2 were isolated.
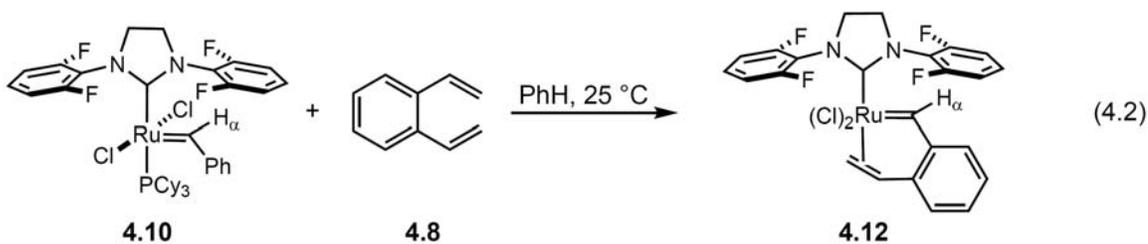
1D ^{1}H$\{^{19}$F$\}$ heteronuclear Overhauser (HOESY) experiments were performed to identify these isomers by examining possible through-space interactions between olefinic protons and the fluorine atoms on the NHC ligand (Figures 4.6, 4.7). The species with a benzylidene resonance at 16.57 ppm is assigned as isomer **4.12a** based on an HOE interaction between H_a and a fluorine resonance at –117.9 ppm in the ^{19}F NMR spectrum. The second species at 16.42 ppm is assigned as isomer **4.12b** due to an observed HOE interaction between H_c and a fluorine resonance at –118.2 ppm. HOE interactions are

also observed between fluorine resonances at −113.7 ppm and −115.7 ppm and benzylidene protons (H$_\alpha$) of **4.12a** and **4.12b**, respectively.
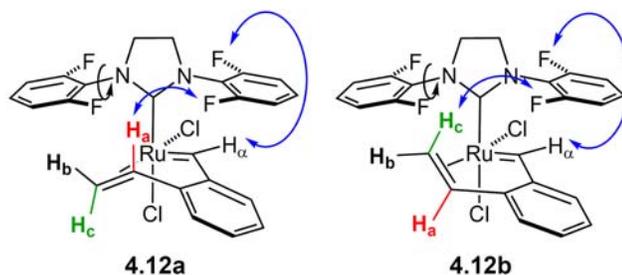

Figure 4.6. Structural assignment of solution isomers of **4.12** based on observed HOEs (blue arrows). Unhindered N–C bond rotation shown with black arrows.
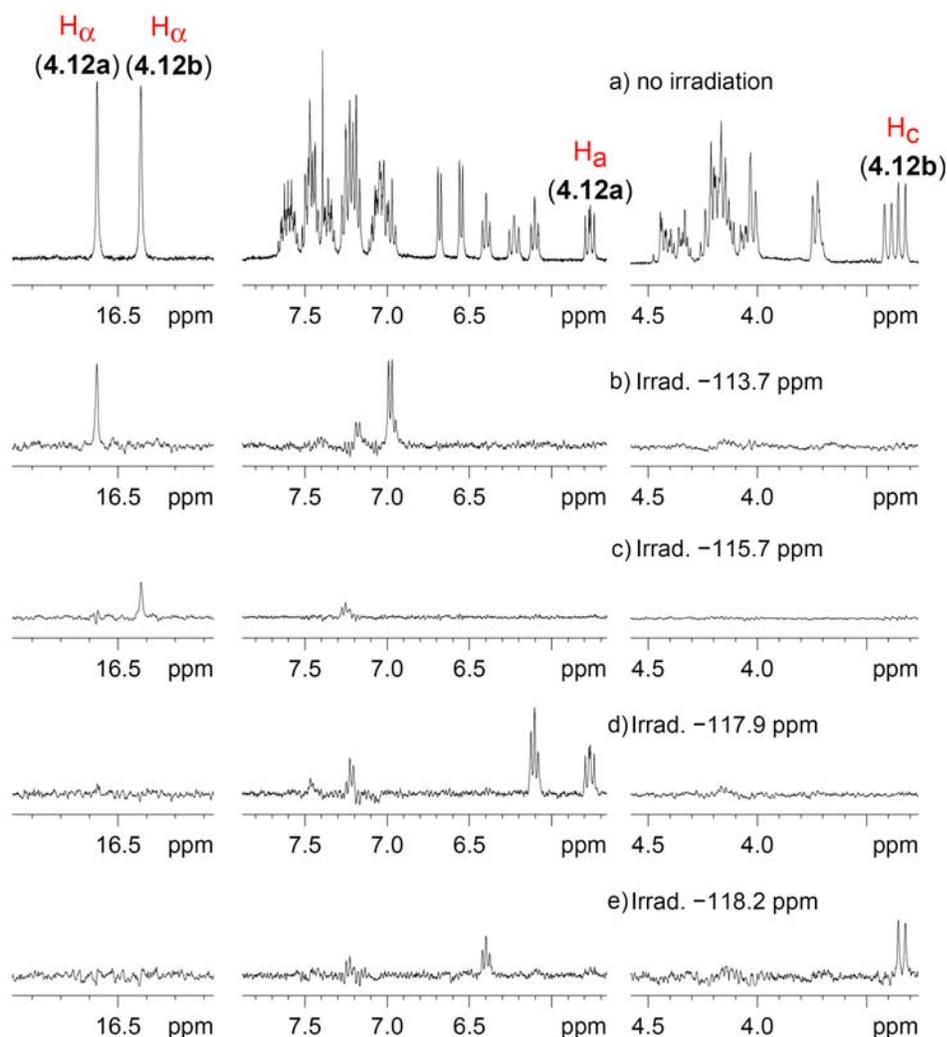

Figure 4.7. Benzylidene (H$_\alpha$) and olefin proton-containing portions of 1D ^{1}H-^{19}F HOESY spectra of **4.12a** and **4.12b** in CD$_2$Cl$_2$ after irradiation at a) no irradiation b) −113.7 ppm c) −115.7 ppm d) −117.9 ppm e) −118.2 pm.

The ^{19}F NMR spectrum of complexes **4.12a** and **4.12b** in 1:1 CD$_2$Cl$_2$:TCE-d_2 at room temperature displays 4 sharp peaks and one broad signal, rather than the 8 signals expected if the system is in slow exchange (Figure 4.8). We hypothesized that fast exchange at room temperature may broaden the 4 unobserved signals in the ^{19}F NMR spectrum; 8 fluorine resonances were observed when the sample was cooled to –85 °C. Together with the 1D HOESY data, these results are consistent with hindered rotation of the aryl ring near the quadrant containing the benzylidene moiety and free rotation of the aryl ring above the open quadrant at room temperature (Figure 4.6). For comparison, N–C bond rotation is not observed for complexes H$_2$IMes-substituted analogs **4.9a** and **4.9b**, although Ru–C$_{NHC}$ bond rotation is observed.
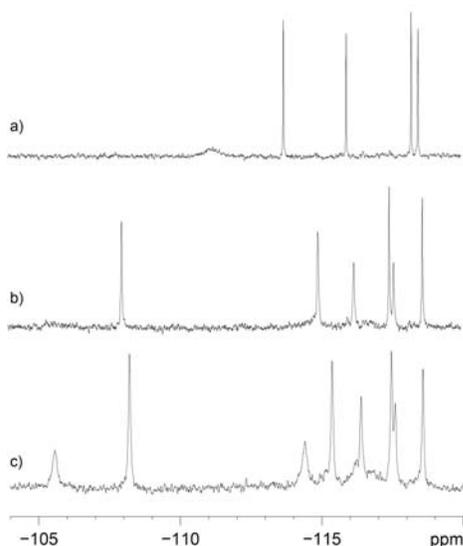

Figure 4.8. Variable-temperature ^{19}F NMR spectra for a solution of isomers **4.12a** and **4.12b** in 1:1 CD$_2$Cl$_2$/TCE-d_2 taken at a) 22 °C, b) –60 °C, c) –80 °C.

Several other NMR experiments were performed. No exchange between isomers **4.12a** and **4.12b** in CD$_2$Cl$_2$ at room temperature was observed in 2D-EXSY experiments. In the ^{1}H NMR spectrum of complexes **4.12a** and **4.12b**, the benzylidene protons are

observed to be quartets (Figure 4.9). ^{1}H-^{1}H coupling is observed between H_α and H_b between H and its ortho-disposed aromatic proton for both isomers (J = 1 Hz). Additionally, ^{1}H{^{19}F} decoupling experiments demonstrated that each benzylidene resonance is also coupled with a single fluorine resonance. We believe that this coupling is a result of a through-space, rather than through-bond interaction. Indeed, the H_a and any of the fluorine nuclei are separated by seven sigma bonds and the couplings involve specific pairs of nuclei. These results are also consistent with the observed HOE interactions between fluorine resonances at −113.7 ppm and −115.7 ppm and benzylidene protons (H_α) of **4.12a** and **4.12b**, respectively.
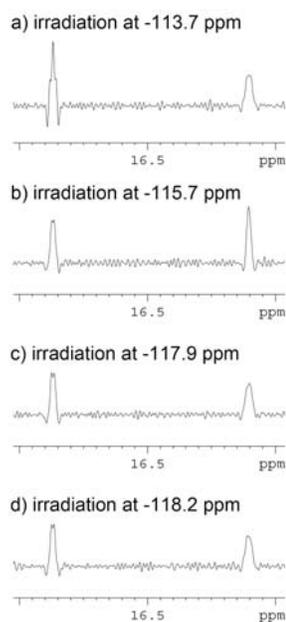

Figure 4.9. Benzylidene (H_α) region of ^{1}H{^{19}F} NMR spectra (Gaussian resolution enhanced) of **4.12a** and **4.12b** acquired with continuous-wave ^{19}F irradiation at frequencies a) −113.7 ppm b) −115.7 ppm c) −117.9 ppm d) −118.2 ppm to demonstrate spin-spin ^{1}H-^{19}F coupling.

Further investigation of the solution conformation of complex **4.10** via ^{19}F-^{19}F EXSY experiments demonstrated exchange of the two broad resonances observed in the

^{19}F NMR spectrum. The interconversion rate is ca. 84–88 s^{-1}. Based upon this exchange process and the two broad signals at room temperature, it is not possible to ascertain whether the source of hindered rotation is about the Ru-C$_{NHC}$ or N-C$_{aryl}$ bond. As a result of fluorine exchange, meaningful 1D ^{1}H-^{19}F HOESY data could not be acquired. Additionally, no discernible coupling of the benzylidene proton (H$_\alpha$) to any other nuclei was observed.

X-ray quality crystals grown from a solution of **4.12a** and **4.12b** provided a solid-state structure of side-bound isomer **4.12b** (Figure 4.10). The ruthenium center has a distorted square-pyramidal geometry. Unlike complex **7**, the NHC plane of complex **4.12a** is not significantly distorted from the ruthenium benzylidene plane. Although complex **4.12a** contains a side-bound olefin, the terminal methylene group of the olefin is directed toward the region of the NHC, unlike the solid-state structure obtained for complex **4.9b**. Interestingly, no evidence for a Ru—F interaction (shortest Ru···F = 3.82 Å) is observed despite a relatively open steric environment near the quadrant of the fluorinated aryl ring. The C–C bond length of the coordinated olefin is 1.383(3) Å, which is ca. 0.05 Å shorter than that of free styrene and complex **4.9b**. All other bond lengths and angles are similar to those observed for complex **4.9b**.
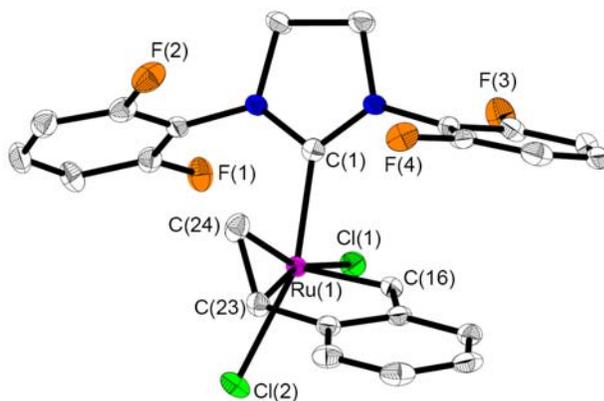
Figure 4.10. Solid-state drawing of **4.12b**. Thermal ellipsoids drawn at 50% and hydrogens omitted for clarity. Selected bond distances (Å) and angles (deg): Ru–C(1) = 2.0397(19), Ru–C(26) = 1.840(2), Ru–Cl(1) = 2.3865(5), Ru–Cl(2) = 2.3768(5), Ru–C(23) = 2.2283(19), Ru–C(24) = 2.203(2), C(23)–C(24) = 1.383(3), Cl(1)–Ru–Cl(2) = 87.941(18), C(1)–Ru–Cl(2) = 153.28(5), C(23)–Ru–Cl(1) = 162.84(5), C(24)–Ru–Cl(1) = 160.75(6).

Bulkier NHC Complex

To explore the effect of increasing the steric bulk of the NHC on olefin binding geometry, H$_2$DIPP-containing (H$_2$DIPP=1,3-di(2,6-diisopropylphenyl)-4,5-dihydroimidazol-2-ylidene) complexes were prepared. Upon addition of 1,2-divinylbenzene (**4.8**) to a solution of complex **4.13**[32] in benzene, two ruthenium-olefin complexes (isomers of **4.14**) with benzylidene resonances (H$_\alpha$) at 16.27 ppm and 16.58 ppm were isolated in a 97:3 ratio (eq 4.3).
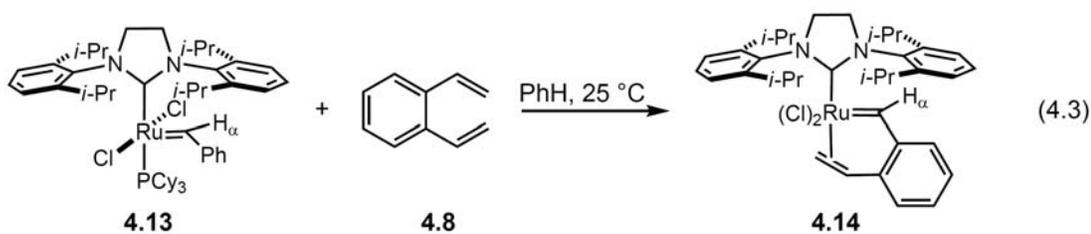
For the major isomer, 2D-NOESY experiments demonstrated Overhauser effects between olefinic proton H$_b$ and one Me group at 1.46 ppm (CD$_2$Cl$_2$), H$_c$ and two Me groups at 0.11 and 1.32 ppm (C$_6$D$_6$) and H$_c$ and an isopropyl methine proton at 2.35 ppm (C$_6$D$_6$) (Figures 4.11, 4.12). No crosspeaks were observed between H$_a$ and the isopropyl groups. Interestingly, an NOE interaction is also observed between the methine protons of proximal isopropyl groups spanning the the olefin binding site. These interactions are consistent with isomer **4.14a** in which the olefin is directed toward the NHC. Due to the low concentration of the minor isomer, no structural assignment could be made. 2D-

EXSY experiments did not show any exchange of the benzylidene protons of the major

(**4.14a**) and minor isomers in CD$_2$Cl$_2$ at 22 °C.
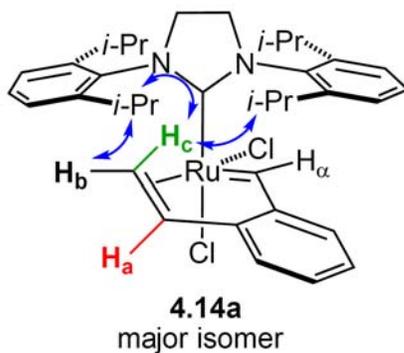
Figure 4.11. Structural assignment of major solution isomer of **4.14** based on observed NOEs (blue arrows).
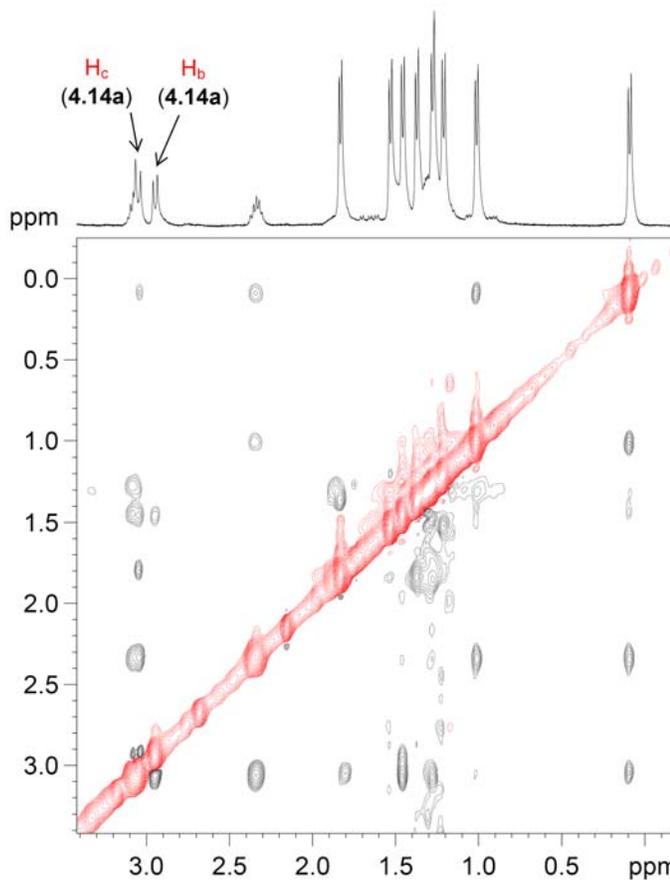

Figure 4.12. Olefin and alkyl-group region of a 2D-NOESY spectrum of **4.14** in CD$_2$Cl$_2$.

Several characteristic NMR shifts and couplings are observed for complex **4.14a**. The vicinal protons H_b and H_c are significantly shifted upfield to 3–4 ppm. Long-range COSY experiments indicate ^1H-^1H coupling between the benzylidene proton (H_α) and H_b of the coordinated olefin.

Interestingly, upon addition of **4.8** to complex **4.13**, a benzylidene resonance at 16.49 ppm is initially observed in the ^1H NMR spectrum of the crude reaction, but disappears after a few hours at room temperature (Figure 4.13). Unlike other observed intermediates, a relatively high conversion (25%) is initially observed. However, attempts to isolate or further characterize this intermediate by VT NMR spectroscopy were unsuccessful.
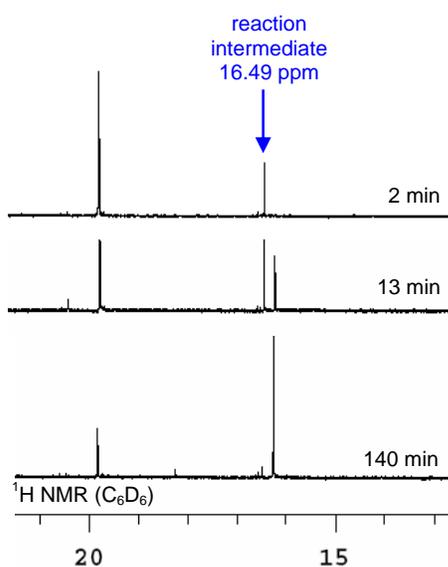
Figure 4.13. Benzylidene region (H_α) of ^1H NMR spectra of the reaction between **4.13** and **4.8** at different time points.

Although no suitable crystals of complex **4.14** could be isolated, ruthenium-containing decomposition products were characterized by X-ray crystallography. The solid-state structure obtained from these crystals show 3 components: free H_2DIPP, $O=PCy_3$ and hexacoordinate ruthenium center **4.15** (Figures 4.14, 4.15). The benzylidene

moiety has been oxidized to a benzoate group which acts as a chelating ligand for the Ru(IV) complex.
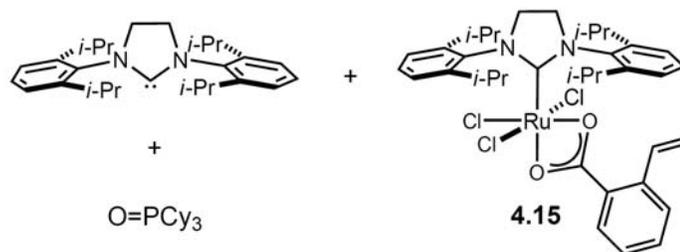
Figure 4.14. Decomposition products of complex **4.13**.
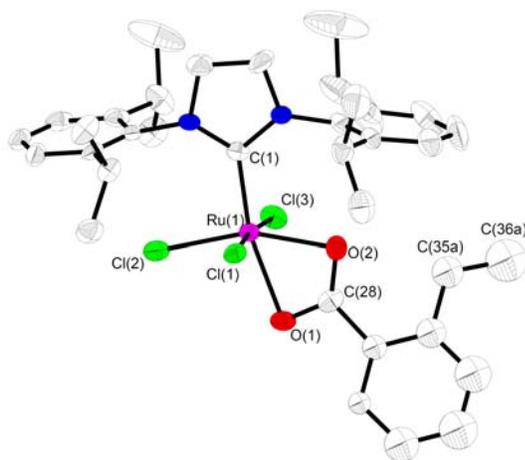
Figure 4.15. Solid-state drawing of **4.15**. Thermal ellipsoids drawn at 50% and hydrogens omitted for clarity. Selected bond distances (Å) and angles (deg): Ru–C(1) = 1.978(3), Ru–O(1) = 2.229(2), Ru–O(2) = 2.114(2), Ru–Cl(1) = 2.3529(8), Ru–Cl(2) = 2.3125(9), Ru–Cl(3) = 2.3247(9), Cl(1)–Ru–Cl(3) = 173.16(3), C(1)–Ru–O(1) = 165.36(10), Cl(2)–Ru–O(2) = 158.62(6).

Chiral NHC Complex

Chiral complex **4.16** was also investigated as a ruthenium precursor. Upon addition of **4.8** to **4.16** in pentane, 3 isomers with benzylidene resonances (H_α) at 16.25, 15.57 and 15.37 ppm are isolated in a 3:6:1 ratio (eq 4.4). Unlike previously investigated complexes, 4 side-bound ruthenium-olefin complexes (**4.17a–d**) are possible due to the mono-*ortho* substituted aryl groups on the NHC (Figure 4.16).

(4.4)
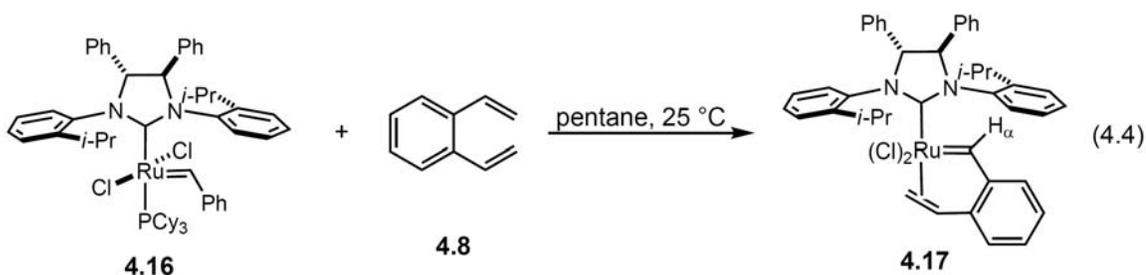
Overhauser effects were observed between H_b of both major isomers and Me groups on the NHC in 2D-NOESY experiments (Figure 4.16, 4.17). These isomers are assigned as **4.17a** and **4.17b** because it would not be expected that H_b of either **4.17c** or **4.17d** would be in close proximity to an isopropyl group. No NOEs are observed for H_c of either isomer with the isopropyl groups. The isomer in largest abundance ($H_\alpha = 15.57$ ppm) is assigned as isomer **4.17a** due to an observed NOE between H_c and an *ortho*-aryl proton on the NHC. The other major isomer ($H_\alpha = 16.25$ ppm) is assigned as isomer **4.17b** based on an observed NOE between H_a and a Me group of an isopropyl moiety. No assignment could be made for the isomer in smallest concentration ($H_\alpha = 15.37$ ppm) due to the absence of any diagnostic NOE crosspeaks.
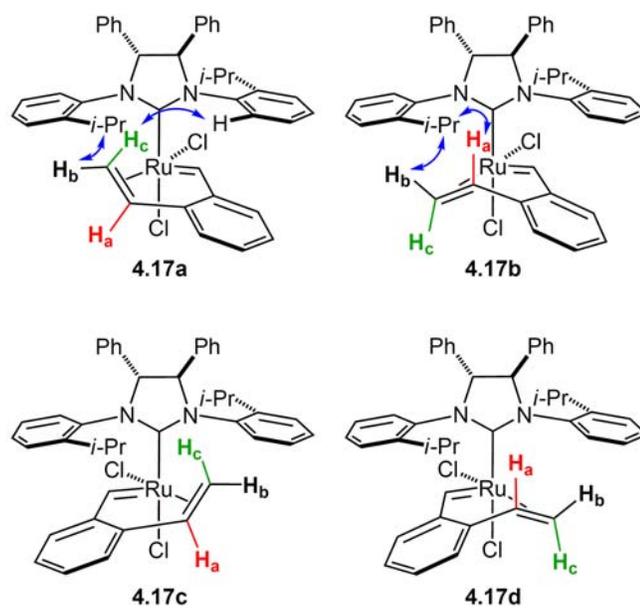
**Figure 4.16**. Possible side-bound geometries for complex **4.17**. Observed NOEs shown with blue arrows.
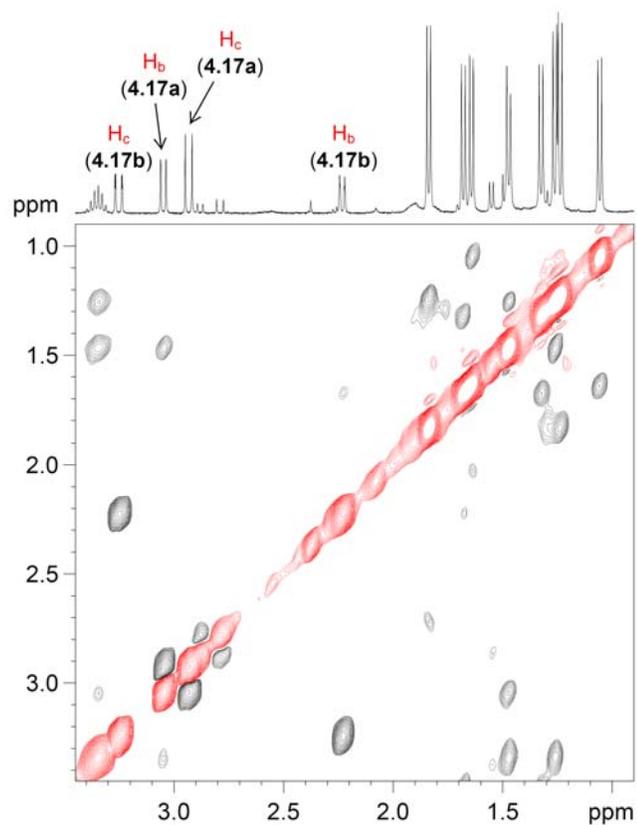
Figure 4.17. Olefin and alkyl-group region of a 2D-NOESY spectrum of **4.17** in CD_2Cl_2.

2D-EXSY experiments performed in CD_2Cl_2 at 19 °C and 40 °C did not reveal any exchange processes in this complex. Several characteristic NMR shifts and couplings are observed for the 3 isomers of **4.17**. Olefinic protons for all 3 observed isomers are shifted upfield to 2–3.5 ppm The benzylidene resonance (H_α) of **4.17a** exhibits a long-range coupling to H_b at 3.05 ppm; similarly, H_α of **4.17b** exhibits a long-range coupling to H_b at 2.23 ppm.

X-ray quality crystals grown from slow diffusion of pentane into a concentrated solution of **4.17** in THF provided a structure of side-bound olefin complex **4.17a** (Figure 4.18). The bond lengths and angles are similar to those observed for other ruthenium-olefin complexes.
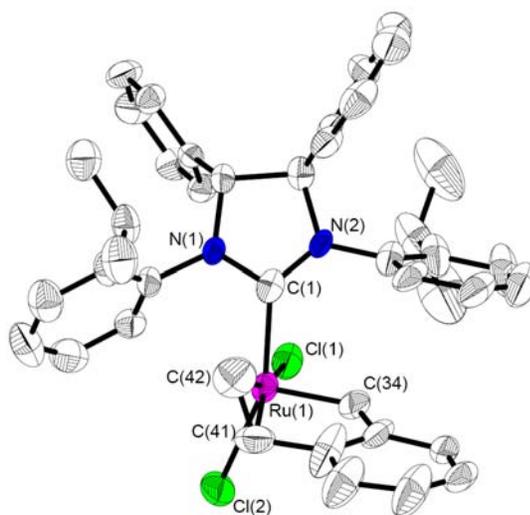
Figure 4.18. Solid-state drawing of **4.17a**. Thermal ellipsoids drawn at 50% and hydrogens omitted for clarity. Selected bond distances (Å) and angles (deg): Ru–C(1) = 2.045(5), Ru–C(26) = 1.849(5), Ru–C(41) = 2.227(6), Ru–C(42) = 2.184(6), Ru–Cl(1) = 2.4027(12), Ru–Cl(2) = 2.3881(12), C(41)–C(42) = 1.318(7), Cl(1)–Ru–Cl(2) = 86.81(5), C(1)–Ru–Cl(2) = 154.55(14), C(41)–Ru–Cl(1) = 163.82(15).

Phosphine Complex

To examine the possibility that phosphine and NHC complexes could have different preferred olefin-binding geometries, a phosphine analog to complexes **4.12**, **4.14**

and **4.17** was targeted. Bisphosphine complex **4.1**, in the presence of 1 equiv
divinylbenzene (**4.8**), showed low reactivity as monitored by ^{1}H NMR spectroscopy.
However, utilizing bispyridine complex **4.18** as a ruthenium precursor in presence of **4.8**,
two new ruthenium-olefin complexes (isomers of **4.19**) with benzylidene resonances (H$_\alpha$)
at 17.85 and 17.62 ppm were isolated in a 9:1 ratio (eq 4.5).

$$\text{(4.5)}$$
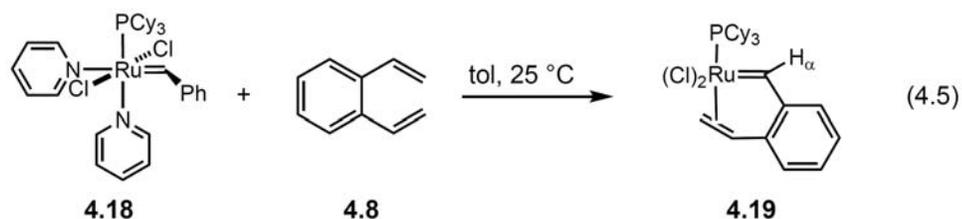
2D-NOESY experiments demonstrated cross peaks between olefinic proton H$_b$ of
the major isomer and cyclohexyl protons (Figures 4.19, 4.20). No NOE crosspeaks are
oberved for H$_a$ and the alkyl region. Olefinic proton H$_c$ overlaps with a cyclohexyl
resonance, thus making it difficult to determine if there are NOEs between H$_c$ and the
cyclohexyl protons. Thus, the major isomer is hypothesized to be either side-bound
isomer **4.19a** or **4.19b**. No cross peaks were observed for the minor isomer, which could
be a result of its low concentration.
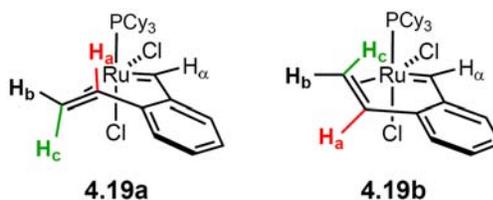
Figure 4.19. Possible side-bound geometries for complex **4.19**.
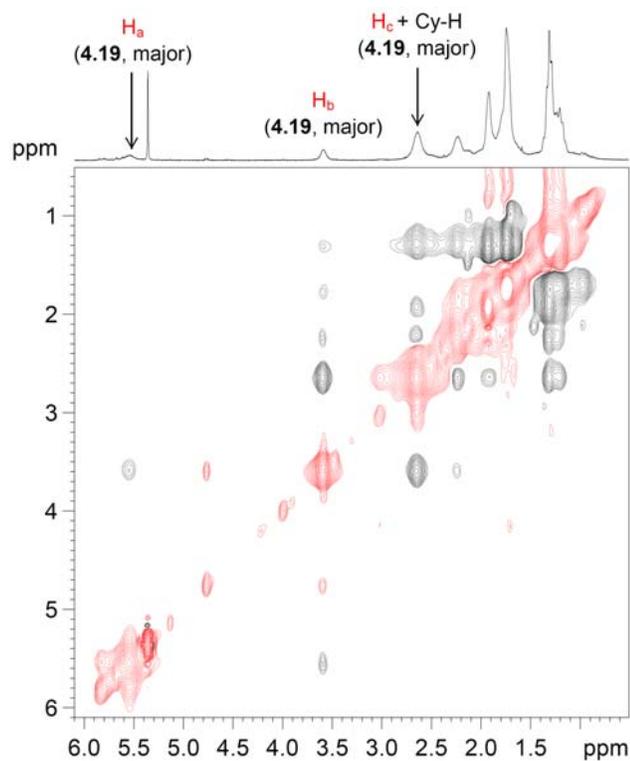
Figure 4.20. Olefin and alkyl-region of a 2D-NOESY/EXSY spectrum of **4.19**.

2D-EXSY experiments conducted in CD_2Cl_2 at room temperature demonstrated exchange between all olefinic protons of the major and minor isomers (Figure 4.20). The benzylidene resonances also undergo exchange (Figure 4.21).
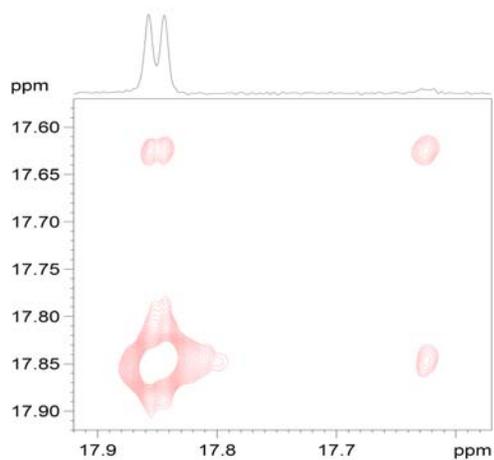
Figure 4.21. Benzylidene-containing region of a 2D-EXSY spectrum of **4.19**.

Crystals of **4.19** suitable for X-ray crystallography were unable to be grown. Unfortunately, the ruthenium olefin complex isomers of **4.19** decompose at room temperature in hours.

Bulkier Olefin Complex

To examine the steric effect of binding a 1,1-disubstituted olefin, diene **4.20** was synthesized in two steps from 2-bromostyrene (eq 4.6). Upon addition of **4.20** to a solution of bispyridine complex **4.7**, several new ruthenium-olefin complexes (isomers of **4.21**) are formed. In CD_2Cl_2, the two major benzylidene resonances are at 15.86 and 15.50 ppm (4:1).

(4.6)

4.7   **4.20**   **4.21**
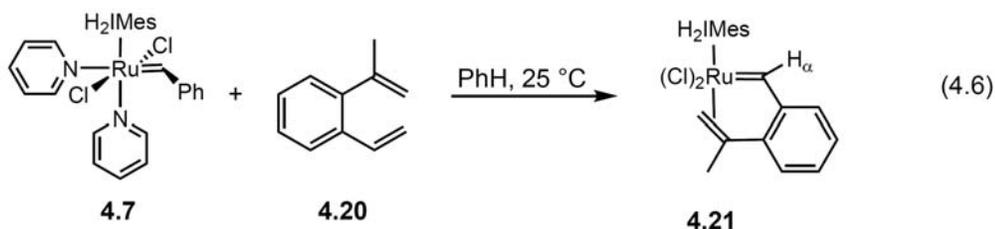
2D-NOESY experiments demonstrate NOEs between olefinic proton H_c of the major isomer (assigned based on HSQC and COSY-LR experiments) and Me groups of H_2IMes at 1.44 and 2.73 ppm (which are in exchange as indicated by 2D-EXSY experiments) (Figures 4.22, 4.23). These interactions are consistent with solution-phase structure **4.21a** in which the terminal methylene group of the olefin is directed toward the NHC.
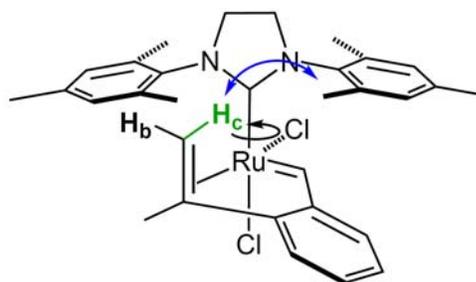
4.21a
major isomer

Figure 4.22. Structural assignment of major solution isomer of **4.21** based on an observed NOE (blue arrow). Ru–C$_{NHC}$ bond rotation shown with black arrow.
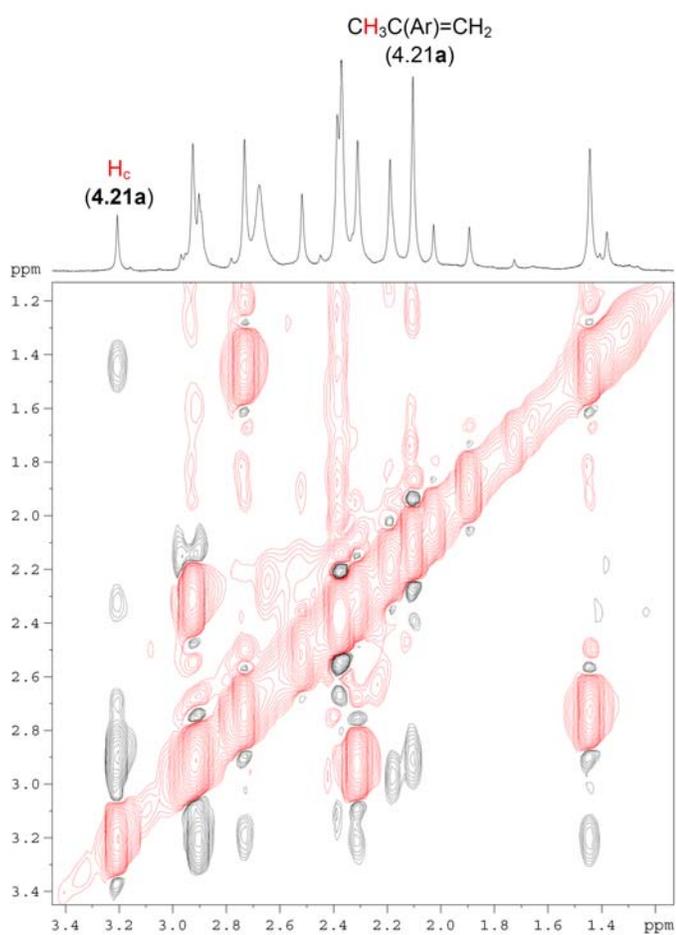
Figure 4.23. Olefin and alkyl-group region of a 2D-NOESY/EXSY spectrum of **4.21**.

2D-EXSY experiments demonstrate exchange of aryl, NHC backbone, and Me protons of **4.21a**, but not of benzylidene or olefinic protons. This data is consistent with hindered Ru–NHC rotation rather than interconversion of the two isomers.

COSYLR experiments indicate interactions between H_α and an adjacent aryl proton of **4.21a**. Additionally, a long-range interaction is observed between H_α and an olefinic proton H_b at 2.94 ppm. NOEs are also observed between H_α and two Me groups that are in exchange.

X-ray analysis of crystals grown from a solution of **4.21** shows a single molecular geometry, **4.21a**, in which H_2IMes and the chelated ligand are bound cis to one another (Figure 4.24). Bond lengths and angles are similar to other ruthenium-olefin complexes.
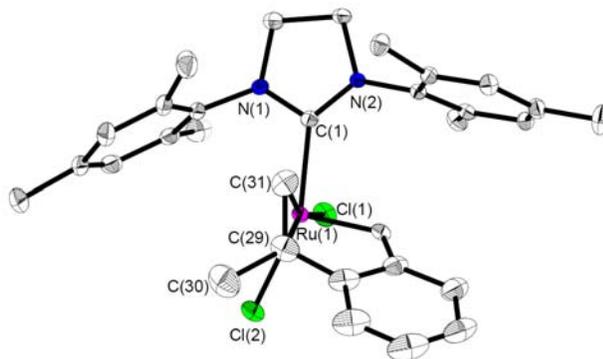
Figure 4.24. Solid-state drawing of **4.21a**. Thermal ellipsoids drawn at 50% and hydrogens omitted for clarity. Selected bond distances (Å) and angles (deg): Ru–C(1) = 2.063(2), Ru–C(26) = 1.825(2), Ru–Cl(1) = 2.4005(6), Ru–Cl(2) = 2.3781(6), Ru–C(29) = 2.249(2), Ru–C(31) = 2.167(3), C(29)–C(31) = 1.402(4), C(1)–Ru–Cl(2) = 153.37(6), Cl(1)–Ru–Cl(2) = 83.75(2), C(29)–Ru–Cl(1) = 160.33(8).

Aryl-substitued Dienes

For other chelating benzylidene or alkylidene complexes, such as chelating ether complexes, an electronic and steric effect of substitution on the linker moiety on catalyst

initiation has been demonstrated.[33,34] To examine electronic and steric effects of the chelating olefin complexes **4.9**, a series of 1,4- and 1,2-disubstituted dienes was targeted (Chart 4.1).

Chart 4.1. Targeted dienes **4.22–4.24**

4.22	**4.23**	**4.24**
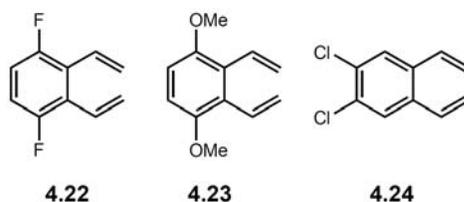
Dienes **4.22** and **4.23** were synthesized from commercially-available 2,3-dimethylbenzene precursors.   After bromination of **4.25** and **4.26** with *N*-bromosuccinimide, addition of PPh₃ enabled the isolation of a phosphonium salt that was utilized in a Wittig reaction to provide the desired substituted dienes **4.22** and **4.23**, respectively (eqs 4.7, 4.8).   Diene **4.24** was synthesized from the corresponding commercially-available anhydride **4.27** (eq 4.9).   Upon reduction of anhydride **4.27**, bromination with PBr₃, and addition of PPh₃, a phosphonium salt was isolated; addition of base and paraformaldehyde resulted in the formation diene **4.24**.

$$(4.7)$$

$$(4.8)$$
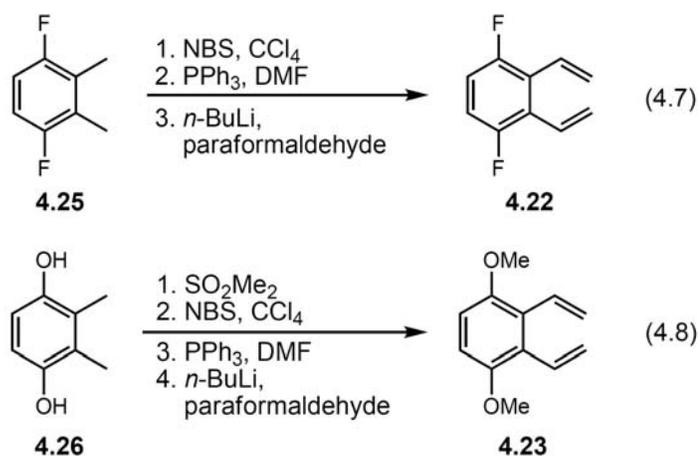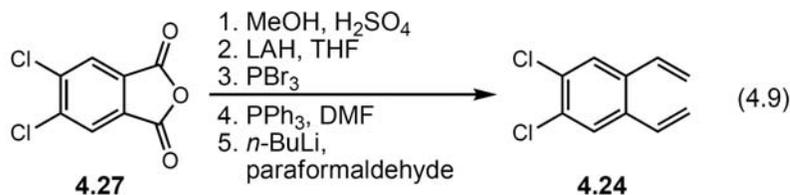
Although fluorinated diene **4.22** showed no reactivity with pyridine complex **4.7** at room temperature, two new benzylidene resonances at 16.45 (d) and 16.74 (d) ppm were observed after heating a solution of diene **4.22** and ruthenium precursor **4.2** in C_6D_6 at 55 °C for 1 h (Scheme 4.3). These new compounds are hypothesized to correspond to be isomers of **4.28**. In addition, a signal corresponding to methylidene complex **4.29** was observed. After 18 h at 65 °C, only resonances corresponding to **4.2** and methylidene complex **4.29** are observed by ^{1}H NMR spectroscopy.

Scheme 4.3. Reactivity studies of **4.2** with **4.22**
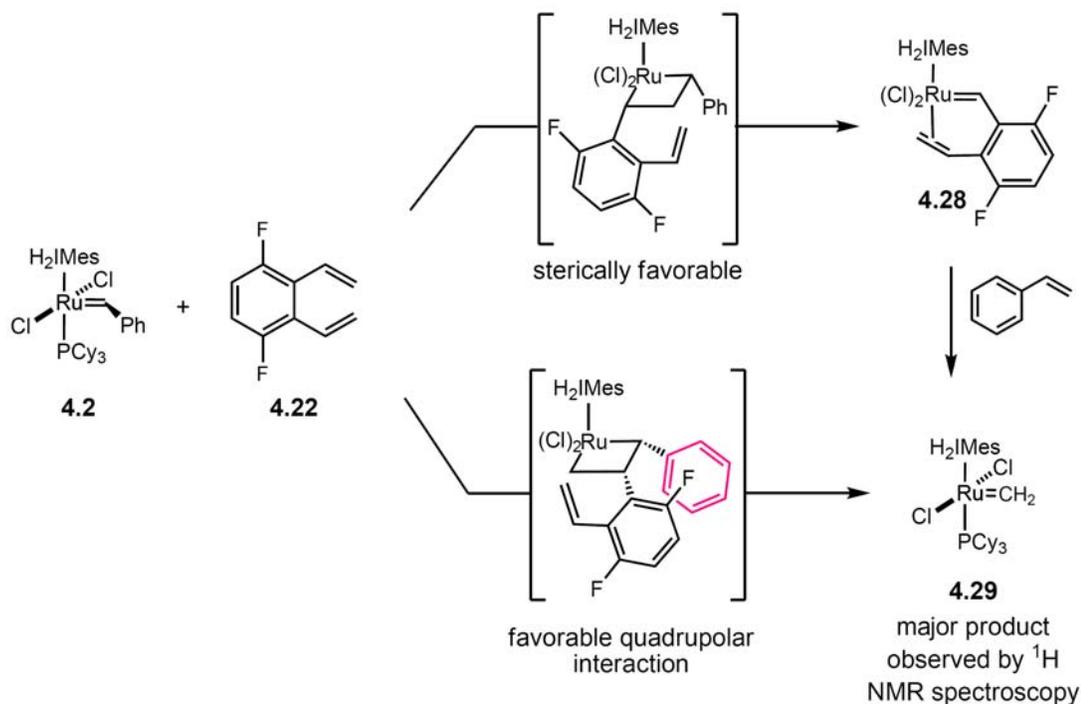
The formation of methylidene **4.29** has not been previously observed in the formation of ruthenium-olefin complexes and could be formed directly from **4.2** or from the reaction of **4.28** with styrene. Ruthenium-olefin complex **4.28** would be expected to exhibit higher reactivity than **4.9** due to the electron-withdrawing fluorine groups, and this could be responsible for the formation of **4.29**. However, **4.29** may also be formed directly from **4.2** through a ruthenacyclobutane intermediate in which a favorable quadrupolar interaction[35] occurs between a phenyl and 1,4-difluoroaryl group. Further examination of this process was not conducted.

No new complexes were observed or isolated from reactions between methoxy-substituted diene **4.23** and ruthenium precursors **4.7** or **4.30** in C_6D_6 at 45 °C, even after extended reaction times (eq 4.10). No further studies were conducted.
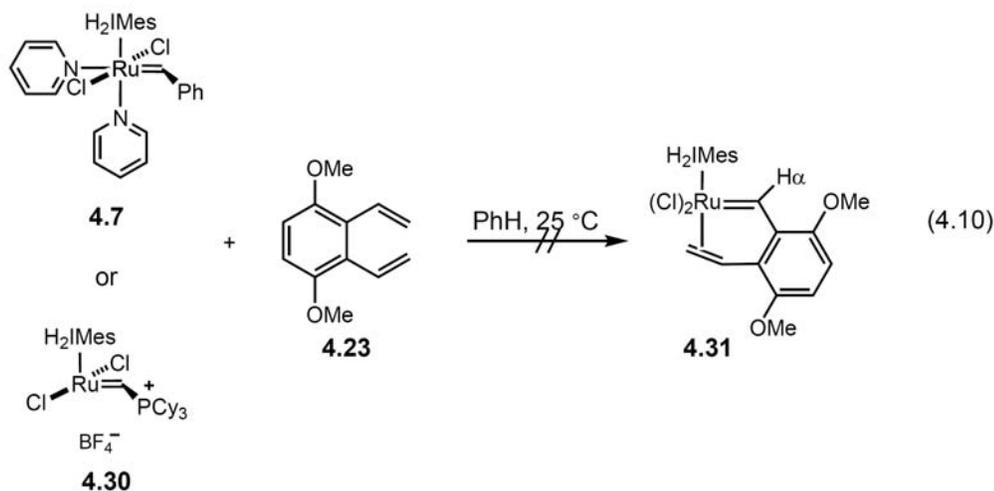
The addition of chloro-substituted diene **4.24** to **4.7** in C_6D_6 results in the formation of several new benzylidene resonances in the ^1H NMR spectrum (eq 4.11). Upon workup, a solid comprised of 5 benzylidene-containing complexes is isolated. The two major isomers are assigned as side-bound complexes based on observed NOEs

between olefinic protons and Me groups on the NHC.[36] Due to the low concentration of

the other isomers, no structural assignment could be made.

(4.11)
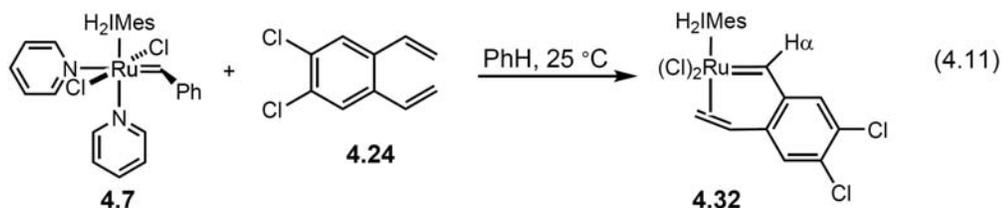
Alkyl-linked Dienes

A series of more conformationally-flexible dienes have also been examined as

possible ligand precursors. 2,5-dimethylhexadiene was initially investigated due to the

low activity of **4.2** for the homodimerization of 1,1'-disubstituted olefins to form

tetrasubstituted olefins. Unfortunately, no reactivity was observed between catalyst **4.7**

and 2,5-dimethylhexadiene under a variety of reaction conditions.

Subsequently, 2-methylhexadiene (**4.33**) was investigated as a ligand precursor.

Upon addition of **4.33** to **4.7** in C_6D_6, a new benzylidene resonance, a triplet, is observed

at 19.46 ppm (eq 4.12). After the addition of 1 equiv **4.33**, 46% conversion and after 3

equiv, 72% conversion is observed. Due to the relatively down-field benzylidene

chemical shift, this new complex is postulated to be pyridine complex **4.34**.

(4.12)
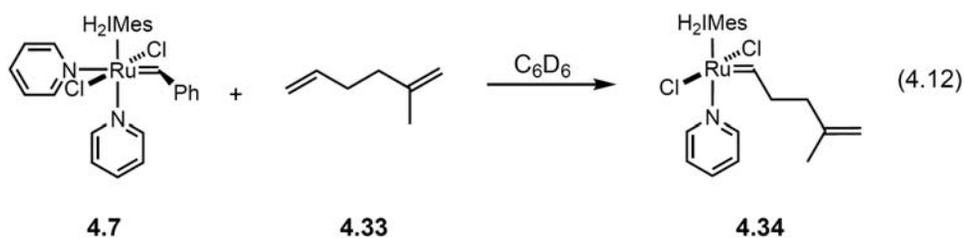
To remove excess pyridine and possibly favor olefin coordination, the reaction was performed in toluene with 1 equiv **4.33** and the solvent subsequently removed. This sequence was repeated three times; the resulting mixture contained significant decomposition with a small, broad benzylidene resonance at ~ 15 ppm and a possible hydride resonance at -0.3 ppm. Performing the reaction in CH_2Cl_2 and Et_2O produced the same resonance at 19.46 (t), but in lower conversion than observed in C_6D_6.

Addition of CuCl to a mixture of **4.33** and **4.7** in C_6D_6 did not significantly change the observed NMR spectrum. After 25 min at 40 °C, no benzylidene resonances were observed, indicating decomposition.

The use of ruthenium precursors **4.2** and **4.30** was also investigated. Upon addition of **4.33** to **4.2** in the presence of CuCl at 40 °C, 55% conversion to the analogous methylidene complex was observed in addition to 22% conversion to a new species with benzylidene resonance at 17.52 ppm. Upon addition of 2-methylhexadiene (**4.33**) to **4.30** in CD_2Cl_2 (used for solubility purposes), several new resonances are observed along with the formation of vinyl phosphonium salt. However, the new products could not be further characterized due to rapid decomposition at room temperature.

Upon addition of 1,5-hexadiene to ruthenium precursor **4.7** in C_6D_6, two new benzylidene resonances were observed at 19.49 (t, 37%) and 18.82 (s, 35%). The resonance at 19.49 ppm is attributed to a pyridine complex analogous to **4.34**. The benzylidene resonance at 18.82 ppm may correspond to a previously unobserved pyridine-containing ruthenium methylidene species. No further studies were conducted.

Summary

In summary, we have developed a model system to study ruthenium-olefin complexes relevant to the mechanism of olefin metathesis. Our studies of the reaction between 1,2-divinylbenzene (**4.8**) and catalyst **4.7** have shown that two ruthenium-olefin adducts are formed and undergo dynamic interconversion. Based on observed NOEs and a low-temperature crystal dissolution experiment, we assign the two isomers as side-bound olefin adducts **4.9b** and **4.9c**. To examine the generality of our initial results, we chose to vary the NHC ligand and ligand precursor. Although not all observed solution-phase isomers could be structurally characterized, the assignable isomers of ruthenium-olefin adducts **4.14**, **4.17**, **4.19** and **4.21** were determined to be side-bound in which the NHC (or PCy$_3$) are coordinated cis to the chelated olefin. The reactivity of ortho- and meta-substituted analogs of **4.8** and alkyl-linked dienes with several ruthenium precursors yielded few isolable ruthenium-olefin complexes.

Experimental

General Considerations

All reactions were carried out under a dry argon atmosphere using standard Schlenk techniques or in a nitrogen-filled glovebox, unless otherwise noted. Toluene, pentane, benzene, and benzene-d$_6$ were purified by passage through activated A-2 alumina solvent columns and were degassed with argon prior to use. Unless otherwise noted, all compounds were purchased from Aldrich or Fisher. Diethyl diallymalonate (**2.9**) was purchased from Aldrich and distilled prior to use. CD$_2$Cl$_2$ was purified by distillation from CaH$_2$ and degassed with argon prior to use. CDCl$_2$CDCl$_2$ was passed through a plug of alumina, degassed with nitrogen and stored over 4Å molecular sieves.

Divinylbenzene (**4.9**),[37] catalysts **4.7**,[38] **chiral**[20,39] were prepared according to literature procedure. Complexes **4.10** and **4.13** were generously donated by Materia, Inc. Diene **4.24** was prepared by Dan Hickstein.[36] High-resolution mass spectrometry (HRMS) data was obtained on a JEOL MSRoute mass spectrometer. ^{1}H and ^{13}C NMR spectra were recorded on Varian Inova (300 and 500) or on a Bruker Avance DPX 400 MHz NMR spectrometer equipped with a 5 mm dual ^{1}H/^{13}C Z-gradient probe. ^{1}H NMR chemical shifts are reported in ppm relative to SiMe$_4$ ($\delta = 0$) and referenced internally with respect to the protio solvent impurity. ^{13}C NMR spectra were referenced internally with respect to the solvent resonance.

NMR Spectroscopy Experiments

2D NMR spectra were obtained on a Bruker Avance DPX 400 MHz NMR spectrometer equipped with a 5 mm dual ^{1}H/^{13}C Z-gradient probe. Unless otherwise specified, spectra were obtained at room temperature. For experiments requiring elevated temperatures, the probe was calibrated with a sample of ethylene glycol containing a trace amount of gaseous HCl.[40] 1D ^{1}H and ^{13}C spectra were acquired with standard pulse sequences and parameters. Details for the 2D experiments are as follows:

Gradient-enhanced 2D COSY experiment.[41] The **cosygs** pulse program was used with the following acquisition parameters: F2 and F1 sweep widths, 7184 Hz. F2 and F1 digital resolution, 7.01 Hz/pt. 256 FIDs recorded, each consisting of 4 scans and 1024 data points (AQ = 0.071 s). A recycle delay of (D1) of 1.5 s was employed. Processing parameters: unshifted sinusoidal apodization was applied in both dimensions prior to the Fourier transformation.

2D COSYLR experiment.[42]   The **cosylr** pulse program was used with the following acquisition parameters: F2 and F1 sweep widths, 7184 Hz. F2 and F1 digital resolution, 7.01 Hz/pt.   128 FIDs recorded, each consisting of 8 scans and 1024 data points (AQ = 0.071 s). Refocussing delays of 100 ms and 200 ms were used in separate experiments. A recycle delay of (D1) of 2.0 s was employed. Zero-filling was applied once to achieve digital resolution of 3.5 Hz/pt in each dimension. Processing parameters: unshifted sinusoidal (SINE, SSB=0) apodization was applied in both dimensions prior to the Fourier transformation.

2D ROESY experiment.[43]   The **roesytp.2** pulse program was used with the following acquisition parameters: F2 and F1 sweep widths, 7184 Hz. F2 and F1 digital resolution, 3.5 Hz/pt.   256 FIDs recorded, each consisting of 16 scans and 2048 data points (AQ = 0.142 s). The 800 ms spin lock consisted of 5404 cycles of phase-shifted pairs of 74 μs 180° pulses. A recycle delay of (D1) of 2.0 s was employed. Processing parameters: $\pi/2$ shifted sine^2 (QSINE, SSB=2) apodization was applied in both dimensions prior to the Fourier transformation.

Representative 2D NOESY/EXSY experiment.[44]   The **noesytp** pulse program was used with the following acquisition parameters: F2 and F1 sweep widths, 2913 Hz. F2 and F1 digital resolution, 2.8 Hz/pt.   256 FIDs recorded, each consisting of 8 scans and 1024 data points (AQ = 0.176 s). A mixing time of 800 ms was set as a simple delay. A recycle delay of (D1) of 2.0 s was employed. Processing parameters: $\pi/2$ shifted sine^2 (QSINE, SSB=2) apodization was applied in both dimensions prior to the Fourier transformation.

Gradient-enhanced 2D ^{1}H-^{13}C HMQC experiment.[45]   The **inv4gp** pulse program was used with the following acquisition parameters: F2 sweep width, 7184 Hz, F1 sweep width, 32,895 Hz. F2 digital resolution, 7.01 Hz/pt, F1 digital resolution, 257 Hz/pt. 128 FIDs recorded, each consisting of 16 scans and 1024 data points (AQ = 0.071 s). The D2 delay was set to 3.57 ms (1/2J = 140 Hz). A recycle delay (D1) of 3.0 s was employed. Processing parameters: Zero-filling was applied once (SI = 2048) in F2 to achieve a digital resolution of 3.5 Hz/pt and eight times (SI = 1024) in F1 to achieve a digital resolution of 32 Hz/pt. Exponential (EM, LB = 5) apodization was applied in the F2 dimension and $\pi/3$ shifted sine^2 (QSINE, SSB=3) apodization was applied in the F1 dimension prior to the Fourier transformation.

2D ^{1}H-^{13}C HMQC experiment without F2 decoupling.[46]   The **inv4nd** pulse program was used with the following acquisition parameters. F2 sweep width, 4789 Hz, F1 sweep width, 17605 Hz. F2 digital resolution, 4.68 Hz/pt, F1 digital resolution, 137.5 Hz/pt. 128 FIDs recorded, each consisting of 64 scans and 1024 data points (AQ = 0.107 s). The D2 delay was set to 3.57 ms (1/2J = 140 Hz). A recycle delay (D1) of 2.2 s was employed. Processing parameters: Zero-filling was applied eight times (SI = 1024) in F1 to achieve a digital resolution of 17.2 Hz/pt. Processing parameters: $\pi/2$ shifted sine^2 (QSINE, SSB=2) apodization was applied in both dimensions prior to the Fourier transformation.

Assignment of the ^{1}H NMR Spectra

The ^{1}H NMR spectra of each ruthenium-olefin complex was assigned utilizing a mixture of 1D and 2D NMR data. Due to the complexity of some samples, full proton

assignment could not be made. Examples of isomer assignment are detailed below for isomer **4.9b** and **4.9c**.
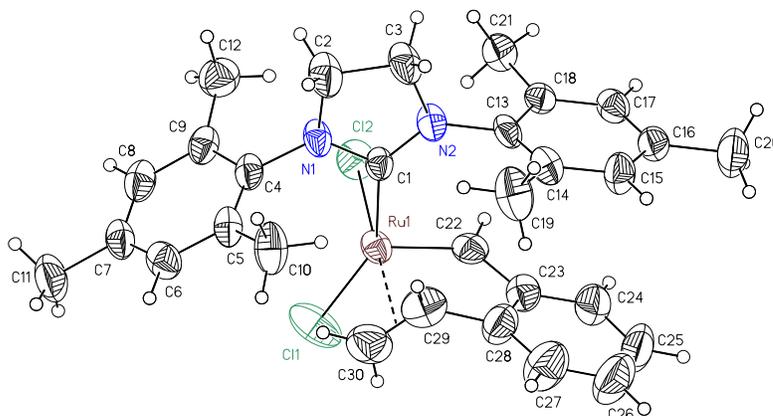
Isomer 4.9b. The olefin resonances were assigned on the basis of coupling constants and the geminal nature of the H-30 (numbering scheme based on crystal structure atom assignment above) resonances was confirmed by a 2D-HMQC experiment which correlated these resonances to a single carbon resonance (**4.9b**: 86.70 ppm). The H-29 resonance was likewise correlated to a carbon resonance, thus identifying the C-29 carbon chemical shift (**4.9b**: 92.20 ppm). These olefinic proton and carbon chemical shifts are discussed in detail in a later section that compares this data with the free ligand (Table 4.A2). To summarize the olefinic proton assignments, H-29 (5.54 ppm) was found to have a large coupling (12.6 Hz) to the trans-disposed H-30(cis) (3.59 ppm, H_c) and a smaller coupling (9.2 Hz) to the cis-disposed H-30(trans) (3.44 ppm, H_b). A small (1.0 Hz) geminal coupling was observed between the H-30 protons. A small coupling (1.1 Hz) was also observed between H-30(trans) and the benzylidene H-22. Formally a six-bond scalar coupling, this small coupling may arise from a favorable orientation of the C-H backside bond vectors.

As predicted from consideration of the internuclear distances, a strong NOE was observed between the benzylidene H-22 and a doublet (J = 7.8 Hz) proton resonance at 6.62 ppm, identifying it as H-24 on the divinylbenzene-derived ligand. Attempts to fully assign the benzylidene aromatic spin system were hindered by overlap between the remaining protons; H-22 couples as shown by 2D-COSY into the 7.00−7.10 ppm region, but this region is further complicated by overlap with the same resonances corresponding to the **4.9c** isomer.

NOEs between the olefin/benzylidene resonances and methyl resonances were used to assign resolved methyl resonances. A benzylidene H-22/Me NOE was used to assign the methyl resonance at 2.55 ppm as Me-21. Me-19 (1.90 ppm) was assigned on the basis of its NOE with H-29. Both H-29 and H-30(trans) showed an NOE to 2.43 ppm, which is in a region of several overlapping methyl groups. Using the Me-19 resonance at 1.90 ppm as a reference point, an NOE from it to a broad singlet at 5.99 ppm identifies that resonance as H-15. The H-15 resonance shows one additional NOE to a methyl resonance at 2.12 ppm, identifying it as Me-20. The Me-20 resonance shows an NOE to a broad singlet at 6.85 ppm, identifying it as H-17. The H-17 resonance shows one additional NOE to a methyl resonance at 2.55, identifying it as Me-21 and supporting the assignment made on the basis of the benzylidene H-22 NOE. It was thus possible to assign the mesityl methyl resonances of the portion of the NHC ligand situated over the divinylbenzene-derived ligand. The greater dispersion of these resonances, seen in both **4.9b** and **4.9c**, is probably due to the chemical shift anisotropy induced by the divinylbenzene-derived ligand.

The methyl resonance at 2.72 ppm was assigned as Me-12 on the basis of exchange crosspeaks, observed at 45 °C, correlating it to Me-19 in both **4.9b** and **4.9c**. The details of the exchange processes are discussed in a separate section (vide infra). To add further support for the Me-12 assignment, the H-30/Me NOE in **4.9b** involved a methyl resonance in the region of overlap (2.36–2.44 ppm), which would be consistent with Me-10 (and not Me-12) being located in the region of overlap.

Isomer 4.9c. For the most part, the strategy used to assign the resonances of **4.9b** was also found successful for **4.9c**. The olefin resonances were assigned on the basis of coupling constants and the geminal nature of the H-30 resonances was confirmed by a 2D-HMQC experiment which correlated these resonances to a single carbon resonance (**4.9c**: 69.60 ppm). The H-29 resonance was likewise correlated to a carbon resonance, thus identifying the C-29 carbon chemical shift (**4.9c**: 107.80 ppm). To summarize the olefinic proton assignments, H-29 (6.13 ppm) was found to have a large coupling (12.5 Hz) to the trans-disposed H-30(cis) (3.37 ppm) and a smaller coupling (9.9 Hz) to the cis-disposed H-30(trans) (3.51 ppm). A small coupling (1.1 Hz) was also observed between H-30(trans) and the benzylidene H-22.

A strong NOE was observed between the benzylidene H-22 and a doublet ($J = 7.8$ Hz) at 6.40 ppm, identifying it as H-24 on the divinylbenzene-derived ligand. None of the remaining divinylbenzene-derived aromatic protons were assigned because of peak overlap problems.

As was done for **4.9b**, NOEs between the olefin/benzylidene resonances and methyl resonances were used to assign resolved methyl resonances in **4.9c**. A benzylidene H-22/Me NOE was used to assign the methyl resonance at 2.91 ppm as Me-

21. Me-19 (1.20 ppm) was assigned on the basis of its NOE with H-30(cis). H-30(cis) also showed an NOE to 2.36 ppm, which is in a region of several overlapping methyl groups. Using the Me-19 resonance at 1.20 ppm as a reference point, an NOE from it to a broad singlet at 6.41 ppm identifies that resonance as H-15. The H-15 resonance shows one additional NOE to a methyl resonance at 2.38 ppm, identifying Me-20 as one of the resonances within the region of overlap. The H-17 resonance was assigned on the basis of its NOE with the well-resolved Me-21 at 2.91 ppm. Data from a 2D-COSYLR experiment was used to provide further corroboration of the assignments for this mesityl ring. In this experiment, which detects small H-H scalar couplings, correlations between aromatic hydrogens and methyl groups were readily detected (Table 4.A1). For example, the H-17 resonance shows correlations with H-15 (6.41 ppm) and three methyl groups: Me-21 (2.91 ppm), Me-19 (1.2 ppm), and Me-20 (2.37 ppm). As was the case for **4.9b**, the mesityl methyl and aromatic resonances of the portion of the NHC ligand situated over the divinylbenzene-derived ligand exhibited a pronounced dispersion in their chemical shifts.

The methyl resonance at 2.75 ppm was assigned as Me-12 on the basis of a room-temperature NOESY exchange crosspeak correlating it to Me-19 at 1.20 ppm. The details of the exchange process will be discussed later. The remaining methyl groups, Me-11 and Me-10, resonate in the region of overlap between 2.36–2.44 ppm. The evidence for this assignment is that Me-21 (2.91 ppm) has an exchange crosspeak with this region, which would be consistent with Me-21 exchanging with Me-10. Me-11 is assigned to the 2.36–2.44 region by virtue of not being assignable to any of the well-resolved methyl resonances corresponding to the major isomer.

Synthesis and NMR Characterization

Complex **4.9**: To a solution of **4.7** (200 mg, 0.275 mmol) in benzene (10 mL) in a 20-mL vial under nitrogen was added **4.8** (40 mg, 1.1 eq., 0.308 mmol). The reaction was stirred for 2 h at room temperature during which time a light green precipitate was formed. The solid was filtered, washed with benzene and dried under vacuum overnight to give **4.9**, a light green powder (89%). HRMS (FAB) m/z (%): 594.1137 $[M]^+$ (3).


do_ct_44 expt 1
Ru−alkene complex 9 in CD2Cl2
400 MHz 1H spectrum
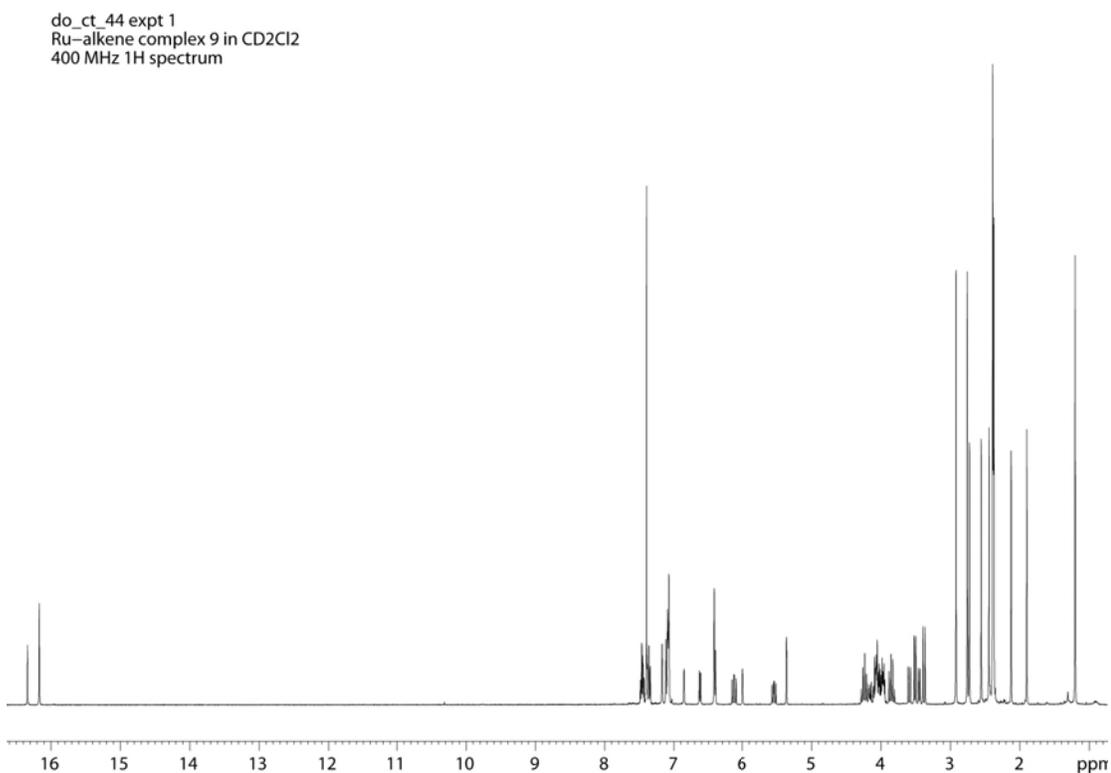
Figure 4.A1. 400 MHz ^{1}H NMR spectrum of **4.9b/c** in CD$_2$Cl$_2$ at 22 °C.

Table 4.A1. Tabulation of ^{1}H NMR data of complex **4.9b/c** in CD_2Cl_2 and observed ^{1}H or ^{13}C crosspeaks (ppm) in 2D spectra. The minor isomer (**4.9b**) is shown in red, the major isomer (**4.9c**) is shown in black.

assignment	proton (ppm)	integral	multiplicity (Hz)	COSY	COSY-LR	NOESY	2D-exchange	HMQC	1J(C13/H)
H-22	16.34	0.75	t, J = 1.1	3.44	7.38, 3.44	2.55, 6.62	16.17	300.300	
H-22	16.17	1	t, J = 1.0	3.51	7.38, 3.51	2.91, 6.40	16.34	296.900	
	7.50-7.41	1.75	M	7.095	6.428				
	7.39-7.32	1.75	M						
H-17	7.17	1	br s		6.41, 2.91, 2.37, 1.20	2.91, 2.38	6.85		
	7.11	1	br s						
	7.10-7.00	4	M		2.72				
H-17	6.85	0.75	br s		5.99, 2.55, 2.12, 1.20	2.55, 2.12	7.17	129.395	
H-24	6.62	0.75	d, J = 7.8	7.09	7.43	16.34, 7.09	6.4	121.616	
H-15	6.41	1	br s		7.17, 2.91, 2.39, 1.20	2.38, 1.2	5.99	130.336	
H-24	6.4	1	d, J = 7.8	7.101		16.17, 7.07	6.62	121.565	
H-29	6.13	1	dd, J = 12.5, 9.9	3.51, 3.37		7.35, 3.37, 3.51	5.54	107.800	163 Hz
H-15	5.99	0.75	br s		6.85, 2.55, 2.12, 1.90	2.12, 1.9	6.62	129.068	
H-29	5.54	0.75	dd, J = 9.2, 12.6	3.59, 3.44		7.35, 3.44, 3.59, 2.43, 1.90	6.13	92.200	160 Hz
	4.23	1	app quart, J = 10.2	4.01, 3.77		3.90, 2.787		52.682	
	4.19-3.92	4.5	M						
	3.84	1	app quart, J = 11.2			4.01, 1.195		52.219	
H-30(cis 28)	3.59	0.75	dd, J = 12.6, 1.6	5.54		3.44, 5.54	3.37	86.700	166 Hz
H-30(trans 28)	3.51	1	dt, J = 9.9, 1.1	6.13		6.13, 3.37, 2.36	3.44	69.600	160 Hz
H-30(trans 28)	3.44	0.75	dt, J = 9.2, 1.5	5.54		5.54, 3.59, 2.43	3.51	86.700	159 Hz
H-30(cis 28)	3.37	1	dd, J = 12.5, 1.0	6.13		6.13, 3.51, 2.36. 1.20	3.59	69.600	160 Hz
Me-21	2.91	3	s		6.41, 7.17, 1.20	7.17, 4.01, 16.17	2.55, 2.36	19.713	
Me-12	2.75	3	s			7.104	1.2		
Me-12	2.72	2.1	s		7.05	7.13			
Me-21	2.55	2.1	s		5.99, 6.85, 1.90	16.34, 6.85			
	2.44-2.36	13	m						
Me-20	2.12	2	s		5.99, 6.85, 1.90	5.99, 6.85	2.39		
Me-19	1.9	2	s		5.99, 6.85, 2.55, 2.12	5.54, 5.99	1.2		
Me-19	1.2	3	s		2.40, 2.91, 6.41, 7.17	6.41, 3.37	1.90, 2.75		

Comparison of NMR Parameters of 4.9b/c with Divinylbenzene (4.8)

Table **4**.A2 summarizes the relevant ^1H and ^{13}C NMR parameters for the divinylbenzene-derived ligand in **4.9b/c** with divinylbenzene (**4.8**).

Table 4.A2. Comparison of olefin NMR parameters for ruthenium-olefin complexes **4.9b**, **4.9c**, and divinylbenzene (**4.8**) in CD_2Cl_2
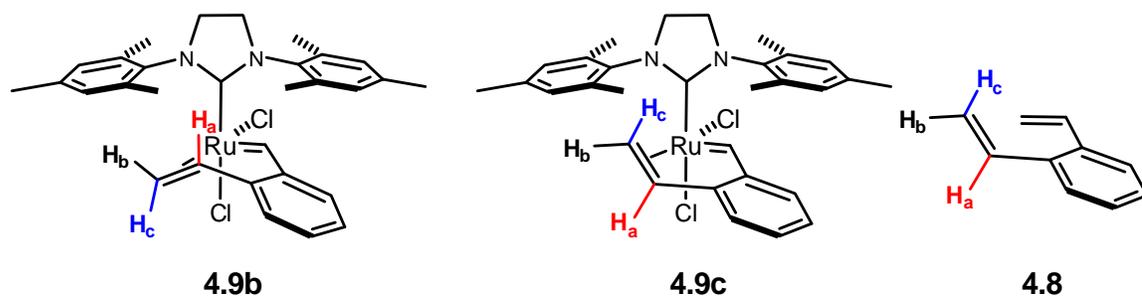
		Compound	
parameter (units)	**4.9b**	**4.9c**	**4.8**
δH_a (ppm)	5.54	6.13	7.07
δH_b (ppm)	3.44	3.51	5.37
δH_c (ppm)	3.59	3.37	5.67
$^3J_{ab}$ (Hz)	9.2	9.9	11.0
$^3J_{ac}$ (Hz)	12.6	12.5	17.4
$^2J_{bc}$ (Hz)	1.1	1.0	1.4
δC_a (ppm)	92.20	107.80	135.1
δC_{bc} (ppm)	86.70	69.60	116.5
$^1J_{C-Ha}$ (Hz)	160	163	155
$^1J_{C-Hb}$ (Hz)	159	160	160
$^1J_{C-Hc}$ (Hz)	166	160	155
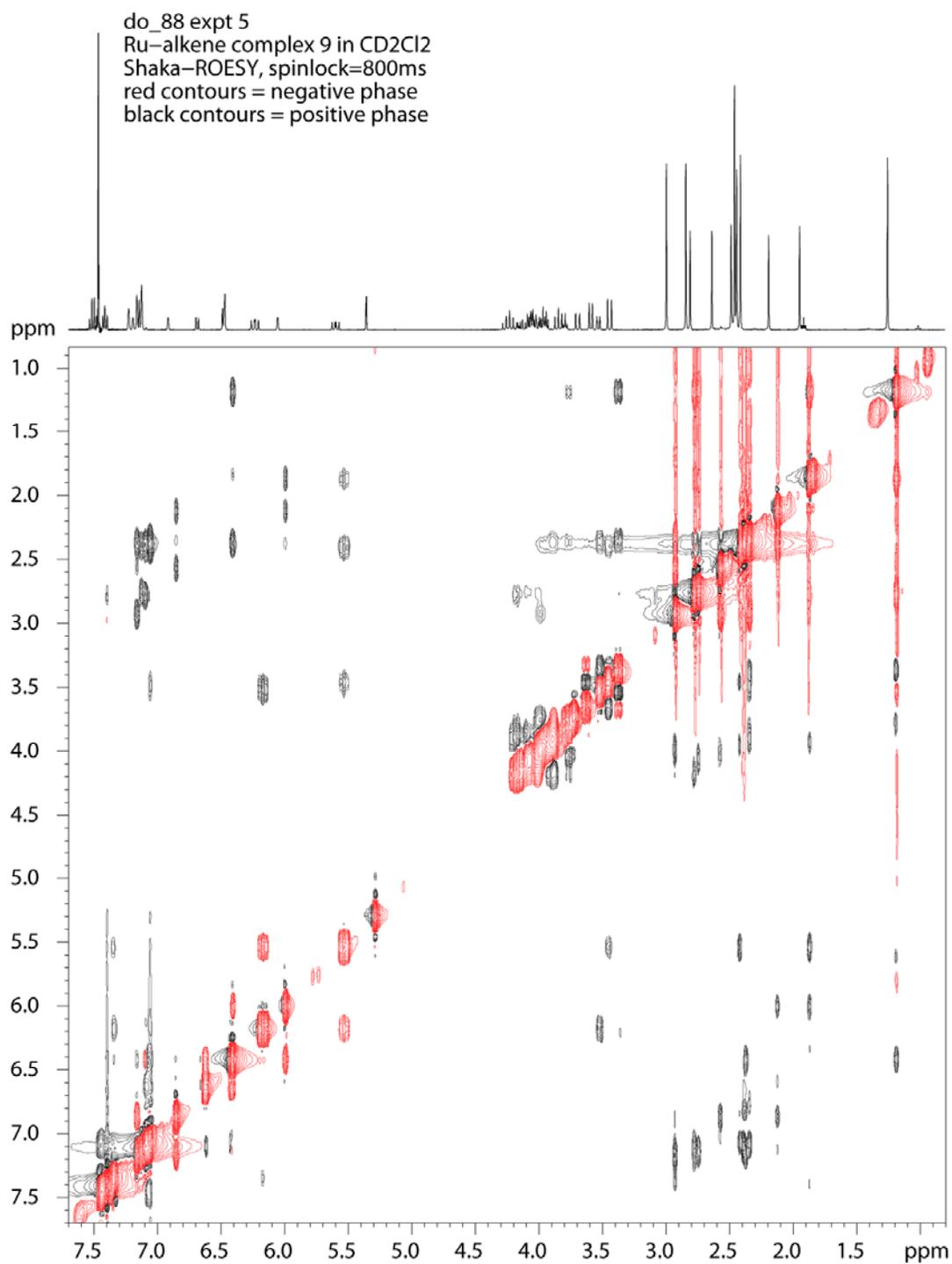
Figure 4.A2. 400 MHz ^{1}H-^{1}H ROESY spectrum of **4.9b/c** in CD$_2$Cl$_2$ at 22 °C. Overhauser-derived crosspeaks are colored black, diagonal and exchange-derived crosspeaks are colored red.

do_88 expt 5
Ru−alkene complex 9 in CD2Cl2
Shaka−ROESY, spinlock=800 ms
Black contours = positive phase
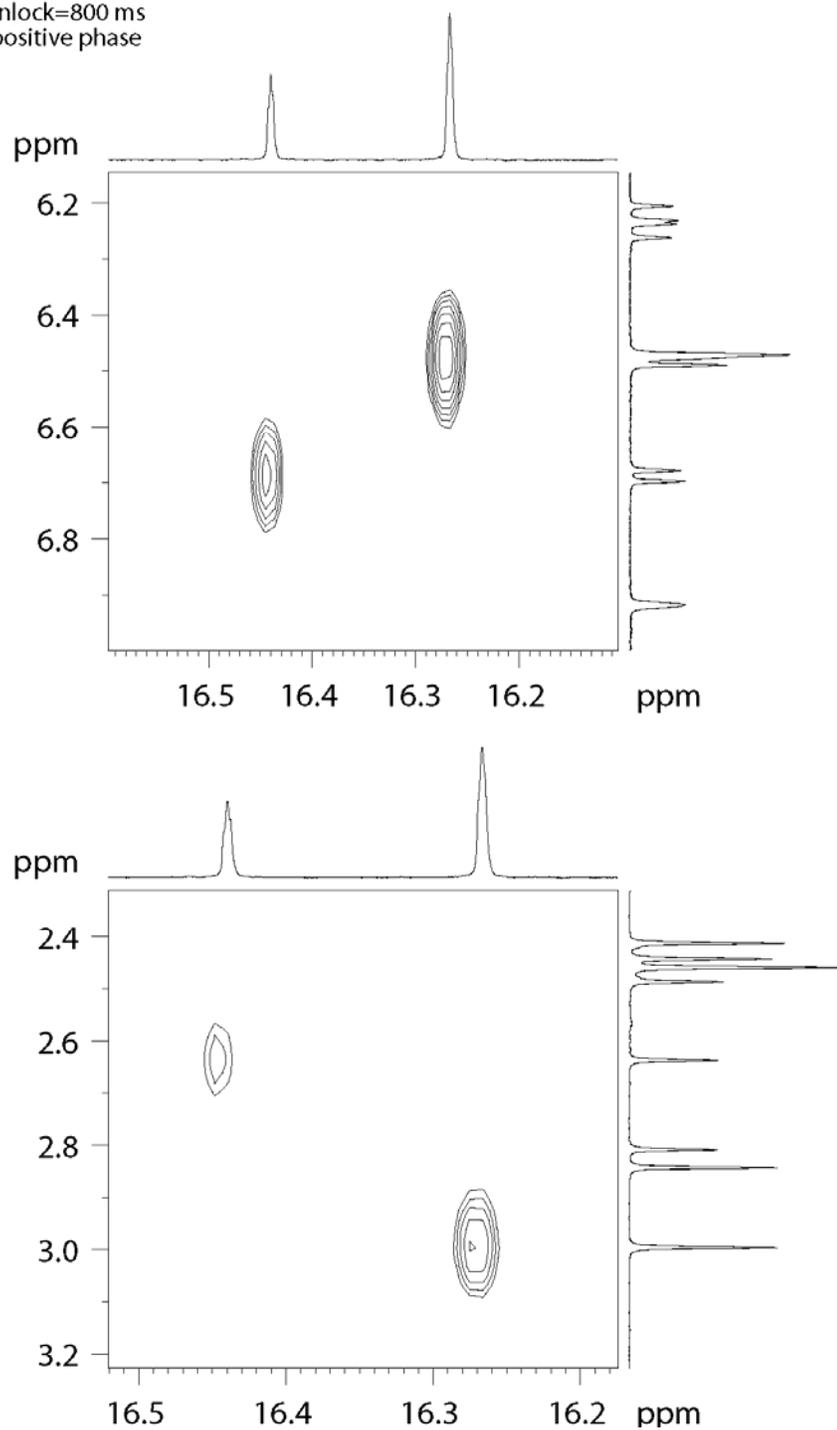
Figure 4.A3. 400 MHz ^{1}H-^{1}H ROESY spectrum of **4.9b/c** in CD$_2$Cl$_2$ at 22 °C. Overhauser-derived crosspeaks are colored black, diagonal and exchange-derived crosspeaks are colored red.
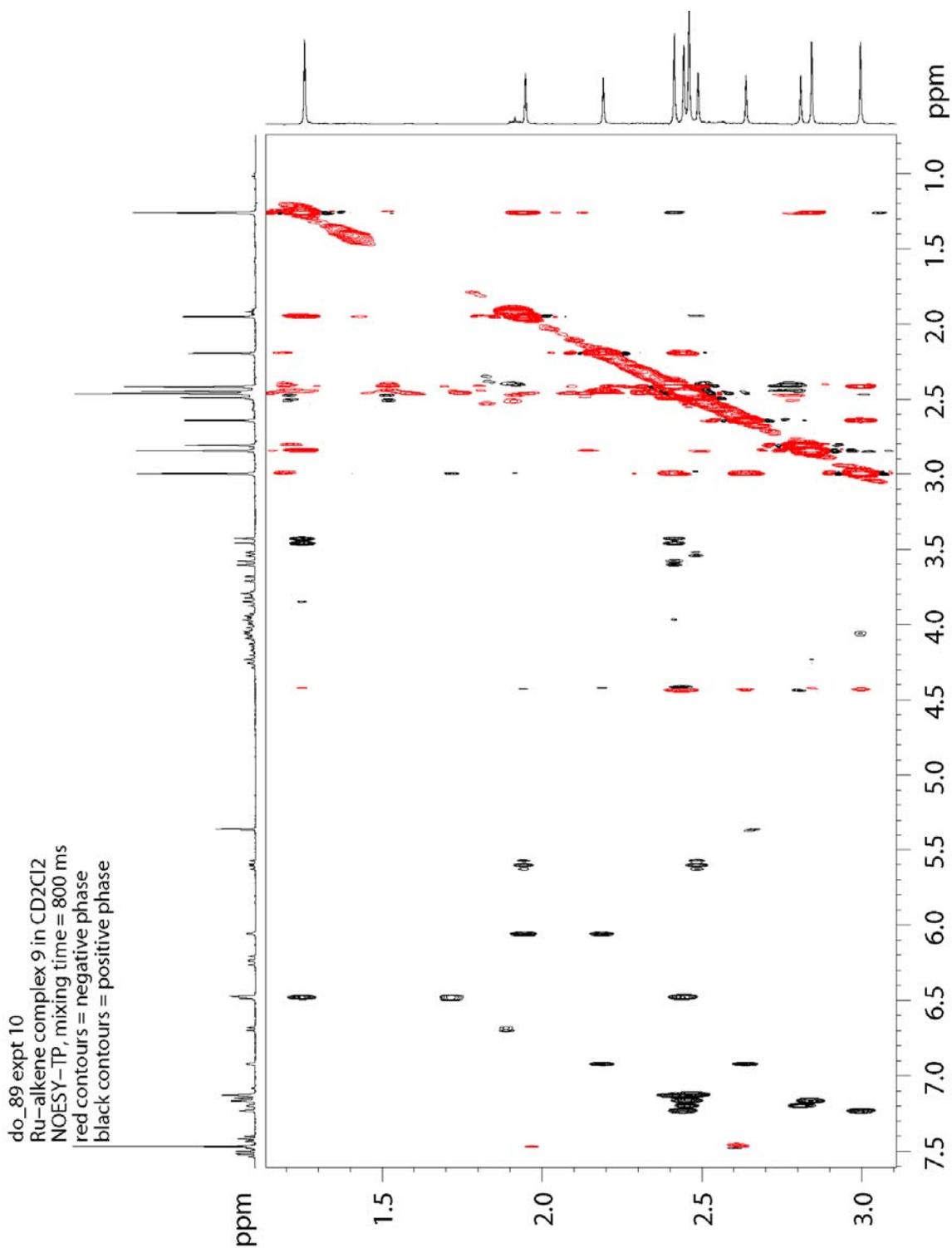
Figure 4.A4. 400 MHz ^{1}H-^{1}H NOESY/EXSY spectrum of **4.9b/c** in CD$_2$Cl$_2$ at 22 °C. Overhauser-derived crosspeaks are colored black, diagonal and exchange-derived crosspeaks are colored red.
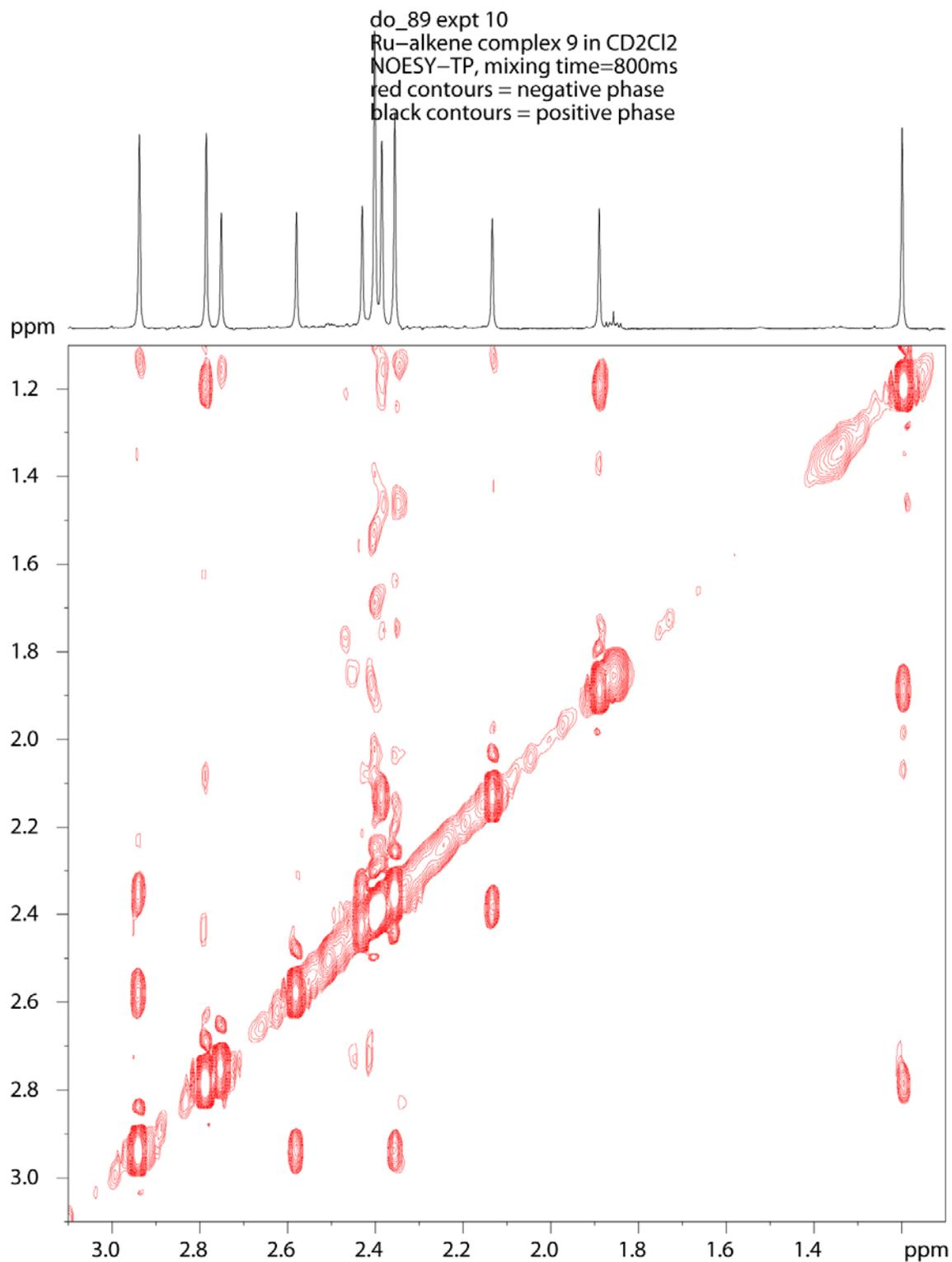
**Figure 4.A5.** 400 MHz ^{1}H-^{1}H NOESY/EXSY spectrum of **4.9b/c** in CD$_2$Cl$_2$ at 22 °C. Overhauser-derived crosspeaks are colored black, diagonal and exchange-derived crosspeaks are colored red.

Complex **4.12**: To a 4-mL vial in the glovebox was added **4.10** (95 mg, 0.12 mmol) and toluene (ca. 2 mL). Vial capped with a screwcap containing a PTFE septum and removed from the glovebox. Divinylbenzene (17.5 μL, 0.12 mmol) added via syringe. Vial taken into the glovebox. The reaction stirred at 22 °C overnight, filtered through a pipette column and washed with toluene (ca. 1 mL) and pentane (2 x 2 mL). Solid eluted with CH_2Cl_2 and concentrated to yellow-green solid (37 mg, 56%). ^1H NMR (CD_2Cl_2, 400 MHz): δ = 16.57 (q, 1H, J = 0.9 Hz), 16.42 (q, 1H, J = 1.1 Hz), 7.60 (m, 2H), 7.47 (m, 4H), 7.37 (m, 2H), 7.22 (m, 6H), 7.23 (m, 4H), 6.68 (d, 1H, J = 7.8 Hz), 6.55 (d, 1H, J = 7.7 Hz), 6.4 (tt, 1H, J = 9.0, 1.4 Hz), 6.22 (br d, 1H, J = 11.3 Hz, H_a of **4.12a**), 6.10 (tt, 1H, J = 9.0, 1.4 Hz), 5.77 (dd, 1H, J = 9.1, 12.8 Hz, H_a of **4.12b**), 4.48-3.96 (m, 9H, H_b of **4.12a** is buried within), 3.73 (dt, 1H, J = 9.1, 1.4 Hz, H_b of **4.12b**), 3.40 (ddd, 1H, J = 0.65, 1.8, 12.8 Hz, H_c of **4.12b**), 3.33, (dd, 1H, J = 12.8, 1.1 Hz, H_c of **4.12a**); ^{19}F NMR (1:1 TCE-d_2/CD_2Cl_2, 376.5 MHz): δ = −111.5 ppm (br s), −113.7, −116.0, −118.2, −118.5. HRMS (FAB) m/z (%): 581.9824 $[M]^+$ (2).

COSYLR NMR data for **4.12**: Benzylidene resonance at 16.57 has long-range COSY interaction with 3.73 ppm (H_b of **4.12b**). Benzylidene resonance at 16.42 has long-range COSY interaction with H_b of **4.12a** (resonance buried within NHC backbone). H_c of **4.12b** has COSYLR interactions with 3.73 ppm (H_b of **4.12b**), which is to be expected on account of a small geminal coupling.

f4-NHC in CD2Cl2
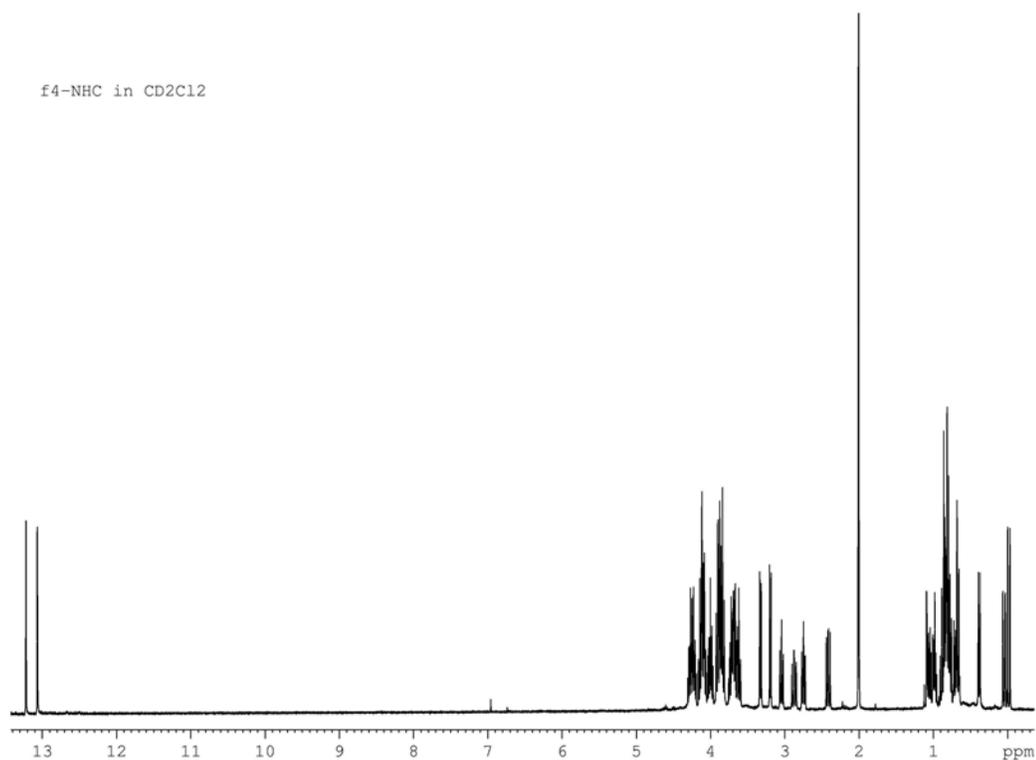
Figure 4.A6. ^{1}H NMR spectrum of **4.12** in CD$_2$Cl$_2$ at 22 °C.

donde F4-DVB
do_ct_92 gaussian enhanced proton
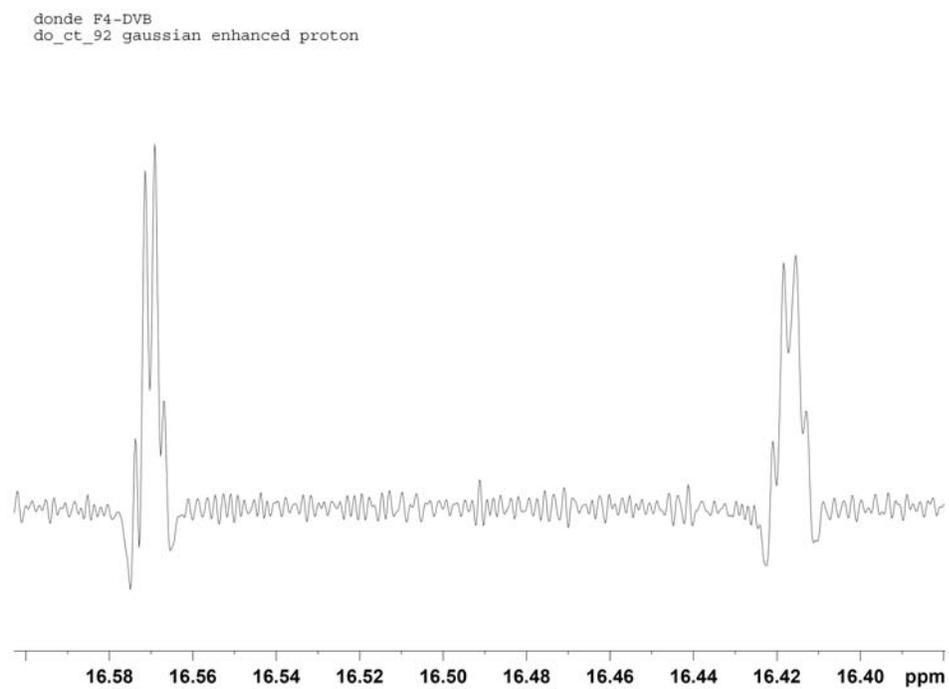
Figure 4.A7. Gaussian-enhanced ^{1}H NMR spectrum of **4.12** in CD$_2$Cl$_2$ at 22 °C.

```
donde F4-DVB
do_ct_92 expt 4
NOESY, 600 ms mixing time
```
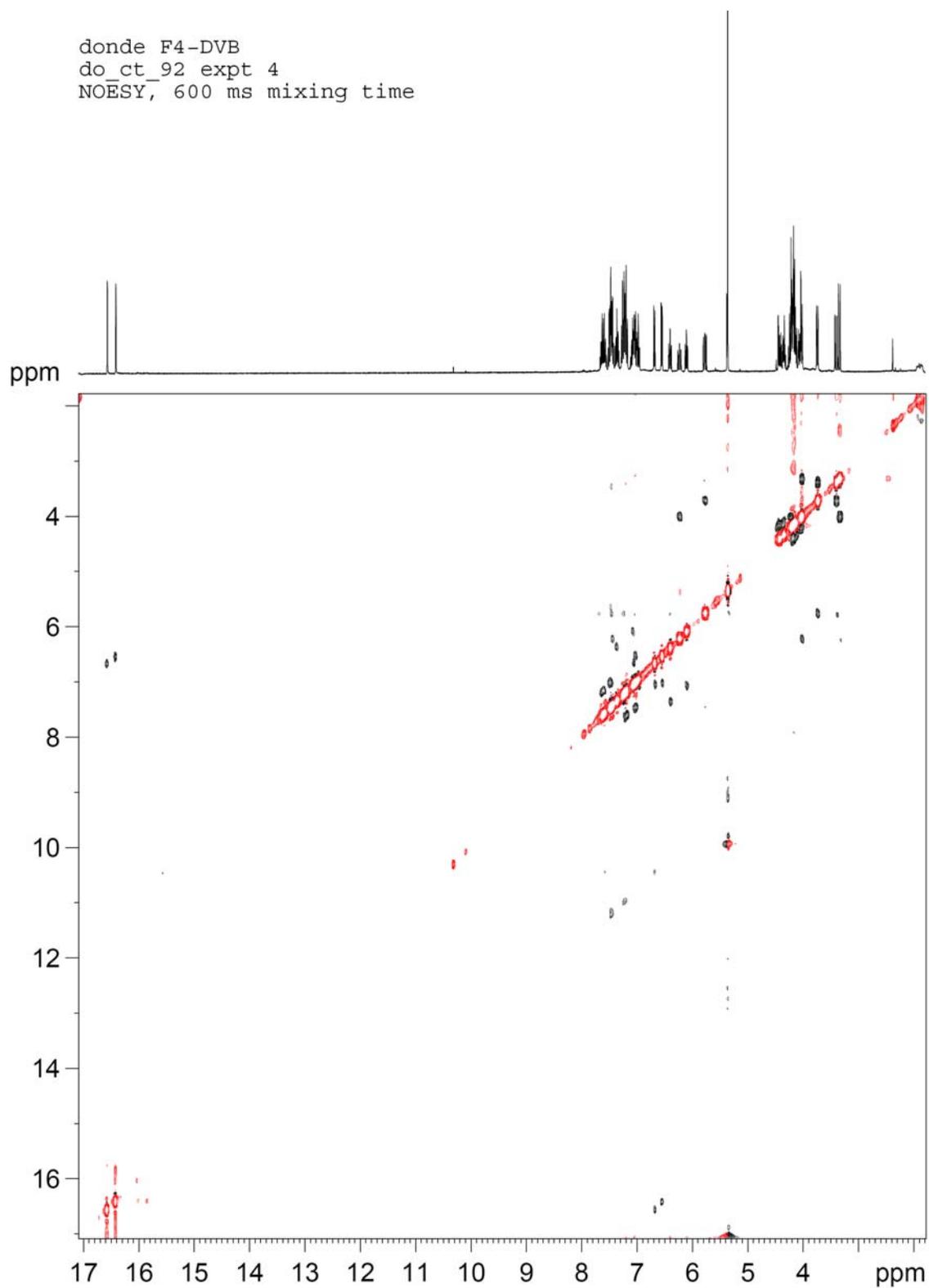
Figure 4.A8. 2D-NOESY/EXSY spectrum of **4.12** in CD$_2$Cl$_2$ at 22 °C.

donde F4-DVB
do_ct_92 expt 4
NOESY, 600 ms mixing time
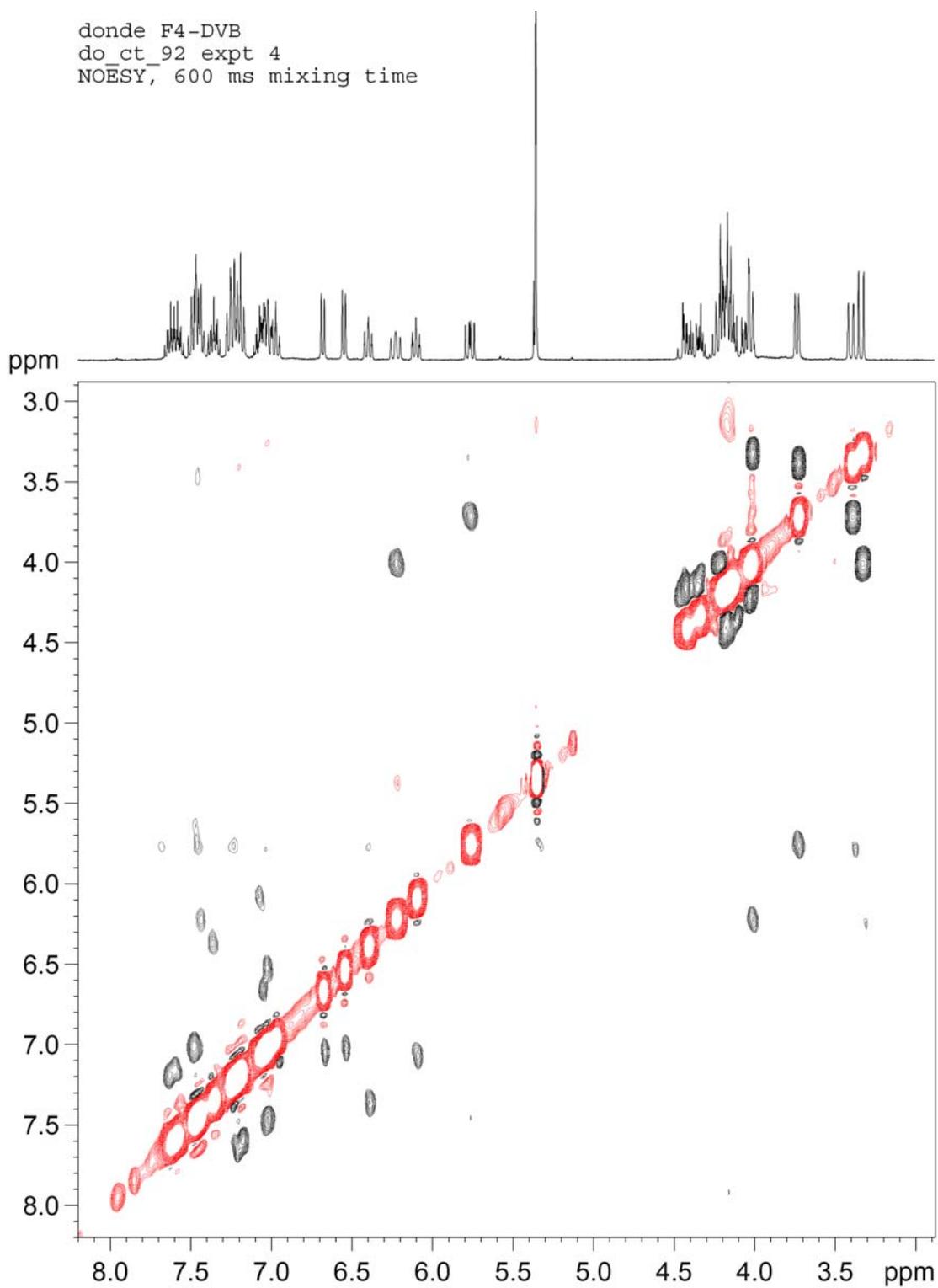
Figure 4.A9. 2D-NOESY/EXSY spectrum of **4.12** in CD$_2$Cl$_2$ at 22 °C.
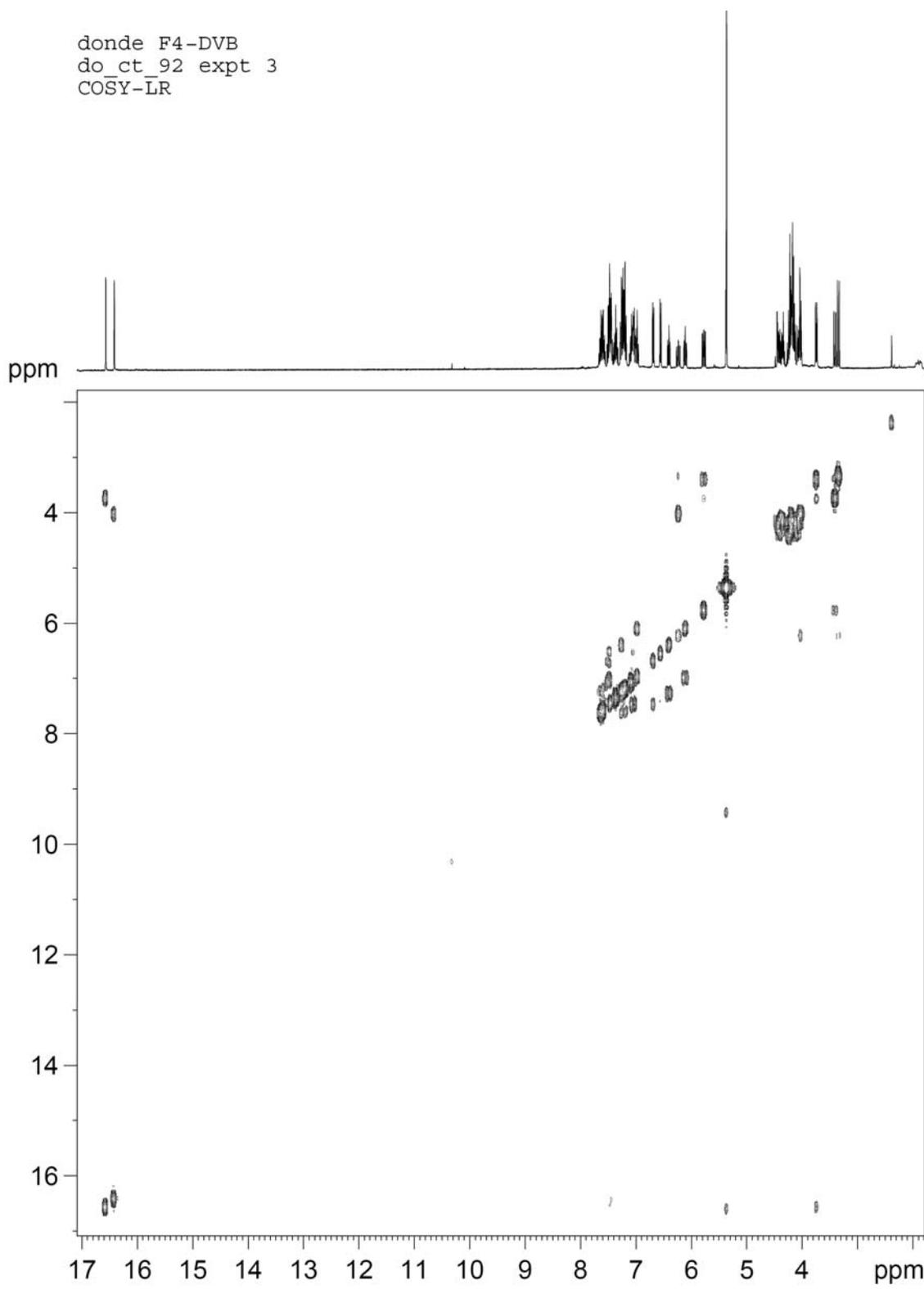
Figure 4.A10. COSYLR spectrum of **4.12** in CD$_2$Cl$_2$ at 22 °C.
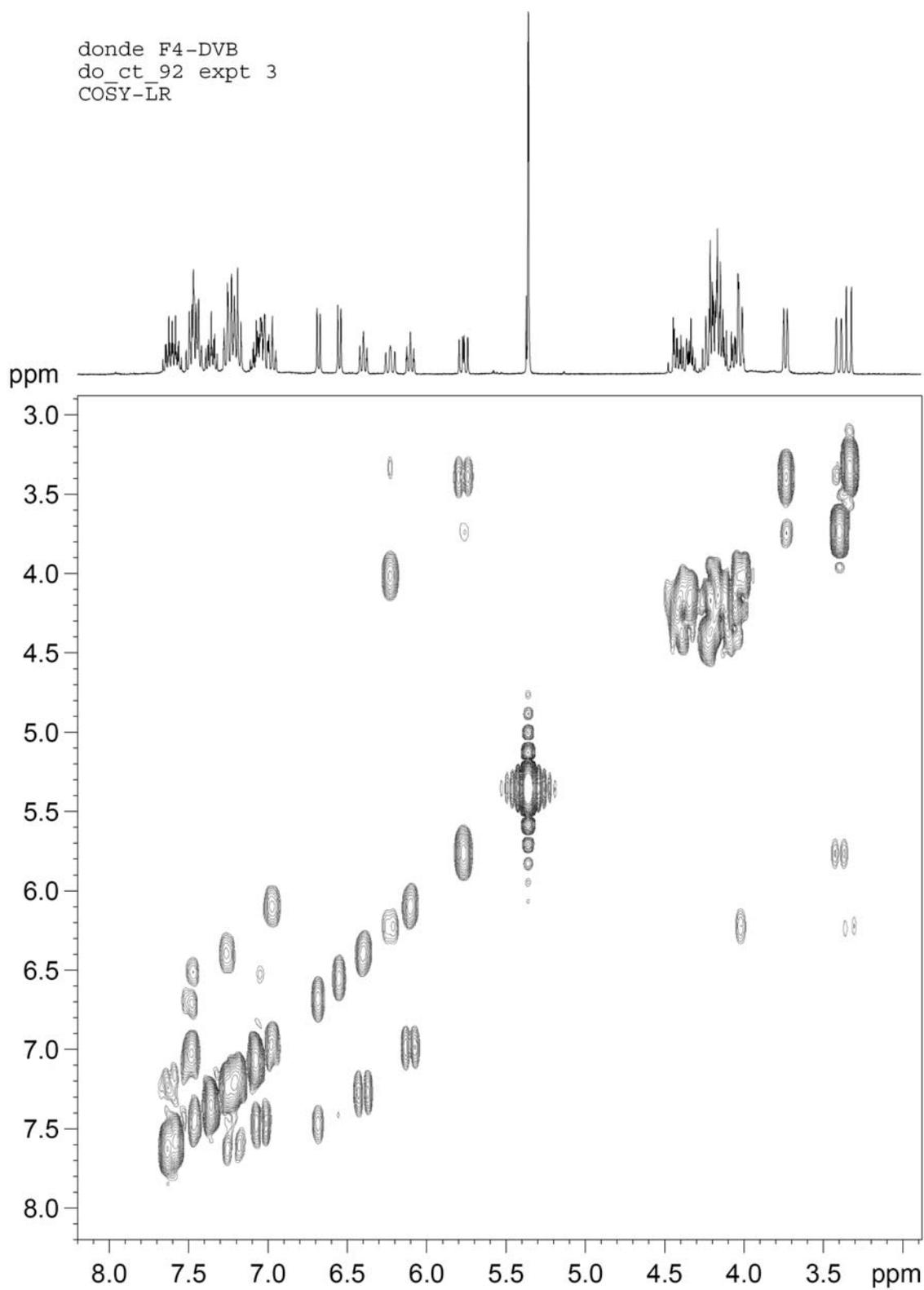
Figure 4.A11. COSYLR spectrum of **4.12** in CD_2Cl_2 at 22 °C.

Complex **4.14**: To a 4-mL vial in the glovebox was added **4.13** (30 mg, 0.032 mmol) and benzene (ca. 1 mL). Vial capped with a screwcap containing a PTFE septum and removed from the glovebox. Divinylbenzene (4.5 μL, 0.032 mmol) added via syringe. Vial taken into the glovebox. The reaction stirred at 22 °C 2 h, concentrated and extracted with pentanes. The resulting solid was dissolved in benzene and precipitated with pentane. After filtration through a pipette column, elution with CH_2Cl_2, and concentration, a green solid (12 mg, 55%) was isolated. ^{1}H NMR (CD_2Cl_2, 400 MHz): δ = 16.14 (br s, 1H, long range couples to 2.93 ppm, 7.32 ppm), 7.6-7.2 (m, 10 H), 7.00 (t, 1H, J = 7.7 Hz), 6.76 (d, 1H, J = 7.2 Hz), 6.24 (d, 1H, J = 7.5 Hz), 6.13 (dd, 1H, J = 9.9. 11.7 Hz, H_a of **4.14a**), 4.44 (m, 2H), 4.28 (m, 2H), 4.12 (m, 1H), 4.03 (m, 1H), 3.08 (sept, 1H, J = 6.7 Hz), 3.05 (d, 1H, J = 12.3 Hz, H_c of **4.14a**), 2.95 (d, 1H, J = 10.1 Hz, H_b of **4.14a**), 2.34 (septet, 1H, J = 7.2 Hz), 1.83 (d, 3H, J = 6.7 Hz), 1.53 (d, 3H, J = 6.7 Hz), 1.46 (d, 3H, J = 6.7 Hz), 1.37 (d, 3H, J = 6.7 Hz), 1.27 (d, 3H, J = 6.7 Hz), 1.21 (d, 3H, J = 6.7 Hz), 1.00 (d, 3H, J = 6.7 Hz), 0.09 (d, 3H, J = 6.7 Hz).

2D-NOESY data utilized to assign the major conformer in solution as **4.14a**: H_c shows an NOE with a Me resonance at 0.09 ppm, H_b shows an NOE to a Me resonance at 1.46 ppm, H_a shows one NOE to H_b. Additional NOE expts were run in C_6D_6 in order to resolve overlap between one olefin resonance and a methine resonance. In this experiment (plot is included in the folder), H_b shows an NOE to a methyl resonance at 1.32 ppm, H_c shows NOEs to 0.11 ppm (Me), 1.32 ppm (Me), and 2.35 ppm (C-H). It is also interesting to note that a methine-methine NOE is readily observed in this data set

(2.35/3.0 ppm)—this is likely the C-H/C-H interaction spanning the gap filled by the

olefin.
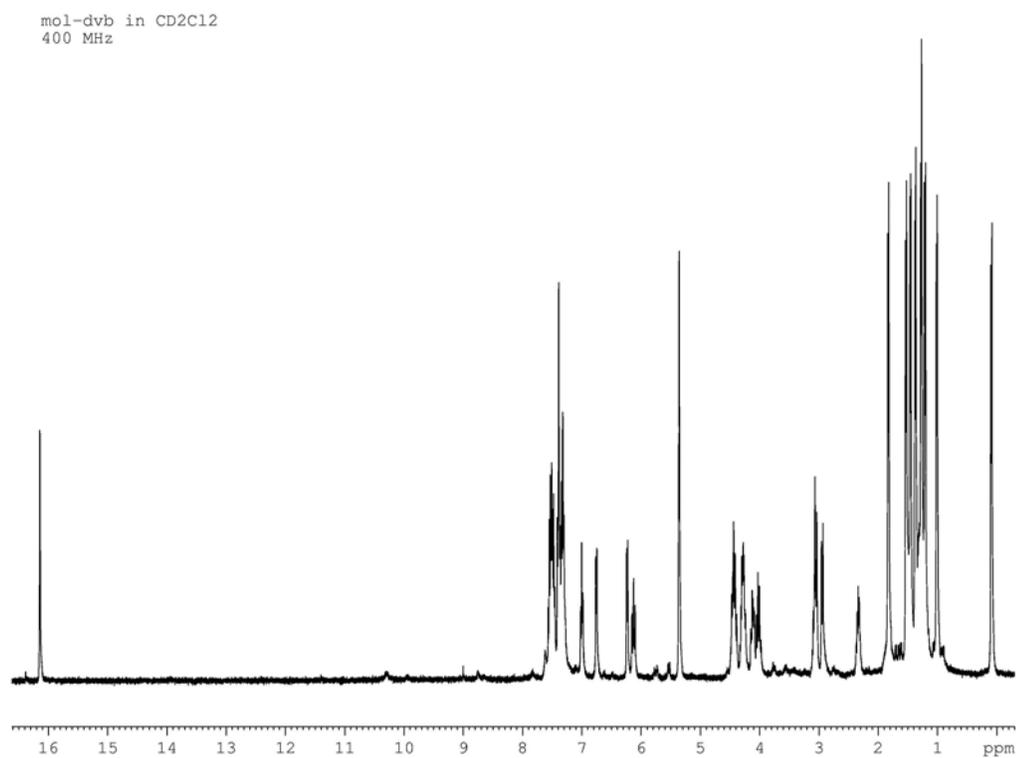
Figure 4.A12. ^{1}H NMR spectrum of **4.14** in CD$_2$Cl$_2$ at 22 °C.
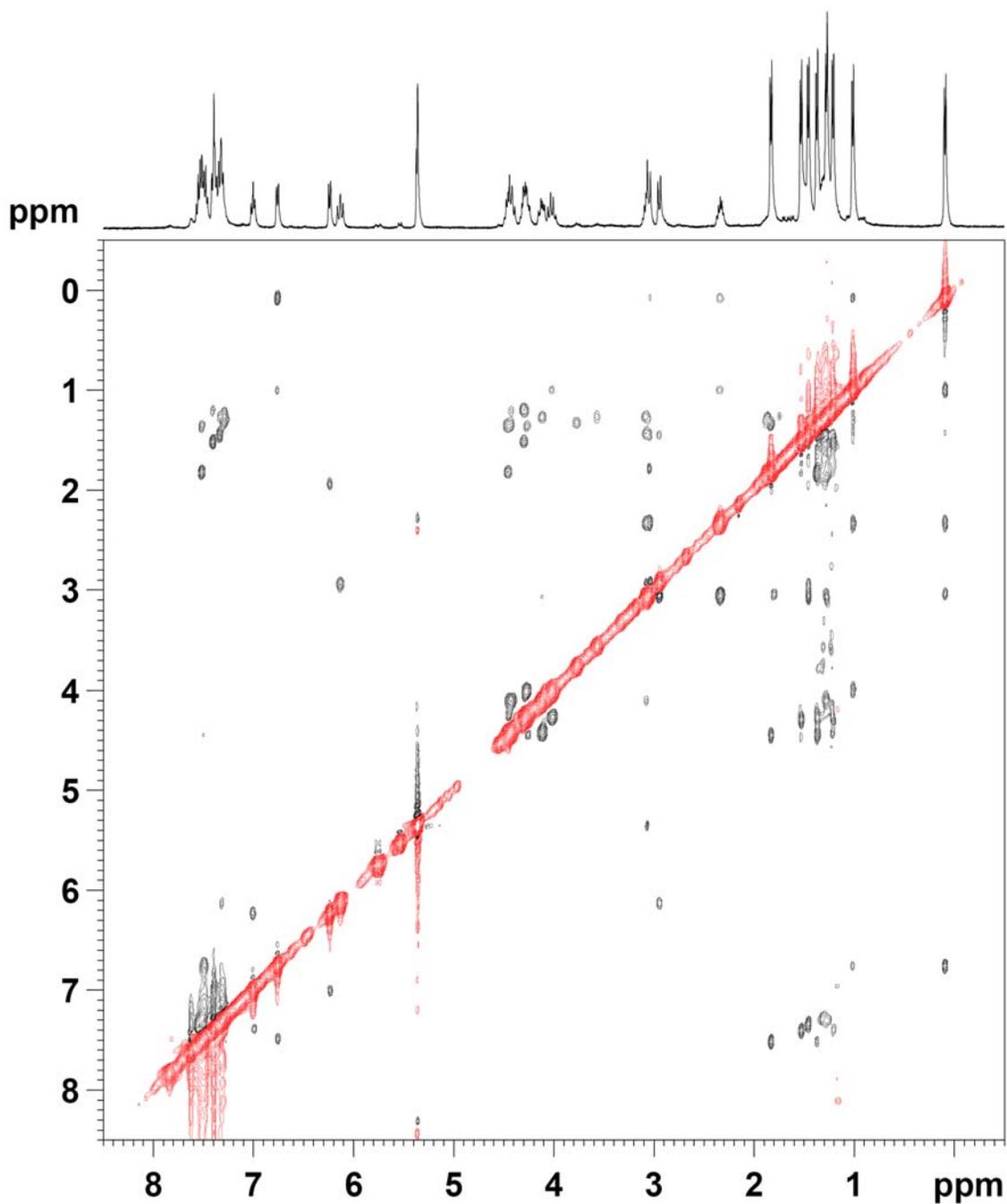
Figure 4.A13. Alkyl and aromatic region of 2D-NOESY/EXSY spectrum of **4.14** in CD$_2$Cl$_2$ at 22 °C.
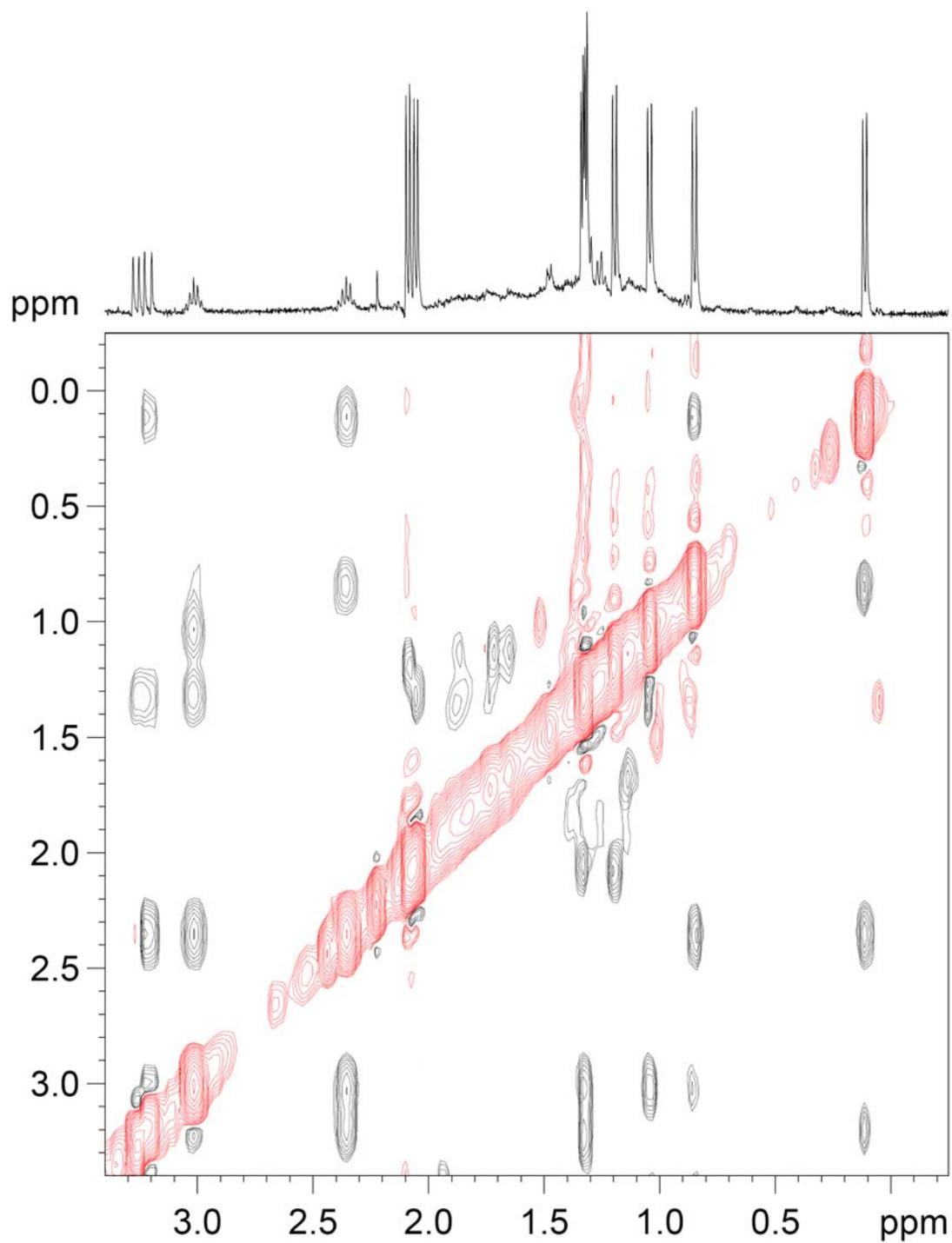
Figure 4.A14. 2D-NOESY/EXSY spectrum of **4.14** in C_6D_6 at 22 °C.
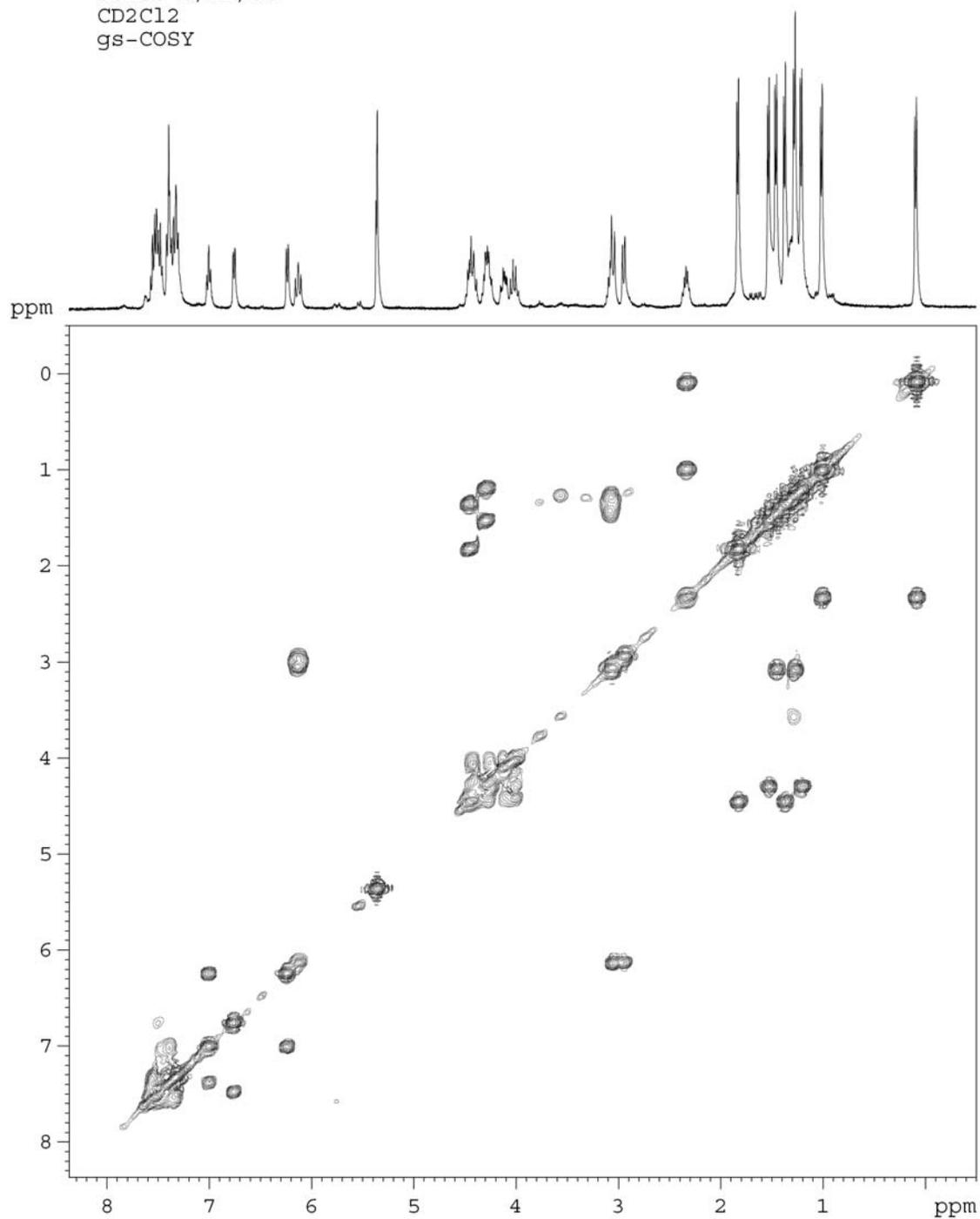
**Figure 4.A15**. COSYLR spectrum of **4.14** in CD$_2$Cl$_2$ at 22 °C.
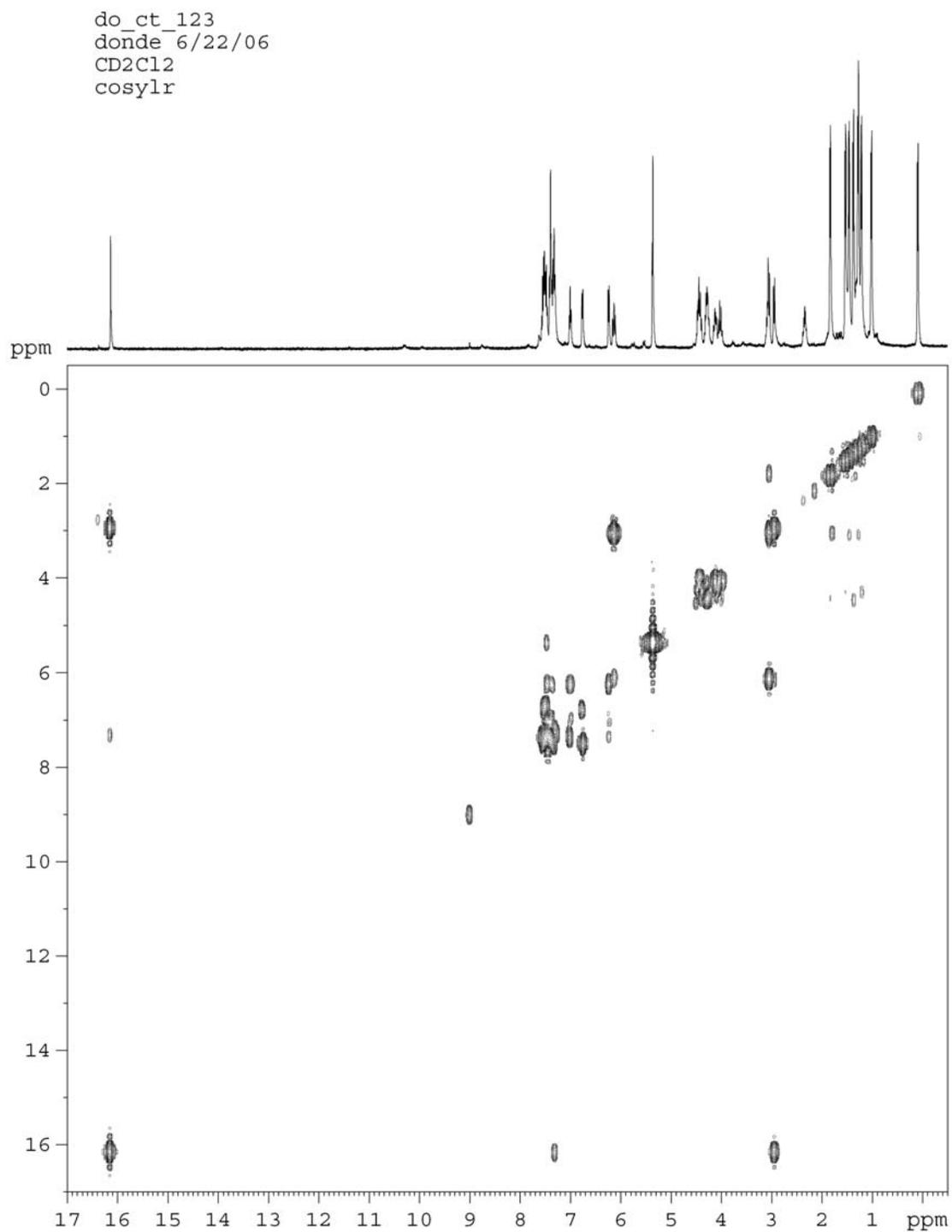
Figure 4.A16. COSYLR spectrum of **4.14** in CD$_2$Cl$_2$ at 22 °C.

do_ct_123
donde 062206, C6D6
C-H correlation for olefin carbon chemical shift assignment
HSQC experiment, 256 scans per fid, 20 hr
olefin carbons at ca. 68 + 107 ppm
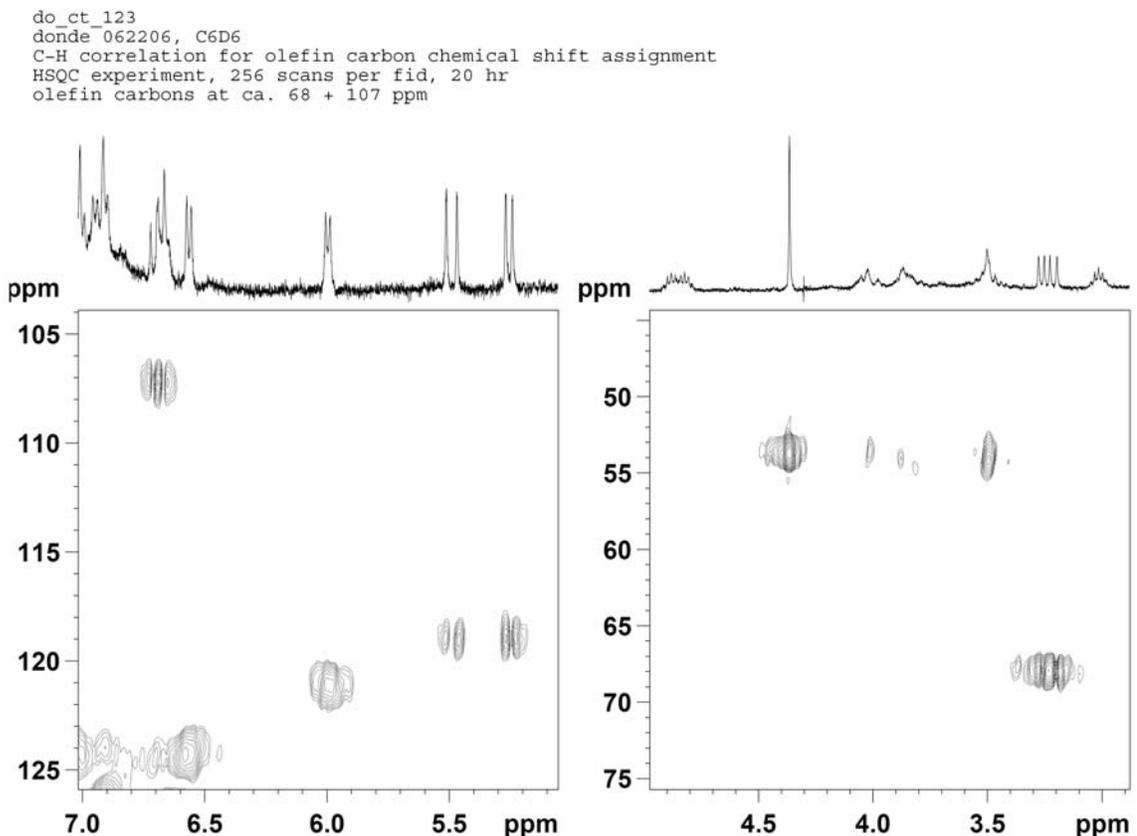
Figure 4.A17. Selected regions of HSQC spectrum of **4.14** in C_6D_6 at 22 °C.

Complex **4.17**: To a 4-mL vial in the glovebox was added **4.16** (12 mg, 0.012 mmol) and pentane (ca. 0.5 mL). Vial capped with a screwcap containing a PTFE septum and removed from the glovebox. Divinylbenzene (1.8 μL, 0.012 mmol) added via syringe. Vial taken into the glovebox. The reaction stirred at 22 °C overnight, filtered through a pipette column and washed with pentane (4 x 2 mL). Solid eluted with CH_2Cl_2 and concentrated to green solid (8 mg, 89%). ^{1}H NMR (CD_2Cl_2, 400 MHz): δ = 16.25 ppm (s, Ru=CHAr of **4.17b**), 15.57 (s, Ru=CHAr of **4.17a**), 15.37 (s, minor isomer C). Olefin resonances for isomer **4.17a**: 2.93 (d, 1H, J = 12.4 Hz, H_c), 3.05 (br d, 1H, J = 9.6 Hz, H_b), 5.93 (dd, 1H, J = 9.6, 12.4 Hz, H_a). Olefin resonances for isomer **4.17b**:

3.25 (dd, 1H, J = 1.3, 12.2 Hz, H_c), 2.23 (dt, 1H, J = 9.4, 1.2 Hz, H_b), 5.41 (overlapping

with other peaks, shift determined by COSY, H_a). Olefin resonances for isomer C: 2.78

(d, 1H, J = 12.5 Hz, H_c), 2.88 (br d, 1H, J = 10.0 Hz, H_b), 5.81 (overlapping with other

peaks, shift determined by COSY, H_a)

Select ^{13}C shifts from HMQC experiments (CD_2Cl_2) for olefin carbons:

Isomer A: CH_2: 84.34 ppm, CH: 101.20 ppm.
Isomer B: CH_2: 64.91 ppm, CH: 92.80 ppm.
Isomer C: can not be determined due to S/N issues.

The proton resonance at 3.05 ppm (H_b of isomer **4.17a**) has an unambiguous NOE to a

methyl group (1.48 ppm) and to an isopropyl methine (3.36 ppm) [and to 5.93 ppm,

which is the cis-disposed H_a]. This NOE might be expected if this conformer is identical

to the X-ray structure. H_c would be expected to have an NOE to an aromatic proton, as it

is facing a region where the *i*-Pr group is facing away. H_c does in fact have an NOE to a

proton at 5.69, which is an aromatic doublet and thus consistent with an H ortho to N(2)

[see X-ray structure].

The proton resonance at 2.23 ppm (H_b of isomer **4.17b**) has an ambiguous NOE to the

methyl region (ambiguous because this proton sits on top of a methine associated with the

minor component, note that a methine would be expected to have a strong NOE to a

methyl group). This is most likely an olefin-methyl NOE however, because methine-

methyl NOEs typically come in pairs (provided there is a chemical shift difference

between the methyl groups). The assignment of isomer **4.17b** to the side-bound, "CH_2

down" conformation is based upon the absence of NOEs involving H_c and the

methyl/methine region and one NOE involving H_a (5.41 ppm) and the methyl region is detected (NOE to 1.67 ppm), in addition to the expected NOE to H_b at 2.22 ppm.
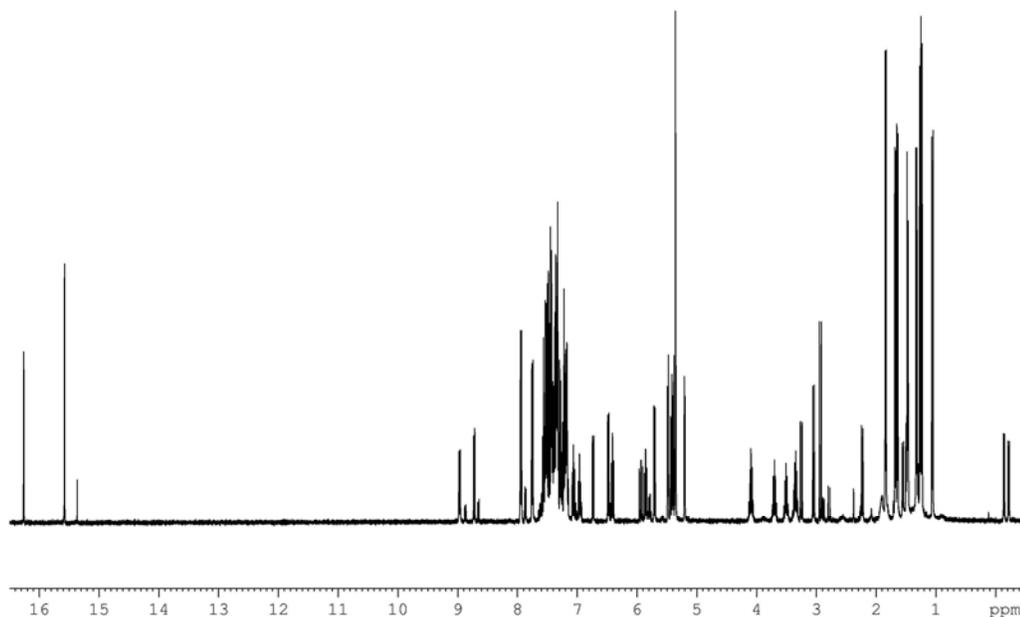
Figure 4.A18. ^1H NMR spectrum of **4.17** in CD_2Cl_2 at 22 °C.
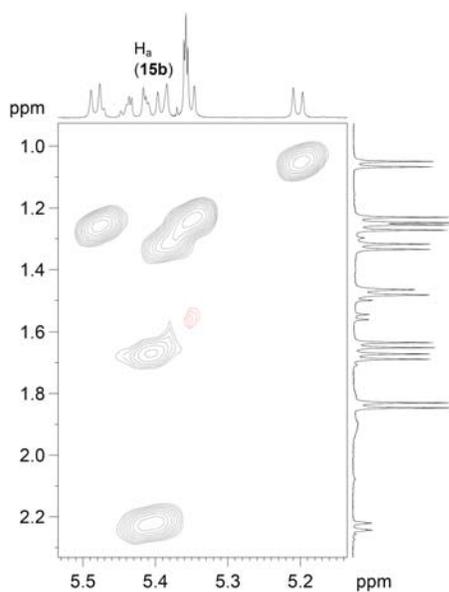
Figure 4.A19. 2D-NOESY/EXSY spectrum of **4.17** in CD_2Cl_2 at 22 °C.
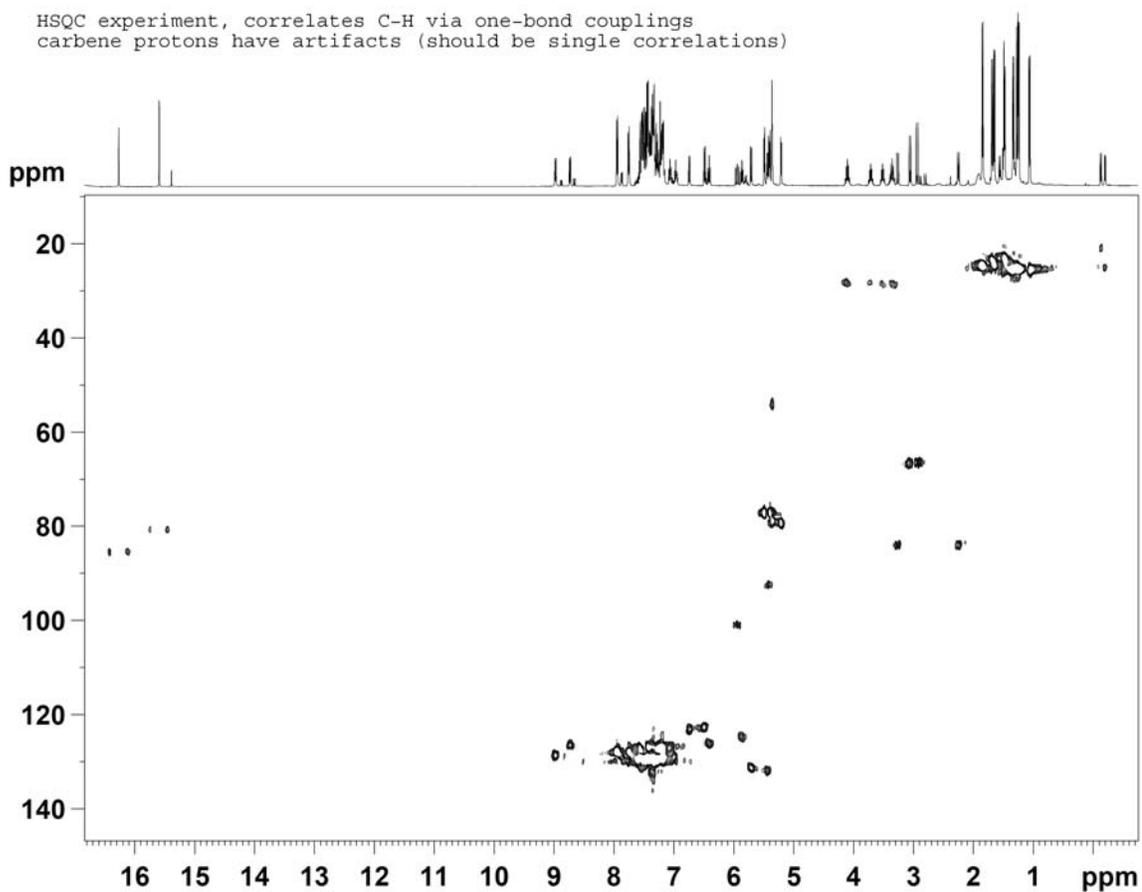
Figure 4.A20. HSQC spectrum of **4.17** in CD$_2$Cl$_2$ at 22 °C.

do_101 expt 10
cosy experiment
detects 'normal' H-H couplings
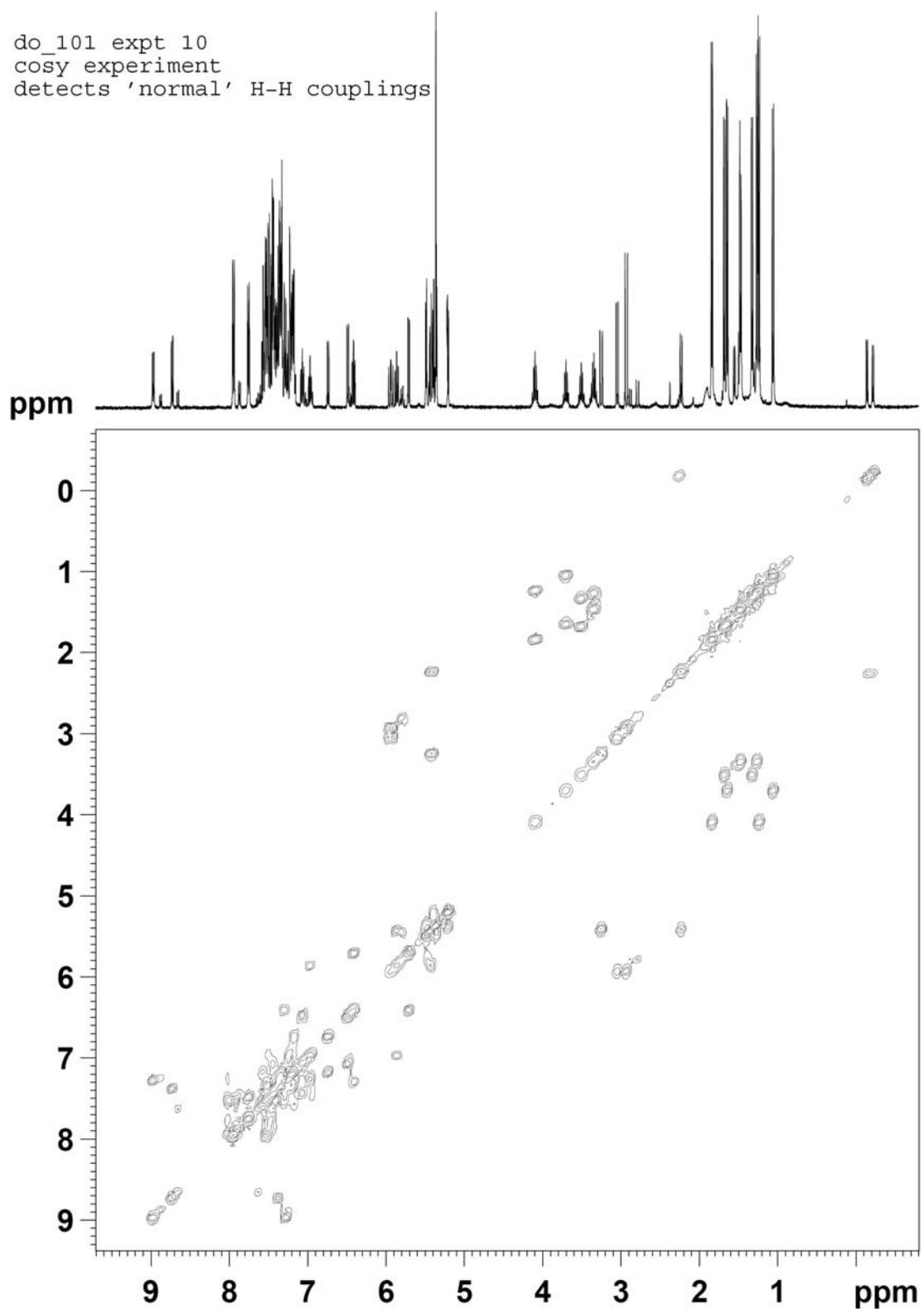
Figure 4.A21. Selected region of a COSY spectrum of **4.17** in CD_2Cl_2 at 22 °C.
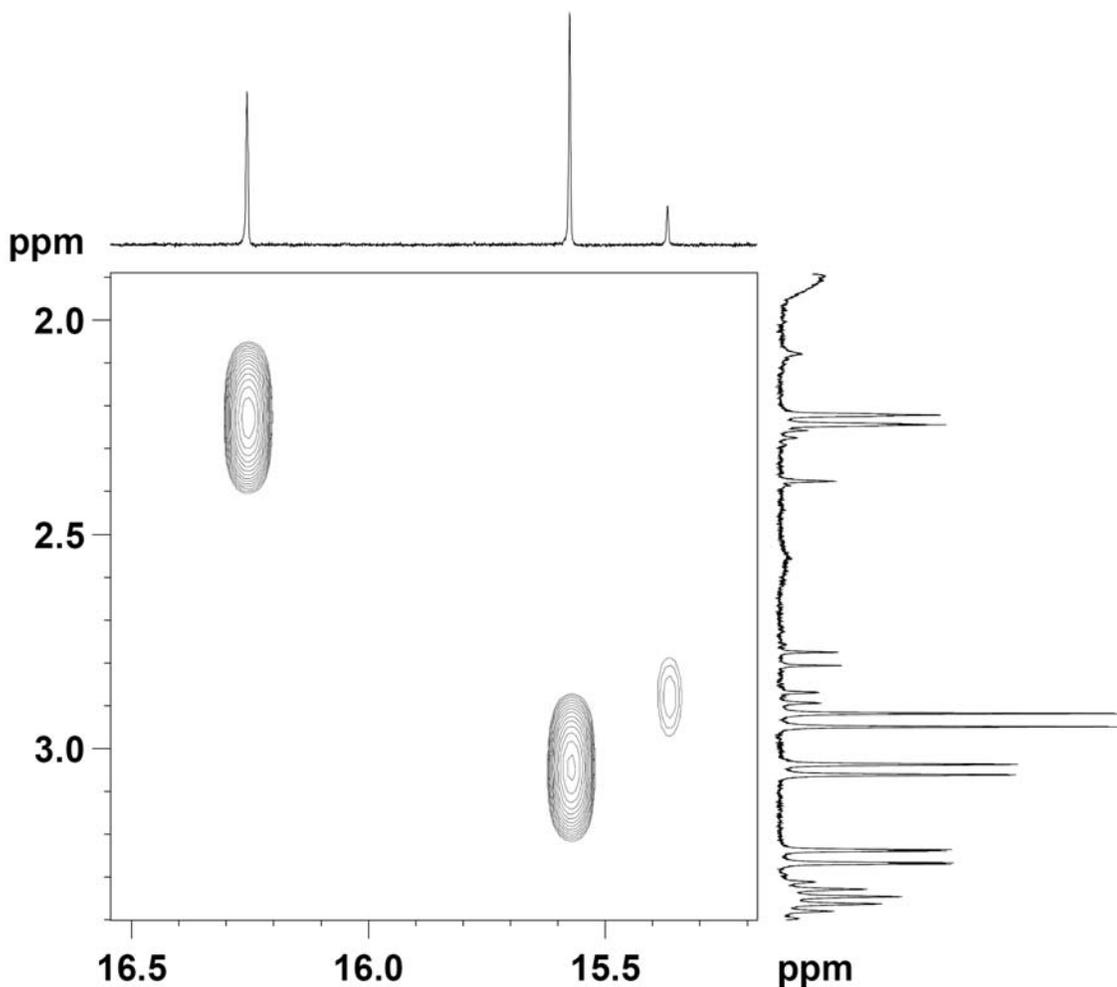
Figure 4.A22. Selected region of a COSYLR spectrum of **4.17** in CD$_2$Cl$_2$ at 22 °C.

Complex **4.19**:   To a 4-mL vial in the glovebox was added **4.18** (99 mg, 0.143 mmol) and toluene (ca. 2 mL). Vial capped with a screwcap containing a PTFE septum and removed from the glovebox. Divinylbenzene (19 μL, 0.14 mmol) added via syringe. Vial taken into the glovebox. The reaction stirred at 22 °C overnight, filtered through a pipette column and washed with toluene (ca. 1 mL) and pentane (3 mL). Solid eluted with CH$_2$Cl$_2$ and concentrated to yellow-green solid (32 mg, 40%). HRMS (FAB) *m*/*z* (%): 568.1392 [M-H]$^+$ (11).

The broad peak at 5.52 is assigned as H_a because it has COSY cross peaks to signals at 3.59 ppm and to 2.68 ppm. Note that 3.59 and 2.68 do not have COSY crosspeaks to each other, which might be expected if they are geminal olefin resonances. A complication is that 2.68 is a region that likely contains Cy resonances as well. Note that 5.52 has an NOE to 3.59 (cis-disposed H_b) and 3.59 has a strong NOE into the 2.68 region (geminal disposed H_a).
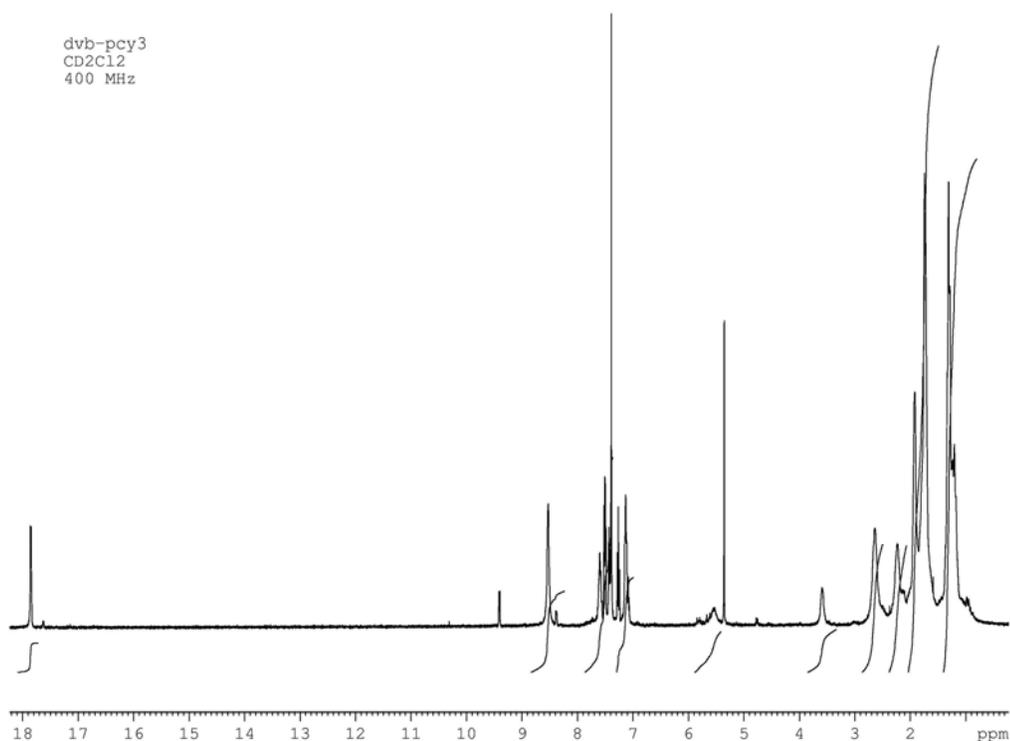
Figure 4.A23. ^{1}H NMR spectrum of **4.19** in CD$_2$Cl$_2$ at 22 °C.
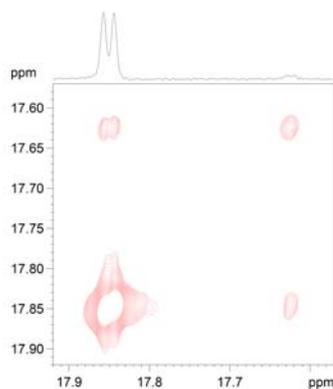
Figure 4.A24. 2D-EXSYspectrum of **4.19** in CD$_2$Cl$_2$ at 22 °C.

NOESY, 600 ms mixing time
red = negative contours
black = positive contours
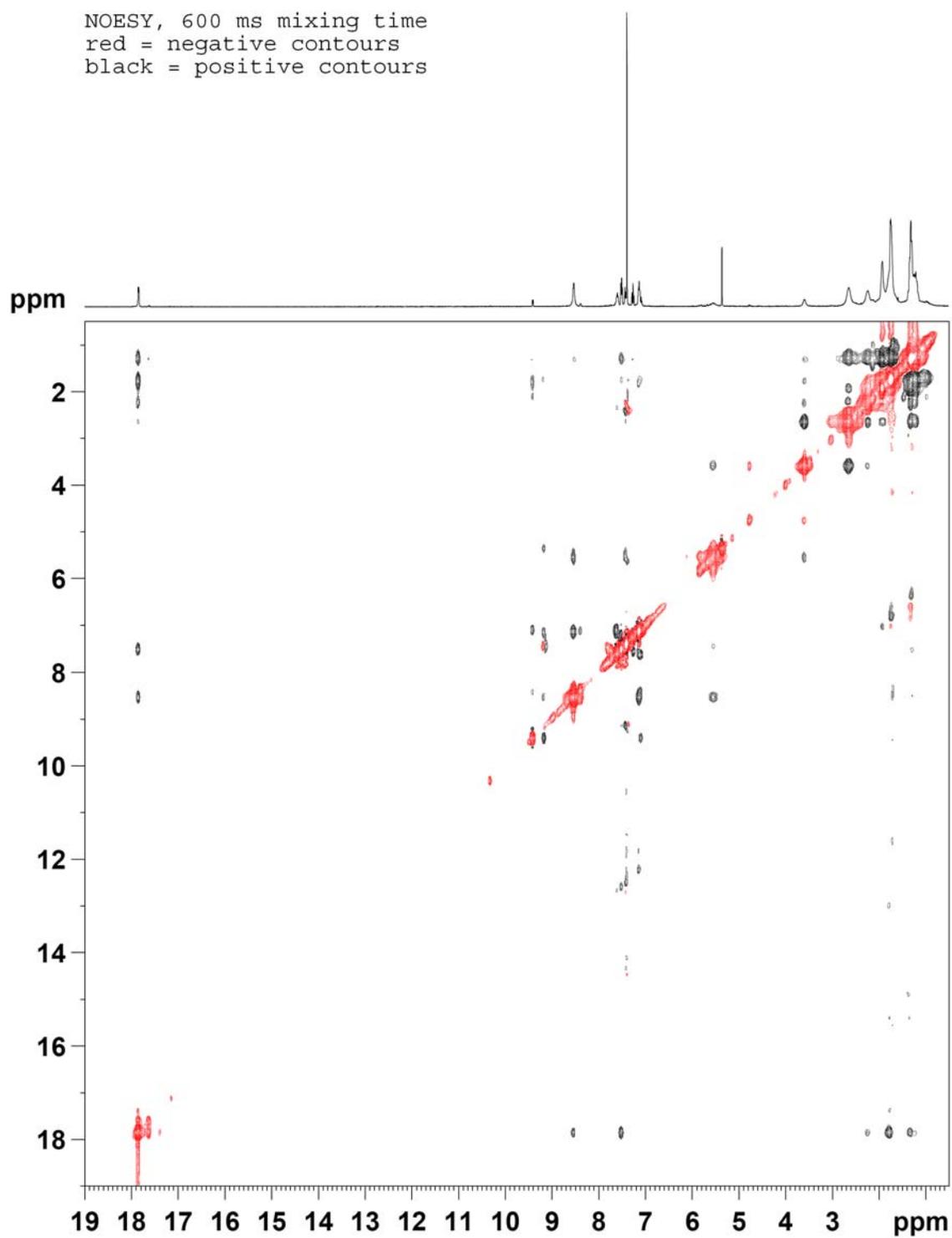
Figure 4.A25. 2D-NOESY/EXSYspectrum of **4.19** in CD$_2$Cl$_2$ at 22 °C.
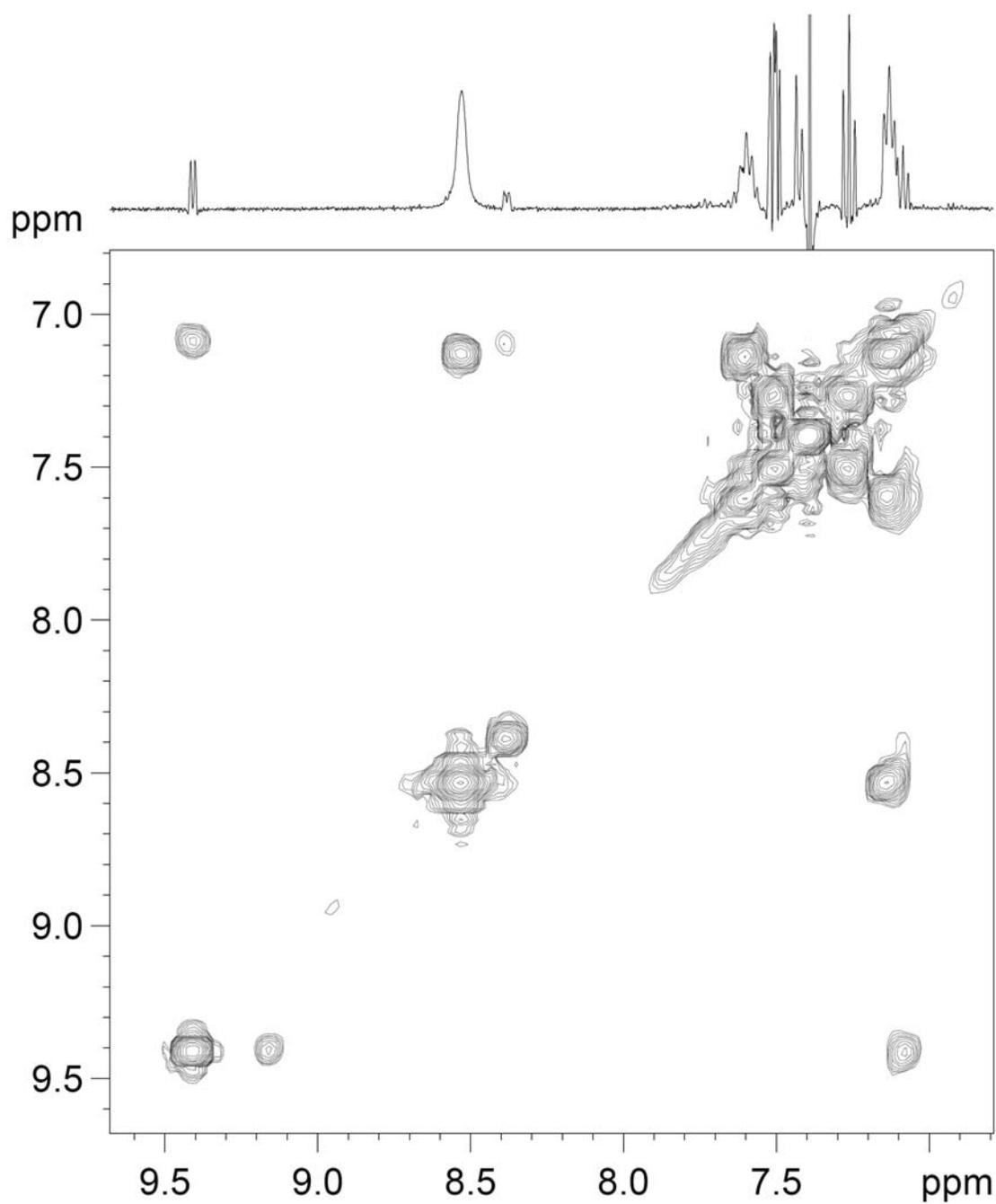
Figure 4.A26. COSY spectrum of **4.19** in CD$_2$Cl$_2$ at 22 °C.
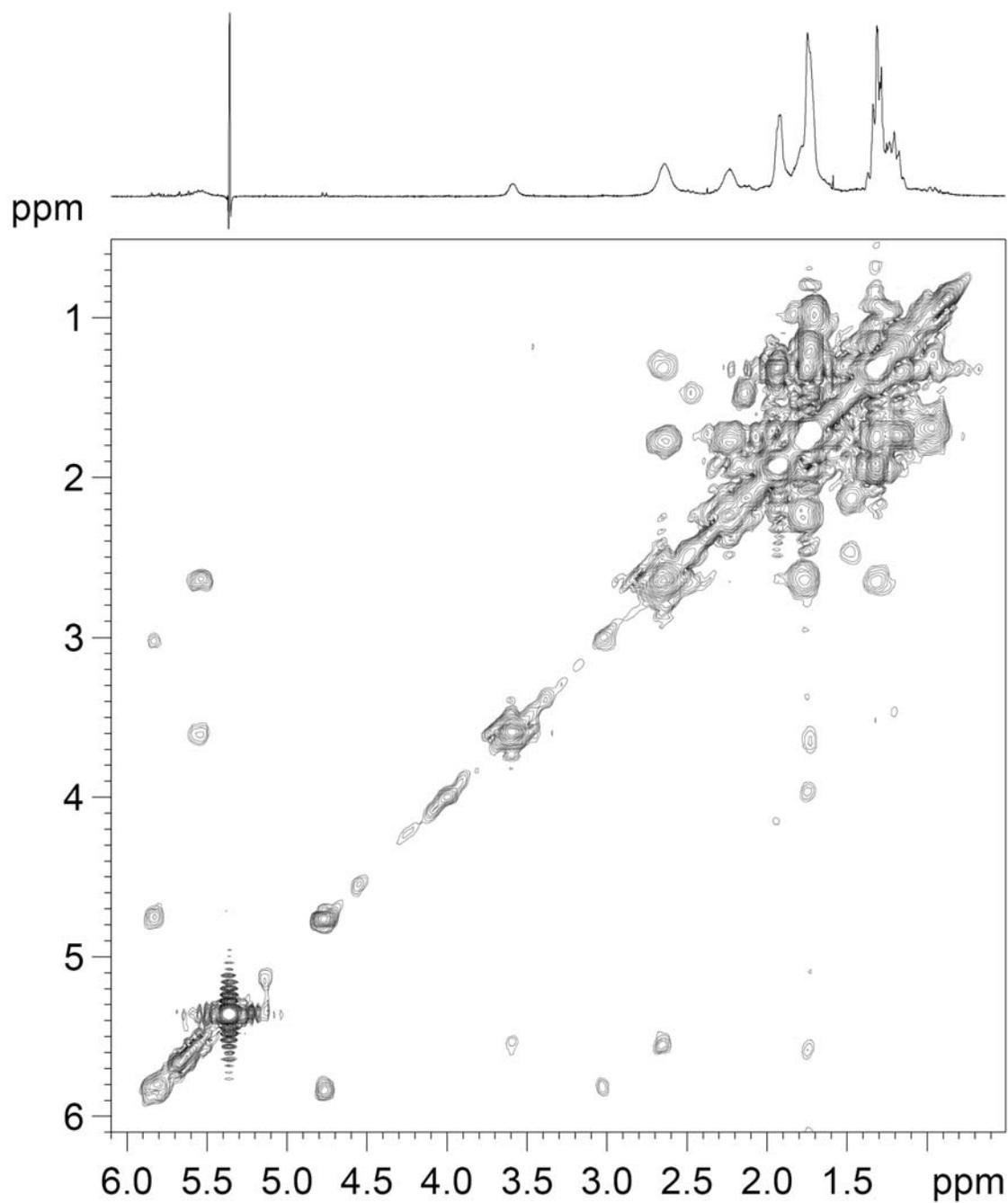
Figure 4.A27. COSY spectrum of **4.19** in CD$_2$Cl$_2$ at 22 °C.
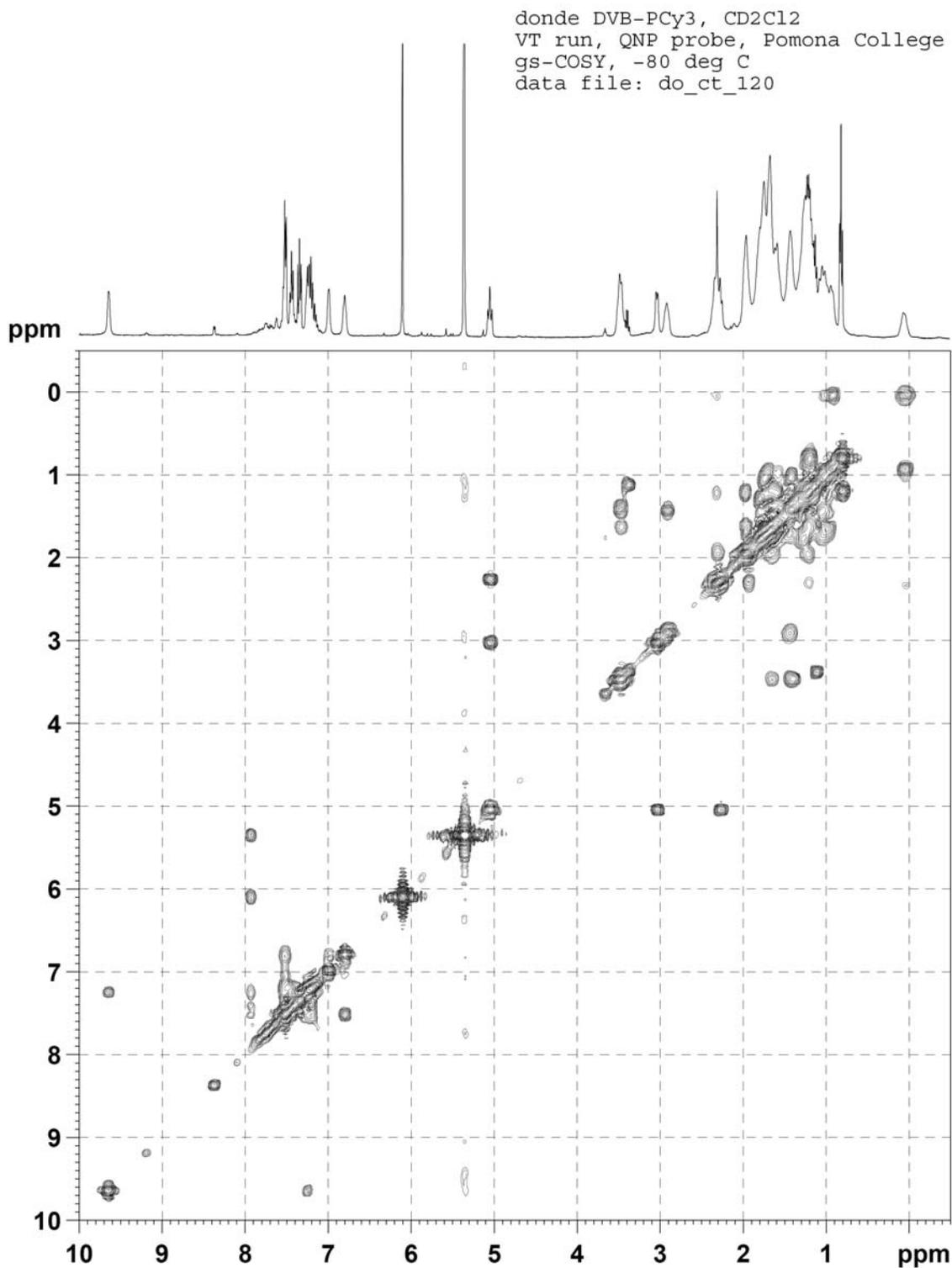
Figure 4.A28. COSY spectrum of **4.19** in CD$_2$Cl$_2$ at −80 °C.

Complex **4.21**: Synthesized utilizing procedure analogous to the synthesis of **4.19**. HRMS (FAB): 608.2 [M]$^+$.

Select data for major isomer: ^{1}H NMR (CD$_2$Cl, 400 MHz): 15.86 ppm (br s, 1H, Ru=C*H*Ar), [15.50 (s, 0.26H, minor Ru=C*H*Ar)], 7.45 ppm (t, 1H, J = 7.4 Hz, H meta to benzylidene moiety), 7.35 ppm (d, 1H, J = 7.4 Hz, H ortho to benzylidene moiety), 7.06 ppm (splitting obscured by overlap, 1H, H para to benzylidene moiety), 6.45 ppm (d, 1H, J = 7.6 Hz, H ortho to alpha olefin), 4.6-3.8 (m, 4H, NHC backbone protons, exchange cross peaks observed between these backbone resonances), 3.2 ppm (br s, H$_c$), 2.94 (1H, H$_b$, overlapping with other resonances), 2.92 ppm (s, 3H, *ortho*-Me grp), 2.73 (s, 3H, *ortho*-Me grp), 2.37 (6H, overlapping *para*-Me grps), 2.35 (s, 3H, *ortho*-Me grp), 2.10 (s, C*H*$_3$C(Ar)=CH$_2$), 1.44 (s, 3H, *ortho*-Me grp).

Select ^{13}C{^{1}H} NMR data (CD$_2$Cl$_2$, 100 MHz) for the major isomer: benzylidene carbon: 295.33 ppm, CH$_2$ carbon of olefin: 67.7 ppm, quaternary carbon of olefin: 117.4 ppm (assignment is tentative), alpha Me group carbon: 26.47 ppm. For the minor isomer: olefin protons at 2.96 and 2.16 ppm and olefinic CH$_2$ carbon at 62.96 ppm.

Major benzylidene NOEs to two methyl groups at 2.35 and 2.89. Note these methyls are in exchange with one another, so the benzylidene likely has an NOE to one site. A strong benzyidene NOE is observed to 6.45 (likely the ortho aromatic H). The general identity of H$_b$, H$_c$, and the alpha-Me group were preliminarily established with COSYLR and HSQC data (below). An NOE between 2.94 and 2.10 ppm establishes the former as H$_b$. A strong NOE is observed between 2.94 and 3.2 ppm, as expected. EXSY crosspeaks are

not observed for the benzylidene nor olefin resonances. EXSY crosspeaks are observed for aromatic singlets and mesityl methyl groups, indicating NHC ligand dynamics at work.

COSYLR data: major benzylidene has a COSYLR interaction to shifts at 2.94 and 7.35 ppm. If this compound is like the others, this implies one olefin resides at 2.94. There is a proton at 2.94 that is attached to a carbon at 68 ppm (HSQC data) bearing an additional attached proton at 3.2 ppm. Both the 3.2 and 2.94 peak have a COSYLR interaction with a resonance at 2.102, which identifies this resonance as that of the alpha methyl group. Further evidence for this assignment is that the 2.10 peak connects to a ^{13}C resonance at 26.47 ppm, which is a unique resonance relative to the mesityl methyl resonances (all at 20 ppm).

Identity of major isomer's conformation: olefin at 3.2 shows a strong NOE to Mes me groups at 1.44 ppm and 2.73 ppm (these Me groups are also in exchange with one another). The benzylidene NOEs to two methyl groups at 2.35 and 2.92 ppm—again these two Me groups are also in exchange with one another.

These data are consistent with a solution conformation similar to the X-ray crystal structure. Further, they suggest that the slow dynamics involve rotation about the Ru-C1 bond, as the benzylidene and olefin to Me NOEs are unique (they would have NOE'd to the same set of methyl groups if there was slow rotation about the N2-Mes bond). The

NHC backbone EXSY behavior is additional evidence for this slow motion—slow rotation about the N2-Mes bond would not exchange the backbone resonances.
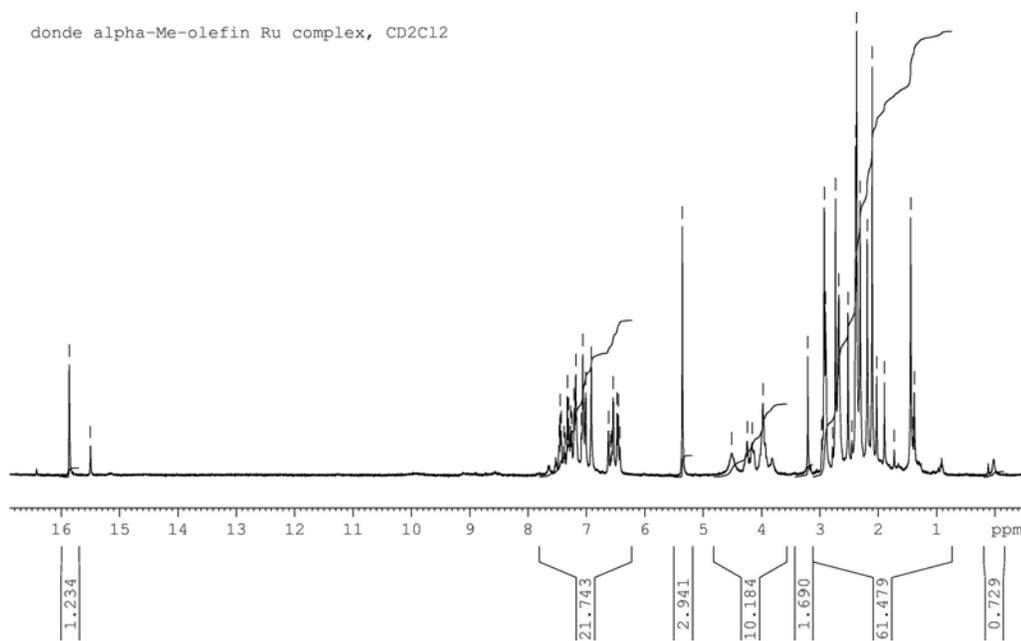
Figure 4.A29. ^{1}H NMR spectrum of **4.21** in CD$_2$Cl$_2$ at 22 °C.
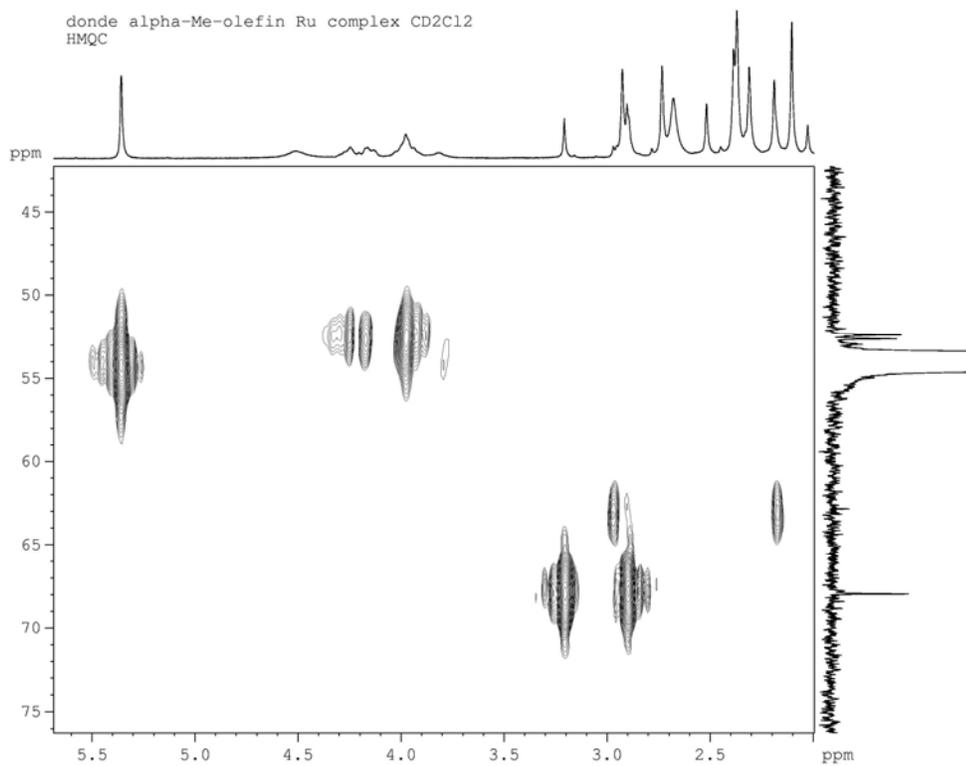
Figure 4.A30. HSQC spectrum of **4.21** in CD$_2$Cl$_2$ at 22 °C.

donde alpha-Me-olefin Ru complex, CD2Cl2
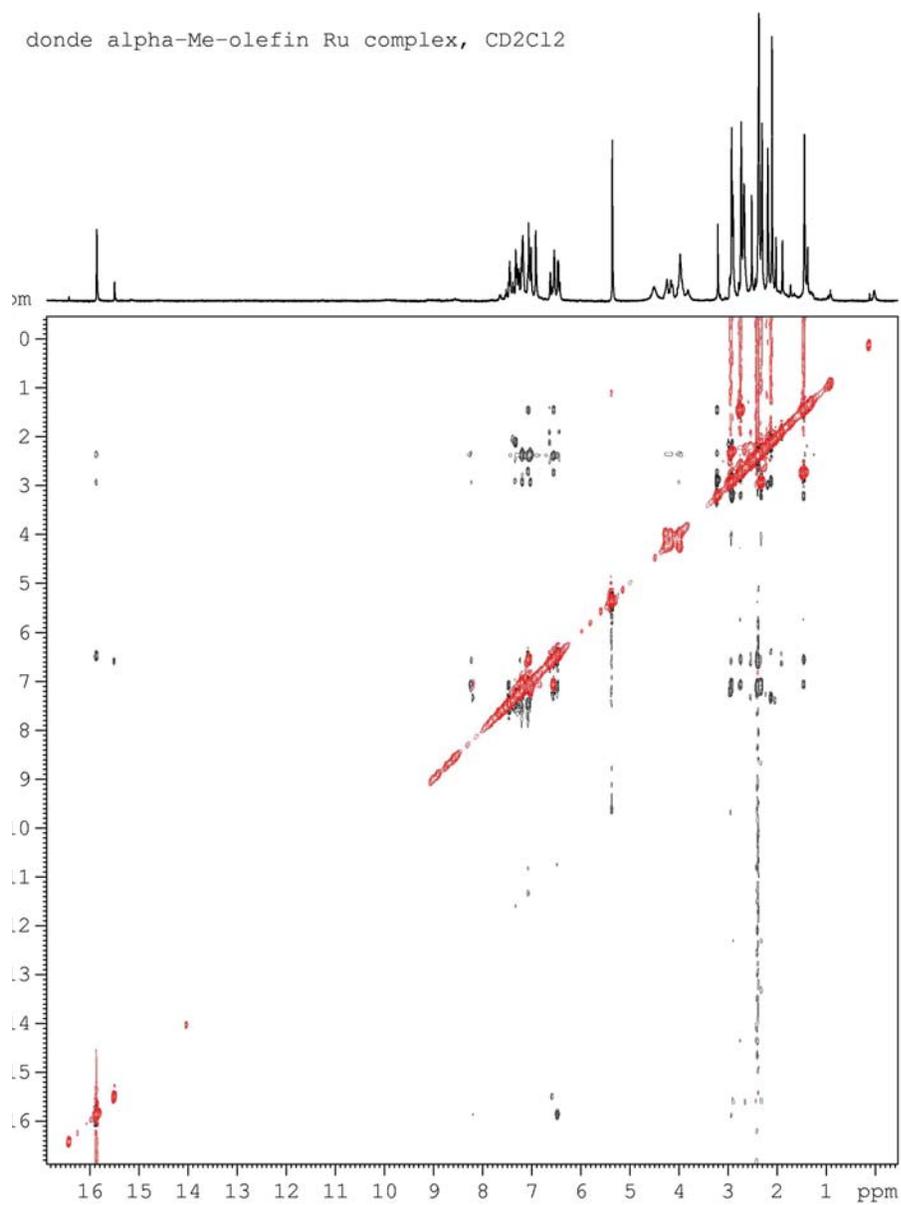
Figure 4.A31. 2D-NOESY/EXSY spectrum of **4.21** in CD_2Cl_2 at 22 °C.
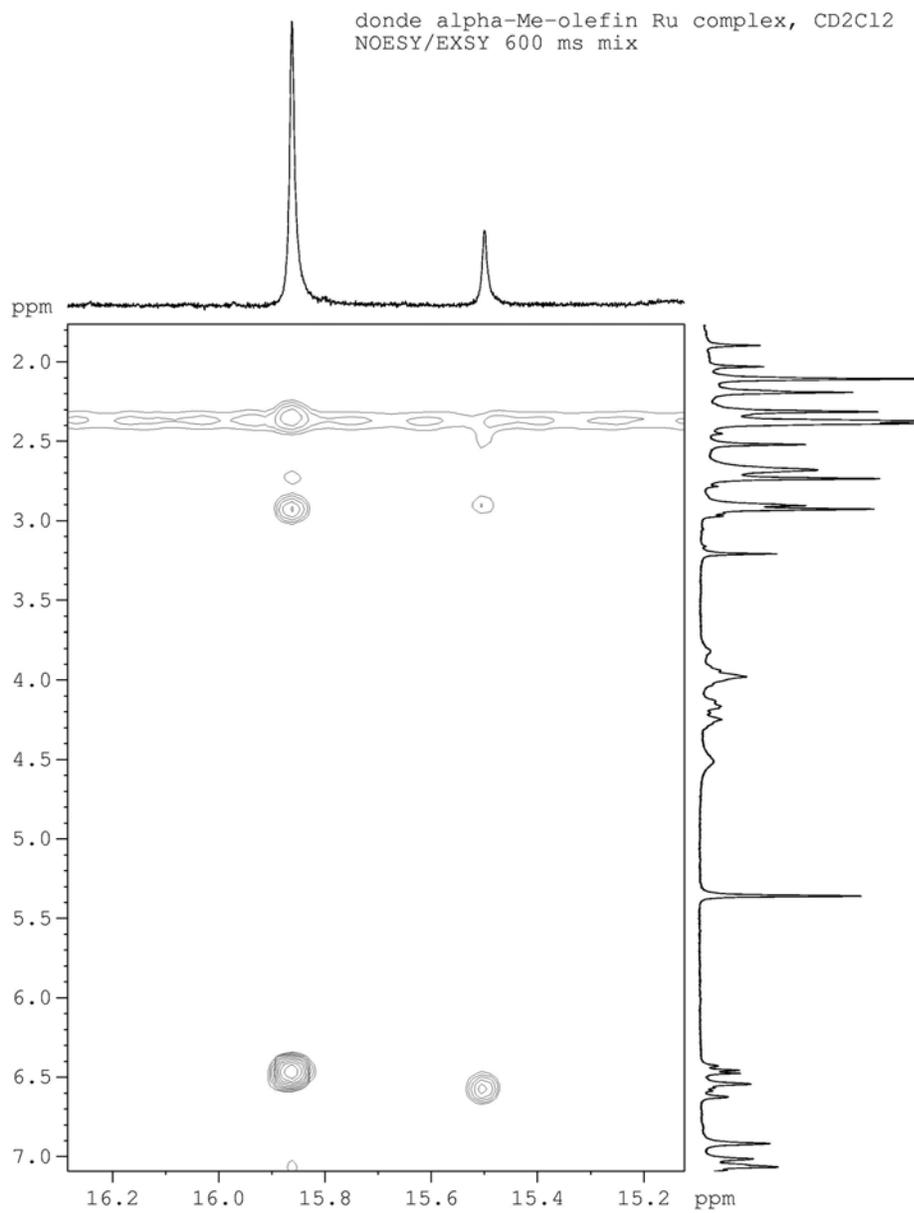
Figure 4.A32. 2D-NOESY/EXSY spectrum of **4.21** in CD$_2$Cl$_2$ at 22 °C.

```
donde alpha-Me-olefin Ru complex, CD2Cl2
COSYLR
```
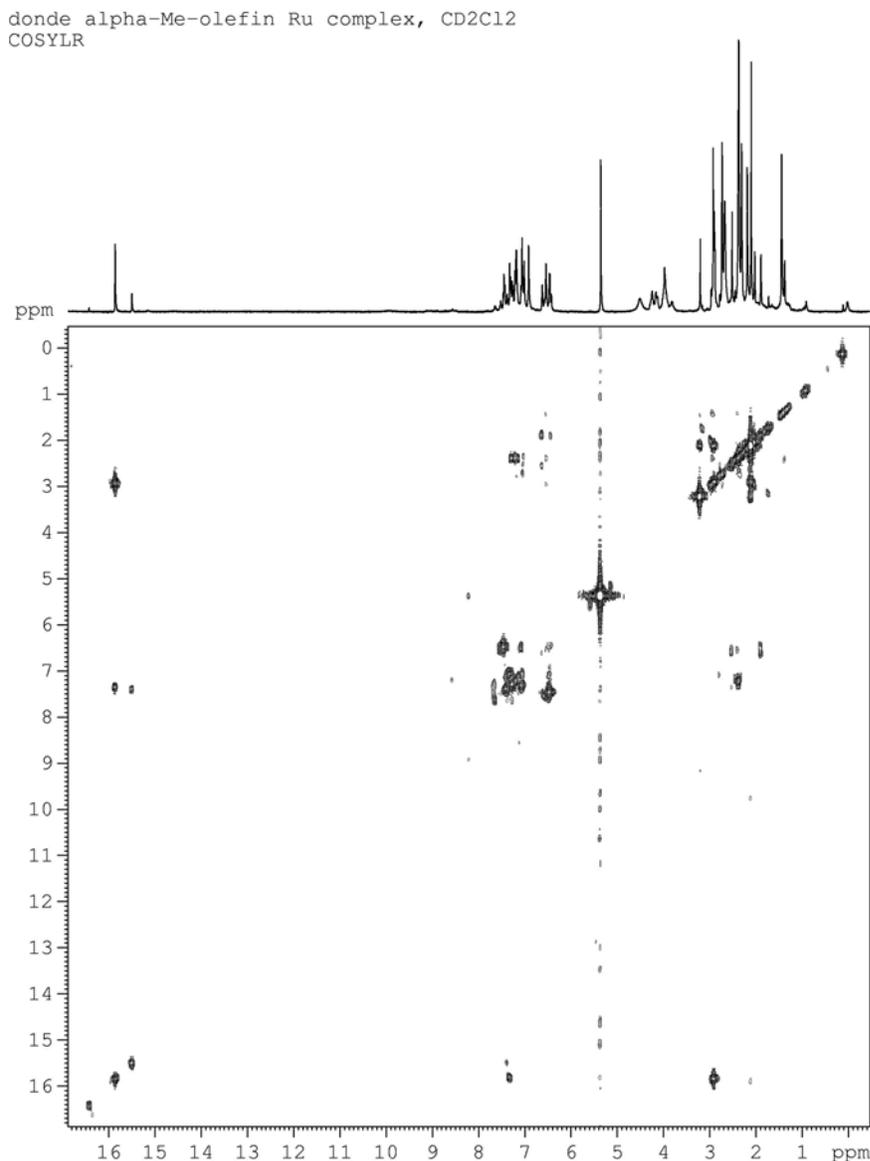

Figure 4.A33. COSYLR spectrum of **4.21** in CD$_2$Cl$_2$ at 22 °C.

Complex **4.32**: To a 4-mL vial in the glovebox was added **4.7** (100 mg, 0.14 mmol) and benzene (2 mL). Vial capped with a screwcap containing a PTFE septum and removed from the glovebox. Divinylbenzene (31 µL, 0.15 mmol) added via syringe. Vial taken into the glovebox. The reaction stirred at 22 °C 30 min, filtered through a pipette column and washed with toluene (ca. 1 mL) and pentane (2 x 2 mL). Solid eluted

with CH_2Cl_2 and concentrated to yellow-green solid (37 mg, 56%). HRMS (FAB) m/z (%): 664.0337 $[M+H-H_2]^+$ (47).

^{1}H NMR (CD_2Cl_2, 400 MHz): 6 benzylidene protons observed: 16.34 (.04 H), 16.26 (.05 H), 16.24 (0.37 H), 16.18 (0.17 H), 16.11 (1 H), 16.04 (0.11 H) ppm.

Major isomer (16.11 ppm) olefin resonances: H_a: 6.04 ppm (dd, 1H, J = 10.3, 12.2 Hz), H_b: 3.60 (d, 1H, J = 10.3 Hz), H_c: 3.50 (d, 1H, J = 12.2 Hz). NOEs observed between: 16.11 ppm (H_α) and 6.41, 2.92, 1.29 ppm; H_a and 3.60 ppm (H_b), 7.437 ppm; H_c and H_b, 6.07 2.396, 1.302 ppm; H_b and one methyl resonance at 2.41 ppm. These NOEs suggest that the 'CH$_2$ up' isomer is the major solution conformation.

Minor isomer (16.24 ppm) olefin resonances: H_a: 5.45 ppm (dd, 1H, J = 9.8, 12.8 Hz), H_b: 3.57 (br d, 1H, J = 10.3 Hz [a doublet of ill-resolved triplets]), H_c: 3.64 (dd, 1H, J = 1.9, 12.2 Hz). NOEs observed for the minor isomer between: H_a and 3.59 (H_b), 2.42, 2.05 ppm. No NOEs were detected for the $H_{a/b}$ resonances into the methyl region.

EXSY summary:

Me at 2.93 ppm is in exchange with 2.52, 2.37 ppm (major-minor exchange)
Me at 2.71 ppm is in exchange with 1.28 ppm (major-major exchange)
Me at 2.04 ppm is in exchange with 1.28 ppm (minor-major exchange)
Me at 2.21 ppm is in exchange with 2.44 ppm (minor-major exchange)

ArH at 6.19 ppm is in exchange with 6.52 ppm (minor-major exchange)
ArH at 6.38 ppm is in exchange with 6.73 ppm (minor-major exchange)
ArH at 6.89 ppm is in exchange with 7.18 ppm (minor-major exchange)
Olefin H_a(major) is in exchange with H_a (minor)
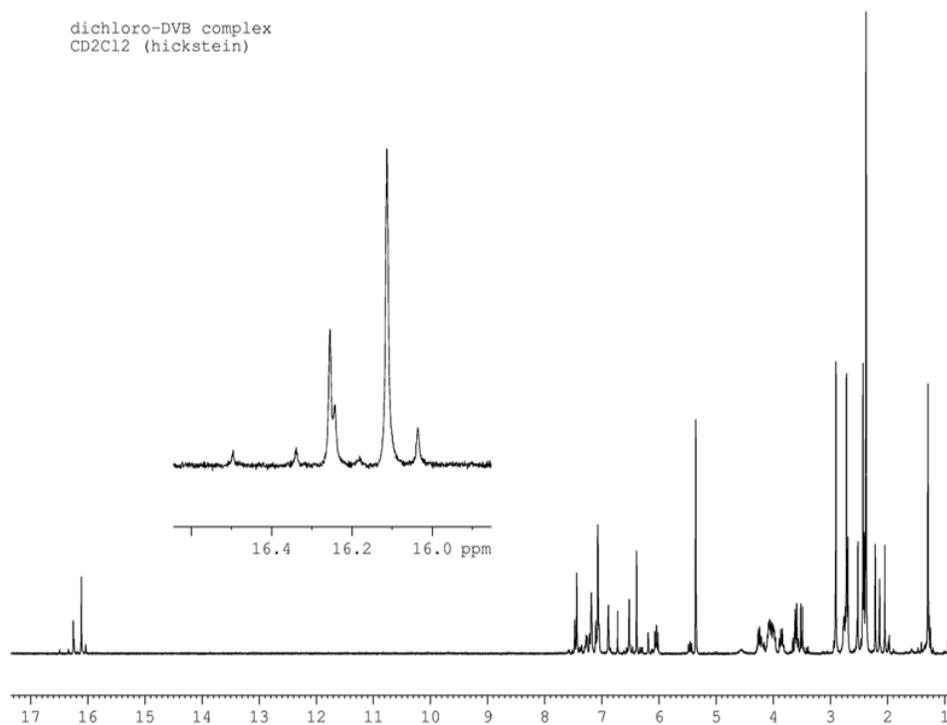
Figure 4.A34. ^{1}H NMR spectrum of **4.32** in CD$_2$Cl$_2$ at 22 °C.
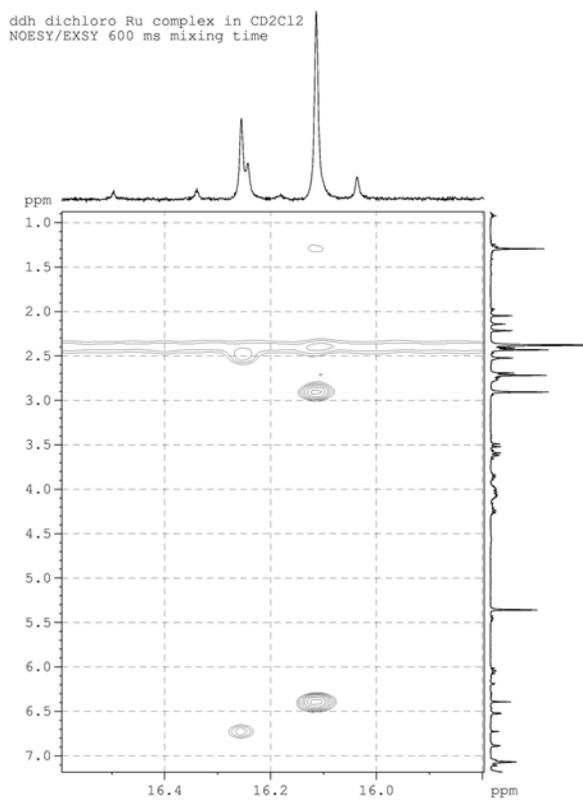
Figure 4.A35. 2D-NOESY/EXSY spectrum of **4.32** in CD$_2$Cl$_2$ at 22 °C.

ddh dichloro Ru complex in CD2Cl2
NOESY/EXSY 600 ms mixing time
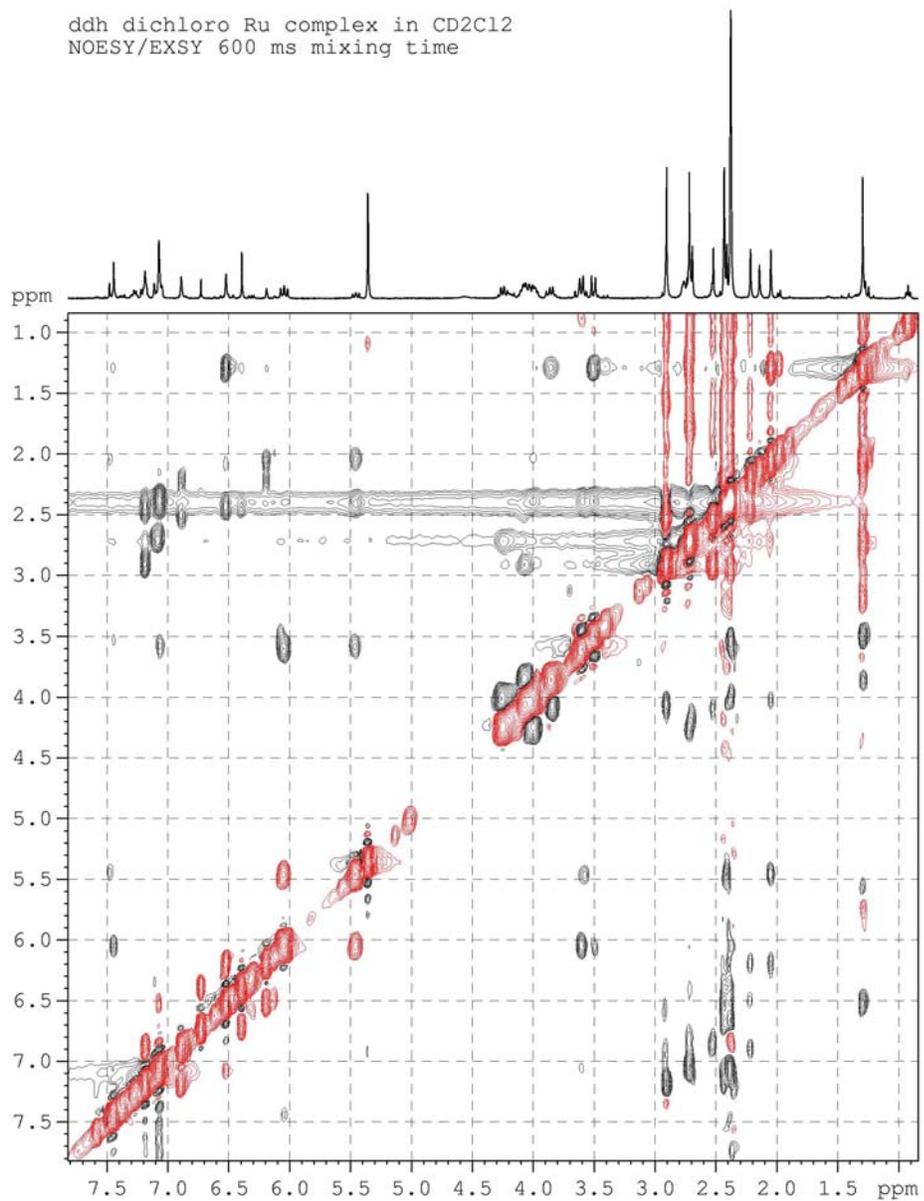
Figure 4.A36. 2D-NOESY/EXSY spectrum of **4.32** in CD$_2$Cl$_2$ at 22 °C.
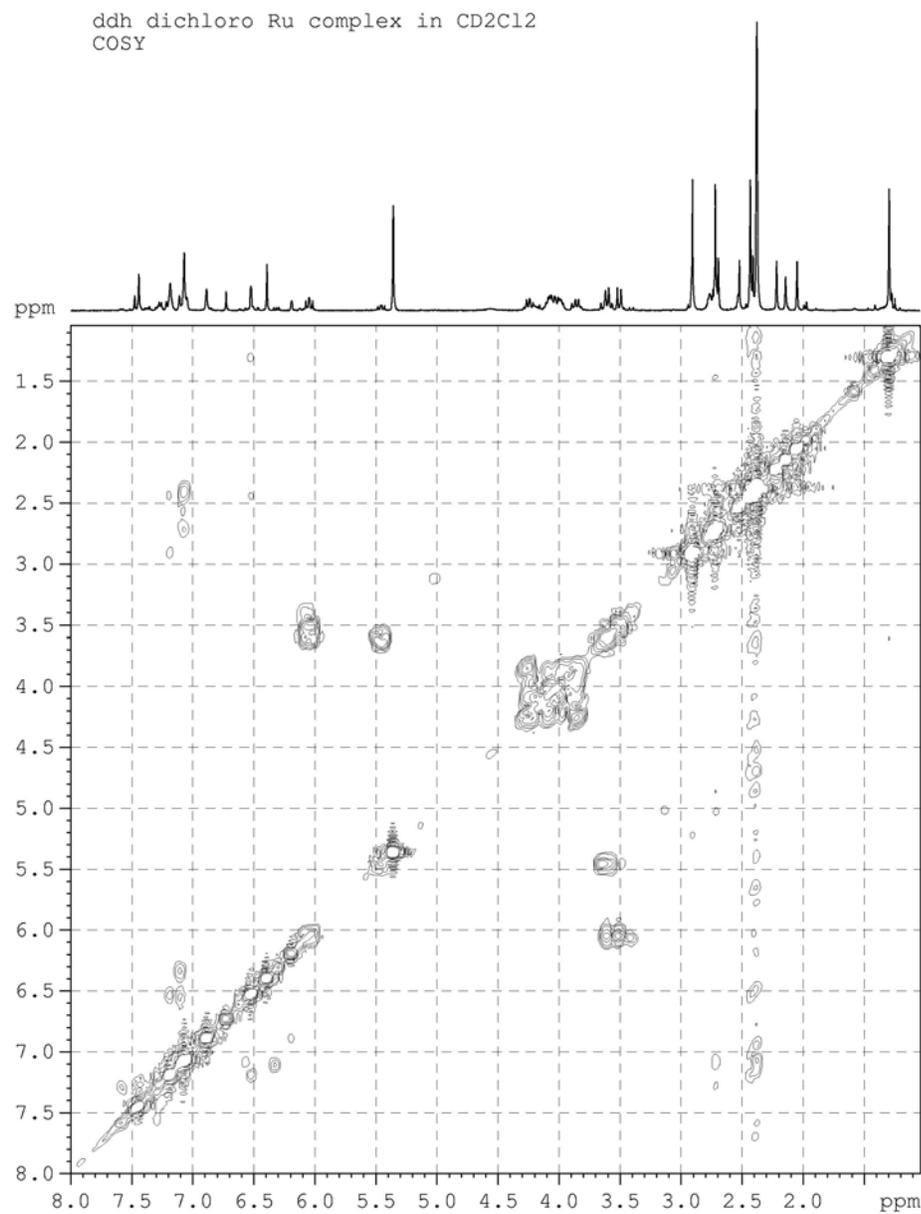
Figure 4.A37. COSY spectrum of **4.32** in CD$_2$Cl$_2$ at 22 °C.
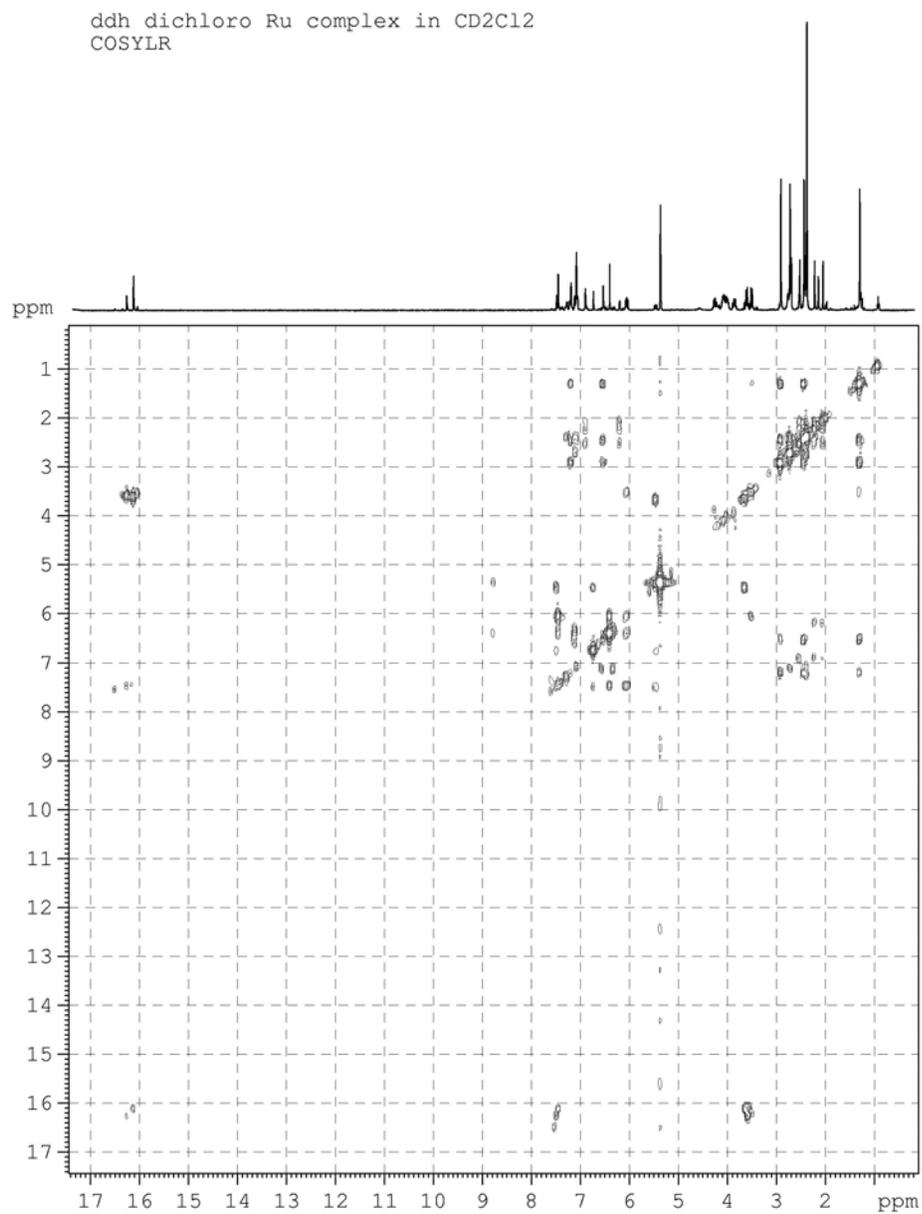
Figure 4.A38. COSYLR spectrum of **4.32** in CD$_2$Cl$_2$ at 22 °C.

ddh dichloro Ru complex in CD2Cl2
COSYLR
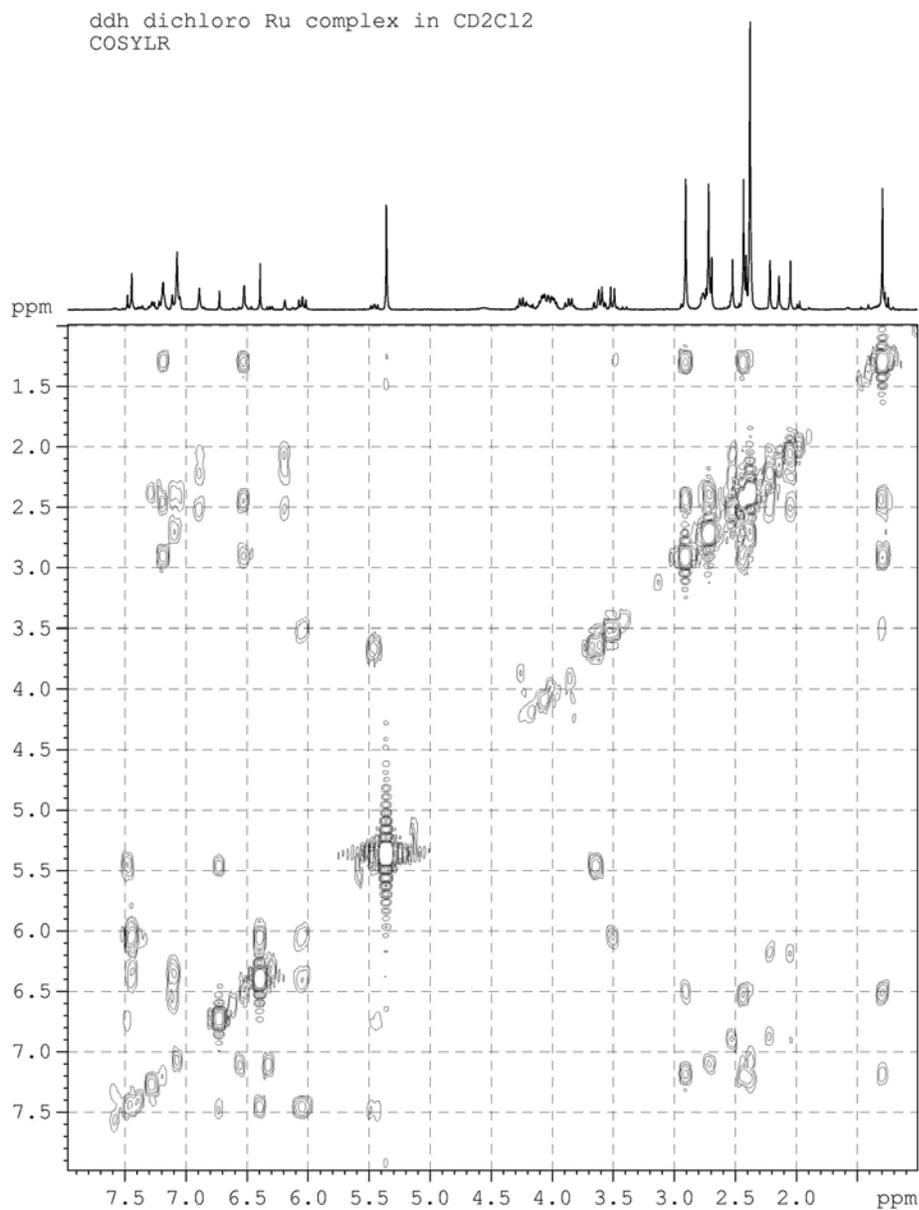
Figure 4.A39. COSYLR spectrum of **4.32** in CD$_2$Cl$_2$ at 22 °C.

4.A1   **4.A2**
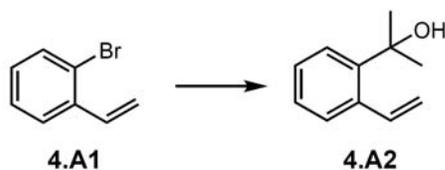
4.A2: To a flame-dried 25-mL Schlenk flask was added 2-bromostyrene (**4.A1**) and dry THF (ca. 5 mL). The flask was cooled in a dry ice/acetone bath and *n*-BuLi (0.87 mL of 2.5M solution in hexanes) added slowly via syringe. After 30 min, acetone (320 μL, 4.4 mmol) added slowly. The reaction was warmed to room temperature and stirred overnight. After aqueous workup, filtration, drying over Na_2SO_4, and removal of solvent under vacuum the crude product was purified by silica gel column chromatography (3:7 Et_2O:hexanes) to provide **4.A2**, a clear oil (309 mg, 87%). ^{1}H NMR (CDCl$_3$, 300 MHz): δ = 7.63 (dd, 1H, *J* = 11.1, 17.4 Hz), 7.49-7.43 (m, 2H), 7.26-7.23 (m, 1H), 5.51 (dd, 1H, *J* = 1.8, 17.4 Hz), 5.27 (dd, 1H, *J* = 1.8, 11.1 Hz), 1.67 (s, 6H).

4.A2   **4.20**
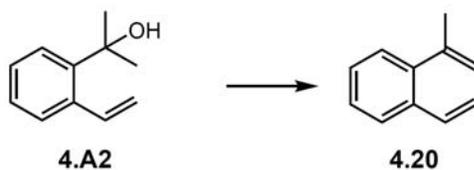
4.20: To a 100-mL round-bottom flask was added alcohol **4.A2** (240 mg, 1.5 mmol), $MgSO_4$ (100 mg, 0.83 mmol), and dry Et_2O (ca. 5 mL). Amberlyst resin (200 mg) added. The reaction was stirred overnight at room temperature (TLC conditions 3:7 Et_2O:hexanes), filtered and solvent removed under vacuum to give **4.20**, a clear oil (155 mg, 73%). ^{1}H NMR (CDCl$_3$, 300 MHz): δ = 7.56-7.43 (m, 1H), 7.26-7.14 (m, 3H), 6.91 (dd, 1H, *J* = 11.1, 17.7 Hz), 5.68 (dd, 1H, *J* = 1.2, 17.7 Hz), 5.25-5.20 (m, 2H), 4.88 (d, 1H, *J* = 0.9 Hz), 2.05 (s, 3H).

4.25   **4.A3**
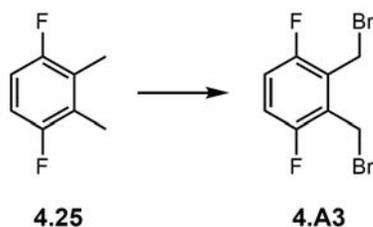
4.A3: To a 50-mL round-bottom flask was added NBS (690 mg, 3.9 mmol) and CCl$_4$ (10 mL). **4.25** (230 μL, 1.8 mmol) and benzoyl peroxide (2–3 mg) added. The reaction was refluxed overnight, cooled to room temperature, and filtered (reaction monitored by TLC in 4:1 hexanes:CH$_2$Cl$_2$). Upon distillation, **4.A3**, a clear oil (460 mg, 87%) was isolated. ^{1}H NMR (CDCl$_3$, 300 MHz): δ = 7.05 (apparent t, 2H, J = 6.6 Hz), 4.64 (t, 4H, J = 1.2 Hz); ^{19}F NMR (CDCl$_3$, 282 MHz): δ = -120.3.

4.A3   **4.A4**
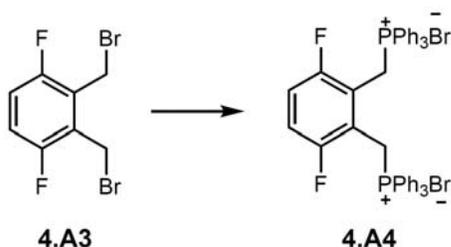
4.A4: To a 10-mL round-bottom flask was added **4.A3** (460 mg, 1.5 mmol), DMF (3 mL) and PPh$_3$ (807 mg, 3.1 mmol). The reaction was refluxed for 1.5 h and cooled to room temperature, during which time a white solid precipitated. Upon addition of toluene, the reaction was filtered and washed with more toluene. A white solid, **4.A4**, was isolated (600 mg, 47%) ^{1}H NMR (CDCl$_3$, 300 MHz): δ = 7.70-7.46 (m, 15H), 6.47 (s, 2H), 5.02 (br d, 4H, J = 13.5 Hz),.; ^{19}F NMR (CDCl$_3$, 282 MHz): δ = -107.5; ^{31}P{^{1}H} NMR (CDCl$_3$, 75 MHz): δ = 24.3.
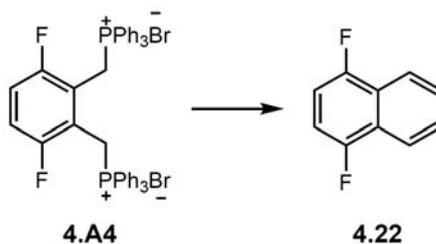
4.22: To a flame-dried 25-mL Schlenk flask was added **4.A4** (590 mg, 0.72

mmol), paraformaldehyde (121 mg, 4.0 mmol) and dry THF (10 mL). The reaction was

cooled to −78 °C and *n*-BuLi (0.58 mL of 2.5 M in hexanes, 1.5 mmol) was added via

syringe. The reaction was warmed to room temperature and stirred overnight. Upon

quenching the reaction with MeOH, an aqueous work up was performed utilizing CH_2Cl_2

to extract the organic components. The organic fractions were dried over Na_2SO_4,

filtered and dried under vacuum. Purification by alumina gel column chromatography

(100% hexanes) afforded **4.22**, a clear oil (42 mg, 35%). ^{1}H NMR ($CDCl_3$, 300 MHz): δ

= 6.77 (dd, 2H, *J* = 12, 18 Hz), 6.77 (s, 2H), 5.67 (dd, 2H, *J* = 2.1, 18 Hz), 5.53 (dd, 2H, *J*

= 2.1, 11.7 Hz); ^{19}F NMR ($CDCl_3$, 282MHz): δ = -121.04.
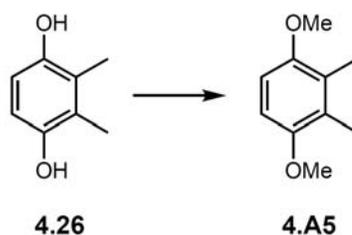
4.A5: To a 250-mL round-bottom flask was added **4.26** (2.02 g, 14.4 mmol),

MeOH (15 mL), and SO_2Me_2 (14 mL, 144 mmol). The reaction was heated to reflux

before a solution of KOH (17 g, 29 mmol) in MeOH (90 mL) was added in 10 mL

portions slowly (very exothermic). The reaction was refluxed overnight, cooled to room

temperature and filtered through a fine frit to give a white solid, **4.A5** (1.2 g, 50%). ^{1}H NMR (CDCl$_3$, 300 MHz): δ = 6.57 (s, 2H), 3.68 (s, 6H, OCH_3), 2.07 (s, 6H, CH_3).

4.A5   **4.A6**
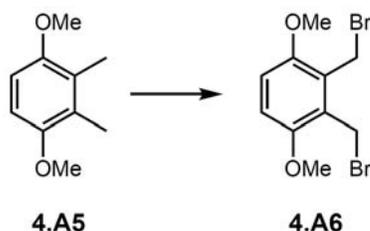
4.A6: To a 50-mL round-bottom flask was added NBS (365 mg, 2 mmol) and CCl$_4$ (10 mL). **4.A5** (153 mg, 0.92 mmol) and benzoyl peroxide (2−3 mg) added. The reaction was refluxed overnight, cooled to room temperature, and filtered (reaction monitored by TLC in 4:1 hexanes:CH$_2$Cl$_2$). Upon distillation, **4.A6**, a clear oil (297 mg, 94%) was isolated. ^{1}H NMR (CDCl$_3$, 300 MHz): δ = 6.85 (s, 2H), 4.74 (s, 4H, CH_2Br), 3.86 (s, 6H, CH_3); ^{13}C NMR (CDCl$_3$, 75 MHz): δ = 151.98, 126.61, 112.35, 56.49, 24.19.

4.A6   **4.A7**
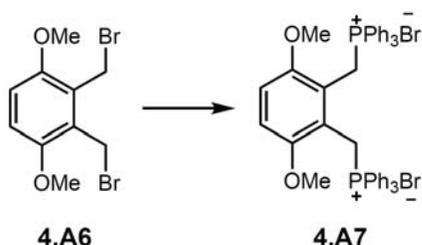
4.A7: To a 10-mL round-bottom flask was added PPh$_3$ (453 mg, 1.73 mmol) DMF (3 mL), and benzyl bromide (280 mg, 0.86 mmol). The reaction was refluxed for 3 h (monitored by TLC in 4:1 hexanes:CH$_2$Cl$_2$). The solvent was removed under vacuum to provide a light brown solid (yield not determined due to inseparable impurities; material used as is). ^{1}H NMR (CDCl$_3$, 300 MHz): δ = 8.03-7.33 (m, 30H), 6.46 (s, 2H),

5.02 (dd, 4H, $J = 2$, 14 Hz), 2.97 (s, 3H), 2.89 (s, 3H); ^{31}P{^{1}H} NMR (CDCl$_3$, 75 MHz): δ = 30.2.

4.A7   **4.23**
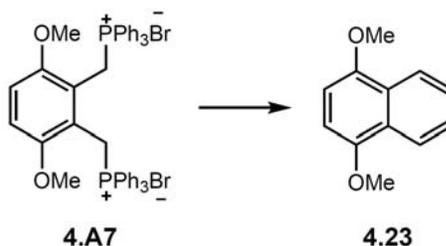
4.23: To a flame-dried 25-mL Schlenk flask was added **4.A7** (732 mg, 0.86 mmol), paraformaldehyde (143 mg, 4.8 mmol) and dry THF (10 mL). The reaction was cooled to −78 °C and *n*-BuLi (0.7 mL of 2.5 M in hexanes, 1.8 mmol) was added via syringe. The reaction was warmed to room temperature and stirred overnight. Upon quenching the reaction with MeOH, an aqueous workup was performed utilizing CH$_2$Cl$_2$ to extract the organic components. The organic fractions were dried over Na$_2$SO$_4$, filtered and dried under vacuum. Purification by alumina gel column chromatography (4:1 hexanes: CH$_2$Cl$_2$) afforded **4.23**, a clear oil (yield not determined due to inseparable impurities; material used as is). ^{1}H NMR (CDCl$_3$, 300 MHz): δ = 6.83-6.73 (m, 4H), 5.69 (dd, 2H, $J = 2.4$, 18.0 Hz), 5.55 (dd, 2H, $J = 2.4$, 11.7 Hz), 3.81 (s, 6H)

DFT Calculations of Ru-olefin Complexes 4.9a–c

DFT calculations were used to explore the gas-phase geometries and gas-phase and solvent-continuum energies of isomers **4.9a**, **4.9b**, and **4.9c**. The relative and absolute energies are summarized in Tables 4.A3–6.

Table 4.A3. Relative gas phase energy comparison (kcal/mol) for **4.9a–c**

	structural isomer		
method	**4.9b**	**4.9a**	**4.9c**
B3LYP/LANL2DZ	5.55	0.00	3.86
B3LYP/LACVP**	4.80	0.00	3.13
MPW1K/LACVP**	5.53	0.00	2.87

Table 4.A4. Relative energy comparison (kcal/mol) for **4.9a–c** using a solvent continuum model (CH_2Cl_2, see following page for details) for single-point energy calculations using structures optimized in the gas phase.

	structural isomer		
method	**4.9b**	**4.9a**	**4.9c**
B3LYP/LANL2DZ	0.51	2.55	0.00
B3LYP/LACVP**	1.12	3.80	0.00
MPW1K/LACVP**	1.53	3.93	0.00

Table 4.A5. Gas phase energies (Hartrees) for **4.9a–c**

	structural isomer		
method	**4.9b**	**4.9a**	**4.9c**
B3LYP/LANL2DZ	-1396.836962	-1396.845806	-1396.839657
B3LYP/LACVP**	-2287.551002	-2287.558644	-2287.553650
MPW1K/LACVP**	-2287.956559	-2287.965370	-2287.960792

Table 4.A6. Solution phase (CH_2Cl_2) energies (Hartrees) for **4.9a–c**

	structural isomer		
method	**4.9b**	**4.9a**	**4.9c**
B3LYP/LANL2DZ	-1396.869770	-1396.866509	-1396.870576
B3LYP/lacvp**	-2287.583968	-2287.579686	-2287.585747
MPW1K/lacvp**	-2287.993397	-2287.989561	-2287.995828

Gaussian '03W[47] was used to optimize geometries using the B3LYP/LANL2DZ level of theory. As described in the Gaussian '03 User's Reference, LANL2DZ uses the D95V basis on first-row elements and Los Alamos Hay-Wadt ECP plus DZ on Ru. The D95V basis is also known as the Dunning/Huzinaga valence double-zeta basis set.

Jaguar[48] was used for geometry optimizations of **4.9a−c** using the B3LYP and MPW1K density functionals, using an effective core potential to describe the core electrons of Ru. The LACVP** basis set was used for each calculation employing the Los Alamos ECP of Hay and Wadt with 18 explicit electrons on Ru and the Pople 6-31G** basis on all other atoms.

Frequency calculations were also performed for each structure optimized with the MPW1K/LACVP** level of theory The MPW1K gas phase optimized structures returned normal modes which were all greater than 40 cm^{-1}.

Once the gas phase structures were optimized, these geometries were subject to single-point energy calculations using a CH_2Cl_2 solvent continuum model at the same level of theory. In Gaussian 03W, this was done using the default PCM methodology [SCRF=(solvent=dichloromethane)]. In Jaguar, the PBF approach was used with parameters input [using MW = 84.9, dielectric constant = 9.08, and density = 1.3255] for dichloromethane [epsout=9.08, radprb=2.33274].

Expected and Observed NOEs in 4.9a−c

The structures of isomers **4.9a**, **4.9b**, and **4.9c** (as shown in Figure 4.A40) were computed with the B3LYP/LACVP** level of theory. The structures are used here for

the purpose of comparing measured nuclear Overhauser effects with those predicted from

a consideration of internuclear distances.
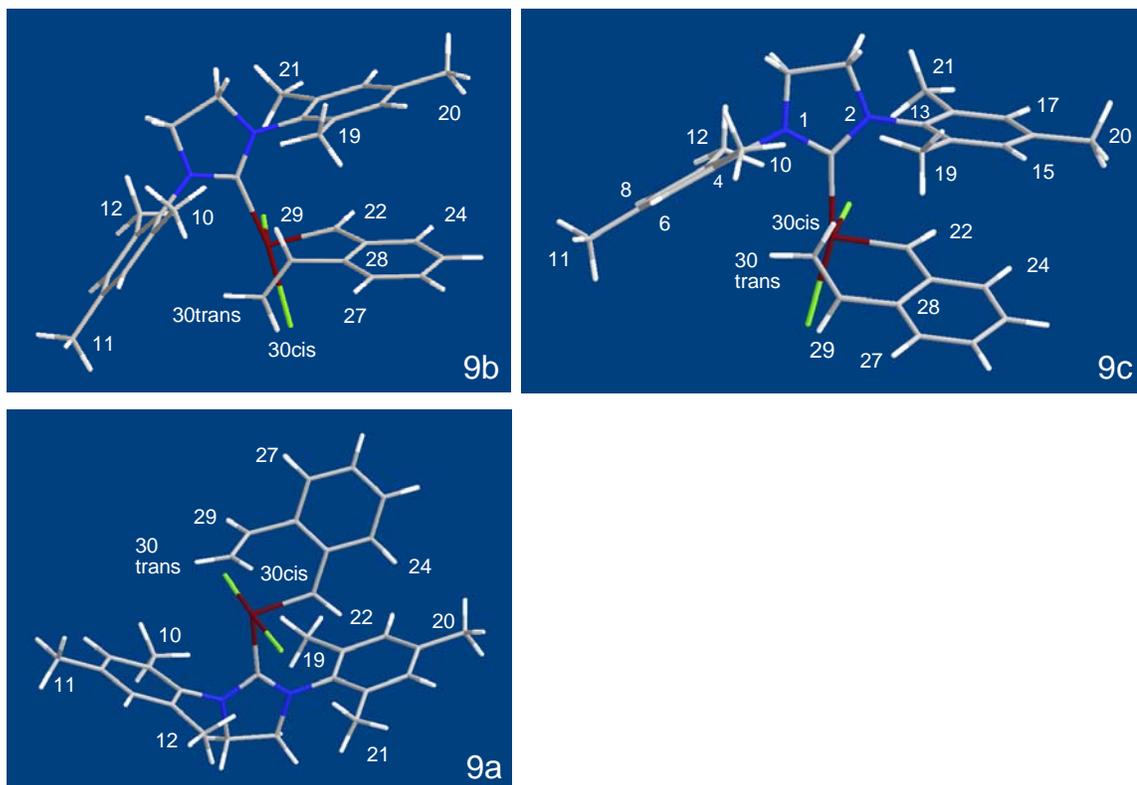
Figure 4.A40. Atom-numbering scheme used to define selected H-H distances in structural isomers **4.9a–c**.

As shown in Table 4.A7, NOEs are expected to arise between the olefin resonances and the mesityl methyl groups in the side-bound isomers **4.9b** and **4.9c**, whereas no such interaction is expected in the bottom-bond isomer **4.9a**. This is not surprising, as the olefin ligand in **4.9a** is trans to and distal from the NHC ligand. In the side-bound isomers **4.9b** and **4.9c**, the benzylidene H-22 is also in proximity to the C-21 methyl group. The only analogous interactions in bottom-bound **4.9a** would arise from the benzylidene H-22, which is in proximity to both mesityl C-21 and C-19 methyl

groups. Examination of the models shows that the side-bound isomers should be differentiable on the basis of the olefin-mesityl methyl interactions: in **4.9b**, H-29 is located roughly equidistant from Me-19 and Me-10 and H-30(trans) is proximal to Me-10. In **4.9c**, olefinic H-29 is oriented away from the NHC ligand and only the geminal protons on C-30 are in proximity to the mesityl methyl groups. In this structural isomer, H-30(cis) is equidistant between Me-10 and Me-19, whereas H-30(trans) is located closer to Me-10.

Table 4.A7. Computed distances (Å) in structural isomers **4.9b**, **4.9c** and **4.9a** $H\cdots CH_3$ and $CH_3\cdots CH_3$ distances are reported as the $H\cdots C$ and $C\cdots C$ distances, respectively. Distances less than 3.8 Å are highlighted; Overhauser effects might be measurable for these interactions. Short-range intra-olefin and benzylidene-*ortho*-H distances, which are expected to produce NOEs, are colored in green. Highlighted in yellow are through-space interactions unique to each structural isomer. Red boxes identify observed NOEs.

Isomer 4.9b

Label	10	11	12	19	20	21	22	24	27	29	30c	30t
10	--											
11	5.033	--										
12	5.117	5.036	--									
19	4.502	9.201	7.159	--								
20	9.221	13.226	9.943	5.028	--							
21	7.112	9.858	5.494	5.117	5.040	--						
22	6.591	8.888	5.951	5.126	5.477	3.677	--					
24	8.038	10.860	8.450	5.548	4.538	5.385	2.578	--				
27	5.433	9.092	8.771	4.181	7.008	7.831	5.542	4.984	--			
29	2.877	6.913	5.926	2.817	6.904	5.839	4.413	5.310	3.020	--		
30cis	4.690	6.305	6.261	5.706	8.532	7.143	4.289	5.171	3.766	3.088	--	
30trans	2.980	4.923	5.250	5.260	8.987	7.048	5.049	6.374	4.298	2.481	1.837	--

Isomer 4.9c

Label	10	11	12	19	20	21	22	24	27	29	30c	30t
10	--											
11	5.034	--										
12	5.108	5.038	--									
19	4.706	9.211	7.127	--								
20	9.452	13.360	9.837	5.036	--							
21	7.099	9.878	5.391	5.115	5.039	--						
22	6.568	9.118	5.819	4.222	4.986	3.555	--					
24	8.043	11.086	8.308	4.490	3.955	5.359	2.555	--				
27	6.653	9.064	8.825	5.381	8.281	8.696	5.534	4.983	--			
29	5.275	6.630	6.189	5.472	8.671	7.344	4.430	5.303	2.954	--		
30cis	3.062	6.755	5.786	2.870	7.329	6.099	4.271	5.216	3.932	3.081	--	
30trans	2.873	5.115	5.044	4.667	8.896	6.915	5.033	6.377	4.360	2.427	1.845	--

Isomer 4.9a

Label	10	11	12	19	20	21	22	24	27	29	30c	30t
10	--											
11	5.037	--										
12	5.095	5.044	--									
19	4.358	8.944	7.050	--								
20	9.196	13.272	9.981	5.048	--							
21	7.049	9.992	5.605	5.099	5.052	--						
22	6.209	9.167	6.064	3.739	4.638	3.423	--					
24	7.996	11.061	8.454	4.759	4.069	5.390	2.482	--				
27	8.214	9.314	8.742	7.290	8.970	8.821	5.537	4.979	--			
29	5.765	6.621	6.203	6.010	8.912	7.492	4.674	5.417	2.805	--		
30cis	7.148	7.813	5.366	6.742	8.222	5.884	3.759	4.917	4.201	3.096	--	
30trans	6.285	6.112	4.633	7.000	9.470	6.804	4.845	6.243	4.497	2.441	1.843	--

Both isomers observed in solution were found to have Overhauser interactions between olefinic resonances and mesityl-derived methyl groups, which is consistent with both isomers being side-bound. Furthermore, NOE interactions arising from each benzylidene resonance were found to involve only one mesityl methyl resonance each, which is additional evidence for a side-bound isomer. We were able to assign the resonances corresponding to the minor form as structural isomer **4.9b** on the basis of Overhauser interactions involving H-29 and two mesityl methyl groups, one well-resolved at 1.90 ppm and one at 2.43 ppm, in a region of several overlapping methyl resonances. The H-30(trans) resonance in the minor form also exhibited an NOE to a methyl resonance at 2.43 ppm. No methyl-derived NOEs were observed for the H-30(cis) resonance of the minor isomer. The resonances corresponding to the major form were assigned to structural isomer **4.9c** on the basis of Overhauser effects between H-30(cis) and two methyl resonances at 1.20 ppm and 2.36 ppm, the latter being in a region of overlapping methyl resonances. The H-30(trans) resonance was found to have an NOE arising from only one methyl group, situated at 2.36 ppm. The H-29 resonance for the major form in solution did not show any measurable NOEs to any methyl resonances, which is consistent with the geometry of **4.9c** (Table 4.A1).

Dynamic NMR Behavior of Complex 4.9b/c in CD$_2$Cl$_2$ at Room Temperature

Evidence from 2D-EXSY experiments suggested that two exchange processes were operative at room temperature. The first, identified as a **4.9b↔4.9c** interconversion, is a process that exchanges all resolved resonances in **4.9b** with those of **4.9c**. This exchange is readily apparent from the 2D-EXSY data, in which exchange crosspeaks have the same phase as the diagonal resonances. We believe this corresponds to a conformational process that involves the Ru-bound olefin changing its orientation by rotation about the C-29/C-28 single bond. The second process involves methyl group interchange in **4.9c** (and not **4.9b**) at room temperature. For example, Me-19 exchanges with Me-12 in **4.9c** (Table 4.A1). Such an exchange is consistent with rotation about the Ru–C bond of the NHC ligand. An alternative process that might be responsible for methyl exchange in **4.9c** is rotation about the N1/C4 or N2/C13 bond within the NHC ligand. We don't believe that this process is responsible for the methyl exchange in **4.9c** because exchange is not observed to occur between Me-19 and Me-21. Rotation about the Ru–C$_{NHC}$ bond appears to occur at a measurable rate at room temperature in **4.9c**. The corresponding bond rotation in **4.9b** does not. If it did, we should see an exchange crosspeak between Me-19 in **4.9b** with Me-12 in **4.9b**. This exchange is not observed at room temperature, but does perhaps become evident at 45 °C. This result could arise from purely a Ru–C$_{NHC}$ bond rotation in **4.9b**. However, a Me-12/Me-19 interchange in **4.9b** could also arise from a combination of the two processes (**4.9b↔4.9c**, Ru–C$_{NHC}$ bond rotation) already described.
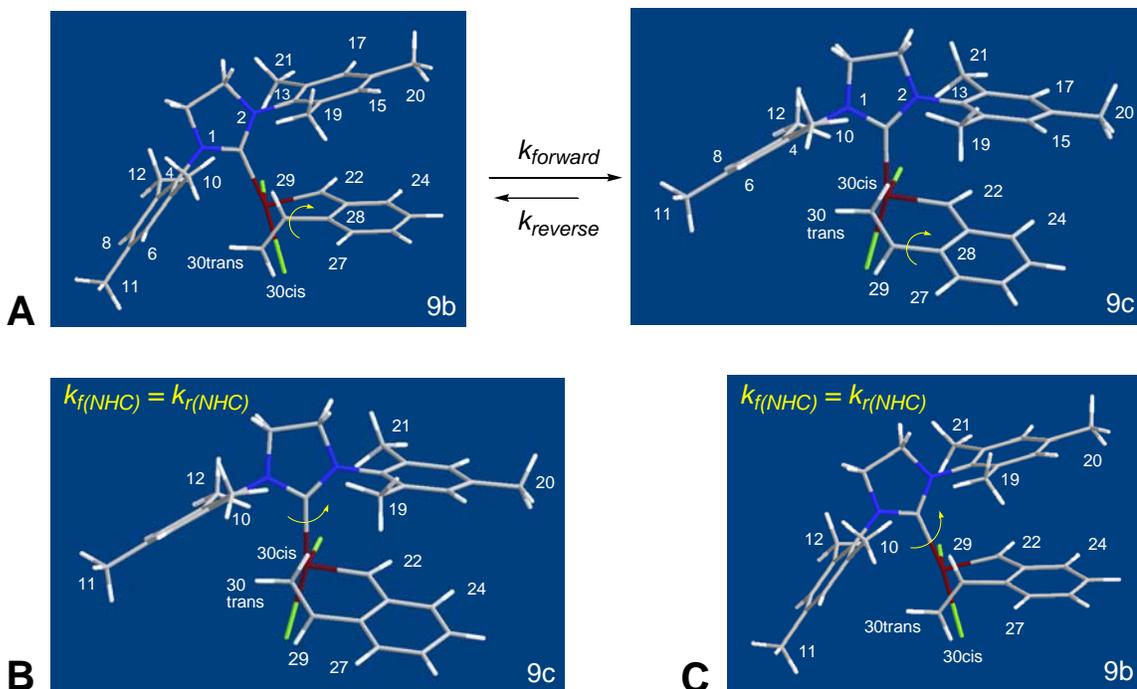
Figure 4.A41. Exchange processes hypothesized as operative in **4.9b/4.9c**. (A) The **4.9b↔4.9c** interconversion is caused by rotation about the C-29/C-28 bond. This process is supported by the presence of exchange crosspeaks between **4.9b/4.9c** resonances (Table 4.A1). (B) and (C) Degenerate interconversion is due to rotation about the Ru–C$_{NHC}$ bond. At room temperature, only the exchange process shown in B is clearly evident.

The dynamics of the **4.9b↔4.9c** interconversion was measured by quantifying the off-diagonal NOESY (this experiment might also be referred to as EXSY) exchange peaks corresponding to the benzylidene resonances (Figure 4.A42). The methodology for extracting the exchange rate constants is well-known. To accomplish this, we have written a Matlab implementation of the Full Matrix Analysis (FMA) method described by Zolnai.[49] In tests, our program (Table 4.A8) provided identical results with those obtained using the now-commercial EXSYCalc[1] program. The forward and reverse rate constants were found to be 0.07 and 0.04 s^{-1}, respectively.

---

[1] http://www.mestrec.com.
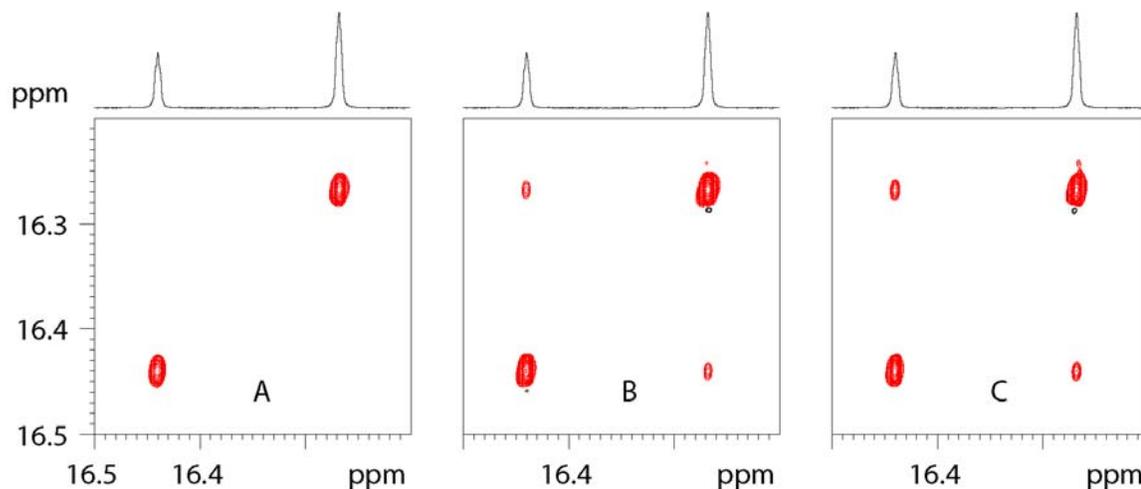
Figure 4.A42. 400 MHz ^{1}H NOESY experiments for the carbene region of Ru-olefin complex **9b/c** in CD$_2$Cl$_2$ at room temperature. Positive peak intensity is colored black and negative peak intensity is colored red. (A) mixing time = 0 s, (B) mixing time = 600 ms, (C) mixing time = 1200 ms. Peak intensities are listed clockwise, starting at the high field diagonal resonance. The off-diagonal intensities have been corrected for background intensity. A: -161.55, -92.75. B: −129.68, −2.67, −73.42, −3.22. C: −102.96, −4.85, −58.34, −4.82.

Table 4.A8. Rate constants for **4.9b↔4.9c** interconversion, using the benzylidene H-22 exchange from matrix analysis of 2D NOESY data

Mixing Time	k_r (s^{-1})	k_f (s^{-1})	Ratio
600 ms	0.035	0.073	0.479
1200 ms	0.040	0.068	0.588
Mean	**0.038**	**0.071**	**0.533**

The dynamics of the **4.9b↔4.9c** interconversion were also measured by an identical analysis of the Me/Me exchange processes in **4.9b/4.9c**. The forward and reverse rate constants determined in this manner were comparable with those determined using the benzylidene resonances.

Table 4.A9.   Forward and reverse rate constants for the methyl region from matrix analysis of two 2D-NOESY spectra

Process	Exchange	Tmix = 600			Tmix = 1200		
		$k_r\,(s^{-1})$	$k_f\,(s^{-1})$	Ratio	$k_r\,(s^{-1})$	$k_f\,(s^{-1})$	Ratio
4.9b↔4.9c	Me-21/Me-21	0.050	0.093	0.538	0.052	0.091	0.572
4.9b↔4.9c	Me-19/Me-19	0.058	0.091	0.630	0.053	0.089	0.598
4.9b↔4.9c	**mean**	**0.054**	**0.092**	**0.584**	**0.053**	**0.090**	**0.585**
Ru–C$_{NHC}$ rotation in **4.9c**	Me-21/Me-10	0.036	0.026	1.406	0.031	0.026	1.189
Ru–C$_{NHC}$ rotation in **4.9c**	Me-19/Me-12	0.030	0.036	0.823	0.030	0.034	0.872
Ru–C$_{NHC}$ rotation in **4.9c**	**mean**	**0.033**	**0.031**	**1.115**	**0.031**	**0.030**	**1.030**

Averaging the four k_f values for the **4.9b↔4.9c** interconversion, we obtain 0.08 ± 0.01 s^{-1}. Using the upper and lower 95% confidence intervals, these rate constants provide an estimate of the Gibbs Free Energy of Activation of 18.9 ± 0.1 kcal/mol at 298 K, according to the expression $\Delta G^{\ddagger} = RT\,[\ln\,(k_B/h) - \ln\,(k/T)]$.

Reported value for 4.9b↔4.9c $\Delta G^{\ddagger}$(25 °C): 18.9 ± 0.1 kcal/mol

The rate of Ru–C$_{NHC}$ rotation in **4.9c** was determined from the Me/Me exchange processes. The rate constant for this process was determined to be 0.03 s^{-1} at room temperature. Interestingly, this rate constant is very similar to that measured for the **4.9b↔4.9c** interconversion. This rate constant corresponds to $\Delta G^{\ddagger} = 19.5$ kcal/mol at 298 K.

Dynamic NMR behavior of complex 4.9b/c in CDCl$_2$CDCl$_2$ from 22−105 °C

To obtain a more accurate estimate of $\Delta G^{\ddagger}$ for the **4.9b↔4.9c** interconversion, we performed a lineshape analysis of a series of 1D ^{1}H NMR spectra of the benzylidene region of complex **4.9** acquired at elevated temperatures. To be able to access the coalescence temperature, the Ru-olefin complex was dissolved in deuterated

tetrachloroethane in a J-Young NMR tube. A preliminary experiment (using a probe not yet temperature-calibrated) showed that complex **4.9** could be heated to ca. 130 °C and returned to room temperature with only a minimal amount of sample decomposition, none of which interfered with the benzylidene resonances (Figure 4.A43).
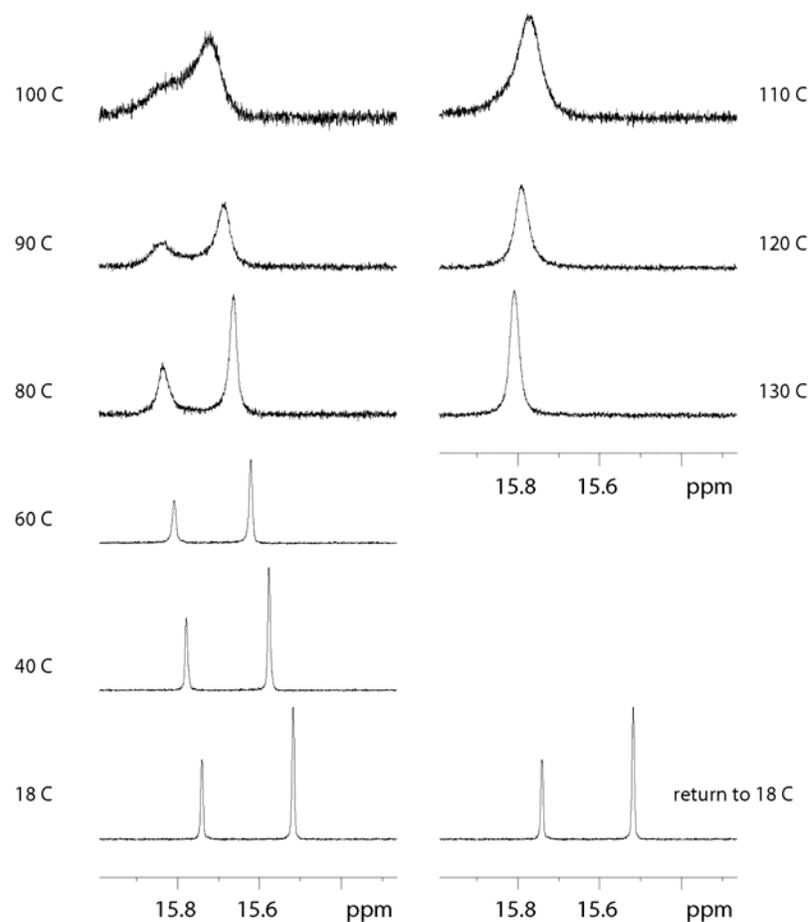
Figure 4.A43. Compound stability test: 400 MHz ^{1}H VT-NMR spectra for Ru-olefin complex **4.9** dissolved in CDCl$_2$CDCl$_2$.

We note that using the benzylidene resonances provides a good estimate for the **4.9b↔4.9c** interconversion because these resonances are 'blind' to the process involving Ru-C$_{NHC}$ rotation in either isomer. Put another way, the NHC ligand rotation is a degenerate process that does not alter the magnetic environment of the benzylidene

resonances. The same is not true for the methyl resonances, as our earlier analysis showed.

Another variable-temperature data set was acquired, this time the probe was calibrated at each temperature with a glycol standard for each measurement. These spectra, together with their overlaid fit spectra, are shown in Figure 4.A44.
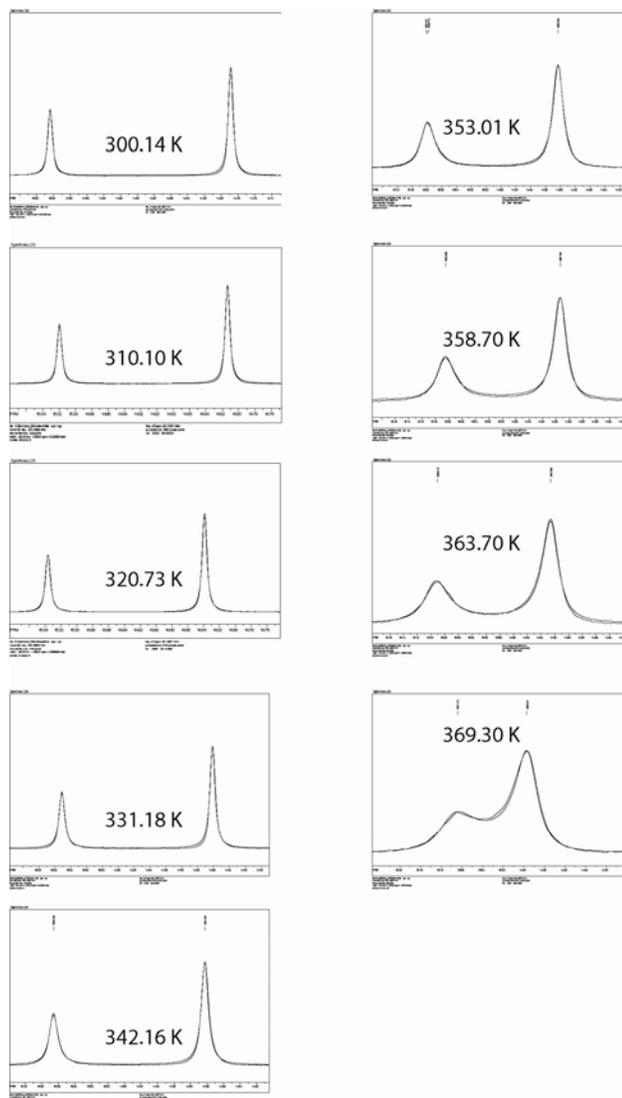
Figure 4.A44. Experimental spectra and MEXICO fits of the benzylidene resonances of Ru-olefin complex **4.9b/c** in CDCl$_2$CDCl$_2$ at temperatures ranging from 300.14 K to 369.30 K.

We simulated our experimental spectra using the MEXICO[2] set of programs written by Professor Alex Bain. We were able to get good results using the non-interative version of MEXICO (mexicon), and we found the most effective way to utilize the manual simulation capability of MEXICO is to use it through SpinWorks[3] NMR program. The SpinWorks program allows the MEXICO simulation to be called from within SpinWorks and displays the simulated spectrum and the RMS value immediately. After getting a good general fit, the RMS value displayed in the upper left corner of the screen can be invaluable for fine-tuning the rate constant and the frequencies of the peaks to get the best possible fit. It is important to note that SpinWorks displays the RMS value for the portion of the spectrum being displayed. Thus, it is important not to change the viewing area while trying to minimize the RMS. The fits are overlaid on the experimental data. The parameters used for each fit are summarized in Table 4.A10. For an exchange process involving unequal populations, as is the case for **4.9b↔4.9c**, MEXICO fits input values of the forward rate constant, k_f.

Table 4.A10. Simulation parameters used for the manual MEXICO fitting. $1/T_1$ was 0.120 s^{-1} and the equilibrium ratio was 1:0.610.

Expt #	Temp (K)	Left Pk (Hz)	Right Pk (Hz)	k_f (s^{-1})	$-1/T$	$R*\ln(hk/k_bT)$
5	310.10	6009.74	5927.36	0.25	−0.0032	−61.371
9	320.73	6016.51	5937.39	0.76	−0.0031	−59.229
11	331.18	6022.48	5946.42	2.25	−0.0030	−57.135
15	342.16	6028.26	5954.96	7.05	−0.0029	−54.931
17	353.01	6033.90	5963.00	20.1	−0.0028	−52.911
22	358.70	6036.60	5967.00	30.9	−0.0028	−52.088
25	363.70	6040.20	5971.60	44.5	−0.0027	−51.391

[2] http://www.chemistry.mcmaster.ca/faculty/bain/
[3] Marat, Kirk. SpinWorks. http://www.umanitoba.ca/chemistry/nmr/spinworks/index.html

An Eyring plot for data collected over the range of 310–363 K was used to extract the entropy and enthalpy of activation from the temperature dependence of the rate constant (Figure 4.A45). Here, $R\ln(hk/k_BT)$ is plotted vs. $-1/T$. From this plot, the slope is the enthalpy of activation ($\Delta H^\ddagger$), and the entropy of activation ($\Delta S^\ddagger$) is equal to the intercept. We found $\Delta H^\ddagger = 21.4 \pm 0.6$ kcal/mol and $\Delta S^\ddagger = 7.5 \pm 1.8$ e.u. Thus, the estimated $\Delta G^\ddagger$ at 298 K is 19.1 ± 0.1 kcal/mol. This is in good agreement with the value of 18.9 ± 0.1 kcal/mol calculated using the 2D-NOESY experiments at room temperature.
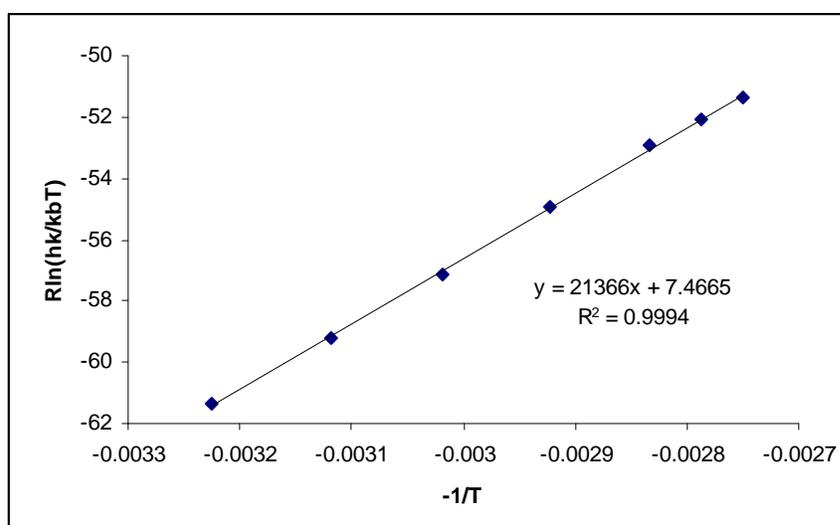
Figure 4.A45. Eyring plot of the MEXICO lineshape data. The slope is $\Delta H^\ddagger$ and the intercept is $\Delta S^\ddagger$.

Eyring Plots and Error Analysis

According to the Activated Complex Theory of Henry Eyring, $k = \dfrac{k_B T}{h} e^{-\Delta G^\ddagger / RT}$ and $\Delta G^\ddagger$

$= \Delta H^\ddagger - T\Delta S^\ddagger$ or $k = \left(\dfrac{k_B T}{h} e^{\Delta S^\ddagger/R}\right) e^{-\Delta H^\ddagger/RT}$. This can be re-worked to yield a linear

equation in traditional y = mx + b format: $R\ln \dfrac{hk}{k_B T} = \Delta S^\ddagger + \left(\dfrac{-1}{T}\right)\Delta H^\ddagger$, where k is the

rate in s^{-1}, k_B is Boltzmann's constant (3.29957x10^{-24} cal K^{-1}), h is Planck's constant (1.58355x10^{-34} cal s), R is the gas constant (1.9872 cal mol^{-1} K^{-1}), and T is the temperature in Kelvin.

The uncertainty in the slope ($\Delta H^\ddagger$) and intercept ($\Delta S^\ddagger$) was determined directly from the output provided by the linear regression function of the NCSS statistical software package.[4]

Reported value for $\Delta H^\ddagger$: 21.4 ± 0.6 kcal/mol

Reported value for $\Delta S^\ddagger$: 7.5 ± 1.8 cal/(mol · K)

Sample calculation for kinetic parameters for 4.9 dissolved in CDCl$_2$CDCl$_2$:

$\Delta G^\ddagger$ (25 °C) = $\Delta H^\ddagger$ − T$\Delta S^\ddagger$ = 21370 cal/mol − (298K)(7.7 cal/mol K)/1000 = 19.135 kcal/mol

Uncertainty in $\Delta G^\ddagger$ (25 °C):

$$S^2_{\Delta G^\ddagger} = S^2_{\Delta H^\ddagger} + T^2 S^2_{\Delta S^\ddagger} - 2TS^2_{\Delta H^\ddagger \Delta S^\ddagger}$$

$$= (239.2 \text{ cal/mol})^2 + (298 \text{ K})^2 (0.7069 \text{ cal/K·mol})^2 - 2(298 \text{ K})(168.83 \text{ cal/mol})$$

$$= 970.8 \text{ cal/mol}$$

$$95\% C.I. = 2.365\sqrt{970.8} = 73.7 (cal / mol)$$

$\Delta G^\ddagger$ (25 °C) = 19.135 ± 0.074 kcal/mol

Reported value for $\Delta G^\ddagger$(25 °C): 19.1 ± 0.1 kcal/mol

Calculation of rate at 25 °C:

$$k_f = 2.084\text{x}10^{10} \text{Te}^{-\Delta G^\ddagger / 1.9872 T} \text{ (units of } \Delta G^\ddagger \text{ is cal/mol)}^{50}$$

$$k_f = 0.06 ± 0.01 \text{ s}^{-1}$$

---

[4] http://www.ncss.com/

References

(1)   Grubbs, R. H. *Handbook of Metathesis*; Wiley-VCH: Weinheim, 2003.

(2)   Ivin, K. J.; Mol, J. C. *Olefin Metathesis and Metathesis Polymerization*; Academic Press: San Diego, CA, 1997.

(3)   Schwab, P.; Grubbs, R. H.; Ziller, J. W. *J. Am. Chem. Soc.* **1996**, *118*, 100.

(4)   Nguyen, S. T.; Grubbs, R. H.; Ziller, J. W. *J. Am. Chem. Soc.* **1993**, *115*, 9858.

(5)   Scholl, M.; Ding, S.; Lee, C. W.; Grubbs, R. H. *Org. Lett.* **1999**, *1*, 953.

(6)   Grubbs, R. H.; Chang, S. *Tetrahedron* **1998**, *54*, 4413.

(7)   Ivin, K. J. *J. Mol. Cat. A* **1998**, *133*, 1.

(8)   Furstner, A. *Angew. Chem. Int. Ed.* **2000**, *39*, 3012.

(9)   Trnka, T. M.; Grubbs, R. H. *Acc. Chem. Res.* **2001**, *34*, 18.

(10)   Connon, S. J.; Blechert, S. *Angew. Chem., Int. Ed.* **2003**, *42*, 1900.

(11)   Herisson, J. L.; Chauvin, Y. *Makromol. Chem.* **1971**, *141*, 161.

(12)   Dias, E. L.; Nguyen, S. T.; Grubbs, R. H. *J. Am. Chem. Soc.* **1997**, *119*, 3887.

(13)   Sanford, M. S.; Love, J. A.; Grubbs, R. H. *J. Am. Chem. Soc.* **2001**, *123*, 6543.

(14)   Sanford, M. S.; Ulman, M.; Grubbs, R. H. *J. Am. Chem. Soc.* **2001**, *123*, 749.

(15)   Choi, T.-L.; Grubbs, R. H. *Angew. Chem., Int. Ed.* **2003**, *42*, 1743.

(16)   Adlhart, C.; Chen, P. *J. Am. Chem. Soc.* **2004**, *126*, 3496.

(17)   Benitez, D.; Goddard, W. A., III *J. Am. Chem. Soc.* **2005**, *127*, 12218.

(18)   Romero, P. E.; Piers, W. E. *J. Am. Chem. Soc.* **2005**, *127*, 5032.

(19)   Seiders, T. J.; Ward, D. W.; Grubbs, R. H. *Org. Lett.* **2001**, *3*, 3225.

(20)   Funk, T. W.; Berlin, J. M.; Grubbs, R. H. *J. Am. Chem. Soc.* **2006**, *128*, 1840.

(21)   Tallarico, J. A.; Bonitatebus, P. J., Jr.; Snapper, M. L. *J. Am. Chem. Soc.* **1997**, *119*, 7157.

(22)   Trnka, T. M.; Day, M. W.; Grubbs, R. H. *Organometallics* **2001**, *20*, 3845.

(23)   Chatterjee, A. K.; Choi, T.-L.; Sanders, D. P.; Grubbs, R. H. *J. Am. Chem. Soc.* **2003**, *125*, 11360.

(24) At 30 °C, low metathesis activity is observed for the ring-closing metathesis of diethyldiallylmalonate; at elevated temperatures (80-100 °C), however, the reaction is complete within 1 h.

(25) Garber, S. B.; Kingsbury, J. S.; Gray, B. L.; Hoveyda, A. H. *J. Am. Chem. Soc.* **2000**, *122*, 8168.

(26) Yasuda, N.; Uekusa, H.; Ohashi, Y. *Acta Crystallographica, Section E: Structure Reports Online* **2001**, *E57*, o1189.

(27) Despagnet-Ayoub, E.; Grubbs, R. H. *J. Am. Chem. Soc.* **2004**, *126*, 10198.

(28) Ung, T.; Hejl, A.; Grubbs, R. H.; Schrodi, Y. *Organometallics* **2004**, *23*, 5399.

(29) Sanford, M. S., Ph.D. thesis, California Institute of Technology, 2001.

(30) We are currently unable to determine whether the crystalline material is comprised of only **4.9b**. X-ray analysis of multiple crystals grown from **4.9** has shown only **4.9b**. Microcrystalline material that also forms could contain **4.9c**. Alternatively, the presence of a small amount of **4.9c** in the low-temperature dissolution experiment could arise from experimental handling errors.

(31) Ritter, T.; Day, M. W.; Grubbs, R. H. *J. Am. Chem. Soc.* **2006**, *128*, 11768.

(32) Dinger, M. B.; Mol, J. C. *Adv. Synth. Catal.* **2002**, *344*, 671.

(33) Grela, K.; Michrowska, A.; Bujok, R.; Harutyunyan, S.; Sashuk, V.; Dolgonos, G. *J. Am. Chem. Soc.* **2004**, *126*, 9318.

(34) Hejl, A.; Day, M. W.; Grubbs, R. H. *Organometallics* **2006**, *25*, 6149.

(35) Meyer, E. A.; Castellano, R. K.; Diederich, F. *Angew. Chem. Int. Ed.* **2003**, *42*, 1210

(36) Hickstein, D. D. Undergraduate thesis, Pomona College, 2007.

(37) Mitchell, R. H.; Ghose, B. N.; Williams, M. E. *Can. J. Chem.* **1977**, *55*, 210.

(38) Sanford, M. S.; Love, J. A.; Grubbs, R. H. *Organometallics* **2001**, *20*, 5314.

(39) Berlin, J. M.; Goldberg, S. D.; Grubbs, R. H. *Angew. Chem. Int. Ed.* **2006**, *45*, 7591.

(40) Braun, S.; Kalinowski, H.-O.; Berger, S. *150 and More NMR Experiments: A Practical Course*; Wiley-VCH: Weinheim, 1998.

(41) Hurd, R. *J. Magn.Reson.* **1990**, *87*, 422.

(42)   Bax, A.; Freeman, R. *J. Magn.Reson.* **1981**, *44*, 542.

(43)   Hwang, T.-L.; Shaka, A. *J. Am. Chem. Soc.* **1992**, *114*, 3157.

(44)   Jeener, J.; Meier, B. H.; Bachmann, P.; Ernst, R. R. *J. Chem. Phys.* **1979**, *71*, 4546.

(45)   Hurd, R. E.; John, B. K. *J. Magn.Reson.* **1991**, *91*, 648.

(46)   Bax, A.; Griffey, R. H.; Hawkins, B. L. *J. Magn.Reson.* **1983**, *55*, 301.

(47)   Frisch, M. J.; Trucks, G. W.; Schlegel, H. B.; Scuseria, G. E.; Robb, M. A.; Cheeseman, J. R.; Montgomery, J., J. A.; Vreven, T.; Kudin, K. N.; Burant, J. C.; Millam, J. M.; Iyengar, S. S.; Tomasi, J.; Barone, V.; Mennucci, B.; Cossi, M.; Scalmani, G.; Rega, N.; Petersson, G. A.; Nakatsuji, H.; Hada, M.; Ehara, M.; Toyota, K.; Fukuda, R.; Hasegawa, J.; Ishida, M.; Nakajima, T.; Honda, Y.; Kitao, O.; Nakai, H.; Klene, M.; Li, X.; Knox, J. E.; Hratchian, H. P.; Cross, J. B.; Bakken, V.; Adamo, C.; Jaramillo, J.; Gomperts, R.; Stratmann, R. E.; Yazyev, O.; Austin, A. J.; Cammi, R.; Pomelli, C.; Ochterski, J. W.; Ayala, P. Y.; Morokuma, K.; Voth, G. A.; Salvador, P.; Dannenberg, J. J.; Zakrzewski, V. G.; Dapprich, S.; Daniels, A. D.; Strain, M. C.; Farkas, O.; Malick, D. K.; Rabuck, A. D.; Raghavachari, K.; Foresman, J. B.; Ortiz, J. V.; Cui, Q.; Baboul, A. G.; Clifford, S.; Cioslowski, J.; Stefanov, B. B.; Liu, G.; Liashenko, A.; Piskorz, P.; Komaromi, I.; Martin, R. L.; Fox, D. J.; Keith, T.; Al-Laham, M. A.; Peng, C. Y.; Nanayakkara, A.; Challacombe, M.; Gill, P. M. W.; Johnson, B.; Chen, W.; Wong, M. W.; Gonzalez, C.; Pople, J. A.; C.02 ed.; Gaussian Inc., 2004.

(48)   6.5 ed.; Schrodinger, LLC: New York, NY, 2005.

(49)   Zolnai, Z.; Juranic, N.; Vikic-Topic, D.; Macura, S. *J. Chem. Inf. Comput. Sci.* **2000**, *40*, 611.

(50)   Eliel, E. L.; Wilen, S. H. *Stereochemistry of Organic Chemistry*; Wiley: New York, 1994.

APPENDIX I

Identification and Optimization of Transition-Metal Promotors of Olefin Hydration

Introduction

The wide abundance of olefin-containing molecules makes the alkene functionality an attractive substrate class in organic synthesis. Olefins can be converted into a variety of other functional groups such as ketones, aldehydes, epoxides, diols, alkyl halides and alcohols. While many of these reactions can be performed utilizing transition-metal-mediated catalysis, the synthesis of alcohols from alkenes via transition-metal catalysis remains an unsolved challenge.

Secondary alcohols can generally be synthesized by the reduction of ketones, which are often derived from unsaturated starting materials, or the stoichiometric oxymercuration-demercuration of alkenes.[1] Electron-deficient olefins such as α,β-unsaturated carbonyl or nitrile compounds undergo nucleophilic addition of water to generate alcohols in the presence of transition-metal catalysts, however these reactions are limited in substrate scope and often generate undesired side products (vide infra). A transition-metal catalyzed method for the synthesis of secondary alcohols from unactivated olefins has yet to be developed.

In the past several decades, publications describing the use of transition-metal complexes for the non-oxidative, catalytic synthesis of alcohols from olefins have been sporadic. Initial reports employed Pd- and Pt-complexes to hydrate electron-deficient olefins. In 1979, Otsuka and co-workers examined several Pt(0) phosphine complexes for the olefin hydration of acrylonitrile and crotonitrile (Scheme A1.1).[2] Pt(P(i-Pr)$_3$)$_3$ was observed to be the best catalyst for the conversion of acrylonitrile to β-hydroxypropionitrile with 49 turnover numbers (TONs) after 20 h, whereas hydration of crotonitrile was most efficiently catalyzed by Pt(PEt$_3$)$_3$ with 42 TONs after 20 h. However, these reactions also produced significant amounts of nitrile hydration and coupling products. Reactions with other electron-deficient

olefins such as methyl acrylate underwent polymerization; reactions with unactivated olefins such as cyclohexene did not proceed.

Scheme A1.1. Pt-catalyzed hydration reactions examined by Otsuka and co-workers
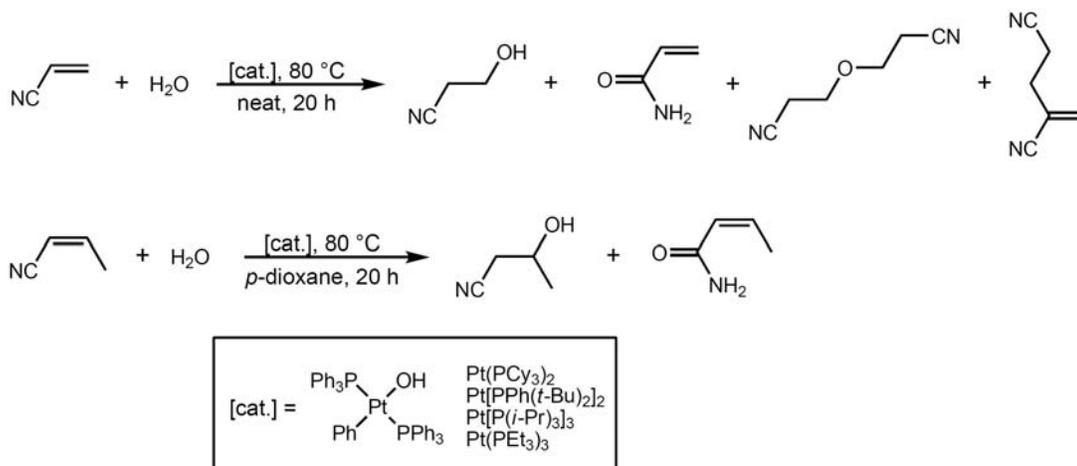
In 1991, Roundhill and co-workers reported the reactivity of Pd(II) hydroxy dimers with diethyl maleate (Scheme A1.2).[3,4] After screening several Pd complexes, [Pd(μ-OH)(DCPE)]$_2^{2+}$[BF$_4^-$]$_2$ (DCPE = 1,2-bis(dicyclohexylphosphino)ethane) was found to have the best activity with 14.3 TON after 30 h at 140 °C. Unfortunately, high levels of olefin isomerization and ester hydrolysis were also observed; separate experiments with each of these side products showed no conversion to alcohol. No other substrates were examined.

Scheme A1.2. Pd-catalyzed hydration reaction examined by Roundhill and co-workers
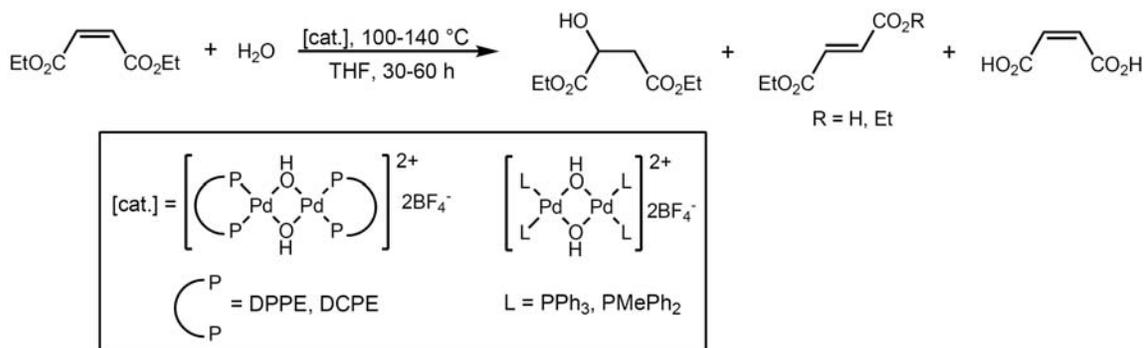
Co(II) complexes represented the first transition-metal catalysts capable of hydrating less-activated substrates such as styrene and 1-octene. In 1982, Drago and co-workers reported the Markovnikov hydration activity of [bis(salicylidene-γ-iminopropyl)-methylamine]cobalt(II) in alcoholic solvents under an atmosphere of oxygen (Scheme A1.3).[5,6] A variety of aliphatic, internal, and terminal olefins was examined and found to be viable substrates, but few yields were reported. In reactions with 1-hexene, a 1:1 mixture of 2-hexanone and 2-hexanol for a total of 12 TON was obtained after 24 h. Although no olefin isomerization was discussed, competitive ketone formation was problematic in all cases.

Scheme A1.3. Co-catalyzed hydration reaction examined by Drago and co-workers
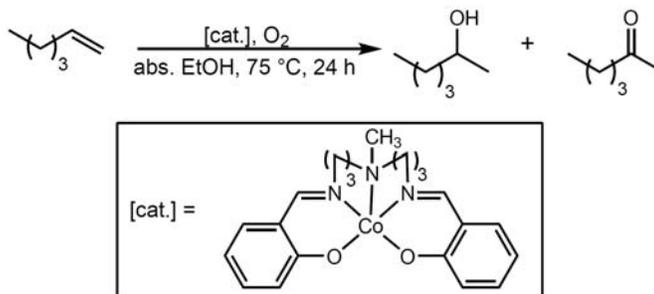
In 1988, Nishinga and co-workers examined Co(II) complexes containing a variety of salen-type frameworks and observed results similar to Drago and co-workers'.[7-9] The use of chiral salen-type ligands yielded poor enantioselectivities.[10] Isayama and co-workers subsequently investigated a series of bis(1,3-diketonato)cobalt(II) complexes for Markovnikov hydration (Scheme A1.4).[11] In all of these reports, low conversion to alcohol (relative to catalyst loading) and significant amounts of ketone and hydrocarbon side products were observed.

Scheme A1.4. Co-catalyzed hydration reactions examined by Isayama and co-workers
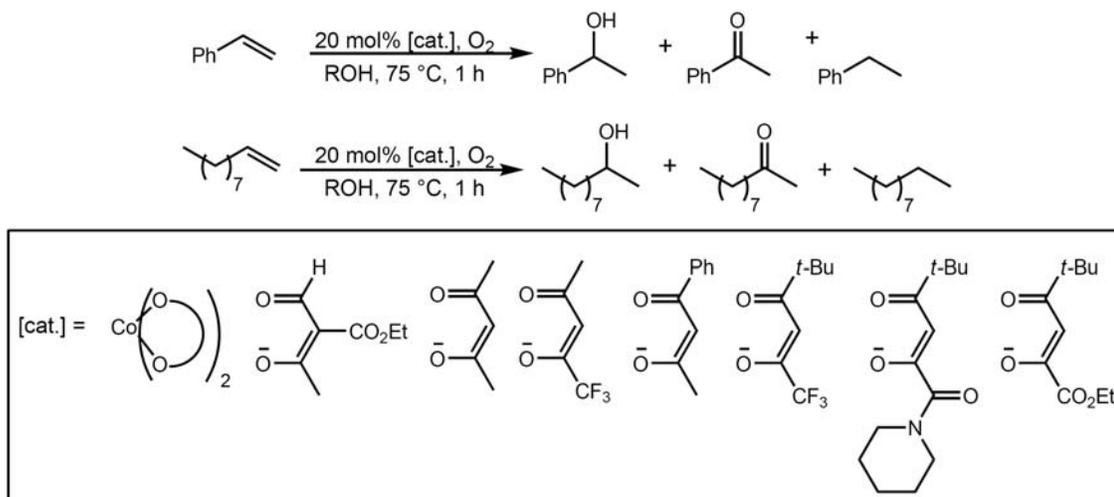
The first report of a transition-metal catalyst for the anti-Markovnikov addition of water to an unactivated terminal olefin was published by Trogler and co-workers.[12] Platinum complexes **A1.1** and **A1.2** were found to catalyze the hydration of 1-octene to 1-octanol with a turnover frequency of 7–8/h.   The reactions were performed in aqueous solutions containing 1 equiv NaOH and a phase transfer catalyst, $[NEt_3(CH_2Ph)]^+Cl^-$; control experiments without either of these components resulted in no reaction. Although **A1.2** was found to be water tolerant and soluble in aqueous media, it was found to be air sensitive, undergoing decomposition in the presence of oxygen.   Based on deuterium labeling experiments, the authors proposed a classical Wacker-type mechanism, as shown in Scheme A1.5, and postulated that anti-Markovnikov addition resulted from hydroxide attack of the more sterically accessible site. No conversion to alcohol was observed in reactions with *cis*- and *trans*-3-hexene, indicating the limitation of this reaction methodology to terminal olefins. Unfortunately, neither the reported catalyst synthesis nor the catalytic activity were reproducible.[13,14]

Scheme A1.5. Mechanism of Pt-mediated anti-Markovnikov olefin hydration proposed by Trogler and co-workers
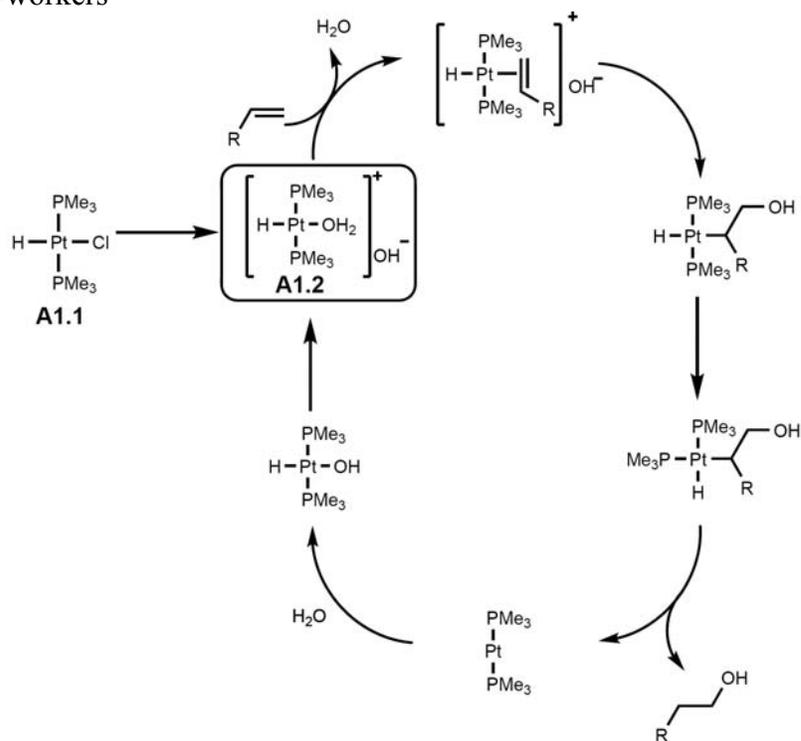
In 1999, Roundhill and co-workers reported new catalysts for anti-Markovnikov olefin hydration.[15] In their theoretical study on the hydration of strained olefins, the authors reported experiments on the hydration of 1-octene with TPPTS (sodium tris(3-sulfonatophenyl)phosphine) complexes of Pd(0) and Ru(II). Although 1-octanol was detected in initial experiments, further experiments could not reproduce this result.

A reproducible, general, and efficient direct olefin hydration catalyst has yet to be developed, despite its numerous potential academic and industrial applications. The catalysts developed to date have demonstrated activity with only a narrow substrate scope, produced significant amounts of side products, and/or were not reproducible. Overall, a relatively small class of transition-metal complexes has been examined for olefin hydration activity; consequently, many catalysts remain to be investigated.

Results and Discussion

Project Design

Our strategy for the design and development of an olefin hydration catalyst is to first screen a variety of early and late transition-metal complexes for hydration activity, irrespective of regiochemistry. After lead compounds are identified and reaction conditions are optimized, subsequent work will center upon controlling the hydration regiochemistry through modifications of the catalyst steric and electronic properties.

Transition-Metal Screen Protocol

To maximize the probability of detecting olefin hydration activity, each metal complex (10 mol%) was evaluated under a standard set of 12 reaction conditions, individually varying solvent, pH, and temperature (Table A1.1). Utilizing H_2O as a reagent in the reaction, THF was selected as the organic co-solvent due to its miscibility with H_2O. To examine both acidic and basic reaction conditions, trifluoroacetic acid (TFA) and NaOH were used as additives. Two temperatures were also examined in each screen. Initially, 25 °C was utilized as the lower temperature, but little activity was typically observed; later, 40 °C and then 60 °C were utilized.   For each reaction, aliquots were taken after 10 h and 40 h and analyzed via gas chromatography.

Table A1.1. Olefin hydration screening reactions

Condition	Aprotic Solvent (mL)	Protic Solvent (mL)	Additive (5 mol%)	Temp. (°C)
1	0.125 THF	0.375 H$_2$O	TFA	25, 40, or 60
2	0.125 THF	0.375 H$_2$O	-	25, 40, or 60
3	0.125 THF	0.375 H$_2$O	NaOH	25, 40, or 60
4	0.375 THF	0.125 H$_2$O	TFA	25, 40, or 60
5	0.375 THF	0.125 H$_2$O	-	25, 40, or 60
6	0.375 THF	0.125 H$_2$O	NaOH	25, 40, or 60
7	0.125 THF	0.375 H$_2$O	TFA	80
8	0.125 THF	0.375 H$_2$O	-	80
9	0.125 THF	0.375 H$_2$O	NaOH	80
10	0.375 THF	0.125 H$_2$O	TFA	80
11	0.375 THF	0.125 H$_2$O	-	80
12	0.375 THF	0.125 H$_2$O	NaOH	80

Styrene was chosen as the test substrate. While highly activated olefins such as acrylonitrile and diethyl maleate have been employed previously to probe for reactivity, these substrates are sometimes easily hydrated in the absence of metal catalyst and thus pose reproducibility issues. However, we did want to utilize a mildly activated olefin. Styrene provided a good compromise; control experiments with styrene in the absence of metal catalyst showed no reaction. Another advantage of styrene is that it cannot undergo olefin isomerization, which could complicate product analysis. Furthermore, styrene and several of its derivatives that are possible reaction products are commercially available, which facilitates the identification of any reaction byproducts (eq A1.1).
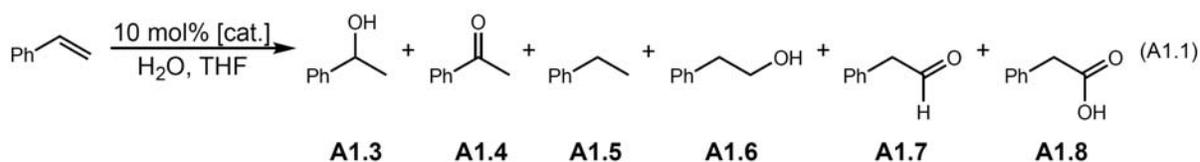
Early-Metal-Oxo-Hydroxo Complexes

While metal-oxo complexes are commonly employed in oxidation reactions,[16] their use in non-oxidative processes has also been demonstrated.[17] For example, Osborn and co-workers developed the rhenium catalyst **A1.9** for the isomerization of allylic alcohols (eq A1.2).[18] The authors proposed a Claisen-like mechanism involving a cyclic transition state. Based on this mechanism, we envisioned that a similar type of intermediate could be possible in an olefin hydration reaction (Scheme A1.6). According to our proposed mechanism, an olefin reacts with an acidic hydroxo ligand and metal-oxo to give a metal alkoxy intermediate via an ene-type reaction. Upon hydrolysis, the hydrated olefin is released and the catalyst is regenerated. The activity of catalysts with the general structure **A1.10**, where X and X' are anionic ligands and M is an early metal such as rhenium, is expected to be sensitive to the acidity of the hydroxo ligand and electrophilicity of the metal-oxo group.
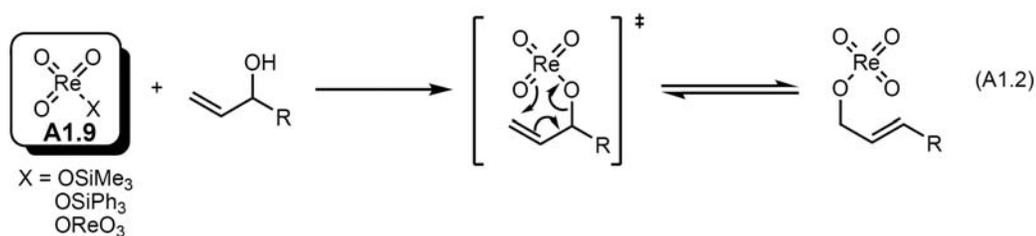
Scheme A1.6. Proposed catalytic cycle for early-metal-oxo-hydroxo complexes
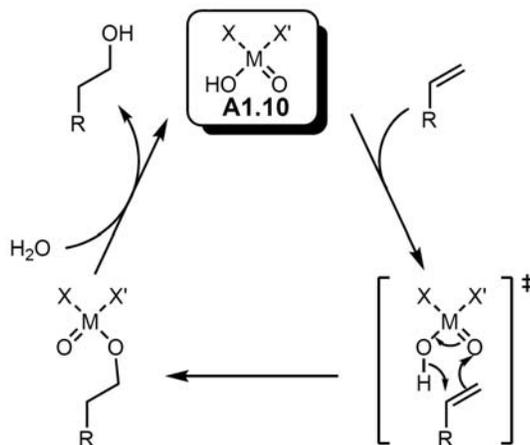
In addition to rhenium-oxo complexes such as **A1.9**, molybdenum-oxo compound **A1.11** was also of interest (Figure A1.1). Recently, Poli and co-workers reported an improved synthesis of **A1.11** and similar complexes bearing different cyclopentadienyl substituents.[19] Stopped-flow kinetics analysis used to study the pH-dependent formation of species **A1.11** demonstrated that acidic conditions favor the formation of **A1.11** over a related dimeric structure.[20] In addition, Tyler and co-workers have shown that the structurally similar compound **A1.12**, while unreactive toward olefins, performs nitrile hydration to produce amides.[21] We hypothesized that complex **A1.11** should be more activated toward nucleophilic attack by an olefin since it bears only one cyclopentadienyl ring and is thus more Lewis acidic.
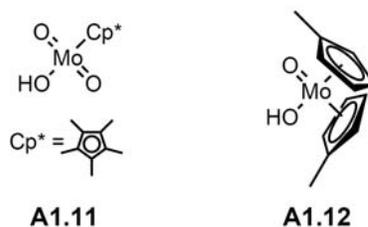
Figure A1.1. Molybdenum-oxo-hydroxo compounds.

Utilizing the aforementioned screening protocol, the following complexes were evaluated for activity with styrene using the standard reaction conditions (Table A1.1): **A1.11**, $Mo(acac)_2O_2$, $WO_3 \cdot H_2O$, $HReO_4$, $ReO_2 \cdot 2H_2O$, ReO_3, $ReO(PPh_3)_2(Cl)$, and $VO(SO_4) \cdot nH_2O$. Unfortunately, either no reaction or only minor amounts (< 2%) of acetophenone were observed.

Late Transition-Metal Catalysts

Although there have been several late transition-metal olefin hydration catalysts reported (vide supra), we decided to conduct a broad transition-metal screen to probe for undiscovered hydration activity. In light of recent progress in olefin hydroamination, we initially focused on Pd(II) complexes with bidentate phosphines;[22,23] however, we subsequently expanded our search to include over 40 commercially available Group VIII–X metal complexes.

The Ni(II), Pd(II), Pt(II), and Pd(IV) complexes screened either showed no reaction or produced small amounts of acetophenone (**A1.4**) and/or ethyl benzene (**A1.5**) (Table A1.2, Figure A1.2). Similar results were subsequently observed with Fe(III), Ru(II), Ru(III), Ru(IV), Co(II), and Rh(I) complexes. However, several Rh(III) and Ir(IV) complexes were found to be active for Markovnikov hydration, producing 1-phenethyl alcohol (**A1.3**) in up to 11% conversion (10 mol% catalyst loading). The highest percent conversion to **A1.3** was obtained at 80 ^{0}C in 1:3 H_2O:THF; the addition of TFA or NaOH did not significantly affect the reaction yield or selectivity. The major products detected were **A1.3**, **A1.4**, and **A1.5**. Interestingly, no terminal alcohol was detected by GC analysis.

Table A1.2. Transition-metal complexes investigated for olefin hydration of styrene[a]

Metal Complex	Ligand or Additive	Temp (°C)	% Conv. **A1.3**[b]	% Conv. **A1.4**[b]	% Conv. **A1.5**[b]
NiCl$_2$	-	25, 80	-	-	-
Pd(OAc)$_2$	-	25, 80	-	-	-
Pd(OAc)$_2$	**A1.14**	25, 80		<5%	<5%
Pd(TFA)$_2$	-	25, 80	-	<10%	-
Pd(TFA)$_2$	**A1.14**	25, 80	-	-	<10%
Pd(TFA)$_2$	**A1.13**	25, 80	-	-	-
Pd(TFA)$_2$	**A1.16**	25, 80	-	<6%	<6%

Metal Complex	Ligand or Additive	Temp (°C)	% Conv. A1.3[b]	% Conv. A1.4[b]	% Conv. A1.5[b]
Pd(TFA)$_2$	**A1.17**	25, 80	-	-	-
Pd(TFA)$_2$	**A1.21**	25, 80	-	<5%	-
PdCl$_2$(**14**)$_2$·CH$_2$Cl$_2$	-	25, 80	-	-	<5%
PdCl$_2$(**14**)$_2$·CH$_2$Cl$_2$	SnCl$_2$·H$_2$O	25, 80	-	<5%	<5%
Pd(dba)$_3$	**A1.14**	25, 80	-	-	<5%
Pt(PEt$_3$)$_2$(C$_2$O$_4$)	-	25, 80	-	<5%	<5%
Pt(acac)$_2$	-	25, 80	-	-	-
Pt(CF$_3$C(O)CHC(O)CF$_3$)$_2$	**A1.14**	25, 80	-	-	-
PtCl$_2$(PMe$_3$)$_2$	-	40, 80	-	-	-
PtCl$_4$	-	60, 80	-	-	<5%
Co(**20**)$_2$	-	25, 80	-	-	-
Co(**20**)$_2$	CuCl$_2$·2H$_2$O	25, 80	-	-	-
Co(**20**)$_2$	CuCl	25, 80	-	-	-
RhCl(PPh$_3$)$_3$	-	25, 80	-	<5%	-
RhCl(CO)(PPh$_3$)$_2$	-	25, 80	-	<5%	-
[Rh(**17**)COD]BF$_4$	-	60, 80	-	-	-
[Rh(cod)(Cl)]$_2$	-	60, 80	-	<5%	<5%
[Rh(C$_2$H$_4$)$_2$(Cl)]$_2$	-	60, 80	-	<5%	-
Rh$_2$(**20**)$_4$	-	25, 80	-	-	-
RhCl$_3$·2.7H$_2$O	-	25, 80	<5%	<5%	-
RhBr$_3$	-	40, 80	<5%	<6%	-
RhI$_3$	-	40, 80	0-11%	1-20%	4-35%
Rh(acac)$_3$	-	25, 80	-	-	-
(NH$_4$)$_3$RhCl$_6$·nH$_2$O	-	25, 80	<5%	<5%	<5%
Rh(C$_2$H$_8$N$_2$)$_3$Cl$_3$·3H$_2$O	-	25, 80	-	-	-
[Rh$_3$(OAc)$_6$-μ-O(H$_2$O)$_3$]OAc	-	60, 80	-	-	-
IrCl(CO)(PPh$_3$)$_2$	-	25, 80	-	-	-
IrCl$_3$	-	25, 80	-	-	-
IrCl$_3$	CuCl$_2$·2H$_2$O	25, 80	<5%	-	-
H$_2$IrCl$_6$·4.7H$_2$O	-	25, 80	<5%	<5%	-
H$_2$IrCl$_6$·4.7H$_2$O	**A1.14**	25, 80	-	-	<5%
H$_2$IrCl$_6$·4.7H$_2$O	**A1.11**	25, 80	-	-	-
Na$_2$IrCl$_6$·6H$_2$O	-	25, 80	<5%	<5%	<10%

Metal Complex	Ligand or Additive	Temp (°C)	% Conv. A1.3[b]	% Conv. A1.4[b]	% Conv. A1.5[b]
IrO_2	-	40, 80	-	-	-
$IrCl_4$	-	40, 80	<5%	<5%	<5%
$Fe(20)_3$	-	25, 80	-	-	-
$RuCl_3$	-	25, 80	-	-	-
$RuHCl(P(i\text{-}Pr)_3)_2$	-	25, 80	-	-	-
$RuH_2(PPh_3)_4$	-	25, 80	-	-	<15%
$K_2RuO_4{\cdot}H_2O$	--	25, 70	-	-	<5%
$CuCl_2{\cdot}2H_2O$		25, 80	-	-	-

[a]For reaction conditions, see Table A1.1. [b]% Conversions refer to the maximum amount of product detected by GC in any individual reaction of the screening protocol.
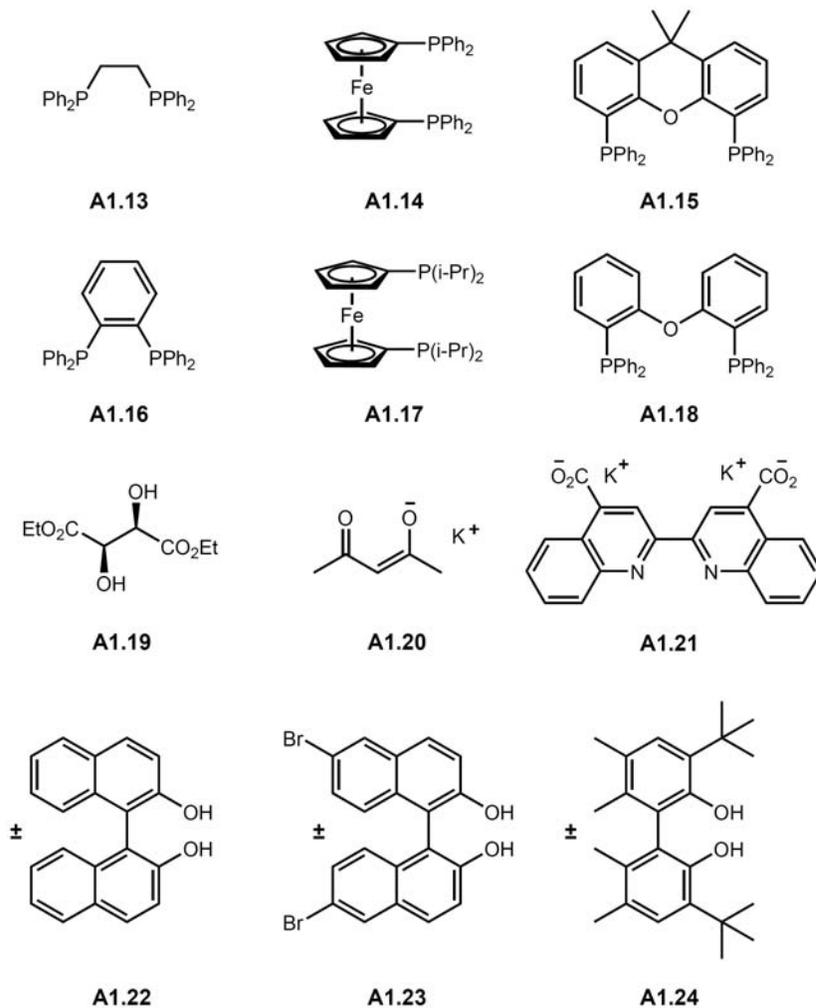
Figure A1.2. Phosphine and oxygen-based ligands examined.

To improve the product yield and selectivity of RhI$_3$-promoted reactions, we investigated the following variables: solvent, temperature, atmosphere, ligands and additives, including acids and bases. These reactions were carried out based on the screen protocol previously described (Table A1.1). For example, when examining solvent conditions, THF and H$_2$O were substituted with other aprotic and protic solvents. In addition, for reactions with added ligands or additives, 1 equiv (relative to catalyst loading) was used unless otherwise specified.

Solvent Systems

Several organic co-solvents were examined for their impact on the product distribution and conversions (Table A1.3). Coordinating solvents such as DMF shut down catalyst activity whereas solvents such as CH$_2$Cl$_2$ and toluene showed no hydration activity. Reactions performed in *p*-dioxane and diglyme produced up to 20% of 1-phenethyl alcohol (**3**), although the side product yields were not diminished; *i*-Pr$_2$O and *n*-Bu$_2$O did not yield any improvements.

Table A1.3. Solvents examined for activity with RhI$_3$

Aprotic Solvent	Protic Solvent	Temp. (°C)
THF	H$_2$O	25, 80
THF	i-PrOH	60, 80
THF	t-BuOH	60, 80
p-dioxane	H$_2$O	40, 80
p-dioxane	t-BuOH	60, 80
MeCN	H$_2$O	40, 80
DMF	H$_2$O	25, 80
CH$_2$Cl$_2$	H$_2$O	25, 40
ClCH$_2$CH$_2$Cl	H$_2$O	60, 80
toluene	H$_2$O	40, 80
i-Pr$_2$O	H$_2$O	60, 80
n-Bu$_2$O	H$_2$O	60, 80
diglyme	H$_2$O	60, 80
1,2-dimethoxybenzene	H$_2$O	60, 80

Protic co-solvents other than water were also studied. Utilizing a THF and i-PrOH solvent combination, nearly quantitative transfer hydrogenation to generate ethyl benzene (**A1.5**) was observed; in contrast, a mixture of THF or p-dioxane with t-BuOH gave similar results as THF and H$_2$O. Interestingly, MeOH and EtOH produced approximately 50−60% of 1-phenethyl methyl ether (**A1.25**) and 1-phenethyl ethyl ether (**A1.26**), respectively, as indicated by preliminary GC-MS data (eq A1.3). The significant increase in conversion and the formation of an ether instead of an alcohol may be indicative of an improved reaction protocol.

R = Me, **A1.25**
R = Et, **A1.26**   **A1.5**
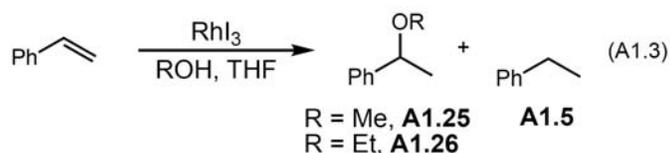
In addition to varying co-solvents, the effect of solvent ratio was examined. Because better results were obtained in runs with more organic co-solvent, reactions with a mixture of 2% or 10% H_2O in THF or p-dioxane were performed. However, no significant difference in the yield of 1-phenethyl alcohol (**A1.3**) was observed with either solvent system in reactions at 80 °C.

Temperature

The initial set of screening reactions performed with RhI_3 indicated that optimal activity was observed at 80 °C rather than at 40 °C. A similar trend was observed in the solvent screen discussed above (Table A1.3). Based on these results, we hypothesized that further elevation of the reaction temperature might result in better reactivity. However, reactions performed in p-dioxane at 100 °C produced diminished conversion to **A1.3** and increased conversion to acetophenone (**A1.4**). For comparison, a series of reactions in aqueous THF or p-dioxane at 40 °C or 60 °C was examined. Under the best conditions obtained from this screen, 1:3 H_2O:p-dioxane at 60 °C, an increase in conversion to **A1.3** to 25% was observed.

Atmosphere

Whereas O_2 inhibited the Pt(II)-based catalysts discovered by Trogler and co-workers, it was required for the Co(II) catalysts previously described. Consequently, we wanted to examine the possible role of O_2 in our catalyst system. For comparison, reactions were set up under an atmosphere of argon and oxygen. The reactions were performed at 80 °C in 3:1 THF:H_2O and sampled after 10 h (Table A1.4). No improvement in conversion to product

was observed under either argon or oxygen, which indicates that O_2 is probably not involved in the major catalytic pathway observed. Combined with the aforementioned results utilizing MeOH and EtOH as protic co-solvents, this evidence also suggests that O_2 is not the source of oxygen in alcohol **A1.3**.

Table A1.4. Comparison of atmospheres examined for activity with RhI_3.

Atmosphere	% Conversion to **A1.3**	% Conversion to **A1.4**	% Conversion to **A1.5**
Air	11%	4%	15%
Oxygen	5%	-	2%
Argon	10%	6%	10%

Ligands

Several monodentate and bidentate phosphorous-based ligands were surveyed to investigate their effect on RhI_3 catalyzed styrene hydration. In comparison to the control reaction, addition of the monodentate ligands PPh_3, $P(p\text{-}FC_6H_4)_3$, and $P(OPh)_3$ did not improve the selectivity for or conversion to 1-phenethyl alcohol (**A1.3**) (Figure A1.3). A series of chelating phosphines with varying bite angles was also examined.[24-27] Reactions with ligands **A1.14**, **A1.15**, and **A1.18** exhibited an improvement in selectivity for **A1.3** over **A1.4** and **A1.5** under most reaction conditions. Additionally, the conversion to **A1.3** increased when a 3:1 H_2O:THF solvent combination was used, but decreased in 1:3 H_2O:THF. The analogous reactions with p-dioxane in place of THF have not yet been performed.

In contrast to the chelating phosphines, chelating oxygen-based ligands exhibited no improvement in overall selectivity for **A1.3**, but showed equal or greater conversions to **A1.3** when a 1:3 H_2O:THF solvent combination was utilized (Figure A1.4). In addition, these

ligands appear to have an effect on the rate of reaction and catalyst lifetime. Although the conversion to **A1.3** typically does not increase after 10 h, reactions employing chelating oxygen-based ligands showed an increase in alcohol yield from 10 h to 40 h. Further studies on these ligands are being conducted.

a)

b)
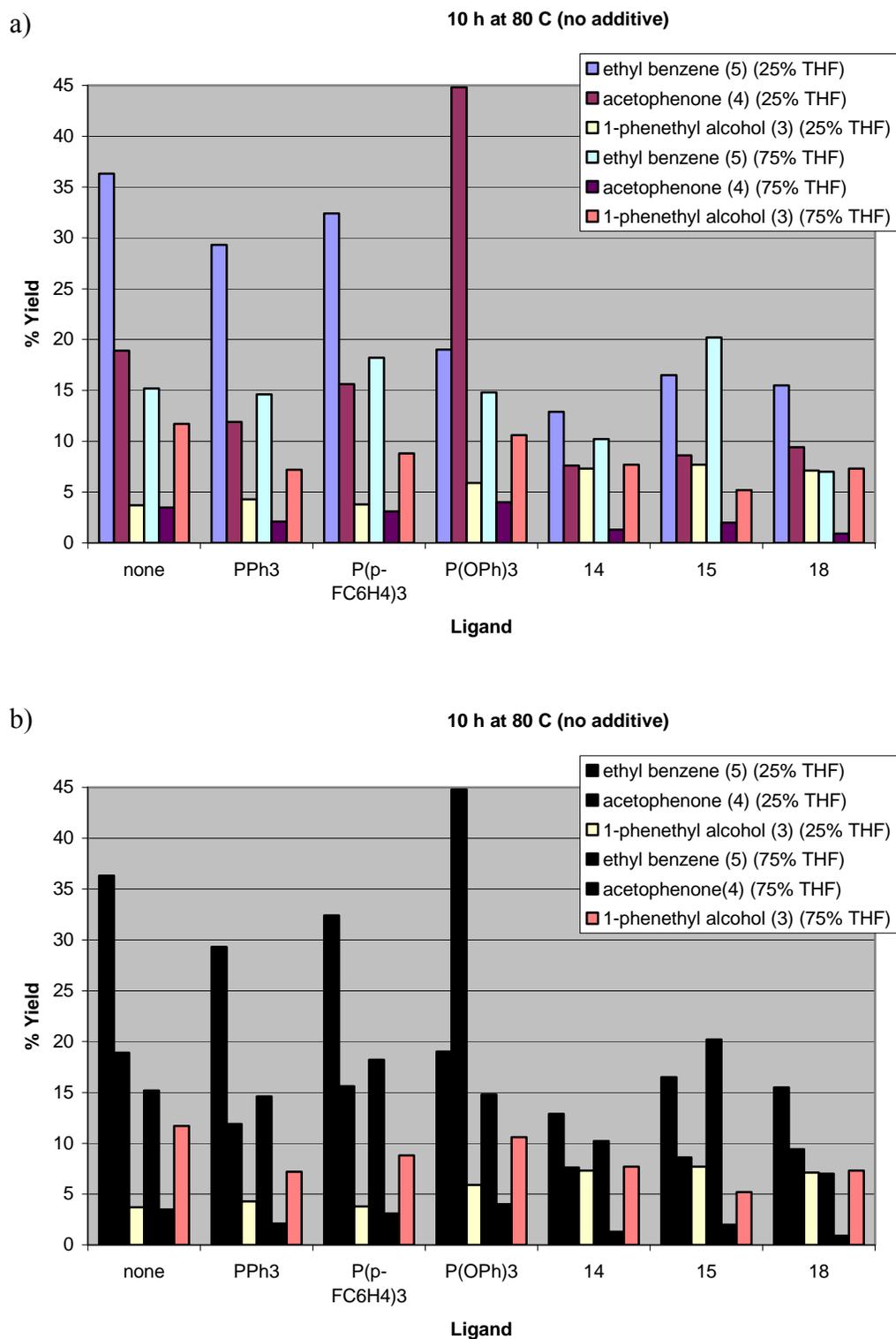
Figure A1.3. a) Product distribution of reactions with RhI3 and phosphorous-based ligands. b) Same as a) with the exception that bars representing conversion to A1.4 and A1.5 are shown in black to clarify the conversion to A1.3.

a) **10 h at 80 C (no additive)**

b) **10 h at 80 C (no additive)**
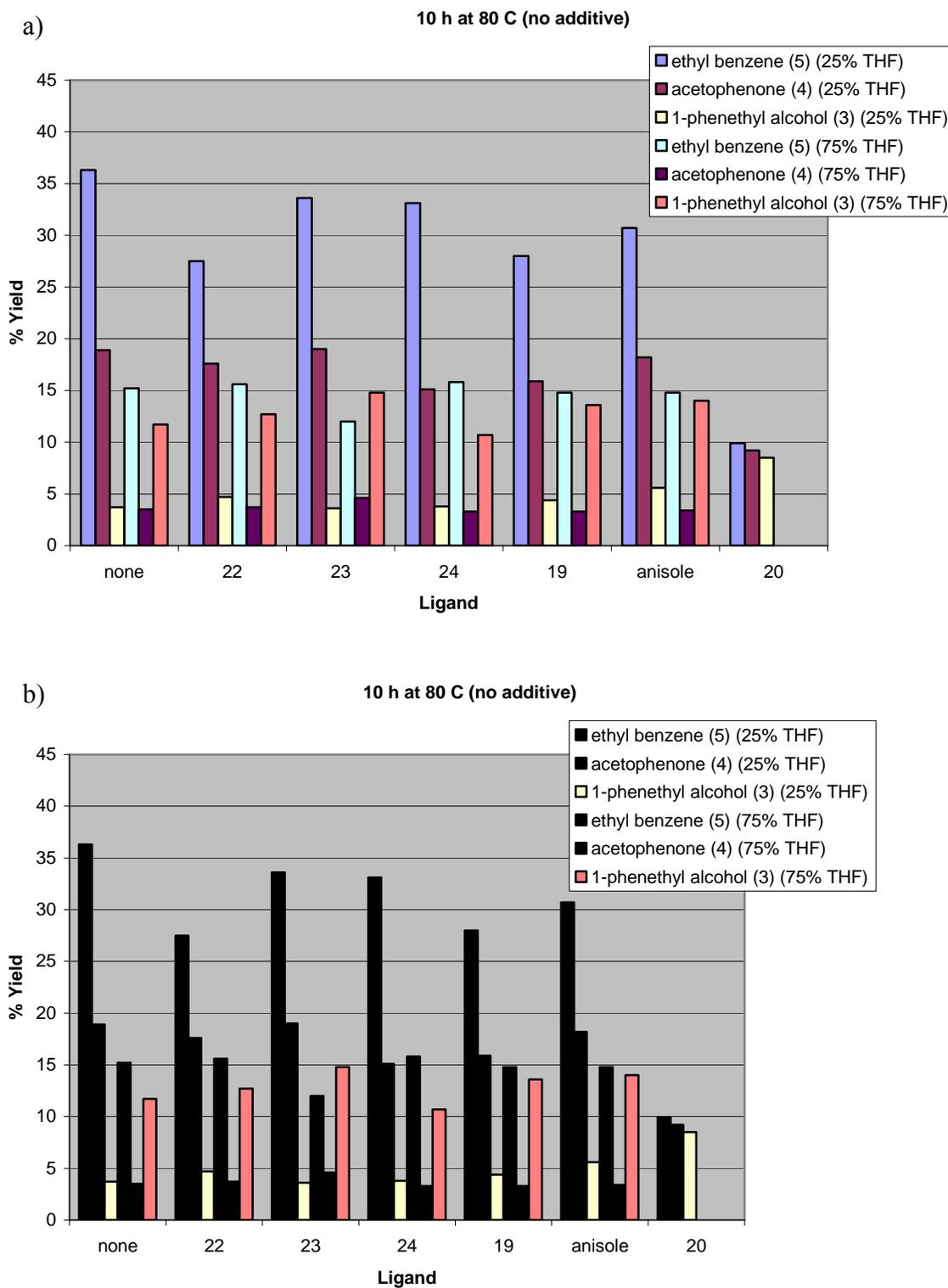
Figure A1.4. a) Product distribution of reactions with RhI$_3$ and oxygen-based ligands. No data was available for **A1.20** in 75% THF. b) Same as a) with the exception that bars representing conversion to **A1.4** and **A1.5** are shown in black to clarify conversion to **A1.3**.

Additives

The Pt(II) olefin hydration catalysts developed by Trogler and co-workers required basic conditions,[8] but the Pd(II) olefin hydroamination catalysts developed by Hartwig and co-workers required acid co-catalysts.[17] Consequently, we wanted to examine the effect of acid and base additives on catalyst reactivity and product distribution. Several acids with varying pKas and counteranion coordinating ability were examined (Figure A1.5). However, the selectivity for and conversion to 1-phenethyl alcohol (**A1.3**) did not differ significantly from the control reaction in which no additives were present. Also, a variety of nitrogen- and oxygen-based bases was examined. Nitrogen bases generally increased selectivity for **A1.3** over acetophenone (**A1.4**) and ethyl benzene (**A1.5**) in 3:1 THF:H_2O reactions; however, overall conversions to **3** decreased significantly. Interestingly, no hydroamination was observed with Et_2NH. Oxygen-based bases also showed an increase in selectivity for **A1.3** in 3:1 THF:H_2O; however, the conversion to **A1.3** was same or slightly decreased relative to the control reaction.

In addition to acids and bases, two other additives were examined for the impact on RhI_3-promoted styrene hydration. Due to the biphasic reaction conditions, a phase-transfer catalyst was added to a series of reactions. Interestingly, the addition of phase-transfer catalyst, $[NBu_4]^+[BF_4]^-$, suppressed catalysis. To test the possibility of catalyst reoxidation being a problem, reactions in the presence of $CuCl_2 \cdot 2H_2O$ as an additive were performed. After 40 h, the conversion to **A1.3** was comparable to that of the control reaction and significant improvement in selectivity for **A1.3** was observed (less than 5% of **A1.4** or **A1.5** was observed).

a)

10 h at 80 C (no additive)

b)

10 h at 80 C (no additive)

Legend:
- ethyl benzene (5) (25% THF)
- acetophenone (4) (25% THF)
- 1-phenethyl alcohol (3) (25% THF)
- ethyl benzene (5) (75% THF)
- acetophenone (4) (75% THF)
- 1-phenethyl alcohol (3) (75% THF)

Y-axis: **% Yield**

X-axis (Additive): 1 HCl, 1 HBF4, .5 TFA, 1 TFA, 1 AcOH, none, 1 pyridine, 1 morpholine, 1 Na2CO3, 1 Et3N, 5 Et3N, 1 Et2NH, .5 NaOH, 1 NaOH, 1 NaOtBu, 1 n-Bu4NBF4, 1 CuCl2*2H2O
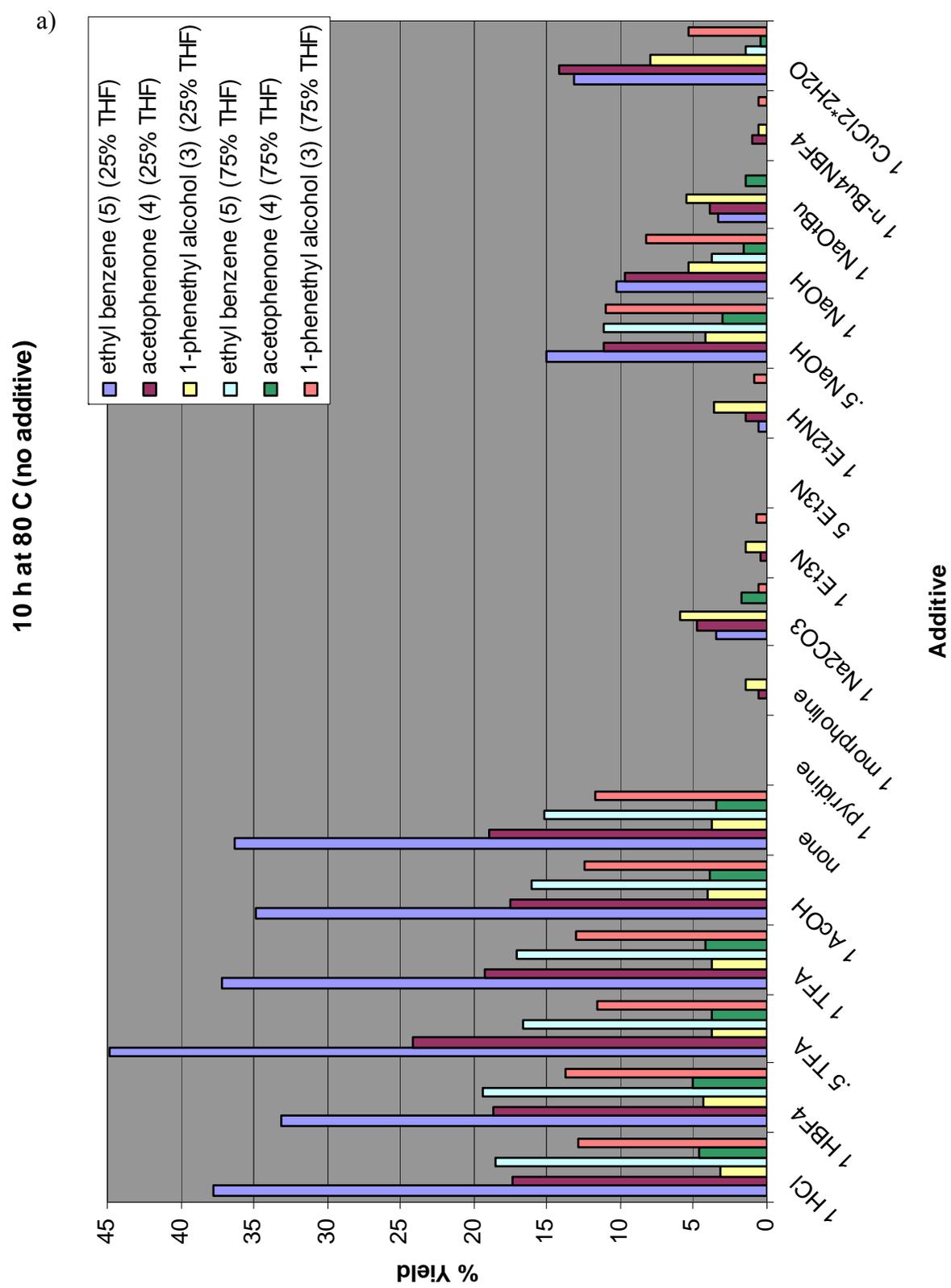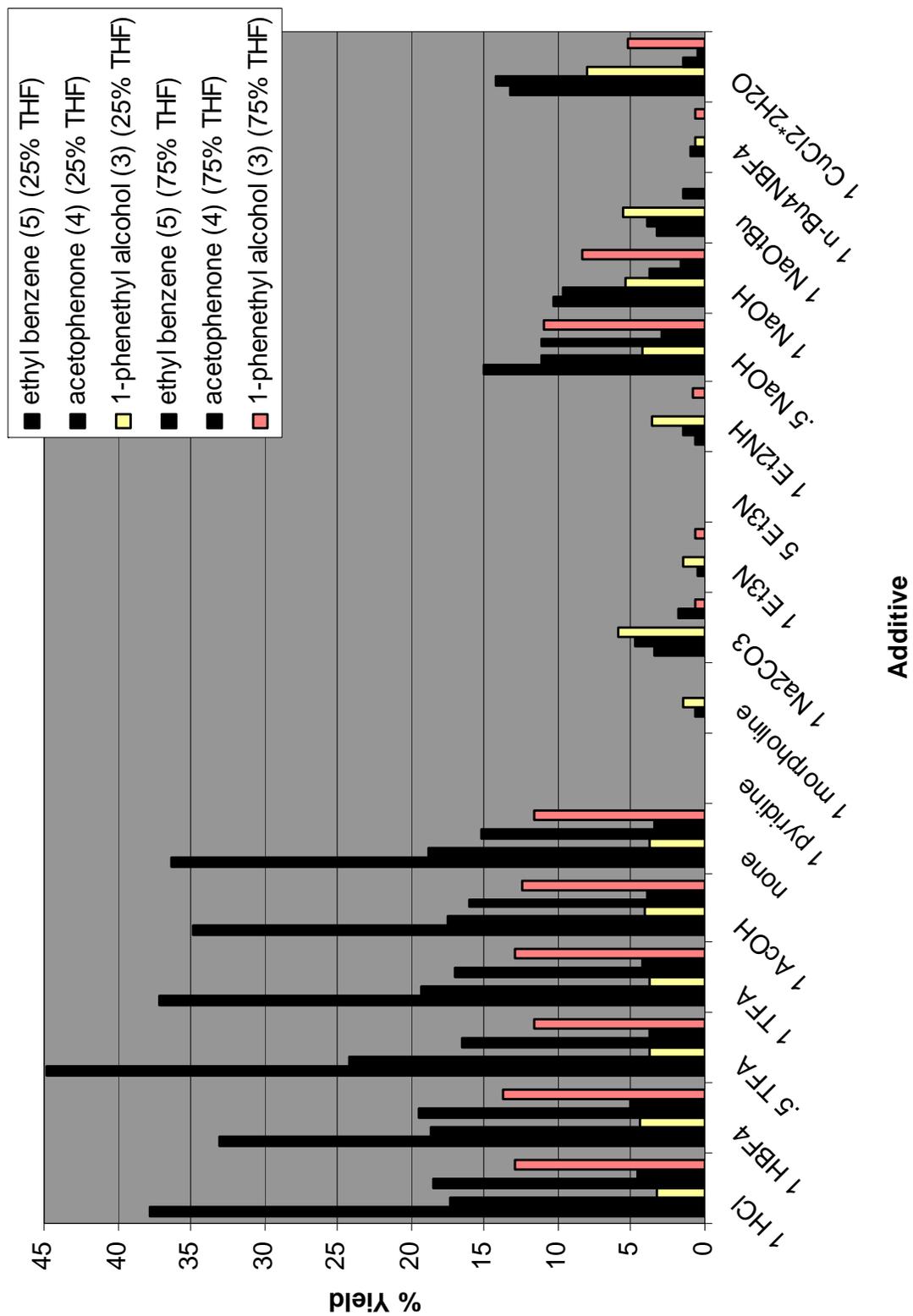
Additive

Figure A1.5. a) Product distribution of reactions with RhI$_3$ and various additives. b) Same as a) with the exception that bars representing conversion to **A1.4** and **A1.5** are shown in black to clarify conversion to **A1.3**.

Product Equilibration

In most reactions with RhI$_3$, the percent conversion to 1-phenethyl alcohol (**A1.3**) after 40 h was either the same or lower after 10 h. A simultaneous, but not always equal, increase in the amount of acetophenone (**A1.4**) was usually detected. Consequently, we examine the reactivity of Rh(III) halide salts with **A1.3** to determine if oxidation to **A1.4** was occurring (eq A1.4). Utilizing the screening conditions outlined in Table A1.1, a series of 12 reactions was performed for RhCl$_3$, RhBr$_3$, and RhI$_3$. Reaction of RhCl$_3$ or RhBr$_3$ with **A1.3** resulted in less than 5% each of **A1.4** and ethyl benzene (**A1.5**) observed after 40 h at 80 °C. However, reactions containing RhI$_3$ and **A1.3** generated surprising results. As shown in Figure A1.6, two thirds of the reactions sampled after 10 h show less than 40% of **A1.3** remaining and after 40 h, less than 10% remained. Significant conversion to both **A1.4** and **A1.5** was observed in all cases and minor (< 10%) amounts of styrene were also observed. Reactions performed in at 60 °C (reaction conditions 1−6) showed less decomposition of **A1.3** than those performed at 80 °C (reaction conditions 7−12). Additionally, reactions 1−6 generally produced a 2:1 mixture of **A1.4** and **A1.5** whereas reactions 7−12 produced an approximate 1:1 mixture of **A1.4** and **A1.5**. These results suggest that RhI$_3$ mediates an equilibration between styrene, **A1.3**, **A1.4**, and **A1.5**. Therefore, previous results in which sampling was performed only after 10 h and 40 h provide limited information about the reaction; sampling after 1 h may show higher percent conversion to **A1.3**.
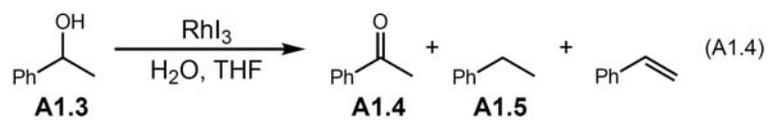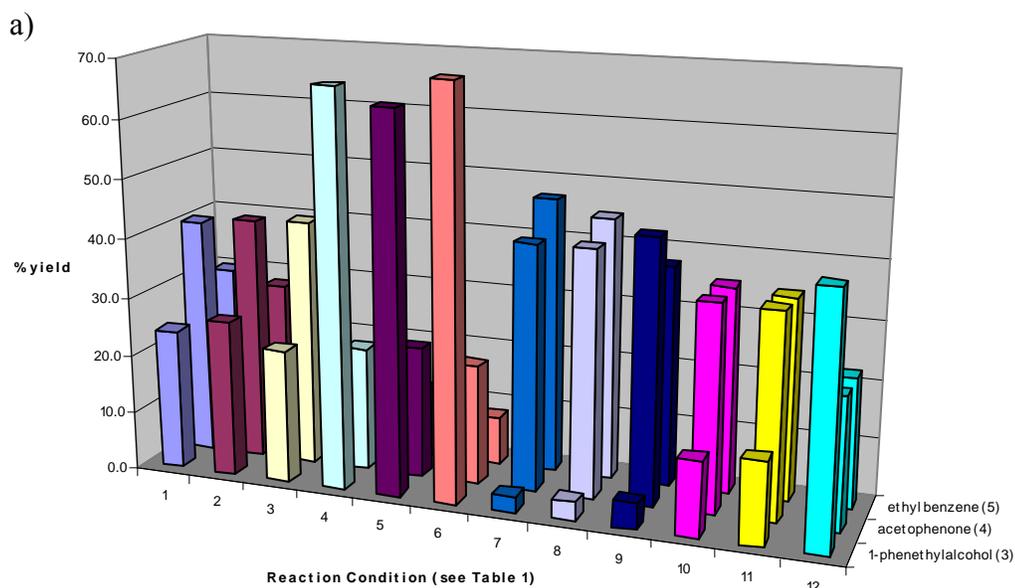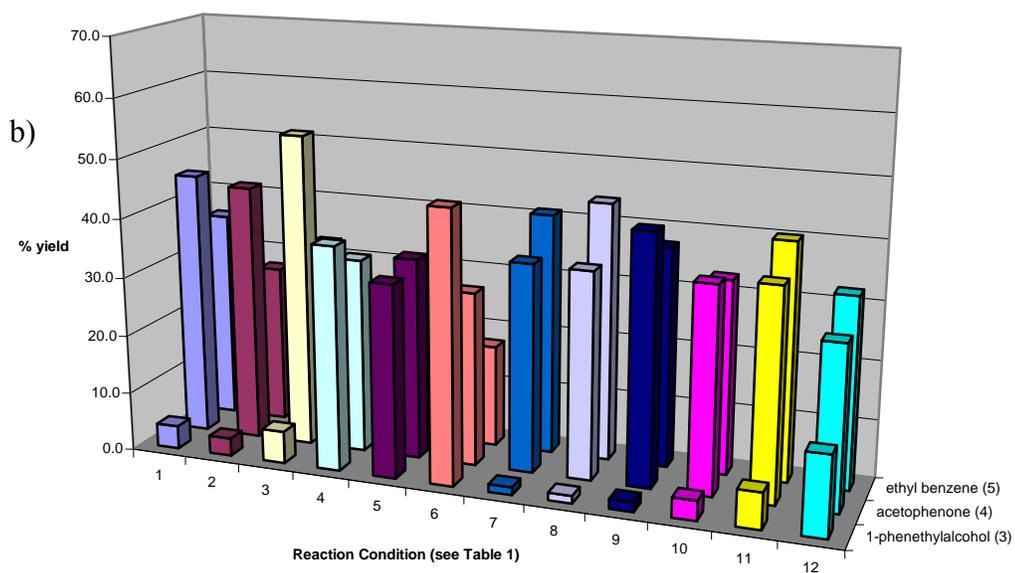
Figure A1.6. Product distribution of reactions of RhI$_3$ and 10 equiv **A1.3** after a) 10 h and b) 40 h.

Following the reaction of 10 mol% RhI$_3$ with 1-phenethylalcohol (**A1.3**) (eq A1.4) at earlier reaction times demonstrated significant oxidation and reduction of **A1.3** to **A1.4** and **A1.5**, respectively, over time (Figure A1.7). After 8 h at 80 °C, approximately 45% conversion to **A1.4** and 15% conversion to **A1.5** is observed. Additionally, monitoring the reaction of styrene with 10 mol% RhI$_3$ at 80 °C at earlier reaction times shows that the conversion to alcohol **A1.3** remains the same or decreases over the first 10 h of the reaction while the conversion to ketone **A1.4** steadily increases. Altogether, these results demonstrate that transformation of the desired alcohol **A1.3** to **A1.4** and **A1.5** occurs competitively with the production of **A1.3**; the utility of RhI$_3$ for the hydration of styrene is thus limited due to competitive side reactions.
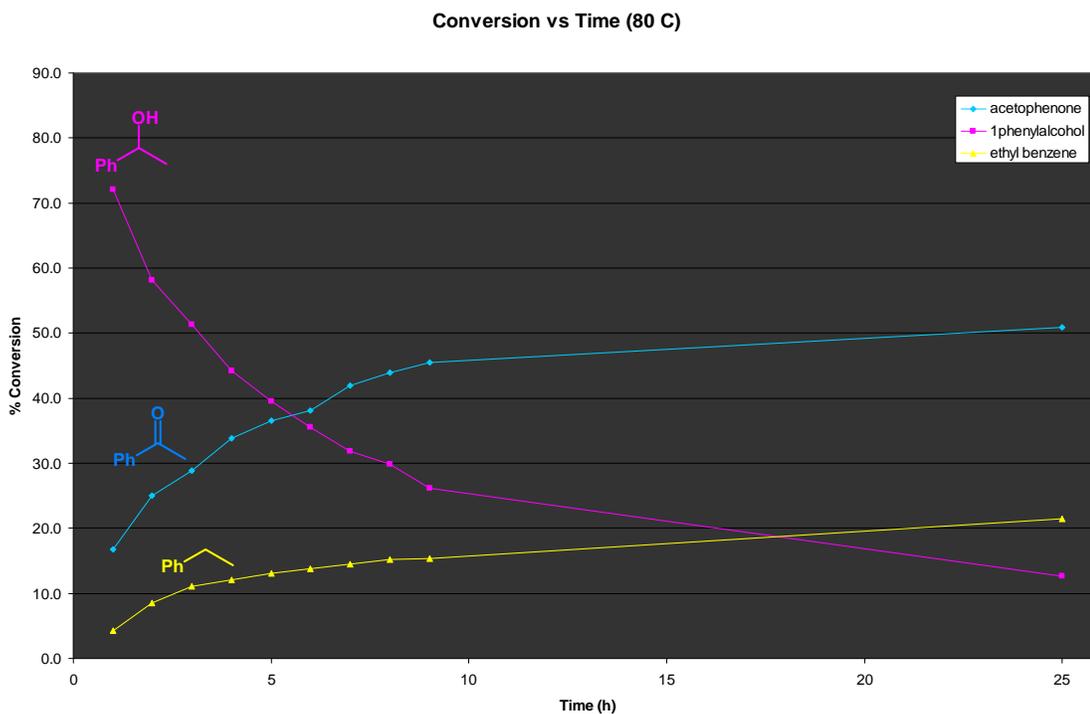
Figure A1.7. Plot of % conversion vs time (h) of **A1.3** (pink square) to **A1.4** (blue diamond) and **A1.5** (yellow triangle) over time with 10 mol% RhI$_3$ in 1:3 H$_2$O:THF at 80 °C.
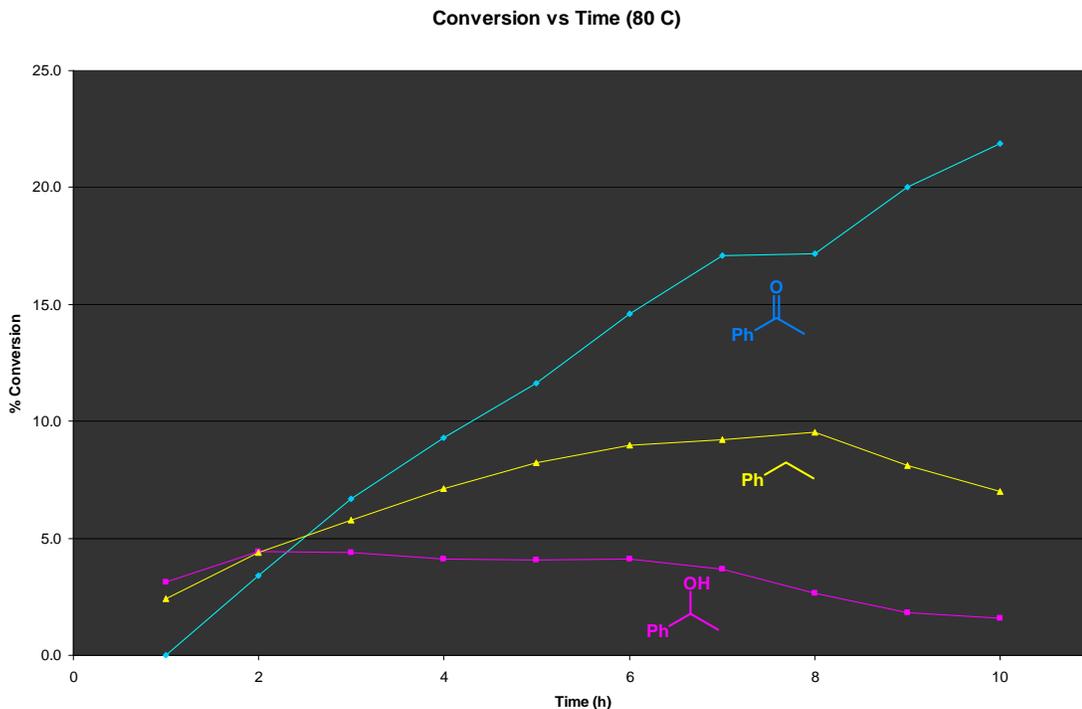
Figure A1.8. Plot of % conversion of styrene to **A1.3** (pink square) to **A1.4** (blue diamond) and **A1.5** (yellow triangle) over time with 10 mol% RhI$_3$ in 3:1 H$_2$O:THF at 80 °C.

To examine the possibility of a heterogeneously-promoted reaction, Hg(0) was added to a standard reaction. Mercury has been previously demonstrated to coat the surface of nanoparticles, thus inhibiting surface chemistry.[28] Two identical reactions were performed and sampled after 4, 10 and 24 h. The % conversion to ketone **A1.4** (diamonds) and alcohol **A1.3** (squares) are shown for both reactions (Figure A1.9). The reaction without mercury (shown in yellow) demonstrates an increasing yield of both **A1.3** and **A1.4** over time. After 10 h, 300 equiv Hg(0) was added and conversion to **A1.3** and **A1.4** (shown in blue) is inhibited relative to the reaction without Hg(0).

Conversion vs Time (80 C)
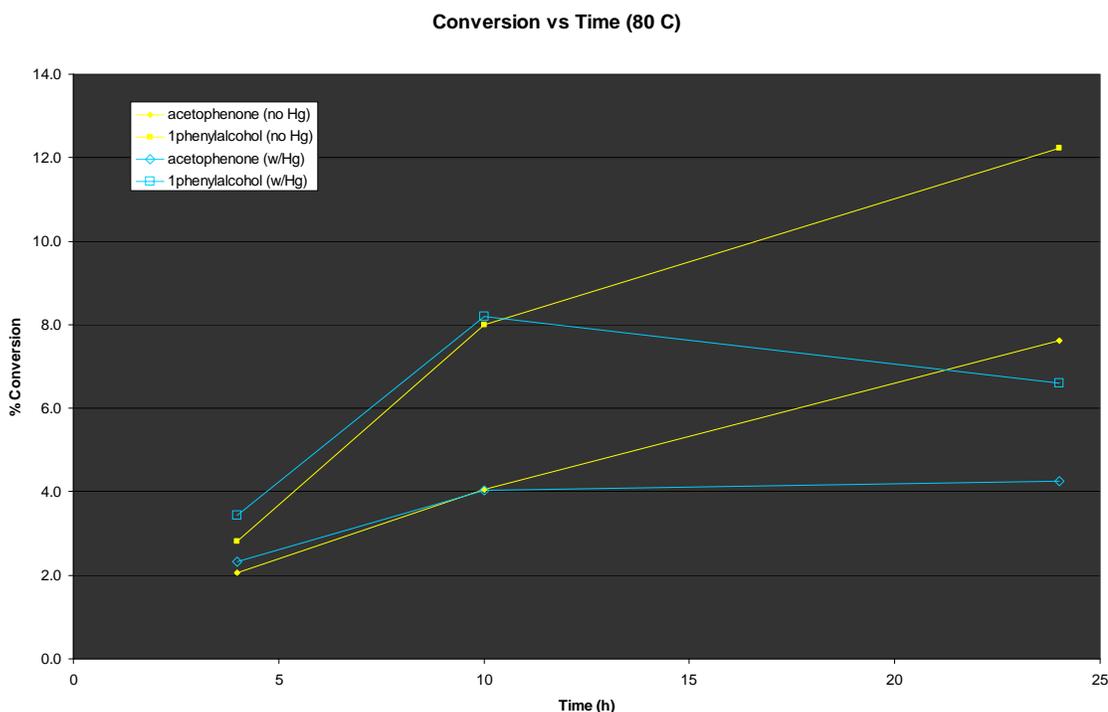
Figure A1.9. Plot of % conversion vs time (h) for the hydration of styrene with 10 mol% RhI$_3$ at 60 °C in 1:3 H$_2$O:p-dioxane in the presence and absence of mercury(0).

Summary

Screening of over 40 early- and late-transition-metal complexes for hydration activity with styrene led to the discovery of new Rh(III)- and Ir(IV)-mediated activity. Among the complexes screened, RhI$_3$ exhibited the highest activity for Markovnikov olefin hydration, producing 1-phenethyl alcohol (**A1.3**) in up to 11% conversion after 10 h stirring at 80 °C in aqueous THF. The major products obtained were 1-phenethyl alcohol (**A1.3**), acetophenone (**A1.4**), and ethyl benzene (**A1.5**).

Subsequent optimization of reaction parameters including temperature, pH, and solvent resulted in a modest increase of 1-phenethyl alcohol to 25% conversion after 10 h utilizing RhI$_3$ in aqueous p-dioxane at 60 °C. The addition of strong and weak acids had no effect on the percent conversion to product and distribution; however, bases were

generally observed to increase the product selectivity for alcohol **A1.3** but decrease the overall conversion. A variety of phosphorous- and oxygen-based ligands were additionally examined with RhI_3. However, none of these additives or ligands significantly improved the percent conversion to 1-phenethyl alcohol.

The use of MeOH or EtOH as nucleophiles rather than H_2O provided significant increases in product (ether) yield to 50−60%. The increased yield for hydroalkoxylation may be a result of the inability for RhI_3 to decompose the product ethers whereas reduction and oxidation of **A1.3** is readily observed at room temperature. Further investigation of this reactivity was not conducted.

Taken together, these results provide some clues about the RhI_3-promoted hydration of styrene. First, the addition of very coordinating species, either as solvent, ligand, or base, generally decreases catalyst activity. Second, experiments with MeOH and EtOH suggest that oxygen incorporation into the product does not involve O_2. Third, it was shown that **A1.3**, in the presence of RhI_3, is easily converted into a mixture of ethyl benzene (**A1.5**) and acetophenone (**A1.4**). Lastly, evidence of a heterogeneously-catalyzed reaction was obtained through demonstration of reaction inhibition upon addition of Hg(0).

Experimental

General Considerations

Reactions were carried out under ambient atmosphere unless otherwise noted. All dry solvents were purified by passage through activated A-2 alumina solvent columns and were degassed with argon prior to use. All other materials were purchased from

Strem, Alfa Aesar, or Aldrich and used as received. All silica gel chromatography was performed with Silica Gel 60. Styrene was passed through a plug of alumina before use.

General Reaction Conditions for Transition-Metal Screen:

To a 2-mL vial containing 10 mol% transition metal (and ligand) and a stir bar was added 22 μL tridecane, 0.5-x mL protic solvent, x mL organic co-solvent, and 34 μL styrene. An additive, if utilized, was then added. The vial was sealed with a cap containing a PTFE septum. The reaction was stirred at 25 °C, 40 °C, 60 °C, or 80 °C for 40 h. After 10 h and 40 h, a 50 μL aliquot was removed and placed onto a micropipette silica gel column. The reaction contents were eluted with 3 volumes of Et_2O and submitted to GC analysis.

References

(1)   Wade Jr., L. G. *Organic Chemistry*; 4th ed.; Prentice-Hall, Inc: Upper Saddle River, 1999.

(2)   Yoshida, T.; Matsuda, T.; Okano, T.; Kitani, T.; Otsuka, S. *J. Am. Chem. Soc.* **1970**, *101*, 2027.

(3)   Ganguly, S.; Roundhill, D. M. *J. Chem. Soc., Chem. Commun.* **1991**, 639.

(4)   Ganguly, S.; Roundhill, D. M. *Organometallics* **1993**, *12*, 4825.

(5)   Hamilton, D. E.; Drago, R. S.; Zombeck, A. *J. Am. Chem. Soc.* **1987**, *109*, 374.

(6)   Zombeck, A.; Hamilton, D. E.; Drago, R. S. *J. Am. Chem. Soc.* **1982**, *104*, 6782.

(7)   Inoki, S.; Kato, K.; Takai, T.; Isayama, S.; Yamada, T.; Mukaiyama, T. *Chem. Lett.* **1989**, 515.

(8)   Mukaiyama, T.; Isayama, S.; Inoki, S.; Kato, K.; Yamada, T.; Takai, T. *Chem. Lett.* **1989**, 449.

(9)   Nishinga, A.; Yamada, T.; Fujisawa, H.; Ishizaki, K.; Ihara, H.; Matsuura, T. *J. Mol. Catal.* **1988**, *48*, 249.

(10)   Nishinga, A.; Yamato, H.; Toshio, A.; Maruyama, K.; Matsuura, T. *Tetrahedron Lett.* **1988**, *29*, 6309.

(11)   Kato, K.; Yamada, T.; Takai, T.; Inoki, S.; Isayama, S. *Bull. Chem. Soc. Jap.* **1990**, *63*, 179.

(12)   Jensen, C. M.; C., T. W. *Science* **1986**, *233*, 1069.

(13)   Grushin, V. V.; Akhrem, I. S.; Vol'pin, M. E. *J. Organomet. Chem.* **1989**, *371*, 403.

(14)   Ramprasad, D.; Yue, H. J.; Marsella, J. A. *Inorg. Chem.* **1988**, *27*, 3151.

(15)   Koch, H. F.; Girard, L. A.; Roundhill, D. M. *Polyhedron* **1999**, 2275.

(16)   Kuhn, F. E.; Hermann, W. A. *Struct. Bonding (Berlin)* **2000**, *97*, 127.

(17)   Kennedy-Smith, J. J.; Nolin, K. A.; Gunterman, H. P.; Toste, F. D. *J. Am. Chem. Soc.* **2003**, *125*, 4518.

(18)   Bellemin-Laponnaz, S.; Gisie, H.; Le Ny, J. P.; Osborn, J. A. *Angew. Chem., Int. Eng. Ed.* **1997**, *36*.

(19)   Saurenz, D.; Demirhan, F.; Richard, P.; Poli, R.; Sitzmann, H. *Eur. J. Inorg. Chem.* **2002**.

(20)   Collange, E.; Garcia, J. A.; Poli, R. *New. J. Chem.* **2002**, *26*, 1249.

(21)   Breno, K. L.; Pluth, M. D.; Tyler, D. R. *Organometallics* **2003**, *22*.

(22)   Kawatsura, M.; Hartwig, J. F. *J. Am. Chem. Soc.* **2000**, *122*, 9546.

(23)   Utsunomiya, M.; Hartwig, J. F. *J. Am. Chem. Soc.* **2003**, *125*, 14286.

(24)   The average bite angle for **14**, **15** and **18** has been experimentally determined to be 99, 102 and 105 degrees respectively. .

(25)   Dierkes, P.; van Leeuwen, P. W. N. M. *J. Chem. Soc., Dalton Trans.* **1999**.

(26)   Kamer, P. C. J.; van Leeuwen, P. W. N. M.; Reek, J. N. H. *Acc. Chem. Res.* **2001**, *34*, 895.

(27)   van Leeuwen, P. W. N. M.; Kamer, P. C. J.; Reek, J. N. H. *Pure Appl. Chem.* **1999**, *71*, 1443.

(28)   Whitesides, G. M.; Hackett, M.; Brainard, R. L.; Lavalleye, J. P. P. M.; Sowinski, A. F.; Izumi, A. N.; Moore, S. S.; Brown, D. W.; Staudt, E. M. *Organometallics* **1985**, *4*, 1819.

APPENDIX 2

Investigation of the Catalytic Intramolecular Hydroalkoxylation of 2-Allylphenol

Introduction

The addition of an alcohol across a carbon-carbon double bond to form an ether is an analogous reaction to the addition of water across a carbon-carbon double bond (eq A2.1). An "atom-economical" reaction, non-oxidative olefin hydroalkoxylation reactions represent a valuable method for the formation of C–O bonds. Both intramolecular[1-5] and intermolecular[6-10] olefin hydroalkoxylation reactions catalyzed by Pt, Pd, Al, Ru, Cu, and Ag have been reported. In 2006, the Hartwig and He groups independently reported triflic acid (TfOH) as a Brønsted acid catalyst for intramolecular and intermolecular olefin hydroalkoxylation reactions.[11,12]
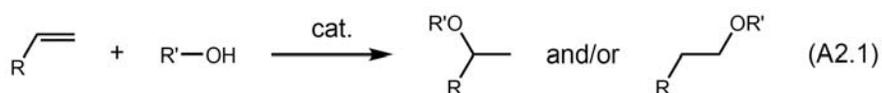
Most publications of transition-metal catalyzed hydroalkoxylation have been reported only recently. In 2004, we became interested in olefin hydroalkoxylation catalysis as a related reaction to olefin hydration. After a literature search, we noted that Furukawa and co-workers reported the use of 10 mol% $RuCl_3 \cdot nH_2O$, 30 mol% AgOTf, 50 mol% $Cu(OTf)_2$ and 20 mol% PPh_3 to transform 2-allylphenol (**A2.1**) to 2,3-dihydro-2-methylbenzofuran (**A2.2**) in 63% yield (Figure A2.1).[1] Each co-catalyst (30 mol% AgOTf, 100 mol% $Cu(OTf)_2$, or 275 mol% TfOH) was independently evaluated under otherwise identical reaction conditions and provided no conversion to furan **A2.2**.
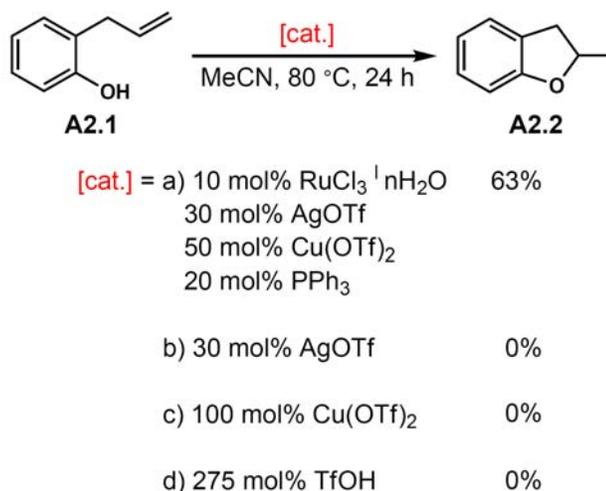
Figure A2.1. Furukawa and co-workers' report of intramolecular hydroalkoxylation.

We wanted to further investigate 1) What is the role of each co-catalyst? 2) Will the addition of ligands accelerate the reaction? 2) Can the substrate scope be expanded?

Results and Discussion

A series of different combinations of reaction promoters was examined. Utilizing identical reaction conditions as reported by Furukawa and co-workers (MeCN, 80 °C, 24 h), only 21% conversion of **A2.1** to **A2.2** was observed (Table A2.1) (Furukawa: 63%). In the absence of PPh_3, no change in conversion was observed. In the absence of $Cu(OTf)_2$, a significant decrease in conversion to 1% was observed. Reactions performed without $Cu(OTf)_2$ & PPh_3, $Cu(OTf)_2$ & AgOTf or AgOTf & $RuCl_3 \cdot nH_2O$ demonstrated lower conversion to **A2.2**. Additionally, utilizing $RuCl_3 \cdot nH_2O$ or AgOTf without any co-catalysts resulted in no conversion to **A2.2**. However, the addition of 50 mol% $Cu(OTf)_2$ afforded 20% conversion to **A2.2**, which is comparable to utilizing the originally reported co-catalyst mixture. The addition of 10 mol% TfOH provided only

4% conversion to the desired product. This experimental evidence suggested that Cu(OTf)$_2$ is the only required promoter for this reaction.

Table A2.1. Examination of different combinations of co-catalysts on conversion to **A2.2** (80 °C, MeCN, 24 h)

RuCl$_3$•nH$_2$O	AgOTf	PPh$_3$	Cu(OTf)$_2$	% conversion A2.1 → A2.2
10	30	20	50	21
10	30	---	50	21
10	30	20	---	1
10	30	---	---	7
10	---	20	---	0
---	---	20	50	13
10	---	---	---	0
---	---	---	100	14
---	---	---	50	20 (4 h)
---	---	---	10	4
---	10	---	---	0
			10 mol% TfOH	4

Based on these results, a solvent and temperature screen was conducted utilizing 10 mol% Cu(OTf)$_2$ as the sole catalyst (Table A2.2); conversions were measured after 24 h. At 40 °C, no conversion to **A2.2** is observed in Et$_2$O, whereas utilizing CH$_2$Cl$_2$ resulted in a 55% yield. Benzene and toluene provided modest conversions to **A2.2** at 40 °C. At 65 °C, reactions performed in MeCN, MeOH, and THF provided poor conversion while reactions in benzene provided 76% conversion to **A2.2**. By increasing the temperature further to 80 °C, conversions measured in benzene, toluene and 1,2-dichloroethane ranged from 60–75% with reaction times reduced to 4 h. Upon reducing the catalyst loading to 2 mol%, an 80% conversion of **A2.1** to **A2.2** in benzene was observed, which was slightly better than conversions measured in toluene (75%) and 1,2-dichloroethane (65%). Based on these results, the optimized reaction conditions were determined to be 2 mol% Cu(OTf)$_2$ in benzene at 80 °C for 4 h.

Table A2.2. Solvent and temperature screen utilizing 10 mol% Cu(OTf)$_2$

Solvent	Temp. (°C)	% conversion A2.1 → A2.2	
CH$_2$Cl$_2$	40	55	
Et$_2$O	40	0	
benzene	40	33	
toluene	40	26	
MeCN	65	4	
MeOH	65	0	
THF	65	1	
benzene	65	76	starting material
benzene	80	75	consumed
toluene	80	71	after 4 h
DCE	80	60	
benzene	80	80	
toluene	80	75	2 mol% cat loading
DCE	80	65	

.

A series of different copper sources were investigated utilizing the optimized reaction conditions (benzene at 80 °C) (Table A2.3). Utilizing 10 mol% of Cu(OAc)$_2$, CuCl$_2$, Cu(acac-F$_6$), CuSO$_4$, Cu(BF$_4$)$_2$ and CuBr, no conversion of **A2.1** to **A2.2** was observed. Utilizing 10 mol% (CuOTf)$_2$ • toluene at 80 °C provided comparable results to utilizing 10 mol% Cu(OTf)$_2$. From these results, it was apparent that the triflate counteranion is important for catalysis.

Table A2.3. Cu-source screen for conversion of **A2.1** to **A2.2**

10 mol% [cat.]	Temp. (°C)	% conversion A2.1 → A2.2 after 2 h	24 h
Cu(OTf)$_2$	65	37	76
Cu(OTf)$_2$	80	74	75
Cu(OAc)$_2$	65	0	0
Cu(OAc)$_2$	80	0	0
CuCl$_2$	65	0	0
Cu(acac-F$_6$)$_2$	80	0	0
CuSO$_4$	80	0	0
Cu(BF$_4$)$_2$	80	0	0
CuBr	80	0	0
(CuOTf)$_2$•toluene	80	56	73

To further examine this reaction, the optimized reaction conditions (benzene, 80 °C) were utilized to re-examine the previously studied co-catalysts to determine if a similar increase in activity could be observed (Table A2.4). Reactions with varying ratios of RuCl$_3$ • nH$_2$O and AgOTf in benzene at 80 °C were performed and conversions of 58−69% of **A2.1** to **A2.2** were observed after 2 h. Utilizing mixtures of RuCl$_3$ • nH$_2$O, AgOTf, and PPh$_3$ provided conversions of 42−59% after 2 h and 78−84% after 24 h. However, RuCl$_3$ • nH$_2$O did not demonstrate any catalytic activity when utilized alone. Indeed, 6−10 mol% AgOTf provided 74−81% conversion after 24 h. To examine if the reaction was acid catalyzed, TfOH, TFA and AgBF$_4$ were evaluated. Although no activity was observed for reactions containing TFA or AgBF$_4$, 57% conversion was observed after 2 h when 10 mol% TfOH was utilized. These results are consistent with a acid-catalyzed hydroalkoxylation reaction as reported independently by the He and Hartwig groups in 2006.[11,12]

Table A2.4. Re-examination of co-catalysts for the conversion of A2.1 to A2.2 utilizing benzene as solvent at 80 °C

RuCl$_3$•nH$_2$O	PPh$_3$	AgOTf	% conversion A2.1 → A2.2 after	
			2 h (**A2.1**)	24 h
10	--	30	67 (0)	
2	--	6	62 (15)	66
2	--	4	69 (1)	63
2	--	2	58 (20)	65
2	2	6	42 (54)	84
2	2	4	59 (31)	78
10	--	--	0 (100)	0
--	--	10	44 (49)	81
--	--	6	30 (65)	74
		10 mol% TfOH	57 (0)	48
		4 mol% TFA	0 (100)	0
		10 mol% AgBF$_4$	0 (100)	0

Summary

Although the original report by Furukawa and co-workers utilized a mixture of Ru, Ag and Cu salts in the presence of PPh$_3$ to catalyze the conversion of **A2.1** to **A2.2**, we could not reproduce their results.[1] Lower conversions were observed utilizing their reaction conditions and it was found that Cu(OTf)$_2$ was the only necessary catalyst for the reaction. After reaction optimization, lower catalyst loadings and shorter reaction times could be achieved. However, further reaction optimization demonstrated that similar activity could be obtained in the presence of TfOH. Trace amounts of acid may be present in Cu(OTf)$_2$ and AgOTf salts, which results in conversion of starting material.

Experimental

Typical reaction procedure: To a 4-mL vial was added metal salt(s) (1−5 equiv, 0.03−0.15 mmol). The vial was taken into the glovebox, dry solvent (1 mL) was added, the vial was capped with a screwcap containing a PTFE septum and removed from the glovebox. Tridecane (3 equiv, 0.09 mmol) and 2-allylphenol (10 equiv, 0.31 mmol) were added via syringe. Aliquots (50 μL) were taken at different time points and flashed through a silica pipette column (eluent: Et$_2$O) and analyzed via GC (50 °C for 2 min, ramp 10 °C/min until 240 °C).

References

(1)   Hori, K.; Kitagawa, H.; Miyoshi, A.; Ohta, T.; Furukawa, I. *Chem. Lett.* **1998**, 1083.

(2)   Ohta, T.; Kataoka, Y.; Miyoshi, A.; Oe, Y.; Furukawa, I.; Ito, Y. *J. Organomet. Chem.* **2007**, *692*, 671.

(3)   Coulombel, L.; Rajzmann, M.; Pons, J.-M.; Olivero, S.; Dunach, E. *Chem. Eur. J.* **2006**, *12*, 6356.

(4)   Yang, C.-G.; Reich, N. W.; Shi, Z.; He, C. *Org. Lett.* **2005**, *7*, 4553.

(5)   Qian, H.; Han, X.; Widenhoefer, R. A. *J. Am. Chem. Soc.* **2004**, *126*, 9536.

(6)   Oe, Y.; Ohta, T.; Ito, Y. *Synlett* **2005**, 179.

(7)   Youn, S. W.; Eom, J. I. *J. Org. Chem.* **2006**, *71*, 6705.

(8)   Zhang, Y.; Sigman, M. S. *Org. Lett.* **2006**, *8*, 5557.

(9)   Gligorich, K. M.; Schultz, M. J.; Sigman, M. S. *J. Am. Chem. Soc.* **2006**, *128*, 2794.

(10)   Utsunomiya, M.; Kawatsura, M.; Hartwig, J. F. *Angew. Chem. Int. Ed.* **2003**, *42*, 5865.

(11)   Li, Z.; Zhang, J.; Brouwer, C.; Yang, C.-G.; Reich, N. W.; He, C. *Org. Lett.* **2006**, *8*, 4175.

(12)   Rosenfeld, D. C.; Shekhar, S.; Takemiya, A.; Utsunomiya, M.; Hartwig, J. F. *Org. Lett.* **2006**, *8*, 4179.

APPENDIX 3

Synthesis and Evaluation of Rhodium(I) Complexes Bearing Chiral N-heterocyclic Carbenes for Acetophenone Hydrosilylation

Introduction

The development and application of N-heterocyclic carbenes (NHCs) as ligands in transition-metal catalysis is abundant.[1,2] Although NHC-metal complexes were prepared by Öfele[3] and Wanzlick and co-workers[4] in 1968, little attention was given to these types of complexes (with the exception of Lappert and co-workers[5-14]) until Arduengo and co-workers[15] reported the isolation of a free carbene in 1991. Since that publication, NHCs have been applied in many areas of catalysis due to their strong σ-donor abilities and their relatively stable bonds to metal centers.[2,16,17] Further advancements include the development of non-traditional NHC frameworks[18-24] and chiral NHCs.[25-28]

NHCs have been exceptionally successful as ligands for olefin metathesis catalysts.[29,30] Our group has synthesized numerous ruthenium-carbene complexes in an effort to develop catalysts with higher activity, stability, selectivity and tailored solubility.[29,31-44] The use of these carbenes in other transition-metal catalyzed processes might provide desirable selectivity or activity, but has been relatively unexplored to date. In particular, novel chiral, monodentate NHC ligands such as **A3.1**, which were initially developed for asymmetric metathesis reactions,[32,37,45] have received little attention in other areas of asymmetric catalyst development. These ligands are synthesized from enantioenriched 1,2-diamines and the chirality of the backbone is translated closer to the metal center through a "gearing" effect with ortho-substituted *N*-aryl groups.

A3.1
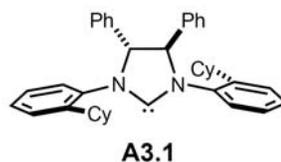
In 2002, Lee and co-workers reported the hydrosilylation of carbonyl groups with Et$_3$SiH or Ph$_2$SiH$_2$ catalyzed by (PCy$_3$)$_2$Cl$_2$Ru=CHPh (**A3.4**) (Table A3.1).[46] **A3.4** demonstrates good activity leading to > 80% conversion for a range of different aldehydes and ketone substrates.

Table A3.1. Hydrosilylation activity of **A3.4** as reported by Lee and co-workers

entry	substrate	silane	temp (°C) / h	silyl ether	yield (%)[b]
1		Me$_2$PhSiH	50 / 3	Silyl = SiMe$_2$Ph	>95
2		Et$_3$SiH	50 / 1	Silyl = SiEt$_3$	>95
3		t-BuMe$_2$SiH	80 / 0.5	Silyl = SiMe$_2$t-Bu	>95
4		Et$_3$SiH	80 / 1	Silyl = SiEt$_3$	>85
5		Ph$_2$MeSiH	80 / 0.5	Silyl = SiPh$_2$Me	>85
6		SiMe$_2$H	50 / 0.5		>95
7		Ph$_2$SiH$_2$	50 / 2		>95
8		Ph$_2$SiH$_2$	50 / 3		>80[c]
9		Et$_3$SiH	80 / 6	Silyl = SiEt$_3$	85
10		t-BuMe$_2$SiH	80 / 6	Silyl = SiMe$_2$t-Bu	42
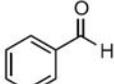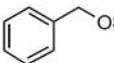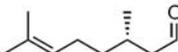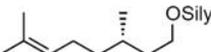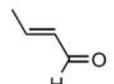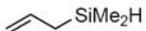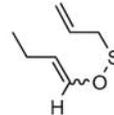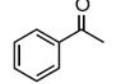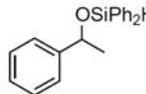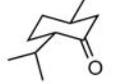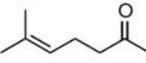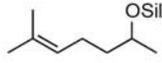
[a]1.0 mol% **1**, 1 mmol silane, 1.1 mmol carbonyl
[b]Yields were reported on the basis of ^{1}H NMR of the crude reaction mixture
[c]3:1 mixture of axial and equatorial silyl ethers

However, Lee and co-workers did not report any experiments utilizing a chiral ruthenium olefin metathesis catalyst. We wanted to further investigate this initial report

to determine: 1) Are NHC-containing ruthenium olefin metathesis catalysts active for ketone hydrosilylation? 2) Can chiral NHC-containing ruthenium olefin metathesis catalysts perform ketone hydrosilylation with high enantioselectivity? 3) Can the chiral NHCs developed by our group be extended to other metal centers that would also exhibit good enantioselectivity for ketone hydrosilylation?

Results and Discussion

Ruthenium Catalysts

Utilizing the hydrosilylation of acetophenone (**A3.2**) to alcohol **A3.3** as a test reaction, a series of reactions employing achiral catalysts **A3.4** and **A3.5** were performed (eq A3.1, Table A3.2). Utilizing the reaction conditions reported by Lee and co-workers, catalyst **A3.4** reduced ketone **A3.2** to alcohol **A3.3** with Ph_2SiH_2 in 80% conversion at 50 °C utilizing. However, employing the bulkier silane $MePh_2SiH$, no conversion was observed at 50 °C in THF, PhH or neat silane. Similar results were observed with NHC-containing catalyst **A3.4**. A slightly higher conversion (95%) was observed utilizing Ph_2SiH_2 at 50 °C.
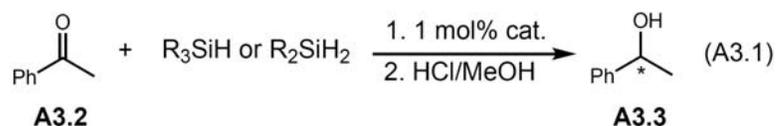
Table A3.2. Comparison of catalysts **A3.4**–**7** in the hydrosilylation of acetophenone (**A3.2**)

catalyst		silane	solvent	temp. (°C)	time (h)	% yield	%ee
A3.4		MePh$_2$SiH	THF	50	18.5	no rxn	
			PhH	50	49	no rxn	
			neat	50	20.5	no rxn	
		Ph$_2$SiH$_2$	neat	50	6	~ 80	
A3.5		MePh$_2$SiH	THF	50	18.5	no rxn	
			PhH	50	49	no rxn	
			neat	50	20.5	no rxn	
		Ph$_2$SiH$_2$	neat	50	6	~ 95	
A3.6	(9:1)^a	Ph$_2$SiH$_2$	neat	50	24	61	8
	(19:1)^a	Ph$_2$SiH$_2$	neat	50	24	77	9
	(9:1)^a	Ph$_2$SiH$_2$ + 2 AgOTf	neat	50	7	61	11
A3.7		Ph$_2$SiH$_2$	neat	50	24	> 90	5
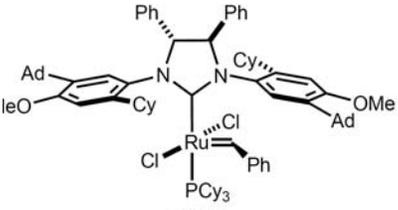
This catalyst is a mixture of **A3.6** and **A3.4** (**A3.6**:**A3.4**) due to separation difficulties during synthesis.

Based on these results, chiral catalysts **A3.6** and **A3.7** were evaluated in the hydrosilylation of acetophenone (**A3.2**) in neat Ph$_2$SiH$_2$ at 50 °C. Unfortunately, both catalysts **A3.6** and **A3.7** provided poor enantioselectivities (5–11%).

Rhodium Catalysts

Rh(I)-NHC complexes have been shown to successfully catalyze the hydrosilylation of ketones. At the time of the work presented herein, Fall 2004, only two

reports of the use of Rh(I) catalysts bearing chiral, monodentate NHCs for ketone hydrosilylation were found (Figure A3.1) in the literature. In 1996, Hermann and co-workers utilized C_2-symmetric chiral NHC **A3.8** as a ligand to synthesize Rh(I) complex **A3.11**.[47] Utilizing 1 mol% **A3.11** for the hydrosilylation of **A3.2** with Ph_2SiH_2, 90% conversion and < 5% ee was observed in 1 h at 20 °C, whereas 90% conversion and 32% ee was observed after 2d at –34 °C. In 1998, Enders and co-workers reported the synthesis of C_1-symmetric triazolinylidenes **A3.9** and **A3.10** and their respective Rh(I) complexes **A3.12** and **A3.13**.[48] The activity and selectivity of these catalysts was measured in the hydrosilylation of **A3.2** with Ph_2SiH_2 at 1 mol% catalyst loading. Catalyst **A3.12** demonstrated 90% conversion and 20% ee in 4 h at 22 °C, whereas catalyst **A3.13** exhibited 60% conversion and 40% ee after 6 d at 11 °C.

A3.8

A3.9: R = Me
A3.10: R = t-Bu

A3.11: L = A3.8
A3.12: L = A3.9
A3.13: L = A3.10
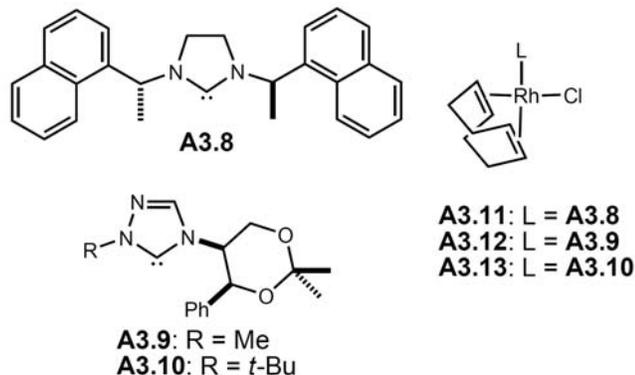
Figure A3.1. Previously studied Rh(I) complexes of chiral, monodentate NHCs.

We thus targeted Rh(I) complexes of the monodentate, chiral NHCs developed within our group. A series of chiral NHCs **A3.14–17** were examined (Figure A3.2). These salts underwent facile deprotonation in the presence of [Rh(cod)(Cl)]$_2$ to provide the air- and moisture-stable rhodium complexes **A3.18–21** in good yield.
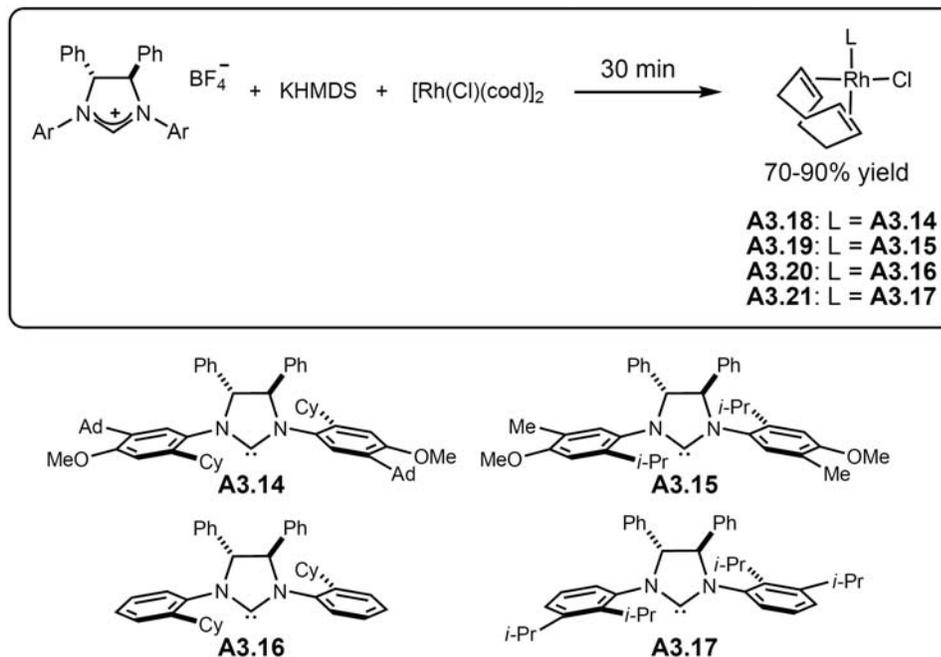
Figure A3.2. Synthesis of Rh(I)-NHC complexes.

These complexes were characterized by X-ray crystallographic analysis; these are the first solid-state structures of chiral ligands **A3.15** and **A3.17** (Figure A3.3). Importantly, these solid-state structures confirm the "gearing" effect proposed to translate chirality from the diamino backbone to the metal center. Bond lengths and angles were similar to previously reported NHC-Rh(I) complexes.
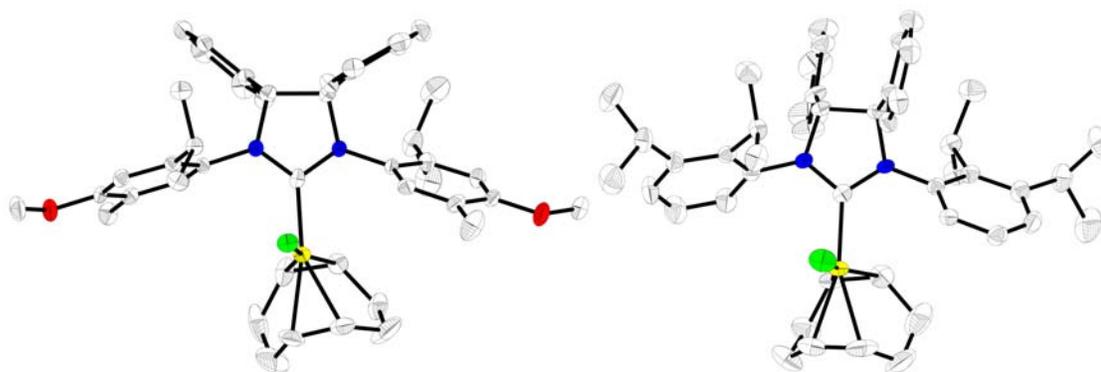
Figure A3.3. X-ray crystal structures of **A3.19** and **A3.21**. Ellipsoids shown at 50% probability and hydrogens omitted for clarity.

At 1 mol% catalyst loading, complexes **A3.18**–**21** were evaluated in the hydrosilylation of acetophenone (**A3.2**) in neat Ph_2SiH_2 (Table A3.3). After 24 h at 50 °C, good yields (72–90%) were observed. Only modest ee's were observed for catalysts **A3.18** and **A3.19**, 5% and 9%, respectively. However, complex **A3.20** and **A3.21** provided promising ee's of 33% and 29%, respectively. Utilizing Et_3SiH or $MePh_2SiH$ in place of Ph_2SiH_2 with catalyst **A3.20** led to decrease in observed ee 12% (78% yield) and 5% (70% yield), respectively. Due to the slightly higher enantioselectivity excess observed and more facile synthetic route to carbene **A3.16**, rhodium complex **A3.20** was chosen for further reaction optimization.

Table A3.3. Selectivity and yield of (*S*)-1-phenethanol from **A3.2**

catalyst	% yield	%ee
A3.18	72	5
A3.19	76	9
A3.20	73	33
A3.21	80	29

First, a solvent and temperature screen was performed utilizing 1 mol% catalyst **A3.20** for the hydrosilylation of acetophenone (**A3.2**) with Ph_2SiH_2 (Table A3.4). Reactions were evaluated after 24 h. Among CH_2Cl_2, toluene and THF at 50 °C, the highest yield (80%) and enantioselectivity (35%) was observed in THF. An increase in enantioselectivity excess to 45% was observed upon lowering the temperature to 22 °C in THF. Examining *p*-doxane and MeCN at 22 °C, significantly diminished yields and enantioselectivities were observed. The optimized reaction conditions included using THF as solvent and performing the reaction at 22 °C.

Table A3.4. Solvent and temperature screen results

solvent	temp. (°C)	% yield	%ee
CH$_2$Cl$_2$	50	38	4
tol	50	69	23
THF	50	80 (79)	35(41)
THF	22	82	45
p-dioxane	22	29	35
MeCN	22	10	10

Further reaction optimization of the reduction of **A3.2** with Ph$_2$SiH$_2$ was performed to determine what reaction time and temperature is optimal and to determine if benchtop THF could be substituted for dry THF (Table A3.5). Sampling a reaction at 22 °C in dry THF, the highest yield was observed after 12 h and the enantioselectivity remained the same at all reaction times. No product was isolated after exchanging dry THF for benchtop THF. Additionally, lowering the temperature from 22 °C to –10 °C or –50 °C resulted in no productive catalysis, even after extending the reaction time to 2.5 d.

Table A3.5. Reaction optimization results

solvent	temp. (°C)	time (h)	% yield	%ee
THF	22	4.25	57	42
		8	89	43
		12	94	43
benchtop THF	22	12	none isolated	
THF	-10	12	none isolated	
		61	none isolated	
	-50	12	none isolated	
		61	none isolated	

Further reaction optimization included the examination of Ag(I) additives that presumably lead to chloride abstraction and a cationic Rh(I) catalyst (Table A3.6). A cationic catalyst might be advantageous by allowing higher conversions at lower temperatures that favor higher ee. The addition of 1 mol% AgOTf or AgBF$_4$ to catalyst

A3.20 in the reduction of **A3.2** with Ph_2SiH_2 resulted in no increase in enantioselectivity. However, upon lowering the temperature to -10 °C, an increase in enantioselectivity to 48–49% was observed.

Table A3.6. Reaction optimization results

additive	temp. (°C)	time (h)	% yield	%ee
1 mol% AgOTf	22	12	71	43
1 mol% AgBF$_4$	22	17	90	32
1 mol% AgOTf	-10	51	78	49
1 mol% AgBF$_4$	-10	24	90	48

Summary

Although chiral NHC-containing ruthenium olefin metathesis catalysts were active for the reduction of acetophenone (**A3.2**) with Ph_2SiH_2, low enantioselectivities were observed. The synthesis of new chiral NHC-Rh(I) complexes led to the development of improved rhodium catalysts for the reduction of **A3.2** with Ph_2SiH_2. Optimized reaction conditions (-10 °C, dry THF, 24 h, 1 mol% AgBF$_4$) achieved 48% ee and 90% yield.

In 2006, Faller and co-workers reported the synthesis and activity of neutral and cationic Rh(I) hydrosilylation catalysts bearing chiral NHCs similar to **A3.1** where Me or *i*-Pr groups have been substituted for the Cy group.[49] Similar enantioselectivities were observed, generally less than 50%, in the hydrosilylation of **A3.2**.

Experimental

General hydrosilylation procedure:

To a 4-mL vial in the glovebox was added catalyst (.01 equiv) and solvent (1 mL) if used. The vial was capped with a screwcap containing a septum and removed from the

glovebox. Acetophenone (**A3.2**, 1 equiv, 1.0 mmol) and silane (1.1 equiv, 1.1 mmol) were added via syringe. The vial was stirred in a heating bath and conversion monitored via TLC (100% CH_2Cl_2, **A3.2** visible by UV irradiation but not I_2). Upon completion, the reaction was quenched with a solution of 1% v/v HCl in MeOH. After an aqueous workup and extraction with EtOAc or CH_2Cl_2, the product was purified by column chromatography (1:4 EtOAc:hexanes for Ru catalysts or 3:7 Et_2O:hexanes for Rh catalysts). The resulting alcohol was analyzed on an HPLC with chiral column OD-H in 2% EtOH in hexanes (1 mL/min, 30 min). A sample HPLC chromatogram is shown below.

Data File C:\HPCHEM\2\DATA\DRA\DRA2-232.D   Sample Name: meph2sih

```
==============================================================================
Injection Date  : 10/14/2004 12:54:35 PM      Seq. Line :   5
Sample Name     : meph2sih                   Location : Vial 83
Acq. Operator   : dra                            Inj :   1
                                          Inj Volume : 5 µl
Acq. Method     : C:\HPCHEM\2\METHODS\2_EOH30.M
Last changed    : 4/3/2003 1:54:36 PM by YKR
Analysis Method : C:\HPCHEM\2\METHODS\BYPASS.M
Last changed    : 10/14/2004 1:16:39 PM by dra
                  (modified after loading)
Position # 1 METHOD : (No Column) Valve to Position # 1 (By-Pass / Flush Line).
```
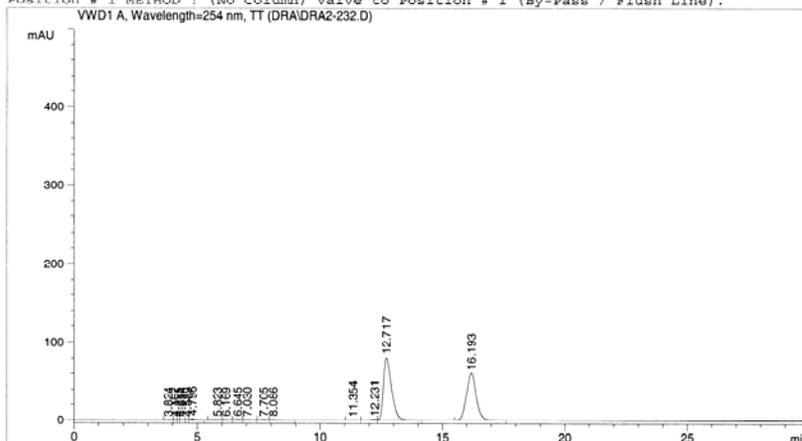


```
==============================================================================
                        Area Percent Report
==============================================================================

Sorted By            :     Signal
Multiplier           :     1.0000
Dilution             :     1.0000


Signal 1: VWD1 A, Wavelength=254 nm, TT

Peak RetTime Type  Width     Area      Height     Area
  #   [min]        [min]   mAU   *s    [mAU   ]     %
----|-------|----|-------|----------|----------|--------|
  1   3.824 RV   0.2206    4.50021 2.84969e-1   0.1205
  2   4.107 VV   0.1012    2.40258 3.08156e-1   0.0643
  3   4.235 VV   0.0857    1.69492 2.89645e-1   0.0454
  4   4.354 VV   0.1453    3.68758 3.48590e-1   0.0987
  5   4.589 VV   0.1096    1.73270 2.19381e-1   0.0464
  6   4.796 VB   0.1876   18.89173    1.40329   0.5058
  7   5.823 BV   0.3156   13.74292 5.51200e-1   0.3679
  8   6.169 VV   0.2554    8.78996 4.39013e-1   0.2353
  9   6.645 VV   0.2108   12.73100 8.24146e-1   0.3409
 10   7.030 VB   0.2556   12.54823 6.38298e-1   0.3360
 11   7.705 BV   0.2474   12.81942 7.33980e-1   0.3432
 12   8.086 VP   0.2791   11.84810 5.94538e-1   0.3172
 13  11.354 BV   0.2269    4.79903 2.58341e-1   0.1285
 14  12.231 VV   0.2412   21.07105    1.32238   0.5641
```

15-16 : 4.8/
15+4

dra7-2326

Instrument 2 10/14/2004 1:31:52 PM dra   Page 1 of 2

Synthesis of Rh(I) complexes

(cod)RhCl(**A3.14**) (**A3.18**): To a 4-mL vial in the glovebox was added **A3.14**•HCl (2 equiv, 126 mg, 0.203 mmol), KHMDS (2 equiv, 42 mg, 0.203 mmol) and ~ 1.5 mL THF. The vial was shaken until clear (no solid remained). The carbene solution was transferred to a 20-mL vial containing [RhCl(cod)]$_2$ (1 equiv, 49 mg, 0.101 mmol). The reaction was stirred 10 min during which time the orange solid dissolved

and the solution turned yellow. The vial was removed from the glovebox and the solvent

was removed under vacuum. The resulting solid was extracted with hexanes and filtered

through celite to give a yellow solution. The complex was recrystallized from EtOAc

and hexanes to give a yellow solid; additional product was isolated from the filtrate (194

mg, 0.187 mmol, 92% yield). ^{1}H NMR spectrum shown below. HRMS (FAB) m/z (%):

1112.542 [M$^+$] (3).
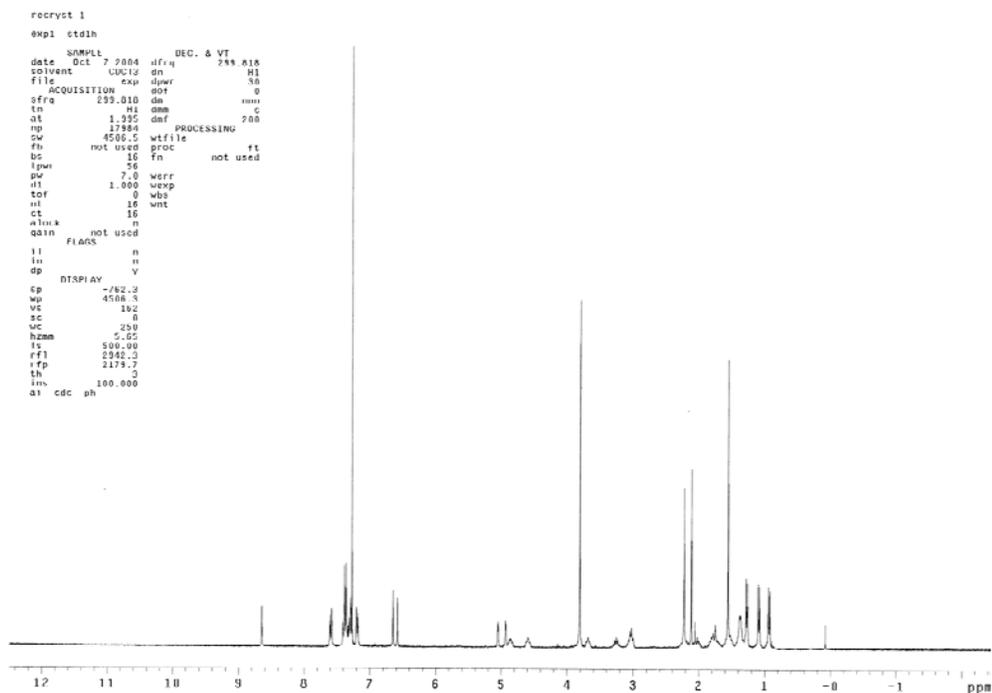
(cod)RhCl(**A3.15**) (**A3.19**): To a 4-mL vial in the glovebox was added **A3.15•**HCl

(2 equiv, 106 mg, 0.158 mmol), KHMDS (2 equiv, 32 mg, 0.158 mmol) and ~ 1.5 mL

THF. The vial was shaken until clear (no solid remained). The carbene solution was

transferred to a 20-mL vial containing [RhCl(cod)]$_2$ (1 equiv, 41 mg, 0.079 mmol). After

stirring 10 min at room temperature, the solution became yellow. The vial was removed

from the glovebox and the solvent was removed under vacuum. The resulting solid was

extracted with hexanes and filtered through celite to give a yellow solution. The complex

was recrystallized from EtOAc and hexanes to give a yellow solid (48 mg, 0.061 mmol,

77% yield). ^{1}H NMR spectrum shown below.
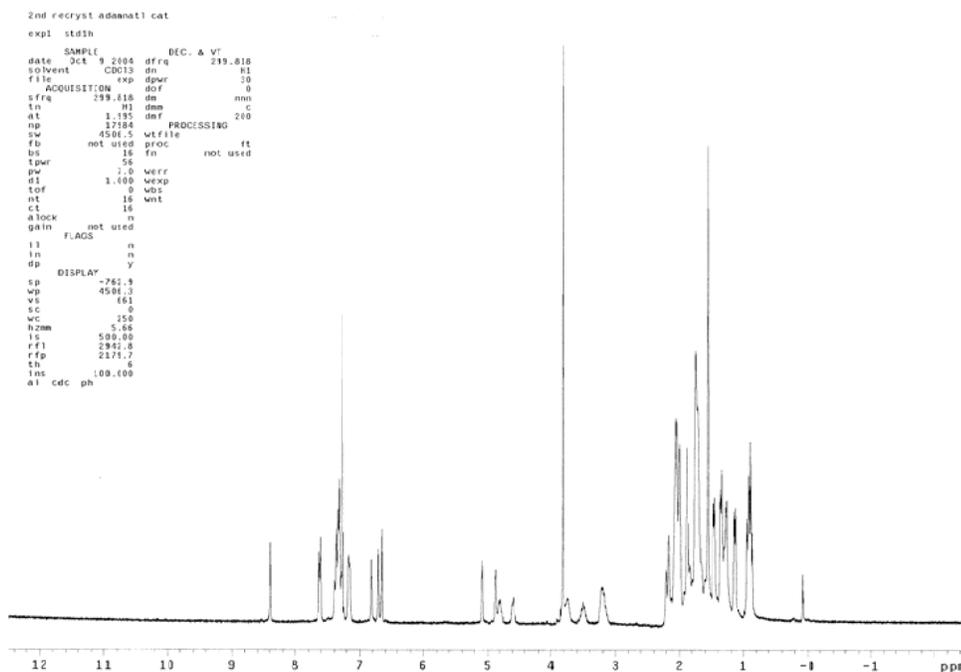
(cod)RhCl(**A3.16**) (**A3.20**): To a 4-mL vial in the glovebox was added **A3.16**•HCl

(2 equiv, 126 mg, 0.203 mmol), KHMDS (2 equiv, 42 mg, 0.203 mmol) and ~ 1.5 mL

THF. The vial was shaken until clear (no solid remained). The carbene solution was

transferred to a 20-mL vial containing [RhCl(cod)]$_2$ (1 equiv, 49 mg, 0.101 mmol). The

reaction was stirred 10 min during which time the orange Rh(I) source reacted to give a

yellow solution. The vial was removed from the glovebox and the solvent was removed

under vacuum. The resulting solid was extracted with hexanes and filtered through celite

to give a yellow solution. The complex was recrystallized from EtOAc and hexanes

(required heating to dissolve all solid) to give a yellow solid (101 mg, 0.128 mmol, 64%

(repeated reaction and obtained 71% yield)). ^{1}H NMR spectrum shown below. HRMS (FAB) *m/z* (%): 784.3030 [M$^+$] (24).
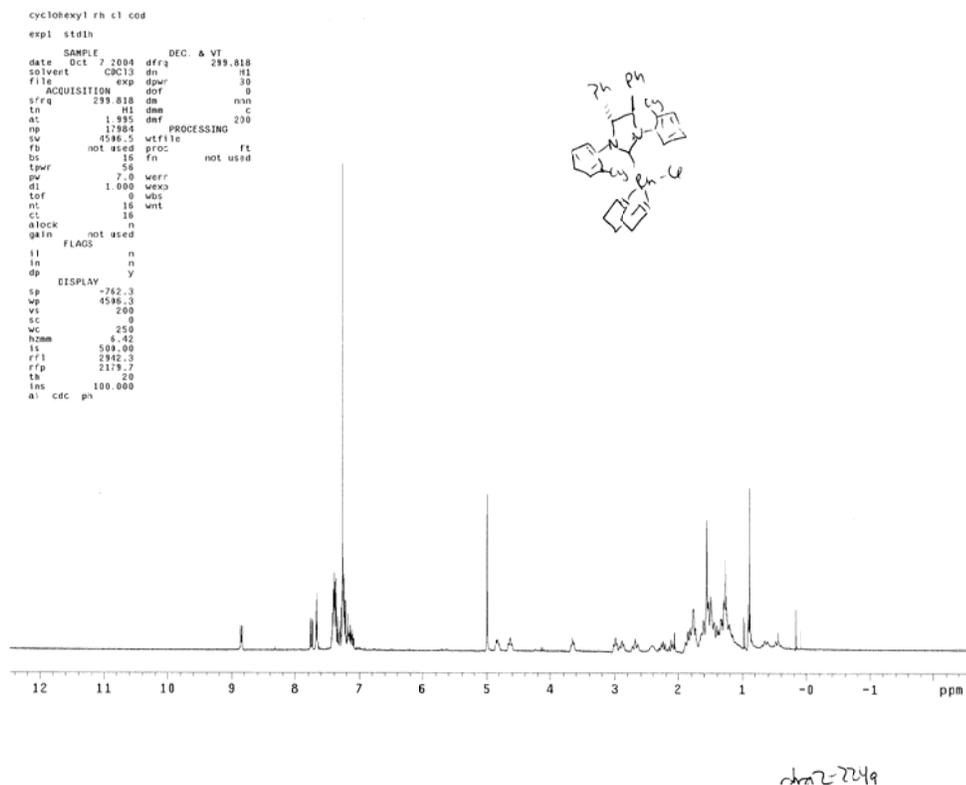

(cod)RhCl(**A3.17**) (**A3.21**): To a 4-mL vial in the glovebox was added **A3.17**•HCl (2 equiv, 124 mg, 0.198 mmol), KHMDS (2 equiv, 39 mg, 0.198 mmol) and ~ 1.5 mL THF. The vial was shaken until clear (no solid remained). The carbene solution was transferred to a 20-mL vial containing [RhCl(cod)]$_2$ (1 equiv, 45 mg, 0.099 mmol). The reaction was stirred for 10 min during which time the orange Rh(I) source reacted to give a yellow solution. Vial removed from the glovebox and the solvent was removed under vacuum. The resulting solid was extracted with hexanes and filtered through celite to give a yellow solution. The complex was recrystallized from EtOAc and hexanes to give a yellow solid (no yield determined). ^{1}H NMR spectrum shown below. HRMS (FAB) *m/z* (%): 788.3359 [M$^+$] (28).
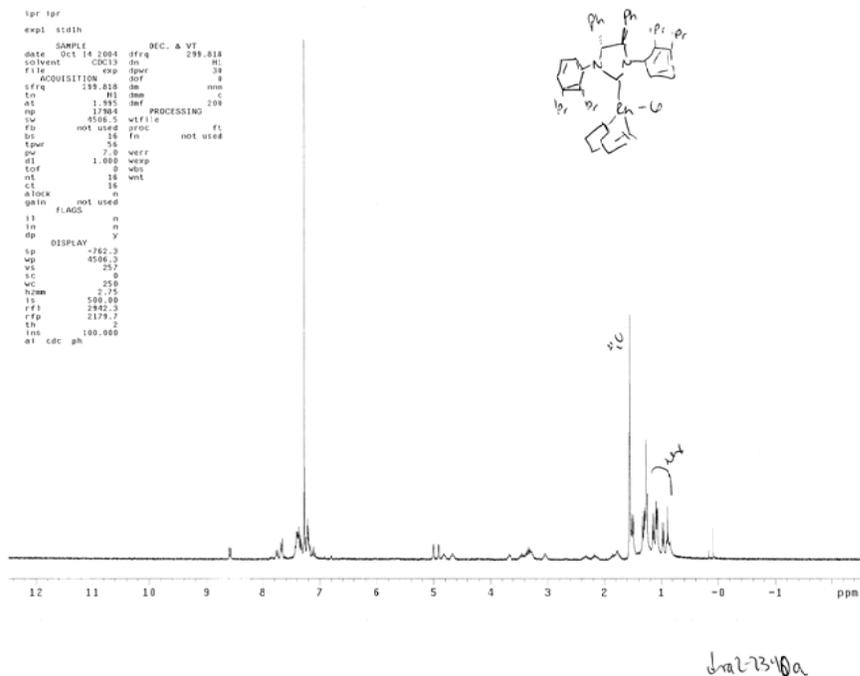
References

(1)   Glorius, F. *Top. Organomet. Chem.* **2007**, *21*, 1.

(2)   Herrmann, W. A. *Angew. Chem. Int. Ed.* **2002**, *41*, 1290.

(3)   Öfele, K. *J. Organomet. Chem.* **1968**, *12*, 42.

(4)   Wanzlick, H. W.; Schönherr, H. J. *Angew. Chem., Int. Eng. Ed.* **1968**, *7*, 141.

(5)   Cardin, D. J.; Cetinkaya, B.; Lappert, M. F. *Chem. Rev.* **1972**, *72*, 545.

(6)   Doyle, M. J.; Lappert, M. F. *J. Chem. Soc., Chem. Commun.* **1974**, 679.

(7)   Doyle, M. J.; Lappert, M. F.; McLaughlin, G. M.; McMeeking, J. *J. Chem. Soc., Dalton Trans.* **1974**, 1494.

(8)   Hitchcock, P. B.; Lappert, M. F.; Pye, P. L. *J. Chem. Soc., Dalton Trans.* **1978**, 826.

(9)   Hitchcock, P. B.; Lappert, M. F.; Terreros, P. *J. Organomet. Chem.* **1982**, *239*, C26.

(10)   Doyle, M. J.; Lappert, M. F.; Pye, P. L.; Terreros, P. *J. Chem. Soc., Dalton Trans.* **1984**, 2355.

(11)   Coleman, A. W.; Hitchcock, P. B.; Lappert, M. F.; Maskell, R. K.; Muller, J. H. *J. Organomet. Chem.* **1985**, *296*, 173.

(12)   Lappert, M. F. *J. Organomet. Chem.* **1988**, *358*, 185.

(13)   Cetinkaya, B.; Hitchcock, P. B.; Lappert, M. F.; Shaw, D. B.; Spyropoulos, K.; Warhurst, N. J. W. *J. Organomet. Chem.* **1993**, *459*, 311.

(14)   Cetinkaya, E.; Hitchcock, P. B.; Kuecuekbay, H.; Lappert, M. F.; Al-Juaid, S. *J. Organomet. Chem.* **1994**, *481*, 89.

(15)   Arduengo, A. J., III; Harlow, R. L.; Kline, M. *J. Am. Chem. Soc.* **1991**, *113*, 361.

(16)   Cavallo, L.; Correa, A.; Costabile, C.; Jacobsen, H. *J. Organomet. Chem.* **2005**, *690*, 5407.

(17)   Crudden, C. M.; Allen, D. P. *Coord. Chem. Rev.* **2004**, *248*, 2247.

(18)   Canac, Y.; Soleilhavoup, M.; Conejero, S.; Bertrand, G. *J. Organomet. Chem.* **2004**, *689*, 3857.

(19)   Lavallo, V.; Canac, Y.; Prasang, C.; Donnadieu, B.; Bertrand, G. *Angew. Chem. Int. Ed.* **2005**, *44*, 5705.

(20)   Martin, D.; Baceiredo, A.; Gornitzka, H.; Schoeller, W. W.; Bertrand, G. *Angew. Chem. Int. Ed.* **2005**, *44*, 1700.

(21)   Praesang, C.; Donnadieu, B.; Bertrand, G. *J. Am. Chem. Soc.* **2005**, *127*, 10182.

(22)   Ishida, Y.; Donnadieu, B.; Bertrand, G. *Proc. Natl. Acad. Sci. U.S.A.* **2006**, *103*, 13585.

(23)   Lavallo, V.; Canac, Y.; Donnadieu, B.; Schoeller, W. W.; Bertrand, G. *Science* **2006**, *312*, 722.

(24)   Masuda, J. D.; Martin, D.; Lyon-Saunier, C.; Baceiredo, A.; Gornitzka, H.; Donnadieu, B.; Bertrand, G. *Chem. Asian J.* **2007**, *2*, 178.

(25)   Gade, L. H.; Bellemin-Laponnaz, S. *Top. Organomet. Chem.* **2007**, *21*, 117.

(26)   Cesar, V.; Bellemin-Laponnaz, S.; Gade, L. H. *Chem. Soc. Rev.* **2004**, *33*, 619.

(27)   Perry, M. C.; Burgess, K. *Tetrahedron: Asymmetry* **2003**, *14*, 951.

(28)   Roland, S.; Mangeney, P. *Top. Organomet. Chem.* **2005**, *15*, 191.

(29)   Scholl, M.; Ding, S.; Lee, C. W.; Grubbs, R. H. *Org. Lett.* **1999**, *1*, 953.

(30)   Schrodi, Y.; Pedersen, R. L. *Aldrichimica Acta* **2007**, *40*, 45.

(31)   Lynn, D. M.; Mohr, B.; Grubbs, R. H.; Henling, L. M.; Day, M. W. *J. Am. Chem. Soc.* **2000**, *122*, 6601.

(32)   Seiders, T. J.; Ward, D. W.; Grubbs, R. H. *Org. Lett.* **2001**, *3*, 3225.

(33)   Trnka, T. M.; Morgan, J. P.; Sanford, M. S.; Wilhelm, T. E.; Scholl, M.; Choi, T.-L.; Ding, S.; Day, M. W.; Grubbs, R. H. *J. Am. Chem. Soc.* **2003**, *125*, 2546.

(34)   Yun, J.; Marinez, E. R.; Grubbs, R. H. *Organometallics* **2004**, *23*, 4172.

(35)   Despagnet-Ayoub, E.; Grubbs, R. H. *Organometallics* **2005**, *24*, 338.

(36)   Gallivan, J. P.; Jordan, J. P.; Grubbs, R. H. *Tetrahedron Lett.* **2005**, *46*, 2577.

(37)   Berlin, J. M.; Goldberg, S.; Grubbs, R. H. *Angew. Chem. Int. Ed.* **2006**, *45*, 7591.

(38)   Hong, S. H.; Grubbs, R. H. *J. Am. Chem. Soc.* **2006**, *128*, 3508.

(39)   Ritter, T.; Day, M. W.; Grubbs, R. H. *J. Am. Chem. Soc.* **2006**, *128*, 11768.

(40)   Anderson, D. R.; Lavallo, V.; O'Leary, D. J.; Bertrand, G.; Grubbs, R. H. *Angew. Chem. Int. Ed.* **2007**, *119*, in press.

(41)   Berlin, J. M.; Campbell, K.; Ritter, T.; Funk, T. W.; Chlenov, A.; Grubbs, R. H. *Org. Lett.* **2007**, *9*, 1339.

(42)   Blum, A. P.; Ritter, T.; Grubbs, R. H. *Organometallics* **2007**, *26*, 2122.

(43)   Stewart, I. C.; Ung, T.; Pletnev, A. A.; Berlin, J. M.; Grubbs, R. H.; Schrodi, Y. *Org. Lett.* **2007**, *9*, 1589.

(44)   Vougioukalakis, G. C.; Grubbs, R. H. *Organometallics* **2007**, *26*, 2469.

(45)   Funk, T. W.; Berlin, J. M.; Grubbs, R. H. *J. Am. Chem. Soc.* **2006**, *128*, 1840.

(46)   Maifeld, S. V.; Miller, R. L.; Lee, D. *Tetrahedron Lett.* **2002**, *43*, 6363.

(47)   Herrmann, W. A.; Goossen, L. K.; Kocher, C.; Artus, G. R. *Angew. Chem., Int. Eng. Ed.* **1996**, *35*, 2805.

(48)   Enders, D.; Gielen, H.; Runsink, J.; Breuer, K.; Brode, S.; Boehn, K. *Eur. J. Inorg. Chem.* **1998**, 913.

(49)   Faller, J. W.; Fontaine, P. P. *Organometallics* **2006**, *25*, 5887.

APPENDIX **4**

Ruthenium-Based Olefin Metathesis Catalysts with Anionic Tin(II) Ligands

Introduction

With the discovery and development of stable ruthenium and molybdenum alkylidenes, olefin metathesis has emerged as a powerful tool for polymer and synthetic organic chemists.[1,2] In an effort to rationally design new catalysts with higher activity, much attention has been given to the mechanism of olefin metathesis. Recent work has provided significant insight into the reaction mechanism of the commercially-available catalysts **A4.1** and **A4.2a** (Scheme A4.1).[3-5] Experimental evidence suggests that the first step of the catalytic cycle involves phosphine dissocation to give the 14-electron species **A4.3**; this step is often referred to as catalyst initiation and has a rate constant of k_1. Intermediate **A4.3** can either rebind phosphine, with rate constant k_{-1}, or bind olefin, with rate constant k_2, and proceed through the metathesis cycle.

Chart A4.1. Ruthenium olefin metathesis catalysts

A4.1

A4.2a: X = Cl
A4.2b: X = Br
A4.2c: X = I
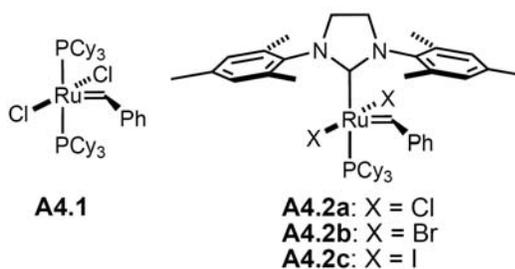
Scheme A4.1. Proposed mechanism of olefin metathesis
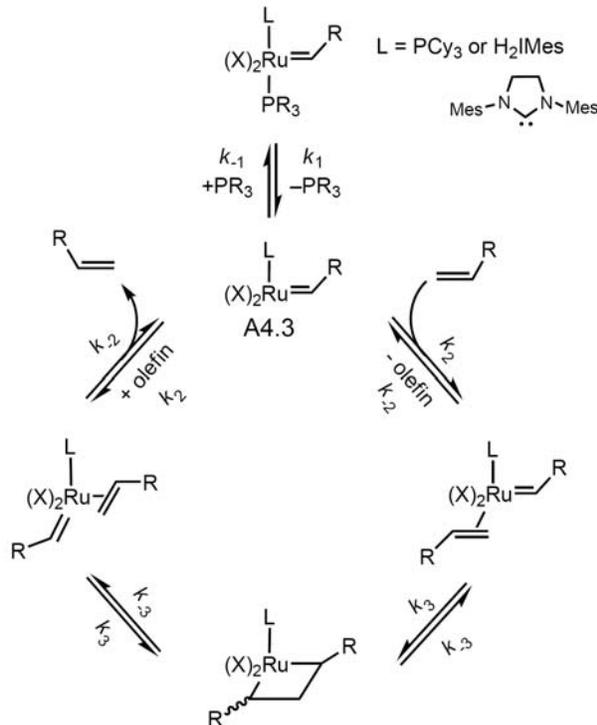
According to this mechanism, the ideal metathesis catalyst should initiate quickly (large k_1), and have a much higher affinity for olefin than phosphine (large k_2/k_{-1}). Experimental evidence has shown that the increased overall activity of **A4.2a** relative to **A4.1** is due to a larger value of k_2/k_{-1}, not an increased k_1. In fact, initiation of catalyst **A4.2a** is slower than catalyst **A4.1**. Thus, much interest lies in designing new catalysts, based on **A4.2a**, that may exhibit large values of k_1 and k_2/k_{-1}.

Although many studies have varied the electronic and steric properties of the L-type donors on ruthenium-based olefin metathesis catalysts,[6-8] analogous work with X-type ligands has been limited primarily to halogens. Recently, Grubbs and co-workers demonstrated that initiation rates increase dramatically from **A4.2a** to **A4.2c**, but that k_2/k_{-1}, which is an estimate of the rate of propagation, decreases from **A4.2a–c**.[4,9] The

overall activity of these catalysts is the same. Interestingly, the enhanced rate of initiation is attributed to the increased sterics of iodide versus chloride, which is hypothesized to drive phosphine dissociation.

Other than halogens, previously explored anionic ligands include alkoxides,[10] aryloxides,[11,12] and carboxylates[13-15] (Figure A4.1). The goal of many of these studies has been to utilize ligands with electronic properties similar to those of halides, but with tunable steric features. However, the catalysts obtained from these substitutions generally exhibit lower metathesis activity than catalyst **A4.2a**. Based on these results, the chemistry of SnY_3^- (Y = halide) substituted catalysts was investigated. This pseudohalide ligand set offers: (*i*) easily tunable electronics through choice of Y; (*ii*) increased steric bulk over traditional halide ions that could facilitate higher initiation rates; (*iii*) potential Lewis acid coordination ability[16] that could increase the tolerance of the ruthenium center to polar functional groups and/or allow for the selective metathesis of olefins in close proximity to functional groups that can coordinate to Lewis-acids (Figure A4.2).
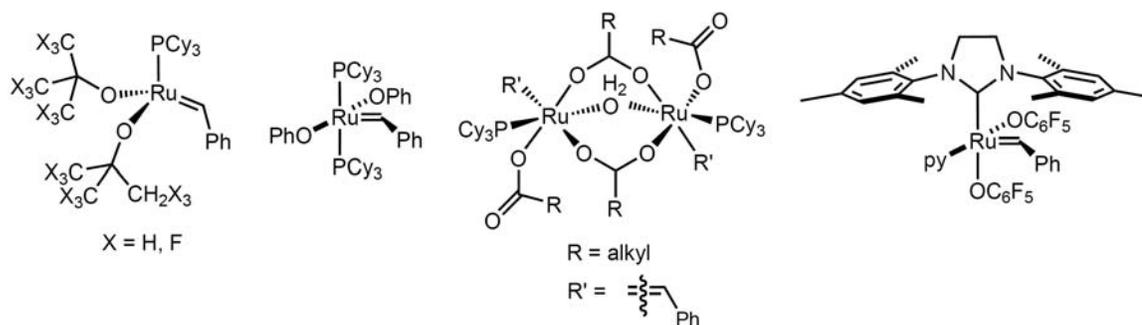
Figure A4.1. Examples of non-halide substituted metathesis catalysts.
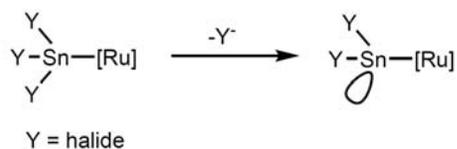
Figure A4.2. Potential Lewis acid coordination site for SnY_3^- substituted catalysts.

<u>Results and Discussion</u>

Bis(phosphine) Catalysts

A common route to transition metal-tin compounds involves insertion of SnY_2 into a metal-halide bond.[16] As shown in eq A4.1, upon addition of 10 equiv of $SnCl_2 \cdot H_2O$ to $(PCy_3)_2(Cl)_2Ru{=}CHPh$ (**A4.1**), ruthenium complex **A4.4a** was obtained. Based on single crystal X-ray crystallographic analysis, complex **A4.4a** contains two ruthenium centers connected by three bridging chlorides (Figure A4.3). Each ruthenium center has a distorted octahedral geometry with a $SnCl_3^-$, PCy_3, and benzylidene moiety. Analogously, the addition of 10 equiv of $SnBr_2 \cdot H_2O$ to **A4.1** produced catalyst **A4.4b**, as shown by X-ray crystallographic analysis (Figure A4.4). Although complex **A4.1** contains two chloride ligands, **A4.4b** contains bridging bromides rather than chlorides; this result is indicative of the facile nature of salt metathesis under these reaction conditions.
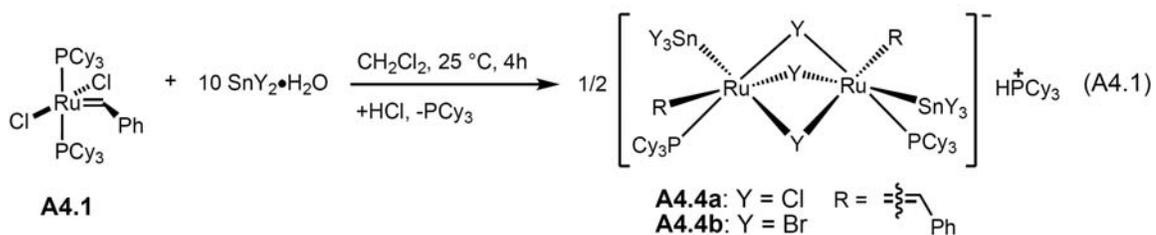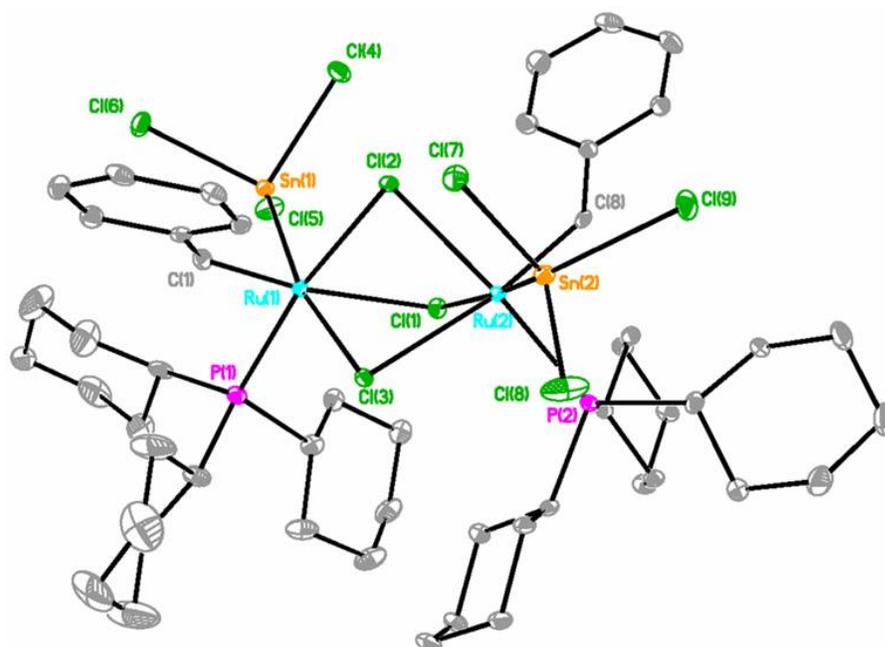
Figure A4.3. X-ray crystal structure of ruthenium dimer **A4.4a** with thermal ellipsoids shown at the 35% probability level. Hydrogen atoms and $HPCy_3^+$ have been omitted for clarity.
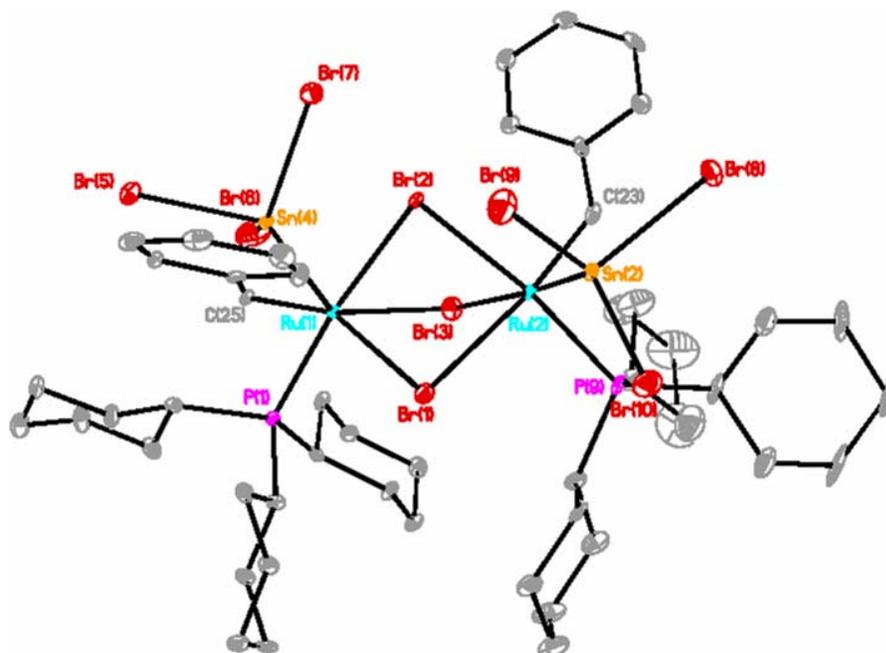
Figure A4.4. X-ray crystal structure of Ru dimer **A4.4b** with thermal ellipsoids shown at the 35% probability level. Hydrogen atoms and $HPCy_3^+$ have been omitted for clarity.

Although complexes **A4.4a** and **A4.4b** have different geometries than **A4.1**, the bond lengths among these complexes are fairly similar (Table A4.1). In comparison with **A4.1**, catalysts **A4.4a** and **A4.4b** have slightly longer (ca. 0.015Å) Ru–C bonds; this bond lengthening is may be due to a combination of the presence of an anionic charge on the complex and the trans influence of the bridging halide. In contrast, the Ru–P bond lengths of **A4.4a** and **A4.4b** are ca. 0.025–0.035 Å shorter than those of **A4.1**. This contraction is attributed to the increased trans influence of a phosphine versus a halide ligand.

Table A4.1. Selected bond lengths (Å)

	Complex **A4.1** (X=Cl)	Complex **A4.4a** (X=Cl)[a]	Complex **A4.4b** (X=Br)[a]
Ru(1)–C(1)	1.839(3)	1.885(6)	1.890(7)
Ru(1)–X(1)	—	2.606(2)	2.6209(10)
Ru(1)–X(2)	2.395(1)	2.403(2)	2.7244(10)
Ru(1)–X(3)	2.401(1)	2.415(2)	2.5275(11)
Ru(1)–P(1)	2.397(1)	2.359(2)	2.371(2)
Ru(1)–P(2)	2.435(1)	—	—
Ru(1)–Sn(1)	—	2.5616(7)	2.5727(8)

[a] average bond lengths

After our initial success in synthesizing complex **A4.4a**, analogous reactions with bis(phosphine) catalysts **A4.5** and **A4.6** were attempted (Chart A4.2). Unfortunately, reactions with 5 equiv of $SnCl_2·H_2O$ with **A4.5** or **A4.6** in CD_2Cl_2 produced several carbene-containing products, as indicated by the multiple benzylidene resonances between 16.5–19 ppm in the ^1H NMR spectra. Reactions in C_6D_6 also produced multiple products.

Chart A4.2. Other bis(phosphine) ruthenium precursors

A4.5   **A4.6**
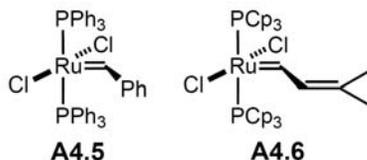
NHC-Substituted Catalysts

Under the same reaction conditions employed to synthesize **A4.4a**, catalyst **A4.2a** produced several products in the carbene region of the ^{1}H NMR spectrum. After 24 h, no carbene signals were observed. Attempts to purify products from the reaction mixture via silica gel chromatography were unsuccessful.

We subsequently expanded our range of catalyst precursors to include bis(pyridine) catalyst **A4.7** and PPh$_3$-substituted catalyst **A4.8** (Chart A4.3). Although ^{1}H NMR spectroscopy experiments of **A4.7** with 5 equiv of SnCl$_2$·H$_2$O in CD$_2$Cl$_2$ indicated the formation of several products, reactions in C$_6$D$_6$ led to one major product with a benzylidene resonance at 17.2 ppm and two additional compounds with benzylidene resonances at 18.6 ppm and 14.2 ppm. However, attempts to isolate pure products were unsuccessful.

Chart A4.3. NHC-containing ruthenium precursors

A4.7   **A4.8**
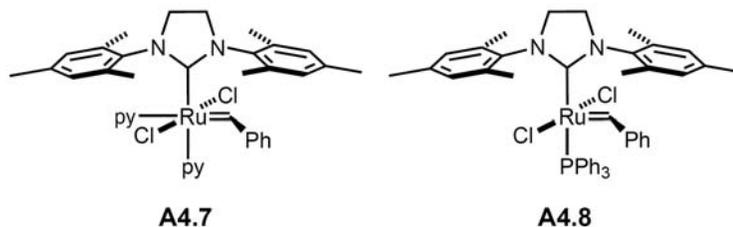
In the reaction of catalyst **A4.8** with 5 equiv of SnCl$_2$·H$_2$O in C$_6$D$_6$, the ^{1}H NMR

spectrum taken after 4 h showed a single product with a benzylidene signal at 17.3 ppm;

a small amount of starting material was also observed. Even after extended reaction

times and heating at 50 °C, ca. 3−5% of **A4.8** was observed in the ^{1}H NMR spectrum.

The product was isolated by evaporation of solvent, followed by several washes with

Et$_2$O to remove **A4.8**. A ^{1}H NMR spectrum of the isolated solid taken 5−10 min after

being dissolved in C$_6$D$_6$ also contained ca. 3% of starting material **A4.8**. ^{1}H NMR

spectra taken at regular time intervals revealed that catalyst **A4.9** slowly reverts to

precursor **A4.8** (eq A4.2); after approximately 24 h, the intensity of both carbene peaks

decreases, indicating decomposition of the ruthenium benzylidene complex. X-ray

crystallographic analysis of catalyst **A4.9** demonstrated that it is isostructural with

precursor **A4.8** (Figure A4.5).
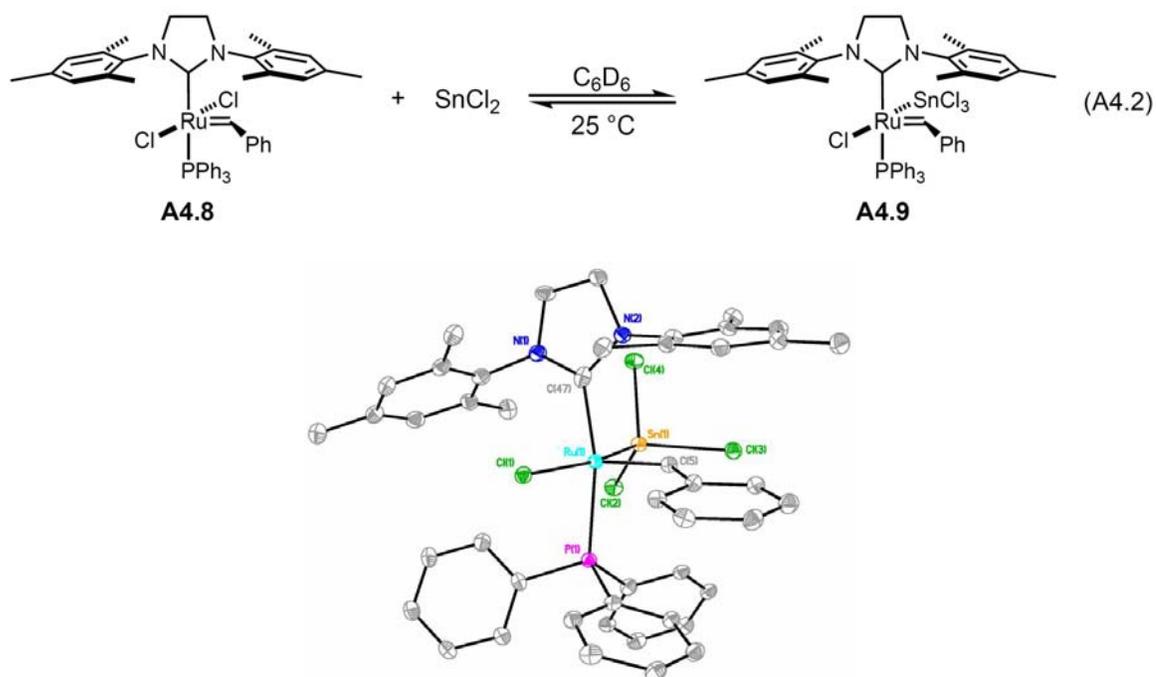
Figure A4.5. X-ray crystal structure of (H$_2$IMes)(PPh$_3$)(Cl)(SnCl$_3$)Ru=CHPh (**A4.9**) with thermal ellipsoids shown at the 35% probability level. Hydrogen atoms have been omitted for clarity.

In comparison to **A4.8**, the Ru–C(5) and Ru–C(47) bond lengths of complex **A4.9** are ca. 0.01–0.02 Å shorter (Table A4.2). In addition, the Ru–P bond length of catalyst **A4.9** is ca. 0.02 Å shorter than that of **A4.8**. The shortening of these bonds is probably due to the increased electron-withdrawing ability of $SnCl_3^-$ versus Cl^-. Complexes **A4.8** and **A4.9** both have a square pyramidal geometry. The largest difference between these catalysts is observed in the Cl–Ru–X bond angle. The 5° compression of catalyst **A4.9** as compared to **A4.8** may be due to steric interaction of the $SnCl_3^-$ moiety and the hydrogen atom of the ruthenium benzylidene.

Table A4.2. Selected bond lengths (Å) and angles (degrees) of **A4.8** and **A4.9**

	Complex **A4.8** (X=Cl(2))[4b]	Complex **A4.9** (X=Sn(1))		Complex **A4.8** (X=Cl(2))[9]	Complex **A4.9** (X=Sn(1))
Ru(1)–C(5)	1.872(3)	1.847(9)	C(5)–Ru–C(47)	98.7(4)	99.31(10)
Ru(1)–C(47)	2.097(3)	2.084(9)	C(5)–Ru–Cl(1)	102.9(3)	109.97(8)
Ru(1)–Cl(1)	2.3894(7)	2.382(3)	C(5)–Ru–X	90.0(3)	87.94(8)
Ru(1)–Cl(2)	—	2.392(2)	C(47)–Ru–X	83.0(3)	85.00(7)
Ru(1)–P(1)	2.4244(7)	2.404(3)	C(47)–Ru–Cl(1)	93.3(3)	90.96(7)
Ru(1)–Sn(1)	2.5942(3)	—	Cl(1)–Ru–X	166.96(9)	162.059(19)
			C(5)–Ru–P(1)	93.5(3)	93.07(7)
			C(47)–Ru–P(1)	167.1(3)	167.61(7)

In an effort to synthesize a more stable tin-substituted catalyst, we attempted to vary both the SnY_3^- and PR_3 ligands of catalyst **A4.9**. Addition of 5 equiv of $SnBr_2 \cdot H_2O$ or $SnI_2 \cdot H_2O$ to complex **A4.8** in C_6D_6 or CD_2Cl_2 produced several benzylidene-containing species with resonances from 16 to 20 ppm in the ^1H NMR spectra. Some of these products may have resulted from incomplete salt metathesis of chloride for bromide

or iodide. Attempts at phosphine exchange of **A4.9** resulted in dissociation of $SnCl_2$ to give dichloride catalysts (eq A4.3).

$$\text{(A4.3)}$$
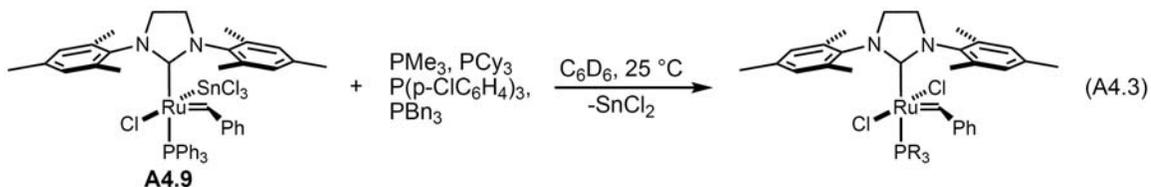
To investigate the electronic effect of phosphine on the equilibrium between catalysts **A4.8** and **A4.9**, catalyst **A4.10** was synthesized. We hypothesized that the equilibrium might require phosphine dissociation before $SnCl_2$ dissociation; consequently a more electron-deficient phosphine was expected to increase the rate of $SnCl_2$ dissociation. Complex **A4.10** reacted with 5 equiv of $SnCl_2 \cdot H_2O$ in C_6D_6 to give a single product **A4.11** as indicated by ^1H NMR analysis. Complex **A4.11** was purified and redissolved in C_6D_6. ^1H NMR spectra taken at regular intervals over 48 h indicate a similar rate of dissociation as catalyst **A4.9** (eq A.4).

$$\text{(A4.4)}$$
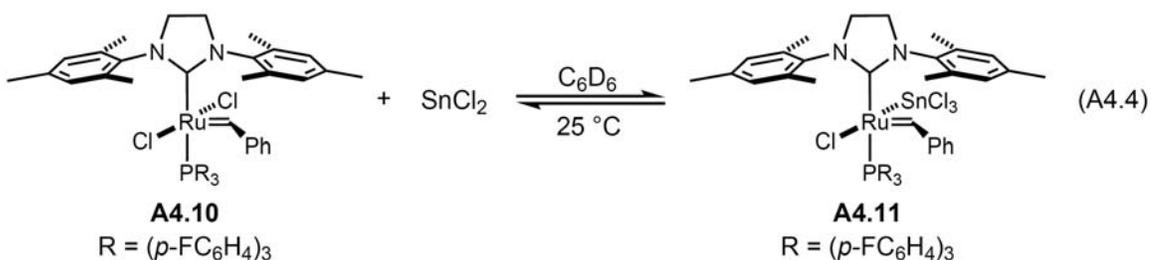
Cross-Metathesis Activity

Catalysts **A4.1**, **A4.4a**, **A4.8** and **A4.9** were evaluated in the cross metathesis reaction of 2 equiv *cis*-1,4-diacetoxy-2-butene and allylbenzene (eq A4.5). The reactions

were performed in CH_2Cl_2 at room temperature and monitored by GC analysis. Comparison of the results from 2.5 mol% catalyst loadings of **A4.1** and **A4.4a** shows that catalyst **A4.4a** produces nearly twice as much **A4.12** as **A4.1**; however, the similar results obtained from utilizing 5 mol% **A4.1** and 2.5 mol% **A4.4a** suggest that catalyst **A4.4a** generates two active metathesis catalysts per dimer (Table A4.3). Catalysts **A4.8** and **A4.9** show nearly identical yields and *cis*:*trans* product ratios. These results imply that $SnCl_2$ is very labile and dissociates from the catalyst during the course of the reaction to generate **A4.8**.
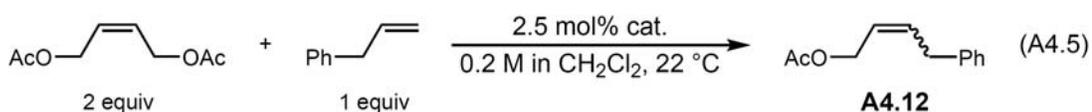
Table A4.3. Results of cross-metathesis experiments

Catalyst	Time (h)	Yield of **A4.12** (%)	(*E*)-**A4.12**/(*Z*)-**A4.12**
A4.1 (5 mol%)	43	57	4.8
A4.1 (2.5 mol %)	7.7	28	3.4
A4.4a (2.5 mol %)	11.2	49	3.9
A4.8 (2.5 mol %)	0.2	76	10.0
A4.9 (2.5 mol %)	0.2	76	9.3

Summary

Both bis(phosphine) and NHC-containing ruthenium olefin metathesis catalysts undergo reactions with tin(II) halides. Catalyst **A4.1** reacts cleanly with $SnCl_2 \cdot H_2O$ and $SnBr_2 \cdot H_2O$ to provide the dinuclear catalysts **A4.4a** and **A4.4b**, respectively. Second-generation derivative **A4.8** reacts with $SnCl_2$ to cleanly provide complex **A4.9**, which is a

mononcular species. However, catalyst **A4.9** is unstable in solution and slowly reverts back to **A4.8**; efforts to increase catalyst stability through changes in the ligand environment were unsuccessful. Both **A4.4a** and **A4.9** are metathesis active complexes; very similar cross metathesis yields and E/Z product ratios were obtained for catalyst pairs **A4.1**, **A4.4a** and **A4.8**, **A4.9**. These results indicate that tin(II) halides are too labile to effect a significant change in the course of a metathesis reaction.

Experimental

General Considerations

All reactions were carried out under a dry argon atmosphere using standard Schlenk techniques or in a nitrogen-filled glovebox unless otherwise noted. All solvents were purified by passage through activated A-2 alumina solvent columns and were degassed with argon prior to use. Ruthenium alkylidene starting materials **A4.2**, **A4.5**, and **A4.6** were gifts from Materia. Catalysts **A4.7**, **A4.8**, and **A4.10** were synthesized from literature procedures.[4] All other materials were purchased from Strem, Alfa Aesar, or Aldrich and used as received. ^{1}H and ^{31}P NMR spectra were recorded on a Varian Mercury 300 FT-NMR spectrometer (300 MHz for ^{1}H NMR, 125 MHz for ^{31}P NMR). ^{1}H and ^{31}P NMR chemical shifts are reported in ppm downfield from tetramethylsilane (TMS, δ scale) with the residual solvent resonances as internal standards.

Synthesis of (H₂IMes)(PPh₃)(Cl)(SnCl₃)Ru=CHPh (A4.9). In an inert atmosphere glovebox, benzene (7 mL) was added to a 20-mL vial containing **A4.8** (248 mg) and $SnCl_2 \cdot H_2O$ (278 mg). After stirring for 4 h at 22 °C the solution was decanted and the solid was placed under vacuum. The solid was washed with Et_2O (4 x 7 mL) and

dried under vacuum to yield **A4.9** as a brown powder (155 mg, 51%). ^{1}H NMR (C_6D_6,

300 MHz): δ = 1.72 (s, 3H, para CH_3), 1.96 (s, 3H, para CH_3), 2.02 (s, 3H, ortho CH_3),

2.36 (s, 3H, ortho CH_3), 3.00 (s, 3H, ortho CH_3), 3.13 (s, 3H, ortho CH_3), 3.55 (m, 2H,

CH_2), 3.94 (m, 2H, CH_2), 5.54 (s, 2H, Mes CH), 6.31–7.17, (m, 20H, PPh_3, para CH,

meta CH, and Mes CH), 7.39 (d, 2H, ortho CH, J = 7 Hz), 17.16 (s, 1H, Ru=CHPh);

^{31}P{^{1}H} NMR (C_6D_6, 125 MHz): δ = 30.82 (s).

Synthesis of (H₂IMes)(P(p-FC₆H₄)₃)(Cl)(SnCl₃)Ru=CHPh (A4.11). In an inert

atmosphere glovebox, C_6D_6 (ca. 0.75 mL) was added to a 4-mL vial containing **A4.10** (13

mg, 0.018 mmol) and $SnCl_2·H_2O$ (15 mg, 0.09 mmol). After stirring for 12 h at 22 °C the

solution was filtered through a plug of celite. The resulting solution was placed under

vacuum to produce **A4.11** (10 mg, 52%) as a dark brown powder. ^{1}H NMR (C_6D_6), 400

MHz): δ = 1.73 (s, 3H, para CH_3), 1.96 (s, 3H, para CH_3), 2.10 (s, 3H, ortho CH_3), 2.36

(s, 3H, ortho CH_3), 2.96 (s, 3H, ortho CH_3), 3.09 (s, 3H, ortho CH_3), 3.54 (m, 2H, CH_2),

3.95 (m, 2H, CH_2), 5.53 (s, 2H, Mes CH), 6.57–7.17 (m, 20H, PPh_3, para CH, meta CH,

and Mes CH), 7.33 (d, 2H, ortho CH, J = 8 Hz), 17.06 (s, 1H, Ru=CHPh) {$^2J_{31P-117Sn}$ =

261 Hz, $^2J_{31P-119Sn}$ = 273 Hz}; ^{31}P{^{1}H} NMR (C_6D_6): δ = 30.08 (s).

References

(1)   Grubbs, R. H. *Handbook of Metathesis*; Wiley-VCH: Weinheim, 2003.

(2)   Ivin, K. J.; Mol, J. C. *Olefin Metathesis and Metathesis Polymerization*;
      Academic Press: San Diego, CA, 1997.

(3)   Sanford, M. S.; Ulman, M.; Grubbs, R. H. *J. Am. Chem. Soc.* **2001**, *123*, 749.

(4)   Sanford, M. S.; Love, J. A.; Grubbs, R. H. *J. Am. Chem. Soc.* **2001**, *123*, 6543.

(5)   Love, J. A.; Morgan, J. P.; Trnka, T. M.; Grubbs, R. H. *Angew. Chem. Int. Ed.*
      2002, *41*, 4035.

(6)   Scholl, M.; Ding, S.; Lee, C. W.; Grubbs, R. H. *Org. Lett.* **1999**, *1*, 953.

(7)   Schwab, P.; France, M. B.; Ziller, J. W.; Grubbs, R. H. *Angew. Chem. Int. Ed.* **1995**, *34*, 2039.

(8)   Schrodi, Y.; Pedersen, R. L. *Aldrichimica Acta* **2007** *40*, 45.

(9)   Love, J. A.; Sanford, M. S.; Day, M. W.; Grubbs, R. H. *J. Am. Chem. Soc.* **2003**, *125*, 10103.

(10)   Sanford, M. S.; Henling, L. M.; Day, M. W.; Grubbs, R. H. *Angew. Chem. Int. Ed.* **2000**, *39*, 3451.

(11)   Conrad, J. C.; Amoroso, D.; Czechura, P.; Yap, G. P. A.; Fogg, D. E. *Organometallics* **2003**, *22*, 3634.

(12)   Coalter, J. N.; Bollinger, J. C.; Eisenstein, O.; Caulton, K. G. *New. J. Chem.* **2000**, *24*, 925.

(13)   Buchowicz, W.; Ingold, F.; Mol, J. C.; Lutz, M.; Spek, Anthony L. *Chem. Eur. J.* **2001**, *7*, 2842.

(14)   Buchowicz, W.; Mol, J. C.; Lutz, M.; Spek, Anthony L. *J. Organomet. Chem.* **1999**, *588*, 205.

(15)   Wu, S.; Nguyen, S. T.; Grubbs, R. H.; Ziller, J. W. *J. Am. Chem. Soc.* **1995**, *117*, 5503.

(16)   Holt, M. S.; Wilson, W. L.; Nelson, J. H. *Chem. Rev.* **1989**, *89*, 11.

APPENDIX 5

X-ray Crystallographic Data for Chapters 2─4 and Appendix 3

Complex	**2.7a**	**2.7b**	**2.16a**	**2.16b**
CCDC #	278154 (DRA09)	279735 (DRA12)	267414 (DRA07)	269308 (DRA08)
Empirical formula	$C_{32}H_{42}Cl_2N_2Ru$	$C_{35}H_{46}Cl_2N_2Ru$	$C_{30}H_{43}Cl_2NORu$	$C_{33}H_{47}Cl_2NORu \cdot C_7H_8$
Formula weight	626.65	666.71	605.62	737.82
Crystallization solvent	C_5H_{12}/THF	C_5H_{12}/THF	CH_2Cl_2/Et_2O	C_7H_8
Crystal color	Dichroic brown-green	Dichroic brown-green	Brown	Brown
T (K)	100(2)	100(2)	100(2)	98(2)
θ range (°)	2.23 to 44.61	2.35 to 42.30	2.40 to 25.03	2.19 to 40.42
a (Å)	9.2313(3)	9.2754(3)	9.7817(9)	10.1023(3)
b (Å)	9.9516(3)	10.5191(3)	33.305(3)	23.9879(7)
c (Å)	18.6772(5)	17.2405(5)	10.1559(9)	15.1952(4)
α (°)	89.9120(10)	90.3080(10)		
β (°)	78.9650(10)	90.6630(10)	120.4450(10)	93.2810(10)
γ (°)	63.2710(10)	108.6120(10)		
V (Å^3)	1497.11(8)	1593.98(8)	2852.4(5)	3676.26(18)
Crystal System	Triclinic	Triclinic	Monoclinic	Monoclinic
Space group	P-1	P-1	P2$_1$/c	P2$_1$/n
d_{calc} (g/cm^3)	1.390	1.389	1.410	1.333
μ (mm^{-1})	0.725	0.686	0.760	0.603
GOF on F^2	1.172	1.086	1.901	1.247
R$_1$, wR$_2$ [I > 2σ(I)]	0.0352, 0.0692	0.0400, 0.0735	0.0597, 0.0856	0.0370, 0.0607

Complex	**2.11**	**2.14**	**2.22**
CCDC #	288533 (DRA18)	284225 (DRA15)	294161 (DRA24)
Empirical formula	$C_{28}H_{40}Cl_2N_2Ru$	$C_{55}H_{93}Cl_2NP_2Ru$	$C_{28}H_{39}Cl_2NORu$
Formula weight	576.59	1002.21	577.57
Crystallization solvent	C_6H_6/C_5H_{12}		C_6H_6/C_5H_{12}
Crystal color	Yellow	Purple	Olive green
T (K)	100(2)	100(2)	100(2)
θ range (°)	2.51 to 37.71	2.27 to 40.32	2.32 to 42.64
a (Å)	16.2330(6)	29.7967(8)	9.5953(3)
b (Å)	9.1913(3)	19.8453(6)	35.0504(10)
c (Å)	17.9441(6)	17.9970(5)	8.9916(4)
α (°)			
β (°)	92.0100(10)	93.0960	115.5570(10)
γ (°)			
V (Å^3)	2675.66(16)	10626.5(5)	2728.16(15)
Crystal System	Monoclinic	Monoclinic	Monoclinic
Space group	P2$_1$/c	C2/c	Cc
d_{calc} (g/cm^3)	1.431	1.253	1.406
μ (mm^{-1})	0.805	0.491	0.791
GOF on F^2	0.999	1.109	1.159

257

Complex	**3.19**	**3.18**
CCDC #	279534 (DRA 11)	284061(DRA14)
Empirical formula	½(C$_{44}$H$_{55}$B$_2$Cl$_2$N$_3$ORu)	C$_{50}$H$_{55}$B$_2$Cl$_2$N$_3$ORu • CH$_2$Cl$_2$
	½(C$_{44}$H$_{55}$B$_2$Br$_2$N$_3$ORu) •	
	2(C$_6$H$_6$)	
Formula weight	1036.18	992.49
Crystallization solvent	C$_6$H$_6$	CH$_2$Cl$_2$/C$_5$H$_{12}$
Crystal color	Brown	Olive green
T (K)	100 (2)	100(2)
θ range (°)	2.28 to 33.09	2.28 to 33.08
a (Å)	12.2175(5)	11.3161(5)
b (Å)	13.3453(6)	12.0058(6)
c (Å)	16.8780(7)	19.9770(10)
α (°)	102.4260(10)	95.6720(10)
β (°)	104.8020(10)	103.7650(10)
γ (°)	96.2280(10)	111.6630(10)
V (Å^3)	2559.01(19)	2397.0(2)
Crystal System	Triclinic	Triclinic
Space group	P-1	P-1
d_{calc} (g/cm^3)	1.345	1.375
μ (mm^{-1})	1.181	0.591
GOF on F^2	1.450	1.153
R$_1$, wR$_2$ [I > 2σ(I)]	0.0490, 0.0916	0.0491, 0.0755

Complex	**4.9b**	**4.12b**	**4.15**
CCDC #	289352 (DRA22)	616546 (DRA28)	653329 (DRA31)
Empirical formula	$C_{30}H_{34}N_2Cl_2Ru$	$C_{24}H_{18}F_4N_2Cl_2Ru \bullet$ CH_2Cl_2	$C_{36}H_{47}N_2O_2Cl_3Ru \bullet C_{27}H_{39}N_2$ $\bullet C_{18}H_{33}OP$
Formula weight	594.56	667.30	1435.19
Crystallization solvent	CH_2Cl_2	CH_2Cl_2	
Crystal color	Green	Olive green	green
T (K)	293(2)	100(2)	100(2)
θ range (°)	2.20 to 25.65	2.31 to 35.22	2.23 to 28.04
a (Å)	16.4420(10)	10.2476(4)	14.1928(12)
b (Å)	16.5926(10)	14.0092(6)	16.5881(14)
c (Å)	22.4396(14)	18.2052(8)	20.1337(17)
α (°)			99.416(2)
β (°)		104.4040(10)	110.3120(10)
γ (°)			100.5130(10)
V (Å^3)	6121.9(6)	2531.40(18)	4236.3(6)
Crystal System	Orthorhombic	Monoclinic	Triclinic
Space group	Pbca	P2$_1$/c	P-1
d_{calc} (g/cm^3)	1.290	1.751	1.125
μ (mm^{-1})	0.706	1.090	0.343
GOF on F^2	1.507	1.233	1.05
R$_1$, wR$_2$ [I > 2σ(I)]	0.0477, 0.0656	0.0425, 0.0642	0.0554, 0.0943

Complex	**4.17a**	**4.21a**
CCDC #	295418 (DRA26)	295508 (DRA27)
Empirical formula	$C_{42}H_{42}N_2Cl_2Ru \bullet C_4H_8O$	$C_{31}H_{36}N_2Cl_2Ru$
Formula weight	818.85	608.59
Crystallization solvent	THF/pentane	
Crystal color	Brown-green	Green
T (K)	100(2)	100(2)
θ range (°)	2.23 to 26.71	2.38 to 35.64
a (Å)	14.2896(14)	10.3527(5)
b (Å)	15.8211(15)	16.2352(7)
c (Å)	18.1127(18)	16.9412(8)
α (°)		
β (°)		103.4140(10)
γ (°)		
V (Å^3)	4094.9(7)	2769.8(2)
Crystal System	Orthorhombic	Monoclinic
Space group	$P2_12_12_1$	$P2_1/c$
d_{calc} (g/cm^3)	1.328	1.459
μ (mm^{-1})	0.550	0.782
GOF on F^2	2.660	1.598
R_1, wR_2 [I > 2σ(I)]	0.0609, 0.0966	0.0479, 0.0880

Complex	ClRh(H$_2$IMes)(cod)	A3.15	A3.17
CCDC #	252907 (DRA03)	254552 (DRA04)	258578 (DRA06)
Empirical formula	C$_{29}$H$_{38}$N$_2$ClRh	C$_{45}$H$_{54}$N$_2$O$_2$ClRh	C$_{47}$H$_{58}$N$_2$ClRh
Formula weight	552.97	793.26	789.31
Crystallization solvent	Ethyl acetate/hexanes	Ethyl acetate/benzene	Et$_2$O/hexanes
Crystal color	Yellow	Yellow	Yellow
T (K)	100(2)	100(2)	100(2)
θ range (°)	2.21 to 32.72	2.16 to 35.07	2.20 to 31.91
a (Å)	15.3728(9)	14.5262(4)	12.7952(4)
b (Å)	11.7889(7)	15.8560(4)	17.7441(5)
c (Å)	14.9779(9)	35.0945(9)	18.5205(6)
α (°)			
β (°)	107.2540(10)		
γ (°)			
V (Å^3)	2592.2(3)	8083.2(4)	4204.9(2)
Crystal System	Monoclinic	Orthorhombic	Orthorhombic
Space group	P2$_1$/c	P2$_1$2$_1$2$_1$	P2$_1$2$_1$2$_1$
d_{calc} (g/cm^3)	1.417	1.304	1.247
μ (mm^{-1})	0.781	0.527	0.503
GOF on F^2	1.229	1.023	0.991
R$_1$, wR$_2$ [I > 2σ(I)]	0.0366, 0,0576	0.0442, 0.0589	0.0383, 0.0541